Molecular and Immunological Mechanisms Underlying Inflammation during SARS-CoV-2 Infection

Alexandru Odainic

ORCID ID:

0000-0002-2806-6904

from Chisinau, Republic of Moldova

Submitted in total fulfilment of the requirements of the joint degree of

Doctor of Philosophy (PhD)

of

The Medical Faculty

The Rheinische Friedrich-Wilhelms-Universität Bonn

and

The Department of Microbiology and Immunology

The University of Melbourne

Bonn/Melbourne, 2025

Performed and approved by The Medical Faculty of The Rheinische Friedrich-Wilhelms-Universität Bonn and The University of Melbourne

1. Supervisor: Prof. Dr. med. Eicke Latz

2. Supervisor: Prof. Dr. Sammy Bedoui

Month and year of the original thesis submission: August 2024

Month and year of the oral examination: September 2025

Institute in Bonn: Institute of Innate Immunity

Table of Contents

List of abbreviations

3CLpro	3C-like proteinase
ACE2	Angiotensin-converting enzyme 2
AIM2	Absent in melanoma 2
ALR	AIM2-like receptor
APC	Antigen presenting cell
ARDS	Acute respiratory distress syndrome
AT2	Alveolar cell type 2
AZ	Vaxzevria AstraZeneca vaccine
BST2	Bone marrow stromal cell antigen 2
BT	Comirnaty BioNTech vaccine
CCL	CC chemokine ligand
CD	Cluster of differentiation
cGAS	Cyclic GMP-AMP synthase
CITE-Seq	Cellular Indexing of Transcriptomes and Epitopes by Sequencing
CLL	Chronic lymphocytic leukemia
CLR	C-type lectin receptors
CoV	Coronavirus
COVID-19	Coronavirus disease 2019
CRP	C reactive protein
CS	Cleavage site
CTSL	cathepsin L

DAMP	Damage-associated molecular patterns
DC	Dendritic cell
DC-SIGN	Dendritic cell-specific intercellular adhesion molecule-3-grabbing non-integrin
DE	Differentially expressed
DEG	Differentially expressed genes
DNA	Deoxyribonucleic acid
E	Envelope of SARS-CoV-2
EBV	Epstein-Barr virus
ECM	Extracellular matrix
ECMO	Extracorporeal membrane oxygenation
EMA	European medicines agency
FDR	False discovery rate
G	Giga (10^9)
GO	Gene ontology
HHV	Human herpesvirus
HS	Heparan sulfate
ICU	Intensive care unit
IFIT	interferon induced protein with tetratricopeptide repeats
IFITM	Interferon-induced transmembrane protein
IFN	Interferon
Ig	Immunoglobulin
IL	Interleukin
ILC	Innate lymphoid cells

ISG	Interferon stimulated gene
ITIM	Immunoreceptor tyrosine-based inhibitory motif
JAK	Janus kinase
JJ	Jcovden Janssen-Cilag vaccine
k.nn	k nearest neighbor
KIR	Killer cell immunoglobulin-like receptor
LLoQ	Lowest limit of quantification
L-SIGN	Liver/lymph node-specific intercellular adhesion molecule-3-grabbing non-integrin
LY6E	Lymphocyte antigen 6 family member E
M	Membrane of SARS-CoV-2
MAIT	mucosal-associated invariant T
MAP	Mean arterial pressure
MDA5	Melanoma differentiation-associated protein 5
ME	Module eigengene
MERS-CoV	Middle east respiratory syndrome coronavirus
MHC	Major histocompatibility complex
MIS-C	Multisystem Inflammatory Syndrome in Children
MO	Spikevax Moderna vaccine
Mtb	Mycobacterium tuberculosis
N	Nucleocapsid protein of SARS-CoV-2
NAb	Neutralizing antibody
NET	Neutrophil extracellular traps
NK	Natural killer

NLR	NOD-like receptors
NOD	Nucleotide oligomerization domain
NRP1	Neuropilin
OAS	Oligoadenylate synthase
ORF	Open reading frame
PAMP	Pathogen-associated molecular patterns
PASC	Post-acute sequelae of SARS-CoV-2 infection
PBMC	Peripheral blood mononuclear cells
PC	Principal component
PCA	Principal component analysis
pDC	plasmacytoid dendritic cell
PoTS	Postural orthostatic tachycardia syndrome
PRR	Pattern recognition receptor
RBD	Receptor binding domain
RIG-I	Retinoic acid-inducible gene I
RNA	Ribonucleic acid
ROS	Reactive oxygen species
S	Spike protein of SARS-CoV-2
SARS-CoV	Severe acute respiratory syndrome related coronavirus
scRNAseq	Single cell RNA sequencing
SEM	Standard error of mean
SIGLEC1	Sialic acid binding immunoglobulin like lectin 1
STAT	signal transducer and activator of transcription protein

STIKO	German Vaccine Committee (Ständige Impfkommission)
STING	Stimulator of interferon genes
T	Tera (10^{12})
TCM	T central memory
TCR	T cell receptor
TEM	T effector memory
Tfh	T folicular helper
TLR	Toll like receptor
TMPRSS2	Transmembrane serine protease 2
TNF	Tumor Necrosis Factor
Treg	T regulatory
UMAP	Uniform manifold approximation and projection
UMI	Unique molecular identifier
VOC	Variant of concern
WGCNA	Weighted gene correlation network analysis
WHO	World health organization
WNN	Weighted nearest neighor
WT	Wild type

1. Introduction

1.1 Coronaviruses

Coronaviruses (CoV), a diverse group of single-stranded, positive-sense ribonucleic acid (RNA) viruses enveloped in a lipid layer, were first identified in the 1960s in patients exhibiting symptoms of the common cold (Tyrrell and Bynoe, 1965; Hamre and Procknow, 1966; McIntosh *et al.*, 1967; Dorothy *et al.*, 1967). These viruses were subsequently classified within the *Coronaviridae* family and taxonomically divided into four distinct genera: alphacoronavirus, betacoronavirus, gammacoronavirus, and deltacoronavirus (Cavanagh *et al.*, 1994; Chang *et al.*, 2020). While the alpha- and betacoronaviruses predominantly affect the respiratory and gastrointestinal systems of mammals, including humans, the gamma- and deltacoronaviruses primarily target avian species, though they can also infect mammals (Yu Chen, Liu, *et al.*, 2020).

Coronaviruses share a conserved genome organization and gene expression pattern, consisting of 16 non-structural proteins and four structural proteins spike (S), envelope (E), membrane (M), and nucleocapsid (N) (Burrell *et al.*, 2017). The distinctive feature of coronaviruses is their crown-like appearance under an electron microscope, a characteristic derived from the S proteins that prominently protrude from their surface (Li, 2016). The spike proteins are key players in the virus's life cycle and represent a focal point in coronavirus research as the S protein facilitates the attachment and entry into the host cells by binding to specific receptors on the host cell surface (McCallum *et al.*, 2020). The Receptor-Binding Domain (RBD) affinity of the spike protein dictates the ability to infect different species and the tissue tropism (Fehr and Perlman, 2015; Ji *et al.*, 2022).

Once inside the cell, through hijacking the host cell machinery, the virus produces the components needed to create new virions. The N protein is self-assembled and binds to the viral RNA to protect the viral genome from extracellular agents and guarantee prompt replication and further transmission (McBride *et al.*, 2014). The M protein represents the core membrane components and is the central organizer of the envelope formation by interacting with all other structural proteins

of the virus, although by itself is not able to produce new virions (Neuman *et al.*, 2011; Schoeman and Fielding, 2019). The E proteins are essential components for virus assembly and release, as deleting the E from the genome leads to impaired viral maturation and production of viruses incapable of effective propagation (de Haan *et al.*, 2000; Ortego *et al.*, 2007). This unique structural organization is crucial for the virus's life cycle and pathogenicity. The interaction

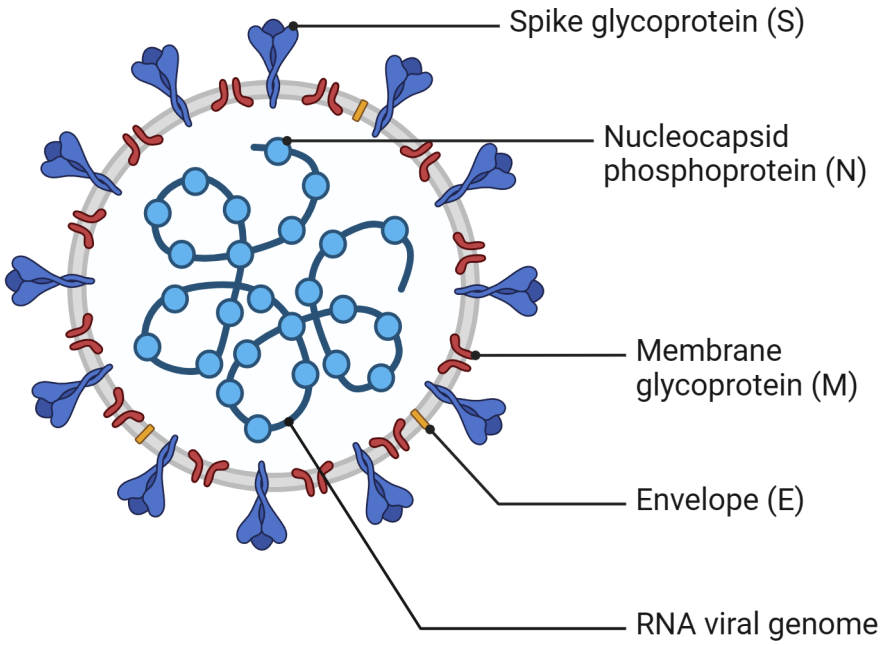

Figure 1: General structure of the coronaviruses. The outer layer of the coronavirus consists of spike (S), membrane (M), envelope (E) glycoproteins. Enclosed within this structure is the viral RNA, wrapped around the nucleocapsid (N) protein. Created with BioRender.com.

of these structural proteins with the host's cellular machinery and innate immune system, in order to modulate the immune response, dictates the efficiency of viral spread and the severity of the disease (Fung *et al.*, 2014; Fung and Liu, 2019). These interactions determine not only how rapidly and widely the virus can propagate within a host population, but also the extent and intensity of clinical symptoms experienced by infected hosts (Gordon *et al.*, 2020; Kasuga *et al.*, 2021).

Recent genomic sequencing data have significantly advanced our understanding of the origins of human coronaviruses, identifying zoonotic spillover events as one of the main cause for the emergence of major pathogenic strains of betacoronaviruses such as Severe Acute Respiratory Syndrome related Coronavirus (SARS-CoV), Middle East Respiratory Syndrome Coronavirus (MERS-CoV) (Forni *et al.*, 2017), and SARS-CoV-2 (Wrobel *et al.*, 2021; Wang *et al.*, 2023). However, current evidence suggests that the human coronaviruses 229E, OC43, NL63, and HKU1 are adapted to the human host, resulting in their persistent circulation within the human population, while there is no substantial evidence to indicate the ongoing maintenance of these viruses in any of the original bat or rodent animal reservoir (Su *et al.*, 2016). Bats have been identified as the high-risk ideal reservoir for both alphacoronaviruses and betacoronaviruses and are considered as the probable source for the emergence of various diseases that have subsequently made the leap to humans (Woo *et al.*, 2012; Letko *et al.*, 2020). This inter-species transmission is facilitated by the plasticity of the spike protein, allowing coronaviruses to adapt to new host receptors (Tian *et al.*, 2022). Additionally, domestic animals have been proven to serve as intermediate hosts in the emergence of novel coronaviruses pathogenic to humans (Cui *et al.*, 2019). Significant populations of SARS-CoV-like viruses in southern China's horseshoe bats, emphasize the elevated risk of new viral pandemics emerging from the consumption of exotic wildlife (Cheng *et al.*, 2007).

Prominent betacoronaviruses, such as SARS-CoV and MERS-CoV, have been responsible for significant epidemics over the past two decades. SARS-CoV, first identified in Southeast Asia in 2002, led to over 8,000 cases of SARS with a case fatality rate of approximately 11 % (Chan-Yeung and Xu, 2003). Similarly, MERS-CoV, first reported in September 2012, resulted in 2,494 infections with a fatality rate of 37 % primarily due to acute respiratory failure or related complications (C. Huang *et al.*, 2020). These outbreaks highlight the public health challenges posed by betacoronaviruses, particularly in terms of transmission and severity of clinical outcomes.

In late 2019, a novel betacoronavirus SARS-CoV-2 was first identified in China. Characterized by its rapid transmission rate and a case fatality rate of 5 %, the outbreak swiftly escalated into a pandemic, impacting nations worldwide (Shu Yang *et al.*, 2020). Three years into the SARS-CoV-2 pandemic, the death rate has been reduced by extensive vaccination efforts and disease mitigation procedures, yet the virus has caused notable footprint on global healthcare systems, challenging hospital capacities and disrupting routine medical care. Additionally, the pandemic impacted remarkably the global economics and escalated psychosocial stress, underscoring the essential need for continued intensive virus and vaccine research and enhanced preparedness for future epidemics (Pak *et al.*, 2020).

1.2 SARS-CoV-2

SARS-CoV-2, the pathogen responsible for the coronavirus disease 2019 (COVID-19) pandemic, represents the seventh coronavirus identified to infect humans (Andersen *et al.*, 2020). Early research efforts to classify the virus, discovered a 80 % similarity to SARS-CoV at nucleotide level (Zhang and Holmes, 2020; Lu *et al.*, 2020). This genomic similarity has been crucial in understanding the virus's mechanisms of infection and pathogenesis. It is known that angiotensin-converting enzyme 2 (ACE2) serves as a cellular entry receptor for SARS-CoV, and it was investigated for its interaction with SARS-CoV-2 (Li *et al.*, 2003; Kuba *et al.*, 2005). Studies revealed infection of ACE2 expressing cells mediated by the S protein of SARS-CoV-2 with a 10- to 20-fold enhanced binding affinity to the receptor compared to SARS-CoV, confirming its use of the same receptor for host cell entry (Wrapp *et al.*, 2020; F. Zhou *et al.*, 2020).

1.2.1 ACE2 expression and the putative impact of comorbidities

ACE2 is a metalloproteinase ectoenzyme that acts as a catalyser of angiotensin II to angiotensin, the latter having a vasodilating function and thus playing an important role in the regulation of cardiovascular and renal functions (Keidar *et al.*, 2007). Analyses of immunofluorescence staining and human transcriptome databases have demonstrated that ACE2 is expressed by the type II alveolar

cells (AT2) in the lower lung, while in the upper respiratory tract the expression is more abundant, largely in the ciliated cells (Zou *et al.*, 2020; Hou *et al.*, 2020). Unlike SARS-CoV, which primarily targets the lungs, SARS-CoV-2 can infect both the upper and lower respiratory tracts efficiently (Meyerholz *et al.*, 2016; Lui *et al.*, 2020). The variance in ACE2 expression across the respiratory tract is strongly reflected in the SARS-CoV-2 infection pattern, with nasal ciliated cells emerging as predominant site for the virus' replication during initial phase of infection (Ahn *et al.*, 2021). In the progressive stages of infection, the organ-specific damage observed in correlates with the distribution of ACE2 expression across various tissues, highlighting the pivotal role of ACE2 availability on cells and the pathophysiological impacts of the virus at a systemic level (Du *et al.*, 2020).

Throughout the body, ACE2 expression has been observed to be most pronounced in the intestine, with subsequent high levels identified in the testis, kidneys, and cardiac muscle tissue (Figure 2) (Y. Wang *et al.*, 2020). In the intestine, the marker is more abundant on the enterocytes of the small intestine relative to the colon, and in patients infected with SARS-CoV-2 immunofluorescence staining revealed the presence of N protein within the cytoplasm of gastric, duodenal, and rectal glandular epithelial cells, as well as in the upper and stratified epithelial cells of the oesophagus (Lamers *et al.*, 2020; Xiao *et al.*, 2020). Renal ACE2 is primarily membrane-bound found on the surface of epithelial and endothelial cells, but N protein was successfully stained in the renal tubules in post-mortem samples of patients who succumbed to SARS-CoV-2 infection, validating the direct infection potential of renal cells by the virus (Kroll *et al.*, 2023). In cardiac tissue, ACE2 expression is specifically localized to pericytes (Liang Chen, Li, et al., 2020). Analysis of myocardial tissue from autopsy samples has confirmed the presence of the SARS-CoV-2 viral genome. Notably, *in situ* hybridization techniques have identified that the predominant localization of SARS-CoV-2 is not within the cardiomyocytes themselves but rather in the interstitial cells or macrophages that infiltrate the myocardial tissue (Lindner *et al.*, 2020). In the liver, ACE2 is not expressed in hepatocytes, Kupffer

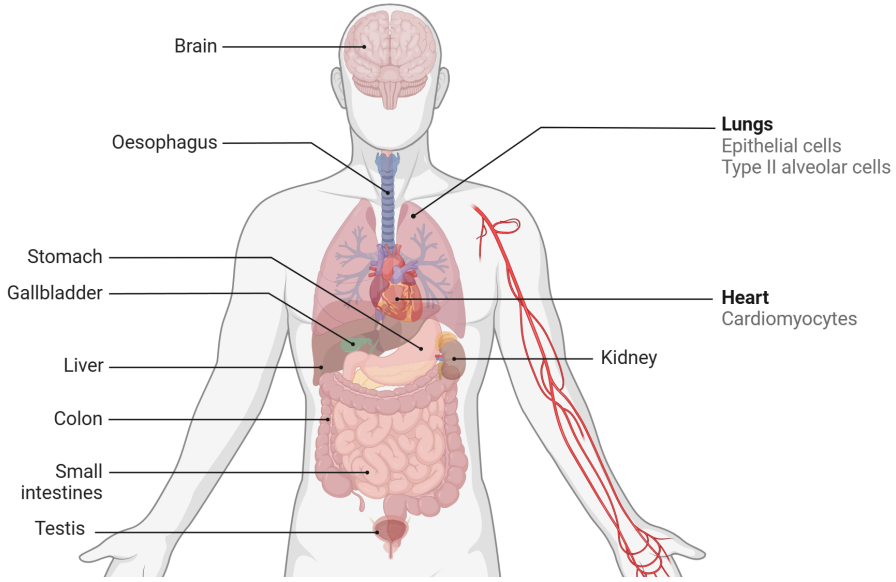

Figure 2: Distribution of ACE2 protein expression across human organs. Summary of tissues expressing ACE2 including gastrointestinal and respiratory tract, heart, kidneys, testes and brain. Created with Biorender.com

cells, or endothelial cells but is detected in cholangiocytes, which can explain liver injury to some extent (Vabret *et al.*, 2020). Although endothelial cells express ACE2, recent studies indicate that endothelial inflammation occurs independently of ACE2 enzymatic activity and viral replication (Montezano *et al.*, 2023).

1.2.2 Processing factors for cell infection

While ACE2 acts as the primary binding receptor for host cells, the successful infection by SARS-CoV-2 depends on the proteolytic activation by cleavage of its S protein, a crucial step for facilitating the fusion between the host cell membrane and the virus (Fraser *et al.*, 2022). The S protein is composed of two subunits: S1, containing the RBD, and S2, responsible for mediating membrane fusion (Walls *et al.*, 2020). Two target-cell proteases have been identified to drive the S protein activation (Figure 3): transmembrane serine protease 2 (TMPRSS2) at the furin cleavage site during “early infection” via the plasma membrane and cathepsin L (CTSL) at the cathepsin cleavage site (CS-1 and CS-2) in the course of “late infection” via endosomal uptake (Essalmani *et al.*, 2022; Jackson *et al.*,

2022; M.-M. Zhao *et al.*, 2022). Inhibiting TMPRSS2 activity with a protease inhibitor significantly reduced SARS-CoV-2's infection efficiency in lung cells

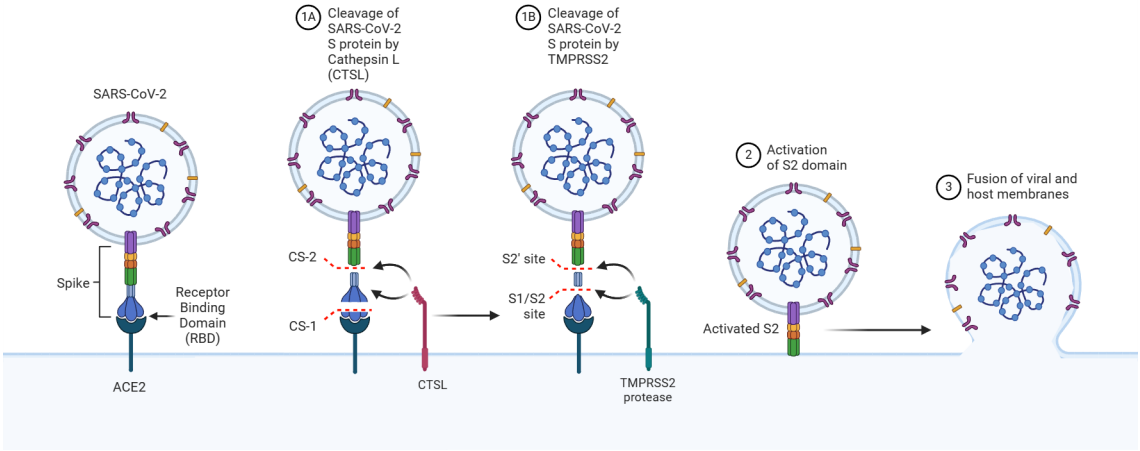

Figure 3: SARS-CoV-2 host cell entry pathways. Following initial binding to the ACE2 receptor via its receptor-binding domain (RBD), SARS-CoV-2 employs two main routes for cellular invasion. Through the “early pathway” (1A) the virus utilizes the host TMPRSS2 on the cell surface to cleave the S protein, thus allowing for the entry via the plasma membrane. Alternatively, in the “late pathway” (1B), SARS-CoV-2 undergoes endosomal uptake and relies on CTSL to cleave the S protein. In both pathways, the activation and cleavage of the S (2) lead to the fusion of the viral and host cell membranes (3), facilitating the release of the viral genome into the host cell's cytoplasm.

(Hoffmann *et al.*, 2020). On the other hand, CTSL overexpression lead to enhanced infection while it’s blockage prevented infection both *in vitro* and *in vivo* (Zhao *et al.*, 2021). Concurrently, removal of the virus's furin site results in asymptomatic disease in hamsters (Johnson *et al.*, 2021). These findings suggest that the focus in combating SARS-CoV-2 should extend beyond just neutralizing antibodies that block the RBD-ACE2 interaction, by targeting the furin cleavage site as a viable strategy, thereby restricting viral infectivity by limiting its ability to effectively prime the spike protein for cell entry (Spelios *et al.*, 2022).

1.2.3 Factors contributing to adhesion of SARS-CoV-2 to host cells

C-type lectins such as dendritic cell-specific intercellular adhesion molecule-3-grabbing non-integrin (DC-SIGN), liver/lymph node-specific intercellular adhesion molecule-3-grabbing non-integrin (L-SIGN) and sialic acid binding immunoglobulin like lectin 1 (SIGLEC1) have been identified to be involved in viral dissemination and increased infectivity, however these cannot support efficient infection in the absence of ACE2 (Amraei *et al.*, 2021; Jackson *et al.*, 2022). Activated dendritic cells (DCs) were observed to be resistant to direct SARS-CoV-2 infection, however these possess the ability to trans-infect cells expressing ACE2 and TMPRSS2 by transporting the virus via the SIGLEC1 receptor to susceptible host cells. This process was significantly reduced in the presence of anti-SIGLEC1 antibodies, suggesting that SIGLEC1-mediated trans-infection by DCs might facilitate the dissemination of the virus to pulmonary and distant tissues (Lempp *et al.*, 2021). Studies indicate that C-type lectins bind the S protein through epitopes located outside the RBD in the S1 region. When mutations were introduced into the S1 RBD, the modified protein lost its ability to bind ACE2, but retained its affinity for C-type lectins. Furthermore, the introduction of soluble mannan, a mannose polymer acting as a ligand for C-type lectins, successfully blocked the S protein's binding to DC-SIGN and L-SIGN in a competitive manner without impacting its interaction with ACE2. Conversely, treatment with endoglycosidase, an enzyme that removes high-mannose oligosaccharides from N-linked glycans, specifically reduced the S protein's binding to DC-SIGN and L-SIGN (Q. Lu *et al.*, 2021).

Beyond the primary mechanisms, additional molecular players like the neuropilin (NRP1) receptor also contribute to the virus's infectious efficiency, serving as a critical component in the development of neurons and the cardiovascular system (Pizzato *et al.*, 2022). The proteolytic cleavage at the S protein's furin site, reveals a region that can bind to and activate NRP1. While NRP1 does not sustain viral uptake, it’s co-expression with ACE2 and TMPRSS2 significantly increases viral infectivity, whereas its inhibition through antibodies or deletion reduces virus uptake in cells co-expressing NRP1 with the main cell entry factors (Cantuti-

Castelvetri *et al.*, 2020). Importantly, NRP1 is highly expressed in olfactory epithelial cells. The detection of the S protein in the olfactory epithelium of SARS-CoV-2 infected individuals, despite the low ACE2 expression in this tissue, suggests that the virus utilizes additional factors to boost its interaction and infection efficiency, thereby enhancing its ability to infect tissues with low levels of the primary entry receptors (Daly *et al.*, 2020).

In addition, other elements such as cluster of differentiation (CD) 147 and heparan sulfate (HS) have been identified to promote SARS-CoV-2 infection of host tissues. HS plays a crucial role in the binding of the virus to the membrane of epithelial cells. Treatment with unfractionated heparin or heparin lyases significantly decreases the binding of S proteins to human primary bronchial epithelial cells, thus reducing infection rates by more than fivefold without affecting cell viability (Clausen *et al.*, 2020). CD147 was reported as a potential alternative binding receptor for cell entry, considering that viral replication was diminished in CD147 knockdown immortalized human bronchial epithelium and anti-CD147 antibodies reduced infection of the cells in a dose-dependent manner (K. Wang *et al.*, 2020). Additionally, overexpression of CD147 enhanced virus infection and viral presence was noted in the lungs of human CD147 (hCD147) transgenic mice following SARS-CoV-2 infection, a phenomenon not observed in wild-type (WT) mice 48 hours post-infection (K. E. Wang *et al.*, 2020).

The various strategies used by SARS-CoV-2 to invade host cells underscore its adaptability to infect the human system and provide insights into the pathogenesis of the disease it causes, offering explanations for the spectrum of symptoms observed in infected individuals.

1.2.4 Proteins restricting infection

The human immune system is continuously engaged in a dynamic confrontation with pathogens attempting to breach anatomical barriers. This requires a balanced and quick immune response that effectively eliminates the pathogen and the infected cells without disrupting the own biological system and also the beneficial symbiotic relationship with the hosts commensals (Latz *et al.*, 2013).

Central to this defence mechanism is the innate immune response, characterized by a range of signalling receptors and cells proficient at recognizing both exogenous molecular structures and endogenous molecules that undergo modification or become abundant during infection (Hornung *et al.*, 2006; Kawai and Akira, 2011). Specifically, in the context of viral infections such as those initiated by SARS-CoV-2, the innate immune machinery is instrumental in limiting viral entry and proliferation, identifying and annihilating the infected cells, and facilitating the transition to an adaptive immune response tailored to the invading pathogen (Diamond and Kanneganti, 2022).

Key players of the innate immune system, including granulocytes, natural killer (NK) cells, monocytes/macrophages, innate lymphoid cells (ILCs), as well as many epithelial cells are equipped with a diversity of pattern recognition receptors (PRRs) located within endosomal compartments, the cytosol, and on the cell surface (Marshall *et al.*, 2018). These receptors are specialized in detecting pathogen-associated molecular patterns (PAMPs) and damage-associated molecular patterns (DAMPs), which are indicative of non-self entities or cellular distress, respectively, thereby activating the immune cascade (Bianchi, 2007). PRRs have been classified in five principal categories: Toll-like receptors (TLRs), nucleotide oligomerization domain (NOD)-like receptors (NLRs), retinoic acid-inducible gene I (RIG-I)-like receptors (RLRs), C-type lectin receptors (CLRs), and absent in melanoma 2 (AIM2)-like receptors (ALRs) (Li and Wu, 2021). Activation of PRRs initiate signalling cascades that ultimately result in the transcription and generation of type I and type III interferons (IFNs), which play a pivotal role in the antiviral defense (Mesev *et al.*, 2019).

Apart from the large PRR classes, various cytosolic detectors also play a pivotal role in identifying viruses and initiating pro-inflammatory responses (Sun *et al.*, 2017; Franz *et al.*, 2018). Among these, the cyclic GMP-AMP synthase (cGAS) and stimulator of interferon genes (STING) pathway is responsible for recognizing cytoplasmic deoxyribonucleic acid (DNA) (Sun *et al.*, 2013; Schoggins *et al.*, 2014). SARS-CoV-2 has been found to cause mitochondrial damage, potentially leading to the release of mitochondrial DNA into the

cytoplasm, thus activating the cGAS pathway and supporting the innate immune pathways (Singh *et al.*, 2020). Nonetheless, SARS-CoV-2's accessory proteins, Open Reading Frame 3a (ORF3a) and 3C-like proteinase (3CLpro), are known to block the cGAS-STING pathway, dampening the body's antiviral immune responses (Rui *et al.*, 2021). Treatment with the STING agonist diABZI, has been shown to limit SARS-CoV-2 replication in primary human bronchial epithelial cells and enhances survival rates in hACE2 transgenic mice (Humphries *et al.*, 2021; Li *et al.*, 2021).

In this context, TLR7 and TLR2 play a crucial role in triggering the pro-inflammatory response upon SARS-CoV-2 infection, leading to subsequent immune activation and cytokine production. TLR7, localized to endosomal compartments, recognizes G/U-rich single-stranded viral RNA (Campbell *et al.*, 2021). Notably, anomalies in the X-chromosomal gene encoding TLR7 have been correlated with severe disease course of coronavirus disease 2019 (COVID-19) in younger demographics, suggesting a protective role for TLR7 against SARS-CoV-2 infection (Van Der Made *et al.*, 2020). Additionally, both murine and human macrophages reduced pro-inflammatory cytokine production when treated with TLR2 antagonist oxPAPC as well as in TLR2 deficiency when stimulated with SARS-CoV-2 E protein (Zheng *et al.*, 2021). In lung epithelial cells, the melanoma differentiation-associated protein 5 (MDA5) receptor, a member of the RLR family located in the cytoplasm, detects RNA of replicating SARS-CoV-2 and triggers the production of IFNs, as the deletion or silencing of the MDA5 gene results in diminished IFN production in these cells upon exposure to SARS-CoV-2 (Rebendenne *et al.*, 2021; Yin *et al.*, 2021). While all types of PRRs play their role in activating the immune system and inducing IFNs, the specific contributions of each PRR during SARS-CoV-2 infection remain subjects of ongoing research. However, the critical role of IFNs in the defense against viruses, including SARS-CoV-2, is underscored by these often redundant mechanisms to ensure a robust antiviral response.

The release of IFNs in response to PRR signalling represents the early defense mechanism against viral infections. IFNs, once secreted, bind to receptors on the

producing cells in an autocrine manner and on neighboring cells. This dual binding strategy not only amplifies the immune response within the initially affected cells but also prepares surrounding cells for potential viral threats, effectively limiting viral spread (Ivashkiv and Donlin, 2014). Moreover, IFNs play a pivotal role in modulating the immune landscape beyond their immediate vicinity. By binding to their receptors on the surface of antigen-presenting cells (APCs), IFNs activate specific signaling pathways with multiple effects (McNab *et al.*, 2015). This activation induces cellular programming, enhancing the antigen presentation capabilities of APCs while simultaneously tempering the production of pro-inflammatory cytokines. This programming ensures that APCs adopt functions that balance immune activation and regulation, helping to prevent excessive inflammation that could lead to tissue damage. (Lee and Ashkar, 2018). Furthermore, IFNs are involved in activating the adaptive immune response, facilitating the development of antigen-specific T and B cells crucial for long-term immunity (McNab *et al.*, 2015). Upon binding to their receptors, IFNs trigger the phosphorylation of the janus kinase (JAK)-signal transducer and activator of transcription protein (STAT) pathway (Katze *et al.*, 2002). This signalling cascade leads to the transcription of a broad array of interferon-stimulated genes (ISGs), which possess diverse antiviral functions, from directly inhibiting viral replication to enhancing the immune system's ability to recognize and eliminate infected cells (Schoggins, 2019).

Several ISGs have been identified to be involved in SARS-CoV-2 infection. Among these, interferon-induced transmembrane protein (IFITMs) have shown conflicting roles. Early studies reported that IFITMs restrict the human coronaviruses from cell entry (Huang *et al.*, 2011). However, as more studies have been published, some suggest that SARS-CoV-2 S proteins may exploit IFITMs to enhance infectivity, with endogenous IFITM expression levels in tissue being sufficient to sustain infection and propagation (Nchioua *et al.*, 2022). Targeting IFITMs with antibodies or usage of the IFITM-derived proteins has been shown to significantly reduce SARS-CoV-2 infection efficacy in lung, heart and intestinal cells (Prelli Bozzo *et al.*, 2021). In individuals infected with SARS-CoV-2 an increased mortality rate correlated with single nucleotide polymorphism in

the *IFITM3* gene (Gholami *et al.*, 2022). Interestingly, it has been observed that IFITM expression can trap the ACE2 receptor in the cytoplasm, thus reducing the infection (Xie et al., 2024).

Lymphocyte antigen 6 family member E (LY6E), another ISG with dual roles in viral infections, facilitates the entry of influenza A virus and flaviviruses but blocks the fusion of the SARS-CoV-2 S protein with the cell membrane, thereby limiting infection (Pfaender et al., 2020). Additionally, CD74 has emerged from a transposon screening as an ISG capable of inhibiting the cathepsin-mediated cleavage of the SARS-CoV-2 S protein, thereby hindering the virus's endosomal entry route (Bruchez *et al.*, 2020).

Beyond entry inhibition, the interferon induced protein with tetratricopeptide repeats (IFIT) family have been described as a family of proteins to curtail viral replication. IFIT proteins specifically target and sequester viral RNA characterized by 5'-triphosphate ends or 2'-O-unmethylated caps, and IFIT1, IFIT3, and IFIT5 are noted for their roles in effective suppression of SARS-CoV-2 viral replication processes (Martin-Sancho *et al.*, 2021; Schindewolf *et al.*, 2023). Similarly, oligoadenylate synthases (OAS) also represent a class of interferon-stimulated proteins which can recognize viral ds-RNA, binding to these molecules and subsequently triggering RNase L activation to dismantle the viral RNA (Hornung *et al.*, 2014). Emerging evidence underscores the critical role of the OAS1p46 isoform; its functional deficit is correlated with an escalated risk of advancing to severe disease in SARS-CoV-2 infected individuals (Wickenhagen *et al.*, 2021; Soveg *et al.*, 2021; Huffman *et al.*, 2022).

Furthermore, bone marrow stromal cell antigen 2 (BST2) was identified as an ISG to restrict viral egress by impeding the production of N protein. Overexpression of BST2 significantly reduced both SARS-CoV-2 replication and release of viral particles, while its deletion resulted in increased secretion of infectious virions (Martin-Sancho *et al.*, 2021). SARS-CoV-2 has evolved a mechanism to circumvent the host defense mechanism, notably through Orf7a protein which counteracts the BST2 inhibitory effect (Shi *et al.*, 2024).

Understanding the elements that sense and constrain the spread of SARS-CoV-2 within the body is crucial for delineating the progression of the disease and developing targeted therapeutic strategies.

1.3 COVID-19

COVID-19 rapidly escalated into a global pandemic, exhibiting an overabundance of challenges for the health systems worldwide (Hu *et al.*, 2021). The disease presents a wide array of symptoms impacting various organ systems such as the respiratory, cardiovascular, gastrointestinal, and nervous system (Cascella *et al.*, 2022). The clinical presentation of COVID-19 spans a broad spectrum, ranging from individuals who remain asymptomatic to those experiencing severe symptoms that require hospitalization and may ultimately result in death (F. Zhou *et al.*, 2020). This variability in clinical manifestations underscores the complex pathophysiology of COVID-19, necessitating a sophisticated approach to diagnosis, treatment, and management. The pandemic's toll, as of March 2024, exceeded 7 million deaths, emphasizing the disease's severe impact worldwide (World Health Organization, 2024).

1.3.1 Severity classifications

The World Health Organization (WHO) has categorized the severity of the disease based on the spectrum of symptoms exhibited by patients (World Health Organization, 2023). Mild disease encompasses individuals presenting symptoms such as fever, cough, and shortness of breath, alongside additional symptoms like sore throat, nasal congestion, headache, muscle pain, fatigue, and sensory impairments, including anosmia (loss of smell) and ageusia (loss of taste) (Wiersinga *et al.*, 2020). Moderate disease is characterized by patients showing signs of pneumonia, including fever, cough, dyspnoea, and rapid breathing, with an oxygen saturation level of ≥ 90% in ambient air (Feng *et al.*, 2020). Severe disease is identified by signs of severe pneumonia coupled with at least one of the following: a respiratory rate exceeding 30 breaths per minute, significant respiratory distress, or an oxygen saturation (SpO2) below 90 % in room air (World Health Organization, 2023). Critical patients are distinguished by

one or more severe clinical manifestations that necessitate immediate and comprehensive medical intervention. These include the development of Acute Respiratory Distress Syndrome (ARDS) within a week of a recognized clinical incident such as pneumonia or the emergence of new or exacerbated respiratory symptoms (Gibson *et al.*, 2020). Additionally, critical severity may be evidenced by multi-organ dysfunction or sepsis, which indicates a systemic infection response that extends beyond the respiratory system (Zaim *et al.*, 2020; Li *et al.*, 2020). Another hallmark of critical COVID-19 cases is septic shock, characterized by persistent low blood pressure despite the administration of fluids, requiring the use of vasopressors to maintain a mean arterial pressure (MAP) of at least 65 mmHg and a serum lactate level greater than 2 mmol/L, indicative of severe metabolic distress (Tao Chen, Wu, *et al.*, 2020). Acute thrombosis is a critical marker of severe COVID-19, characterized by conditions such as acute venous thromboembolism, including pulmonary embolism, acute coronary syndrome, and acute stroke (Gu *et al.*, 2021). These manifestations indicate significant vascular complications, highlighting the extensive impact of the virus beyond the respiratory system.

While most children experience mild or asymptomatic forms of COVID-19, a notable condition termed Multisystem Inflammatory Syndrome in Children (MIS-C), emerges in a subset of youth around four up to six weeks following a mild or asymptomatic SARS-CoV-2 infection (Riphagen *et al.*, 2020). MIS-C is characterized by a broad spectrum of symptoms that suggest a systemic cytokine storm, impacting various body systems including gastrointestinal, cardiovascular, hematologic, neurological, and respiratory systems (Whittaker *et al.*, 2020; Ramaswamy *et al.*, 2021). This syndrome often escalates to critical conditions, with up to 80 % of affected children developing distributive/cardiogenic shock, and it carries a mortality rate of 2 % (Feldstein *et al.*, 2020).

The diverse and potentially devastating impact of SARS-CoV-2 across different populations and organ systems, emphasizes the critical need for early identification of patients at risk for severe disease development and comprehensive treatment approaches.

1.3.2 Immunopathology

1.3.2.1 Viral evolution and immune activation

The increasing number of infections enhances the likelihood of the virus mutating, aiming to boost its infectivity and further evade the host immune system (Jiahui Chen, Wang, *et al.*, 2020). Some variants were defined as variants of concern (VOC) due to their potential for increased pathogenesis, immune escape, and the capability to cause more severe disease, thus were encoded by the Greek alphabet (Harvey *et al.*, 2021). Particularly, variants such as Alpha and Delta have shown to possess heightened transmissibility and viral loads, which complicates the task of distinguishing between elevated rates of infection and the intrinsic severity of the disease (Liu and Rocklöv, 2021; P. Wang *et al.*, 2021; Merad *et al.*, 2022).

COVID-19 pathogenesis involves complex interactions between the virus and the host immune response, particularly within the respiratory system, the primary site for SARS-CoV-2 entry and subsequent immunological activation. In the lungs, where gas exchange is vital, SARS-CoV-2 infection triggers an immune response that can vary significantly in intensity (Paludan and Mogensen, 2022). While a balanced immune reaction can control the viral infection with minimal symptoms, an excessive or dysregulated response may lead to severe disease characterized by a "cytokine storm," extensive tissue damage, and impaired oxygen-carbon dioxide exchange (F. Zhou *et al.*, 2020). This inflammatory overdrive is marked by the excessive production of pro-inflammatory cytokines and chemokines, such as Interleukin 6 (IL6), IL8, Tumor necrosis factor α (TNFα), and IL1β, which correlate with disease severity and poor outcomes (Del Valle *et al.*, 2020).

To understand the molecular mechanisms of COVID-19 pathology, various multi-omics studies across tissues have been performed. In mild COVID-19, the pneumocytes and alveolar macrophages detect the viral presence and produce IFNs (Katsura *et al.*, 2020; Yoshida *et al.*, 2022). The macrophages contribute to the generation of an inflammatory environment to limit viral replication, increase antigen presentation in local and invading APCs, attraction of phagocytic cells to clear the virus and dead cells, and an overall activation of the adaptive immune

system (Lee *et al.*, 2009; Iwasaki and Medzhitov, 2015; Barrat *et al.*, 2019; Vanderheiden *et al.*, 2020). Conversely, in the context of severe COVID19, the lung-resident immune cells along with AT2 cells, exhibit a compromised production of IFNs (Blanco-Melo *et al.*, 2020; Hadjadj *et al.*, 2020; Galani *et al.*, 2021). This deficiency, leads to infiltration of plasmacytoid dendritic cells (pDCs) to the lung tissue initiating a delayed production of high levels of IFNs (Yoshida *et al.*, 2022; Venet *et al.*, 2023).

1.3.2.2 Innate immune dysregulation and hyperinflammation

As the disease progresses, there is a notable reduction in alveolar macrophages that are essential for maintaining lung homeostasis. These macrophages are characterized by their anti-inflammatory actions, high phagocytic activity, and antigen-presentation capabilities, which include the expression of *CCL18*, *CCL22*, major histocompatibility complex (MHC) I/II, and *MERTK* genes. (Wauters *et al.*, 2021). The persistent viral replication, coupled with increased levels of pro-inflammatory cytokines, promotes a pronounced dysfunction of endothelial and epithelial cells and extensive apoptosis (Varga *et al.*, 2020; Ackermann *et al.*, 2020; Melms *et al.*, 2021). The impaired endothelial cells cannot support the homeostasis and promote arteriopathy and thrombosis (Gu *et al.*, 2021). This is accompanied by the enhanced recruitment of inflammatory immune cells to the lung, including monocyte-derived macrophages, which excessively secrete pro-inflammatory chemokines and cytokines such as TNFα, IL6, CXCL10, IL8, and IL1β (Liao *et al.*, 2020; Ren *et al.*, 2021). It was previously shown that, in the peripheral blood of critically severe patients the HLA-$DR^{low}S100A^{high}$ monocytes are more abundant, indicating that the myeloid cells invading the lung tissue are already pre-primed in the periphery to express alarmins and pro-inflammatory cytokines, instead of presenting antigens and licensing T cells (Schulte-Schrepping *et al.*, 2020; Gressier *et al.*, 2023).

Neutrophils are recruited to the lung during infection and play a pivotal role in exacerbating inflammation, cell death, and microthrombosis by releasing neutrophil extracellular traps (NETs), reactive oxygen species (ROS), and alarmins (Veras *et al.*, 2020; Middleton *et al.*, 2020). Moreover, neutrophils

secrete S100A8/A9, which act as DAMPs, initiating the TLR4 signaling pathway which promotes immunopathology (Chakraborty *et al.*, 2017; Liting Chen *et al.*, 2020). Evidence from studies show that treatment with paquinimod, which inhibits the S100A8/A9 interaction with TLR4, significantly reduces exaggerated inflammatory responses in human macrophages and reduces fatalities in SARS-CoV-2 infected mice (Tan *et al.*, 2017; Guo *et al.*, 2021; Sahanic *et al.*, 2023; Nakazawa *et al.*, 2023).

The excessive secretion of pro-inflammatory cytokines such as TNFα, IL6, IL1β, and IFNγ activates caspase-8, leading to a type of unspecific programmed cell death known as PANoptosis (Christgen *et al.*, 2020; Karki *et al.*, 2021). This cell death process further releases more DAMPs, which then exacerbate the cytokine storm, amplifying the pro-inflammatory response. Consequently, this cycle of inflammation can result in multisystem immune dysregulation, multiorgan failure, and ultimately, death (Diamond and Kanneganti, 2022).

1.3.2.3 Adaptive immune response and disease severity

The complex interplay between the innate and adaptive immune systems during SARS-CoV-2 infection highlights the necessity of maintaining balance to ensure a coordinated immune response (Du and Yuan, 2020). This equilibrium is essential not only for an efficient clearance of the virus but also for preventing excessive inflammation that can lead to severe pathology (Shen *et al.*, 2023). Central to the adaptive immunity are the T cells, which play a pivotal role in eliminating infected cells, facilitate antibody production and establishing lasting memory against SARS-CoV-2 (Sun *et al.*, 2023). Upon SARS-CoV-2 infection, the adaptive immune system's primary goal is to tailor its response specifically to the invading pathogen (Chaplin, 2010).

CD4+ T cells, also known as helper T cells, are crucial in this process, aiding both CD8+ T cells and B cells (Swain *et al.*, 2012). The T follicular cells (Tfh) activate B cells that present the appropriate antigens on their surface, prompting these B cells to undergo class switching and affinity maturation (Crotty, 2014). For CD8+ T cells, the CD4+ T cells offer support by producing cytokines that enhance the cytotoxic function of CD8+ T cells, co-stimulate CD8+ T cells alongside antigen-

presenting cells (APCs) to ensure their full activation, and help in the formation of memory CD8+ T cells (Laidlaw *et al.*, 2016). The rapid induction of SARS-CoV-2-specific CD4+ T cells is associated with milder disease courses and faster viral clearance (Tan *et al.*, 2021). These specific CD4+ T cells can be detected early in the infection, as soon as 2–4 days post-symptom onset. Conversely, a delayed or absent CD4+ T cell response is correlated with severe disease and even death, underscoring the critical role of timely and effective CD4+ T cell activation on disease resolution (Moderbacher *et al.*, 2020). In the context of SARS-CoV-2 infection, CD4+ T cells predominantly adopt a Th1 phenotype, characterized by the production of pro-inflammatory cytokines such as IFNγ, TNFα, and IL-2 (Sekine *et al.*, 2020; Braun *et al.*, 2020; Peng *et al.*, 2020). Interestingly, some CD4+ T cells exhibit a cytotoxic transcriptional signature, expressing markers such as *CD107a*, *PRF1*, and *GNLY*, which suggests a direct involvement of CD4+ T cells in clearing the virus through cytotoxic activity against infected cells (Meckiff *et al.*, 2020; Peng *et al.*, 2020). The presence and level of activity of these cytotoxic CD4+ T cells can vary among individuals, indicating a degree of variability in the immune response to SARS-CoV-2.

In acute COVID-19 virus specific CD8+ T cells present robust cytotoxic effector functions characterized by the production of IFNγ, granzyme B, perforin, and CD107a (Schulien *et al.*, 2021). In patients with moderate COVID-19, cytotoxic CD8+ T exhibit a transcriptional profile that overlaps with the antiviral CD8+ T cell response, marked by high levels of *IFNG*, *TNFA*, *CCL5*, and *PRF1*, along with *GZMB* and *GZMA*, and the genes for cytotoxic receptors *KLRB1*, *KLRC1*, and *KLRD1* (Chua *et al.*, 2020). Severe COVID-19 cases further distinguish themselves from moderate disease by an increased abundance of naïve CD8+ T cell clusters and a reduced abundance of activated effector T cells (Su *et al.*, 2020). In contrast, cytotoxic CD8+ T cells in individuals with critical COVID-19 show a notable decrease in the levels of *CCL5*, *IFNG*, and *TNFA*, yet paradoxically, they exhibit an enhanced cytotoxic capability, suggesting a complex modulation of CD8+ T lymphocytes function in dependence of disease stage (Chua *et al.*, 2020).

The cytokine storm, alongside active killing of infected cells lead to extensive cell depletion and significant damage that increases the vascular permeability and impairs the humoral metabolism in the lung (Cui *et al.*, 2021; Grant *et al.*, 2021). Consequently this cascade causes fluid accumulation, impaired gas exchange and increased respiratory distress in infected individuals (Fernandes *et al.*, 2019). Hypoxemia emerges as a significant indicator of severe COVID-19 pneumonia, with the potential to progress to ARDS, characterized by alveolar oedema and substantially increasing the risk of respiratory failure (Ferrando *et al.*, 2020).

1.3.3 Long COVID

After the initial infection with SARS-CoV-2, some patients continue to experience persistent symptoms, even after the virus has cleared and regardless of whether their initial COVID-19 infection was mild or asymptomatic (Carfì *et al.*, 2020). These ongoing and relapsing symptoms are recognized as post-acute sequelae of SARS-CoV-2 infection (PASC), commonly referred to as Long COVID (Bowe *et al.*, 2023). According to the WHO Delphi Consensus, Long COVID is defined as a multisystem condition that typically emerges three months after the onset of COVID-19 in individuals with a confirmed past infection (Soriano *et al.*, 2022). The symptoms, lasting at least two months, cannot be attributed to any alternative diagnosis (Altmann *et al.*, 2023). Common manifestations include weakness, shortness of breath, general malaise, headaches, impaired concentration which significantly impact daily activities (Hastie *et al.*, 2022). Symptoms can be newly developed following initial recovery or persist from the original illness and may fluctuate or relapse over time (Fernández-de-Las-Peñas, 2022).

Studies indicate that between 8 % to 17 % of individuals report symptoms of Long COVID at 12 weeks post-infection, and several hypotheses regarding the underlying mechanisms have been proposed (Thompson *et al.*, 2022). One theory suggests the presence of a gastrointestinal viral reservoir, with SARS-CoV-2 detected in stool samples months after the acute infection phase (Y. Wu *et al.*, 2020; Proal and VanElzakker, 2021; Swank *et al.*, 2023). Additionally, reactivation of herpesviruses such as Epstein-Barr virus (EBV) and human

herpesvirus 6 (HHV-6) has been implicated in long COVID (Gold *et al.*, 2021; Zubchenko *et al.*, 2022). Patients with long COVID have shown increased antibody levels against these viruses and antigen compared to those who recovered from COVID-19 without persistent symptoms (Su *et al.*, 2022; Klein *et al.*, 2023). However, it is important to note that while there is a correlation between Long COVID and EBV reactivation, causality has not been established. Other multi-omics studies have identified low serum cortisol levels as a potential biomarker for Long COVID (Su *et al.*, 2022; Klein *et al.*, 2023). Immune dysregulation might drive the pathology in patients with prolonged symptoms. Studies have observed persistent alterations in T cell functions, including an increased number of exhausted T cells, reduced numbers of CD4+ and CD8+ effector memory cells, and elevated PD1 expression on central memory cells, persisting for at least 13 months post-infection in donors who experienced mild acute COVID-19 (Glynne *et al.*, 2022; Davis *et al.*, 2023). Additionally, the neuropathological aspects of Long COVID may involve several potential mechanisms, including neuroinflammation, vascular damage from coagulopathy and endothelial dysfunction, as well as direct neuronal injury (Charfeddine *et al.*, 2021; Proal and VanElzakker, 2021; Haffke *et al.*, 2022; Glynne *et al.*, 2022). These various observations highlight the complexity of Long COVID and underscore the need for continued research into its pathophysiology and treatment.

1.3.4 Adaptive immune response and vaccination

The adaptive immune response to SARS-CoV-2 is highly epitope specific and relies on both the B and T cell immune response against epitopes located within the structural and non-structural viral proteins (Cheng *et al.*, 2021). From convalescent sera the majority of B cell produced antibodies target the S protein, especially the RBD domain, accounting for approximately 90 % of neutralizing activity (Lapuente *et al.*, 2024). Vaccination is a crucial preventive measure in combating various viral infections, offering a primary line of defense by arming the immune system against future attacks. In the specific case of SARS-CoV-2, vaccination plays an essential role by introducing neutralizing antibodies (NAbs)

that actively prevent the virus from binding and infecting cells (Atyeo *et al.*, 2020). Early research in a rhesus macaque model demonstrated that the level of NAbs targeting the S protein was the most reliable indicator of protection (Chandrashekar *et al.*, 2020). As a result, the epitopes against the spike and it's RBD are the primary target of the COVID-19 vaccines (Pinto *et al.*, 2024). Unfortunately, as a result the immune pressure on these sites has driven the viral evolution to escape variants, as for example the Omicron variants carry mutations that escape the pre-existing antibodies against parental strains (Cao *et al.*, 2022).

Vaccines prepare the immune system for potential exposure to the virus, enabling it to quickly recognize and combat the virus upon contact by promoting an early IFN response, thus diminishing the likelihood of severe disease development (Guang Chen, Wu, *et al.*, 2020; Hadjadj *et al.*, 2020; McMahan *et al.*, 2021). Furthermore, non-neutralizing antibodies (non-NAbs) also contribute significantly to protection through mechanisms such as Fc-mediated effector functions, including antibody-dependent phagocytosis, antibody-dependent cellular cytotoxicity, and antibody-dependent natural killer cell activation (Mercado *et al.*, 2020; Atyeo *et al.*, 2020; Rieke *et al.*, 2022).

The T cell response was previously described to be targeted against a broad array of epitopes across spike and other proteins such as NSP7, NSP12 and NSP13 (Tye *et al.*, 2022; Swadling *et al.*, 2022). The breadth of of T cell immunogenicity against SARS-CoV-2 is spread across approximately 30 epitopes and largely is preserved to induce cross-protectivity against multiple strains (Moss, 2022). Additionally, evidence shows that even individuals with compromised B cell response, such as multiple sclerosis patients treated with anti-CD20 monoclonal antibody, after mRNA vaccination against SARS-CoV-2 induce a robust $CD8^+$ T cell response thus likely to offer a protection against the SARS-CoV-2 severe disease (Apostolidis *et al.*, 2021). Indeed, while new variants can evade many neutralizing antibodies, studies show that over 80% of vaccine-induced memory T cell responses still recognize variant epitopes (Wang *et al.*, 2024).

Overall, the immune system's focus on particular viral epitopes (such as the spike RBD) determines the efficacy of protection and memory, and antigenic drift within those epitopes can lead to immune escape, while the broad targeting by T cells provides a resilient layer of defense against evolving SARS-CoV-2 (Moss, 2022; Wang *et al.*, 2024).

As of 2024, six vaccines have been officially authorized by the European Medicines Agency (EMA) for the prevention of COVID-19 and severe disease progression (European Medicines Agency, 2024). These include recombinant protein-based vaccines such as Bimervax (HIPRA Human Health S.L.U) and Nuvaxovid (Novavax CZ), novel mRNA-based vaccines like Spikevax (Moderna) and Comirnaty (BioNTech Manufacturing GmbH), and adenovirus vector-based vaccines such as Jcovden (Janssen-Cilag International NV) and Vaxzevria (AstraZeneca AB). All of the vaccines were designed to induce production of NAbs against the S protein of SARS-CoV-2. Initially, a single dose of the vector-based Jcovden (Sadoff *et al.*, 2021) and two doses of Vaxzevria (Voysey *et al.*, 2021; Hung and Poland, 2021) were reported necessary for primary immunization. However, to enhance and prolong immune protection, a booster dose using an mRNA-based vaccine has been recommended (World Health Organization, 2022). For the mRNA-based vaccines, the typical regimen involves two initial doses spaced four to eight weeks apart, followed by a booster shot six months later (Polack *et al.*, 2020; Jackson *et al.*, 2020; Thomas *et al.*, 2021).

The COVID-19 pandemic caused significant advancements in vaccine research, marked by the deployment of novel technologies that promise utility beyond just infectious diseases (Lorentzen *et al.*, 2022; Deng *et al.*, 2022). The unprecedented speed with which these vaccines were developed and authorized for human use highlights a new era for drug discovery (Sadarangani *et al.*, 2021). As SARS-CoV-2 continues to evolve and establish itself as one of the seasonal viruses, there remains a persistent need to adapt and improve vaccine formulations (Notarte *et al.*, 2022; Khoury *et al.*, 2023).

1.4 Aim of the thesis

These three studies were initiated during the first wave of the COVID-19 pandemic, a period marked by overwhelmed health systems worldwide, a surge in patients requiring medical assistance, and limited knowledge about the novel virus's pathological mechanisms and potential treatment strategies. At a time when every piece of information was critical to addressing the emerging crisis, this research aimed to provide comprehensive insights into the immune responses to SARS-CoV-2 using a multi-omics approach.

The primary aim of the first study is to elucidate the complex immune responses to SARS-CoV-2. Through single-cell RNA sequencing, the study deciphers the immune pathways activated in various immune cells within peripheral blood. This analysis focuses on identifying the specific cell populations and pathways involved in the immune response to SARS-CoV-2. Particular attention is given to the low interferon response, antigen presentation capabilities, and the highly pro-inflammatory state observed in severe COVID-19 patients.

The second study delves into the development of antibodies in response to both SARS-CoV-2 infection and vaccination. By comparing antibody titers produced by individuals under different vaccination regimens, we aim to understand the dynamics of antibody development against the SARS-CoV-2 Spike protein. Given that precise infection-preventing antibody titers are still undetermined, this comparison is crucial for evaluating the efficacy of various vaccination strategies. Cytokine levels are also assessed to evaluate potential inflammatory responses to the vaccines, providing a comprehensive view of the immune response.

In the third study, by employing bulk RNA-Sequencing, the study investigates gene expression profiles in monocytes isolated from patients with varying disease severities. This approach allows for the identification of transcriptomic programming that may contribute to the severity of SARS-CoV-2 infection, highlighting differences between severe and mild cases.

2. Material and methods

2.1 Assessing the immune response in COVID-19 using single cell RNA sequencing

2.1.1 Study design and data source

A total of 139 donors were recruited from the COVIDBB, DISCOVER, DRASTIC, SETREP, and VDBR studies in Melbourne, Australia. From each donor, single-cell RNA sequencing (scRNAseq) and Cellular Indexing of Transcriptomes and Epitopes by Sequencing (CITE-Seq) with 137 markers was conducted using 10x Genomics technology. The data generated were then aligned and demultiplexed by Peter Hickey at the Walter and Eliza Hall Institute of Medical Research. Stefano Mangiola (Walter and Eliza Hall Institute of Medical Research) carried out several preprocessing steps, including empty droplet filtering, doublet filtering, automatic annotation and count scaling. The processed data was subsequently organized into individual files for each donor, categorized by major immune cell type, and supplied as Seurat objects containing both RNA and CITE-Seq (also called ADT) counts, as well as metadata for each donor and sample.

2.1.2 Data preprocessing and background removal

The h5 output files from the *cellranger* pipeline containing all droplets were processed using the *CellBender* package (version 0.2.2) to eliminate background noise (Fleming *et al.*, 2023). The parameters configured for this procedure included setting the expected number of cells to 26,000, including a total of 35,000 droplets, establishing a false positive rate of 0.01, and applying a low count threshold of 150. The model was trained over a period of 200 epochs. Following this cleanup process, the refined counts were added as a new layer to the original Seurat object, added to the pre-existing raw counts prior to background removal.

For investigation of the efficacy of the background removal, the difference in counts pre- and post-correction was calculated using *CellBender_Feature_Diff()* function from the *scCustomize* package (Marsh, 2022). To easy access and

manipulate the data layers within Seurat objects *tidyseurat* package was used (Mangiola, Doyle, *et al.*, 2021).

Each Seurat object, representing different donors for the same cell type, was loaded into R (version 4.3.1) using the Seurat package (version 4.4.4) (Hao *et al.*, 2021). For each donor and cell type, the most variable features were identified, explicitly excluding ribosomal, mitochondrial, TCR, and immunoglobulin genes from consideration. Across all donors for each cell type, an overlap of variable features, termed 'integration features', was established, from which 3,000 were selected for further analysis. These selected features were then utilized as variable features for downstream analysis specific to each cell type.

The individual Seurat objects were merged, *sctransform()* normalized and scaled counts were uniformly rescaled using the same scaling factor through the *PrepSCTfindMarkers()* function (Hafemeister and Satija, 2019). Following this, the rescaled counts of the defined variable features were employed to compute the first 50 principal components (PCs), which are essential for dimensionality reduction and subsequent analysis.

To mitigate the impact of donor variability on cell clustering, which is crucial for accurate subgroup identification, these principal components were then adjusted using the Harmony integration method by sex (Korsunsky *et al.*, 2019). This step ensures that the clustering is more reflective of biological variations rather than inter-donor differences. The Harmony-corrected principal components were subsequently utilized to generate a uniform manifold approximation and projection (UMAP).

To enhance the signal-to-noise ratio when calculating PCs and UMAP from ADT data, variable features have been selectively identified. This was achieved by first calculating the 0.9 quantile of counts for isotype controls to establish a baseline of noise or background expression levels. Subsequently, the same quantile was calculated for all markers in the assay data. Genes were then filtered to retain

only those whose quantile values exceed the highest quantile identified among the isotype controls or specified patterns. This method ensures that the selected genes are those with expressions significantly above the background.

Subsequently, the ADT counts have been normalised using Centered Log-Ratio (CLR) transformation and subsequently scaled (Stoeckius *et al.*, 2017). Utilizing the filtered variable features from the ADT data, the first 50 PCs were calculated. These principal components were integrated using the Harmony algorithm by sample. Using both RNA and ADT data, 'weighted-nearest neighbor' (WNN) analysis was applied to improve clustering resolution.

2.1.3 Clustering and annotation of cell subtypes

To achieve cell clustering that incorporates both RNA and ADT data, WNN analysis was performed. This unsupervised framework assesses the relative importance of each data type for each cell, facilitating an integrative analysis of multiple modalities. Specifically, the WNN was calculated using the first 30 principal components of both RNA and ADT data, which had been previously harmonized. The parameters for this calculation included a k nearest neighbor (k.nn) value of 30, a k.nn range of 350, and a prune.SNN ratio of 1/30.

Following the WNN analysis, a UMAP was generated to visually represent the data. Clustering of cells was performed based on the WNN using the Louvain algorithm with multilevel refinement to optimize community detection (Stuart *et al.*, 2019). To annotate the cell subtypes identified through the Louvain clustering method, differentially expressed genes (DEGs) between the clusters were determined using the Wilcoxon Rank Sum test. This approach helped to pinpoint significant differences in expression levels between the clusters by plotting the expression of top 50-100 most differential genes per cluster, whereas in the thesis for visualization only top 20 are represented. Thus, accurate characterization of each cell subtype based on their unique gene expression profiles was performed.

2.1.4 Compositional analysis

To investigate the differences in cell subpopulation proportions relative to disease severity, a compositional analysis was performed on the annotated cell types using the *sccomp* package (version 1.7.3) (Mangiola *et al.*, 2023). This analysis was specifically focused on samples collected within the first eight days since symptom onset to capture the early immune response dynamics.

The variability in cell composition was analyzed using the *sccomp_estimate()* function, which modeled the cell type composition as a function of several variables including disease severity, sex, study cohort, and intensive care unit (ICU) status. Before modeling, outliers were removed using the *sccomp_remove_outliers()* function to ensure the robustness of the analysis.

Significant differences between groups were tested using the *sccomp_test()* function, with results considered significant if they demonstrated a log2 fold change of at least 0.2 and an False Discovery Rate (FDR) adjusted p-value less than 0.1. The significant findings were visualized using boxplots, where each dot represents the proportion of a specific cell subtype within a donor per cell type, clearly illustrating the variation across individuals and conditions.

2.1.5 Pseudobulk analysis

To perform pseudobulk analysis of the scRNA-seq dataset, RNA counts were aggregated by the *aggregate_cells()* function from the *tidyseurat* package, using sample and manually annotated cell type columns to guide the aggregation. The resulting matrix was then converted into a *SummarizedExperiment* object using the *as_SummarizedExperiment()* function from the *tidybulk* package (version 1.15.6) (Mangiola, Molania, *et al.*, 2021).

Differential gene expression analysis for each cell type was carried out using the *tidybulk* package. The analysis pipeline included filtering, normalizing, and scaling genes using *keep_abundant()* and *scale_abundance()* functions. DE genes were identified with the *test_differential_abundance()* function, employing the "edger_robust_likelihood_ratio" method. A log2 fold change cutoff of at least 0.2 and FDR corrected p-value of at least 0.1 was applied, and the analysis model

included the formula “~ age_scaled + study + sex*severity”. Several contrasts were tested, including complex comparisons of different severity levels:

1. A combined effect of critical, severe, and moderate conditions compared against mild severity.
2. A combined effect of critical and severe conditions compared against a combination of mild and moderate severity.
3. A combined effect of severe, moderate, and mild conditions compared against critical severity.
4. Additional contrasts factored in sex alongside severity conditions.

For biological interpretation of the DE genes, pathway enrichment was performed using the *enrichPathway()* function from the *ReactomePA* package (version 1.46.10).

Expression of selected genes was visualized in boxplots that were prepared using normalized and scaled counts, adjusted for batch effects with *adjust_abundance()* function considering sex as the unwanted variable. The plots were generated using the *ggplot2* package (version 3.4.4).

2.2 Comparative analysis of antibody titers against the spike protein of SARS-CoV-2 variants in infected patient cohorts and diverse vaccination regimes

2.2.1 Study design

This study was performed at the University Hospital Bonn, where all participants were recruited. All participants were confirmed to have SARS-CoV-2 through quantitative real-time reverse transcription polymerase chain reaction (qRT-PCR) or antigen tests using nasopharyngeal swabs, along with assessments of N-protein levels in SARS-CoV-2 and serum anti-N antibody titers. The specific virus strains were not identified. Samples from individuals with mild COVID-19 symptoms were collected between January and March 2020, and from critically ill patients between November 2020 and February 2021, all within North-Rhine-

Westphalia, Germany following the guidelines of the Declaration of Helsinki. The local ethics committee at the University Hospital Bonn (ethics approval number 468/20) approved the collection of blood samples from individuals infected with or recovered from SARS-CoV-2, as well as from healthy volunteers. Detailed clinical, demographic, medical history, comorbidities, and vaccination data were gathered for all subjects.

Participants were designated as having mild COVID-19 if they experienced symptoms like fever, loss of smell and taste, headache, and diarrhea, and recovered at home. To collect samples from these mildly infected individuals at their residences, the study was supported by the Medical Corps of the German Armed Forces, obtaining samples up to six times within the first 21 days of the study enrollment.

Patients diagnosed with acute respiratory distress syndrome (ARDS) due to SARS-CoV-2 and required treatment with invasive mechanical ventilation or extracorporeal membrane oxygenation (ECMO), following the Berlin Definition, were classified as "Critical" and were enrolled into the study upon their ICU admission. These patients had samples collected up to six times in the 21 days after joining the study.

Individuals who had recovered from SARS-CoV-2 infection but were experiencing persisting COVID-19 symptoms for eight weeks to 12 months were identified as "Long COVID" patients. Recruitment for these patients occurred at the Long COVID clinic of the University Hospital Bonn and through Long COVID support groups on social media platforms like Twitter and Facebook in the UK. Symptoms for this group included fatigue, reduced stamina, cognitive issues, headache, postural orthostatic tachycardia syndrome (PoTS), tachycardia, palpitations, chest pain, and difficulty breathing.

Vaccinated participants were monitored at several points before and after receiving their vaccine doses (BNT162b2, Spikevax mRNA-1273, Vaxzevria, or Janssen), with follow-up extending to one year post-initial vaccination. Individuals

without a SARS-CoV-2 infection and no previous COVID-19 history were labeled as "Control" (Ctrl) and had samples collected up to five times over two weeks.

2.2.2 Sample collection and storage

For collecting peripheral blood, 7.5 ml Z-Gel S-Monovettes from Sarstedt (Nümbrecht, Germany) were used. Additionally, 9 ml of blood for flow cytometry analysis was drawn into K3E S-Monovettes (Sarstedt). The serum gel tubes underwent centrifugation at room temperature (RT) for 10 minutes (min) at a force of 2500 × g. After centrifugation, the cell-depleted serum was moved to sterile, barcoded polypropylene tubes from Azenta (Chelmsford, MA, USA) and stored at -80 °C until analysis was required.

2.2.3 Quantification of SARS-CoV-2 N-Protein, α-Spike-Antibodies Titers and Neutralization

Levels of SARS-CoV-2 N-protein in serum were quantified using the S-PLEX SARS-CoV-2 N Kit by Meso Scale Diagnostics, Rockville, MD, USA, following the provided guidelines. Likewise, the levels of α-SARS-CoV-2 IgG antibodies and their ability to neutralize were measured with the SARS-CoV-2 Plate 7 (Meso Scale Diagnostics). The MESO QuickPlex SQ 120 imager was used for capturing immune assay data, which was then processed using the MSD Discovery Workbench software, both provided by Meso Scale Diagnostics.

2.2.4 Quantification of Cytokines and Markers for Neuroinflammation

At selected timepoints during the course of SARS-CoV-2 infection, the presence of pro-inflammatory and anti-inflammatory cytokines in serum was assessed using the Simoa CorPlex Human Cytokine 10-plex Panel 1 assay (Quanterix, Billerica, MA, USA). This assay targeted a range of analytes, including IFNγ, IL1β, IL4, IL5, IL6, IL8, IL10, IL12p70, IL22, and TNFα. Moreover, indicators of neuroinflammation were evaluated with the Simoa Human Neurology 4-Plex E assay (Quanterix), which measured Abeta 40 (Aβ40), Abeta 42 (Aβ42), Glial Fibrillary Acidic Protein (GFAP™), and Neurofilament light (Nf-L). The CorPlex data were collected and analyzed using the SP-X Imaging and Analysis System™

(Quanterix), while the Neurology 4-Plex E data were processed on the Simoa® HD-X Analyzer™ (Quanterix). Both assays were performed in strict accordance with the instructions from the manufacturer.

2.2.5 Quantification of B Cell Subtypes and T Follicular Helper Cells by Flow Cytometry

Blood samples collected in K3-EDTA tubes were centrifuged at 1200 × g for 10 minutes, after which the cell pellet was washed with PBS once and the erythrocytes were lysed using ACK lysis buffer from Thermo Fisher, Waltham, MA, USA, for 5 minutes. The lysis reaction was halted with another PBS wash, and cells were then resuspended in PBS. Each sample, containing up to 2 million viable peripheral blood mononuclear cells (PBMCs), was stained to differentiate between living and dead cells as well as lineage markers using a cocktail of antibodies for 30 minutes at 4 °C: LIVE/DEAD™ Fixable Far Red Dead Cell Stain, FITC-labeled anti-CD45 (HI30), eFluor™ 506-labeled anti-CD19 (HIB19), PerCP-eFluor™ 710-labeled anti-IgD (IA6-2), eFluor™ 450-labeled anti-IgM (SA-DA4), PE-labeled anti-CD38 (HB7), PE-eFluor610-labeled anti-CD27 or Super Bright™-labeled anti-CD24 (eBioSN3), PerCP-labeled anti-CD4 (SK3), PE-Cyanine7-labeled anti-CD25 (CD25-4E3) and Alexa Fluor™ 660-labeled anti-CD127 (eBioRDR5) from Invitrogen, alongside FITC-labeled anti-CD3 (OKT3), Brilliant Violet™ 650-labeled anti-CD4 (RPA-T4), Brilliant Violet™ 421-labeled anti-CXCR5 (J252D4) and FITC-labeled anti-CD3 (OKT3) from Biolegend. Following the surface staining, cells were rinsed and fixed with 4% PFA for 10 minutes at room temperature. Flow cytometry analyses were conducted using an Attune Next Generation (Thermo Fisher) and FlowJo software (version 10.0.7, Tree star).

2.2.6 Software and Tools for Statistical Analysis

R software (version 4.1.2) was utilized for statistical analyses, with the *rstatix* package (version 0.7.0) aiding in these calculations. The *gtsummary* package (version 1.5.2) was used for table creation, while the *ggplot* (version 3.3.5) and *ggpubr* (version 0.4.0) packages were employed for figure generation. The

Kruskal-Wallis and Mann-Whitney U tests determined p values, considering adjusted p values below 0.05 as statistically significant. Any deviations are noted within the figure legends.

2.3 Programming of peripheral classical monocytes during COVID-19

2.3.1 Patient cohort

Blood samples were collected from the same subjects in the critical cohort as well as from the healthy controls and donors with mild infections as described in the previous chapter on days 1, 3, 5, 8, and 15 following their inclusion in the study. These samples were processed within 2 hours of collection to ensure the integrity and reliability of the data.

2.3.2 PBMC isolation

Fresh blood was collected from SARS-CoV-2 infected patients and healthy controls using 9 ml S-Monovette K3 EDTA tubes (Sarstedt). Following collection, the blood was processed for automated PBMC isolation using the RoboSep™ (STEMCELL Technologies, Vancouver, Canada). PBMCs were extracted from 6 ml of blood following the EasySep™ PBMC Isolation Kit (STEMCELL Technologies) protocol.

For accurate quantification of PBMCs, the Tali Image Based Cytometer (Thermo Fisher Scientific, Waltham, MA, United States) was employed alongside Tali Cellular Analysis slides (Thermo Fisher Scientific) to reduce experimenter bias during cell counting. Subsequently, the isolated cells utilized for the negative selection of CD14+ monocytes.

2.3.3 CD14+ monocyte isolation

The isolated PBMCs were centrifuged for 5 minutes at 210 × g, after which the supernatant was removed and the cells were resuspended in 0.5 ml of RoboSep™ Buffer (STEMCELL Technologies). Using the EasySep™ Human Monocyte Isolation Kit (STEMCELL Technologies), CD14+CD16- monocytes were automatically separated from PBMCs through immunomagnetic labeling,

allowing for negative selection. Monocytes were then counted with the Tali Image Based Cytometer (Thermo Fisher Scientific), and 300,000 cells were transferred to a new Eppendorf tube for RNA extraction.

These monocytes were subsequently centrifuged for 5 minutes at 250 × g at 4 °C, the supernatant was discarded, and the cell pellet was resuspended in 350 µl of RA1 lysis buffer from the NucleoSpin Mini kit for RNA Isolation (Macherey-Nagel, Düren, Germany), then stored at -80 °C until further use. Any remaining monocytes underwent another round of centrifugation under the same conditions and were resuspended in 1 ml of freezing medium (10 % DMSO in FBS) for long-term storage at -80 °C.

2.3.4 RNA isolation and quality control

The cells stored in RA1 lysis buffer were thawed on ice, and RNA was subsequently extracted using the NucleoSpin Mini RNA kit (Macherey-Nagel) strictly according to the manufacturer's guidelines without any modifications. To evaluate the RNA quality, we utilized the Agilent High Sensitivity TapeStation (Agilent Technologies, Santa Clara, CA, United States) system with High Sensitivity RNA ScreenTape (Agilent Technologies). Meanwhile, RNA concentration was determined using the Qubit 4 Fluorometer (Thermo Fisher Scientific) and Qubit High Sensitivity Assay Kit (Thermo Fisher Scientific), adhering to the manufacturer's protocols.

2.3.5 RNA sequencing and quality control

The RNA samples were sent to the Next Generation Sequencing Core Facility at the University of Bonn, headed by Dr. rer. nat. André Heimbach, for sequencing. Libraries were prepared according to the QuantSeq 3’-mRNA sequencing protocol from Lexogen Inc by the core facility. Each sample was sequenced to a depth of 15 million reads, using single-end 100 base pair reads. The resulting sequencing counts were provided as FASTQ files.

2.3.6 Data analysis

The reads were initially processed using *Cutadapt* (version 4.1) with the *Trim Galore* wrapper (Krueger, 2015), aimed at reducing low-quality bases and removing sequencing adapters, which are common artifacts in sequencing data. In the first step bases with a quality score below 30 were trimmed off to efficiently eliminate poor-quality segments of the reads. *Cutadapt*, is also designed to allow partial matches between the read and adapter sequences, thus sometimes leading to short, erroneous matches that result in the incorrect trimming of bases. In the second step, to minimize these false trims, the alignment algorithm of *Cutadapt* was adjusted to require a minimum match of five consecutive base pairs.

Following trimming, the quality of the reads was assessed using *FastQC* (version 0.11.9) (Andrews *et al.*, 2012). The trimmed reads were then aligned to the human reference transcriptome (hg38) using the *Salmon* pseudo-aligner (version 1.10.2) (Patro *et al.*, 2017), which includes a built-in decoy for genomic regions to prevent the misalignment of reads to similar genomic sequences. Salmon was configured to run with a minimum score fraction of 0.5 and to perform Gibbs sampling iterations with the *--numGibbsSamples 20* parameter, enhancing the accuracy of transcript quantification.

To consolidate and summarize the statistics from alignment, quality control, and trimming results, *MultiQC* (version 1.13) was utilized to generate a comprehensive HTML report (Ewels *et al.*, 2016). This report provides a unified view of the data, facilitating an efficient analysis of the sequencing workflow's overall performance.

The transcript counts obtained from *Salmon* were subsequently aggregated transcript-level quantifications to gene-level data using *tximport* (version 1.28.0) (Soneson *et al.*, 2015). The transcript annotation to RefSeq was performed using the *tximeta* (version 1.18.3) (Love *et al.*, 2020) and the data matrix was contained in a SummarizedExperiment object (Morgan *et al.*, 2023).

The count data were normalized using the *DESeq2* package (Love *et al.*, 2014), with a filtering criterion set to include only genes that exhibit a maximum expression of at least 100 counts across samples resulting in 10,725 genes further used in the analysis, here also referred to as present genes. Subsequently, a variance stabilizing transformation was applied to these normalized counts to create a matrix with constant variance across a range of mean values.

To explore the relationship between gene expression and the disease severity over time, Weighted Correlation Network Analysis (WGCNA) (Langfelder and Horvath, 2008) was employed on the normalized and transformed counts. This analysis identified Eigengene modules that correlate with specific days of the disease state using the *WGCNA* package (v1.72.5) in R, configured for a signed network. The Module Eigengene Threshold (MEthreshold) was set at 0.28, and the minimum module size was defined as 30. Modules of interest were selected based on a Pearson correlation threshold of at least 0.3 and a p-value of no more than 0.05, ensuring statistical significance in the correlations found. The biological interpretation of the genes from the specific modules was performed with *enrichGO()* from *clusterProfiler* package (version 4.10) (Yu *et al.*, 2012) or *enrichPathway()* from *ReactomePA* package (version 1.46.10) (Yu and He, 2016).

R software (version 4.3.1) was utilized for the usage packages. The *gtsummary* package (version 1.7.2) was used for table creation, while the *ggplot* (version 3.4.4) package were employed for figure generation.

3. Results

The severity of SARS-CoV-2 infection varies widely among individuals, ranging from mild symptoms to critical cases requiring hospitalization, intubation, or leading to multi-organ failure and death. The factors behind these varying outcomes remain poorly understood, emphasizing a gap in our knowledge of the disease progression. This thesis aims to bridge this gap by examining the results of three separate studies investigating immune response to SARS-CoV-2 across

different disease severities and comparing these responses to those in healthy individuals by employing a range of techniques.

3.1 Assessing the immune response in COVID-19 using single cell RNA sequencing

The first cohort analyzed in this study comprises samples collected in Melbourne, Australia, from patients enrolled across several ongoing COVID-19-related clinical studies. Due to the nature of sample acquisition and integration from multiple sources, comprehensive patient metadata was limited. The primary objective of this investigation was to collect a broad and diverse set of samples to enable a robust single-cell RNA sequencing (scRNA-seq) analysis, focusing on maximizing cell numbers across a wide immune landscape.

This section serves a dual purpose. First, to explore immune cell composition and transcriptional states across COVID-19 disease severities. The second, to develop a harmonized immune cell atlas that can support future analyses and translational research. By using multi-modal data, including both transcriptomic and surface marker information, this analysis provides foundational insights into the cellular mechanisms underlying COVID-19 immune responses.

To investigate the programming of immune cells and the shifts within these populations in the periphery, scRNA-seq and cellular indexing of transcriptomes and epitopes by sequencing (CITE-seq) were performed on PBMCs from 139 donors with COVID-19 (Table 1). Donors for this study were recruited from five different sites, encompassing a broad spectrum of COVID-19 disease severity-comprising 39 mild, 36 moderate, 28 severe, and six critical cases-along with 30 individuals serving as healthy controls. The cohort was meticulously selected to ensure age and sex balance across groups. After processing and filtering, the generated dataset comprised a total of 822,221 cells.

		Severity				
Variable	**Overall**, N = 139[1]	**healthy**, N = 30[1]	**mild**, N = 39[1]	**moderate**, N = 36[1]	**severe**, N = 28[1]	**critical**, N = 6[1]
Study						
COVIDBB	58 (42%)	12 (40%)	34 (87%)	7 (19%)	5 (18%)	0 (0%)
DISCOVER	9 (6.5%)	19 (30%)	0 (0%)	0 (0%)	0 (0%)	0 (0%)
DRASTIC	41 (29%)	0 (0%)	5 (13%)	18 (50%)	12 (43%)	6 (100%)
SETREP	22 (16%)	0 (0%)	0 (0%)	11 (31%)	11 (39%)	0 (0%)
VBDR	9 (6.5%)	9 (30%)	0 (0%)	0 (0%)	0 (0%)	0 (0%)
Sex						
female	58 (42%)	12 (40%)	16 (41%)	20 (56%)	7 (25%)	3 (50%)
male	81 (58%)	18 (60%)	23 (59%)	16 (44%)	21 (75%)	3 (50%)
Age	56 (48, 66)	55 (48, 63)	52 (47, 59)	57 (46, 67)	59 (52, 70)	54 (42, 67)

[1] Median (IQR) or Frequency (%)

Table 1: Metadata of the sampled donors. Indicated are the COVID-19 disease severity, study site of recruitment, sex and age of the participants.

3.1.1 Droplet-based single cell experiments are prone to background

To begin the analysis, all cells which passed the QC were initially loaded into a single Seurat object to ensure unified handling of the dataset. After performing normalization and log-transformation, automated annotation tools were used to assign major immune cell identities and generate a consensus annotation across the dataset. Given the large size of the dataset of approximately one million cells, we opted to streamline our analysis by dividing the cell populations according to

major immune cell types (e.g., myeloid cells, $CD4^+$ T cells, $CD8^+$ T cells). This approach not only reduced computational resources and time but also circumvented the need for clustering all cells together and manually annotating them based on differentially expressed markers among identified clusters. Within each of these cell-type-specific objects, dimensionality reduction, dataset integration, and manual annotation of finer immune cell subsets were subsequently performed through clustering.

To annotate cells into major immune cell types, we employed two automated and unbiased cell type identification tools, leveraging three reference transcriptomic datasets for annotation. Specifically, we used the *SingleR* tool, built on the *celldex* Monaco and Blueprint datasets, in conjunction with the *Seurat* package's built-in *Azimuth* tool, to achieve a consensus on unbiased cell annotation. This consensus was established by identifying common annotations across the three

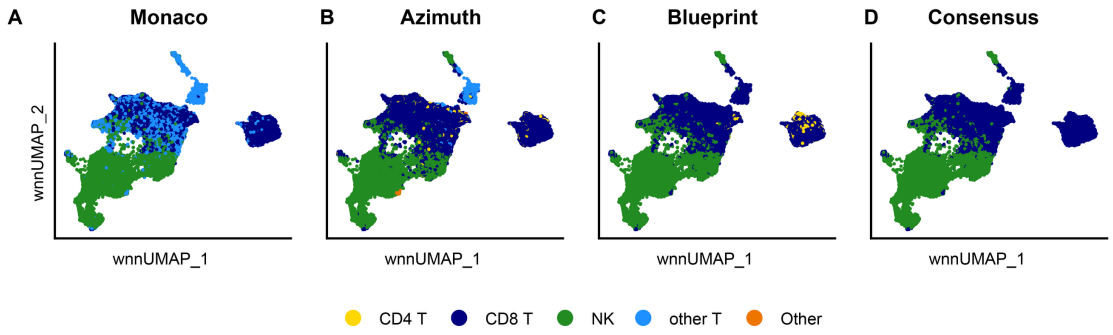

Figure 4: UMAP visualization of clusters identified using automated cell type identification tools (CD8 T and NK cells). Cells were annotated using *SingleR* with *celldex* Monaco **(A)** and Blueprint **(C)** reference databases, alongside *Seurat* built-in *Azimuth* mapping tool **(B)**. A consensus annotation **(D)** was derived from all three databases to consolidate cell identities of CD8 T and NK cells.

datasets. When annotations matched in two datasets, we accepted that consensus; if all three annotations diverged, the cell was excluded from further analysis. Due to the distinct transcriptional profiles characteristic of immune cells, this method yielded accurate annotations for the majority of cells. For instance, as illustrated in Figure 4, this approach was effectively applied to annotate CD8

T and NK cells. These were sub-setted and subsequently re-analysed for presence of subclusters.

The identification of specific cell subpopulations of CD8 T and NK cells, based on their programming or function, involved categorizing the consensus-annotated cells into groups. This categorization was based on their transcriptional profiles using Louvain clustering. First, highly variable features were recalculated, data were normalized and scaled, and principal components (PCs) were computed. Integration was performed across donors, followed by UMAP generation based on integrated PCs. Using both RNA and ADT data, WNN analysis was applied to improve clustering resolution.

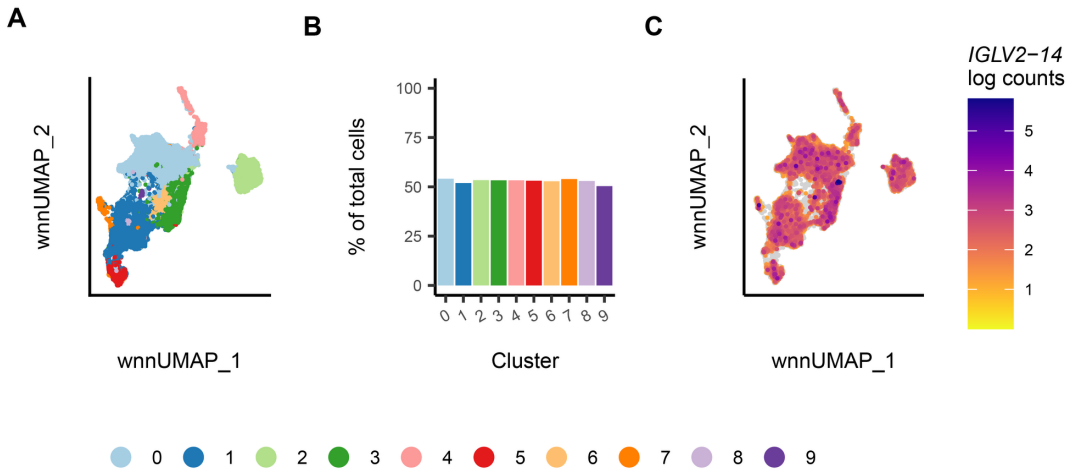

Figure 5: Overview of identified clusters in CD8 T and NK cells and Ig gene expression. The CD8 T and NK cells were selected in a separate dataset and WNN analysis was performed on this subset. The two cell types were clustered to identify groups based on similar gene expression profiles. (A) UMAP representation of grouped cells based on Louvain clustering. (B) Proportion of cells expressing at least one Ig gene. (C) Exemplified expression of *IGLV2-14* across CD8 T and NK cells.

Ten different clusters were identified (Figure 5A). To distinguish between these clusters, we conducted differential gene expression (DGE) analysis, identifying the top 20 most differentially expressed (DE) genes for each cluster. Among the top 20 DE genes across all clusters, 21 immunoglobulin (Ig) genes were

discovered. Notably, approximately 50 % of the cells within these clusters expressed at least one of the DE Ig gene (Figure 5B). Although the expression levels of Ig genes (e.g. *IGLV2-14*) were generally low the expression was not limited to a specific group of cells (Figure 5C).

To determine whether the CD8 T and NK cells were incorrectly annotated by the automated tools or if the observed transcripts represent unspecific counts typically associated with B cells, the expression of the 21 DE Ig genes was plotted

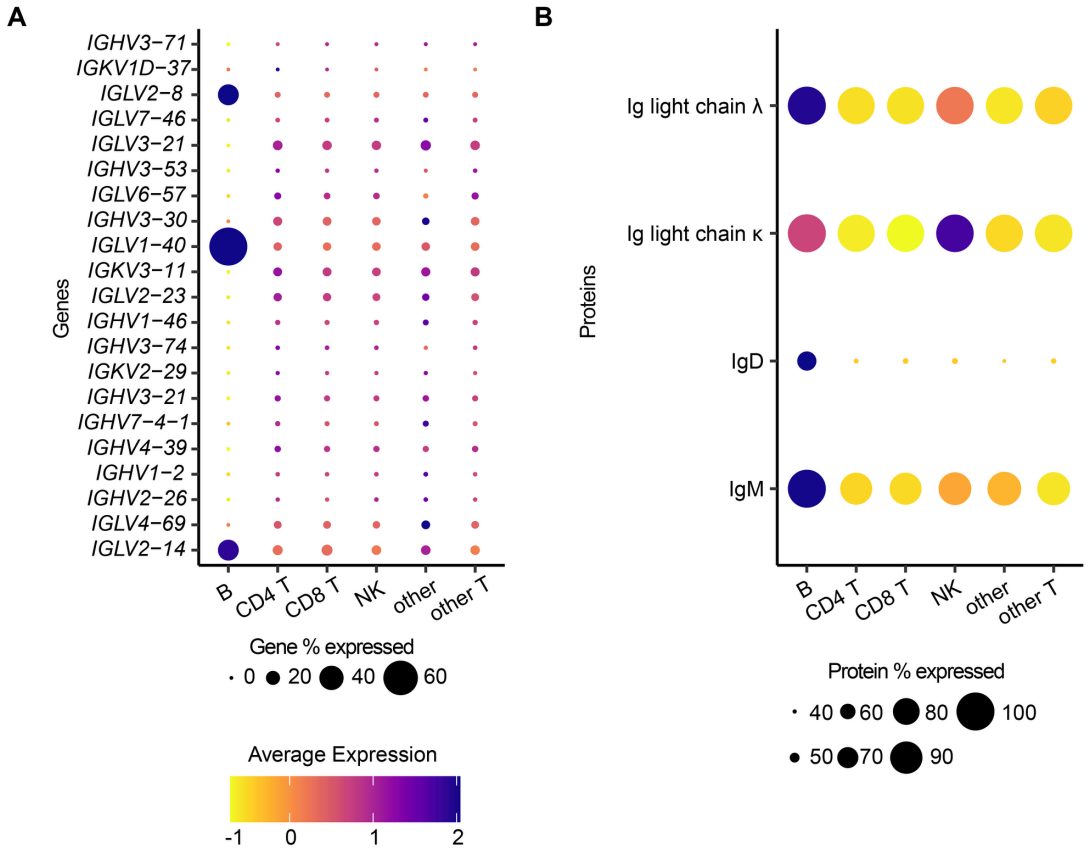

Figure 6: Expression of Ig genes identified as DE across clusters and Ig expression on the surface of CD8 T and NK cells. (A) Expression of all identified DE Ig genes across cells. **(B)** Expression of Ig markers on the surface of the cells. Plotted annotation is the *Azimuth* predicted cell type across the consensus annotated CD8 T and NK cells.

against the cell types predicted by *Azimuth*, alongside B-cell-specific epitopes such as Ig light chains κ and λ, IgD, and IgM (see Figure 6). The Ig transcripts

were found to be uniformly distributed at low levels across all cell types. Notably, markers such as Ig light chains and IgM were present at low levels in about 90% of the cells. This consistent low-level expression of B-cell-associated genes and

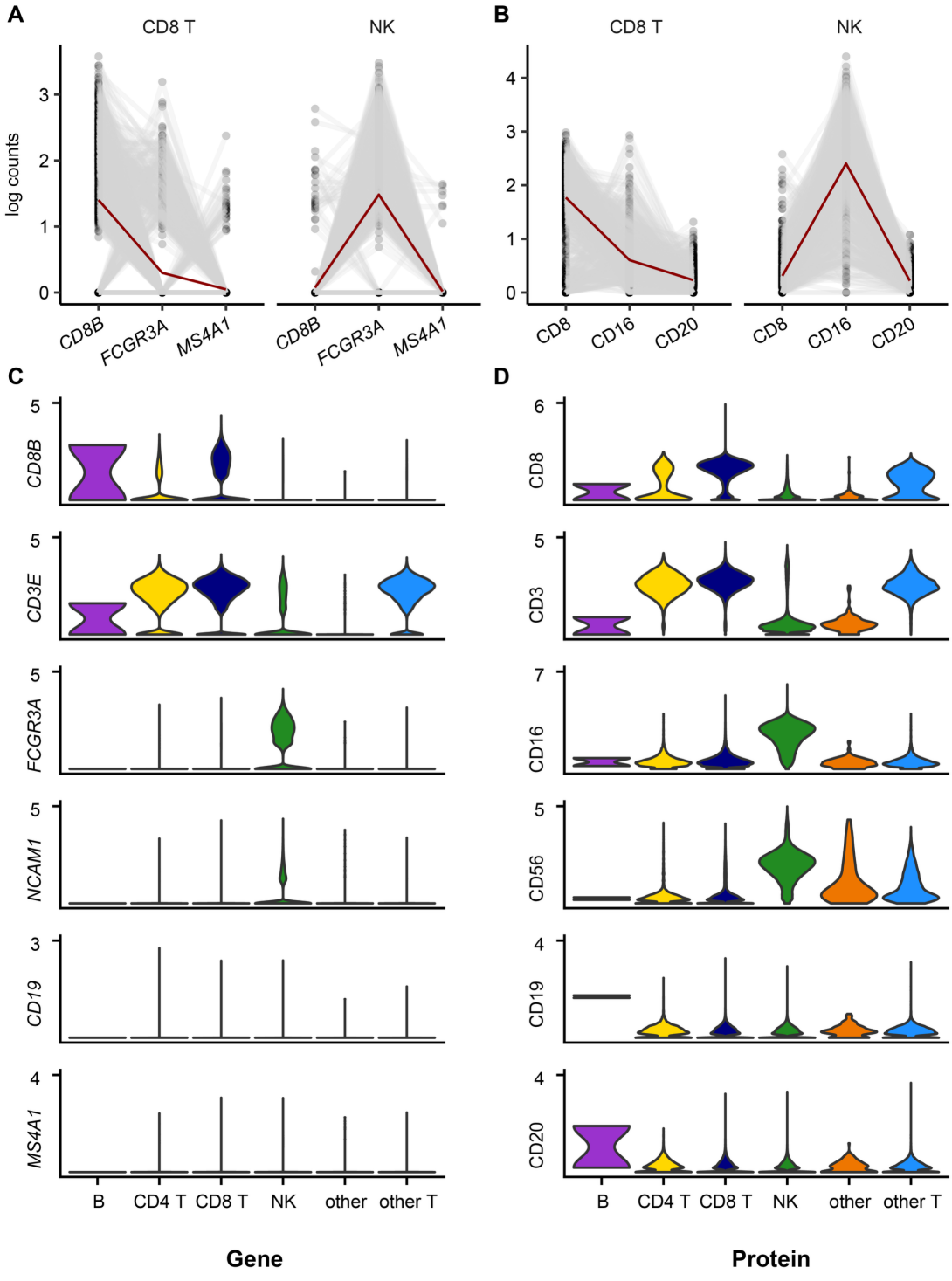

Figure 7: Expression of B, CD8 T and NK cell markers on transcript and protein level in consensus annotated CD8 T and NK cells. Concomitant expression of CD8, CD16 and CD20 genes **(A)** and proteins **(B)** on the surface of 1000 randomly selected CD8 and NK cells. Grey lines interconnect gene expression of the markers within same cell, and the red line depicts the mean expression across cells. Expression of CD8 T cell (*CD3E*, *CD8B*, CD8 and CD3), NK cell (*FCGR3A, NCAM1*, CD16, CD56) and B cell (*CD19, MS4A1*, CD19, CD20) markers on transcript **(C)** and protein **(D)** level across all consensus-annotated CD8 T and NK cells.

proteins across the dataset suggests presence of technical artifacts in the populations of CD8 T and NK cells.

To confirm the accuracy of the consensus annotation, the expression of marker proteins and gene specific to CD8 T, NK and B cells was analysed (Figure 7). A random subset of 1,000 NK and CD8 T cells was selected for this analysis. Concurrent expression of CD8B, FCGR3A, and MS4A1, along with CD8, CD16, and CD20 was assessed, by mapping the connections between marker expressions within the same cell and overlaying the average expression across all selected cells (Figure 7A-B). The findings reveal exclusive expression of cell-type-specific markers, namely CD8B and CD8 for CD8 T cells, and CD16 and FCGR3A for NK cells, without any expression of CD20 or MS4A1. Moreover, B cell markers (CD19, CD20) were not detected at either the transcript or protein level in any of the CD8 T or NK cells from the whole dataset (Figure 7 C-D). These results underscore the precise annotation of cells as either CD8 T cells, characterized by high expression of CD8 and CD3, or NK cells, marked by high expression of CD16 and CD56 at both the gene and protein levels. The absence of B-cell lineage markers, alongside the low expression of Ig genes and pronounced expression of NK and T cell lineage markers, validates the notion of contamination with ambient transcripts from other cell types. A correction of the

ambient noise is critical to improve the cell annotation and DGE analysis accuracy.

3.1.2 *CellBender* accurately evaluates the contamination across cell types and corrects it

Ambient RNA contamination is a recognized challenge in droplet-based scRNA-seq techniques, with several tools available to address this issue. We employed a novel tool, *CellBender*, which utilizes a deep generative model to learn the background noise, thereby enabling a noise-free quantification of transcript counts. Prior to advancing to cell type identification, manual annotation curation, and DGE analysis, the extent of the count correction facilitated by *CellBender* was assessed.

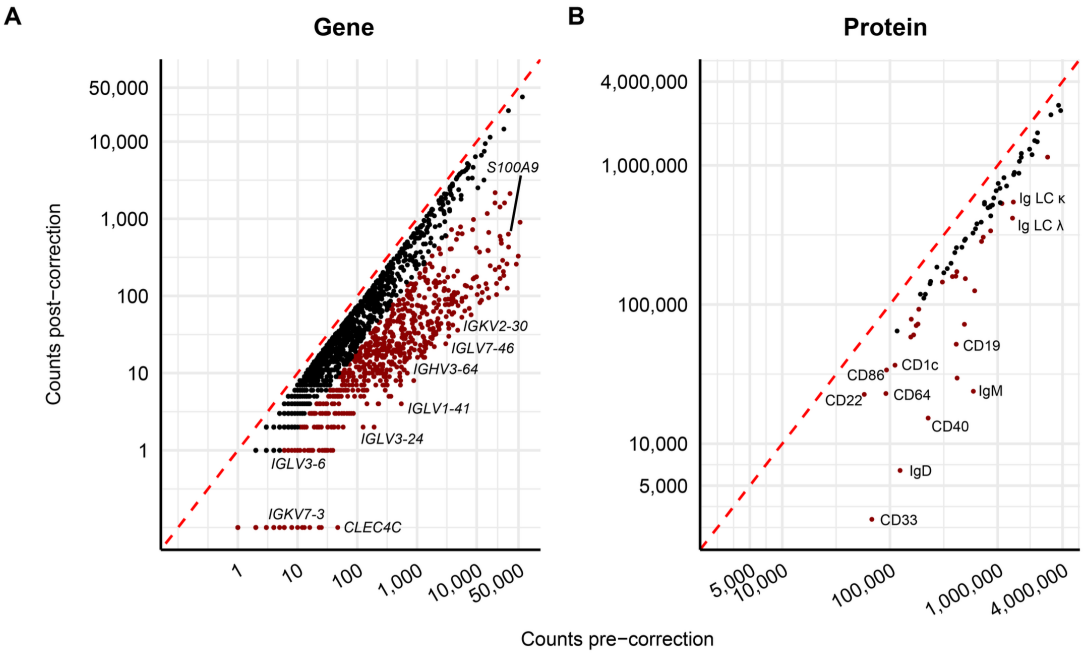

C

Gene	Raw	Corrected	Count Diff.	% Diff.
PTPRC	1.1M	1.1M	3451	0.3
CD3E	0.8M	0.8M	1120	0.1
CD8B	0.4M	0.4M	40	0.0
CD8A	0.5M	0.5M	45	0.0

D

Protein	Raw	Corrected	Count Diff.	% Diff.
CD45	12.3M	11.7M	627K	5.1
CD3	20.0M	19.3M	716K	3.6
CD7	2.8M	2.8M	50K	1.8
CD8	7.5M	7.4M	67K	0.9

Figure 8: Overview of most and least changed genes and proteins after ambient noise decontamination in CD8 T cells. Comparison of genes **(A)** and protein **(B)** expression before and after correction with a change of at least 25 %. Red dots represent transcripts and proteins presenting reductions greater than 80 % and 50 % post-correction, respectively. **(C-D)** Tables indicating initial and corrected counts of transcripts and proteins percentage decrease of marker genes for the CD8 T cell lineage.

For each predicted cell type, the difference in counts before and after correction was analysed, highlighting the genes and proteins that resulted in most and least change. In the case of CD8 T cells, the most changes at the transcript level were observed in Ig genes such as *IGKV7-3, IGLV3-6, IGLV3-24*, etc. The counts of

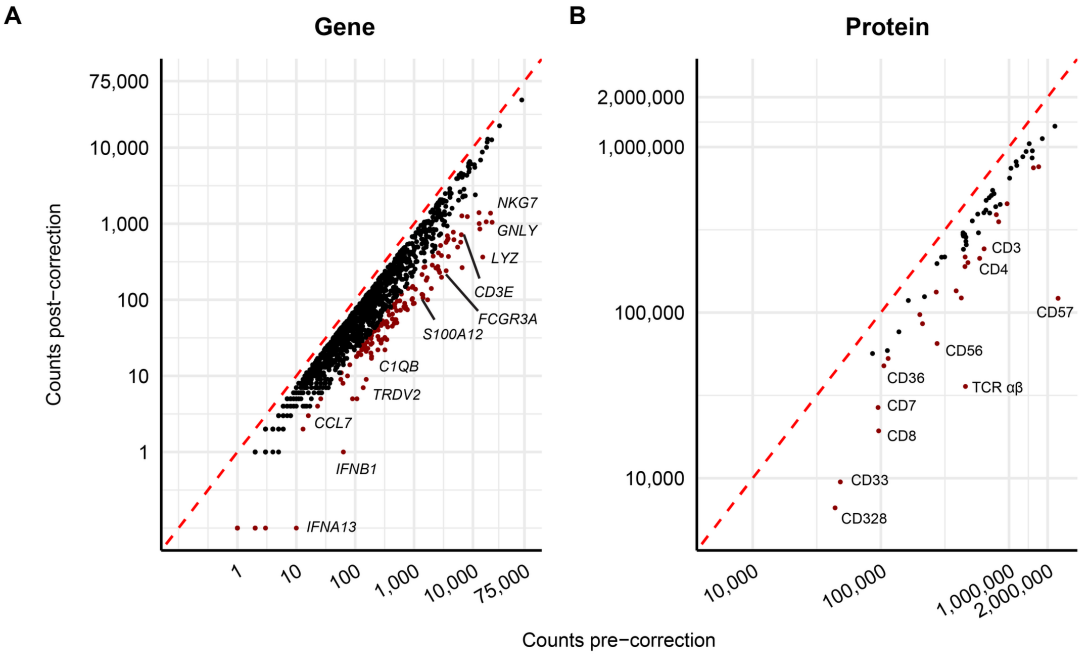

C

Gene	Raw	Corrected	Count Diff.	% Diff.
PTPRC	389.8K	383.7K	6095	1.6
CD79B	172.2K	172.2K	82	0.0
CD79A	624.4K	624.3K	124	0.0
CD19	68.4K	68.4K	11	0.0
MS4A1	452.3K	452.2K	56	0.0
CD22	76.8K	76.8K	8	0.0

D

Protein	Raw	Corrected	Count Diff.	% Diff.
CD79b (Igβ)	4.0M	3.7M	287K	7.1
CD45	6.3M	5.9M	374K	5.9
IgM	10.2M	9.8M	368K	3.6
CD19	16.8M	16.6M	193K	1.1
CD20	9.3M	9.2M	97K	1.1
IgD	4.7M	4.7M	9K	0.2

Figure 9: Overview of most and least changed genes and proteins after ambient noise decontamination in B cells. Comparison of genes **(A)** and protein **(B)** expression before and after correction with a change of at least 25 %. Red dots represent transcripts and proteins presenting reductions greater than 80 % and 50 % post-correction, respectively. **(C-D)** Tables indicating initial and corrected counts of transcripts and proteins percentage decrease of marker genes for the B cell lineage.

Ig genes were dramatically reduced by more than 90 %, dropping from thousands of transcripts to fewer than ten (Figure 8A-B). At the protein level, the most substantial alterations were seen in markers typically associated with B cells (e.g., IgM, IgD, CD19) and myeloid cells (e.g., CD86, CD1c). Conversely, lineage-specific T cell markers, such as CD45 and CD3, exhibited minimal corrections of less than 0.3 % at the gene level and 5.1 % at the protein level, respectively (Figure 8C-D). This precise correction process effectively reduced ambient noise in the CD8 T cells without impacting the expression of lineage markers, thus preserving their utility for subsequent analyses.

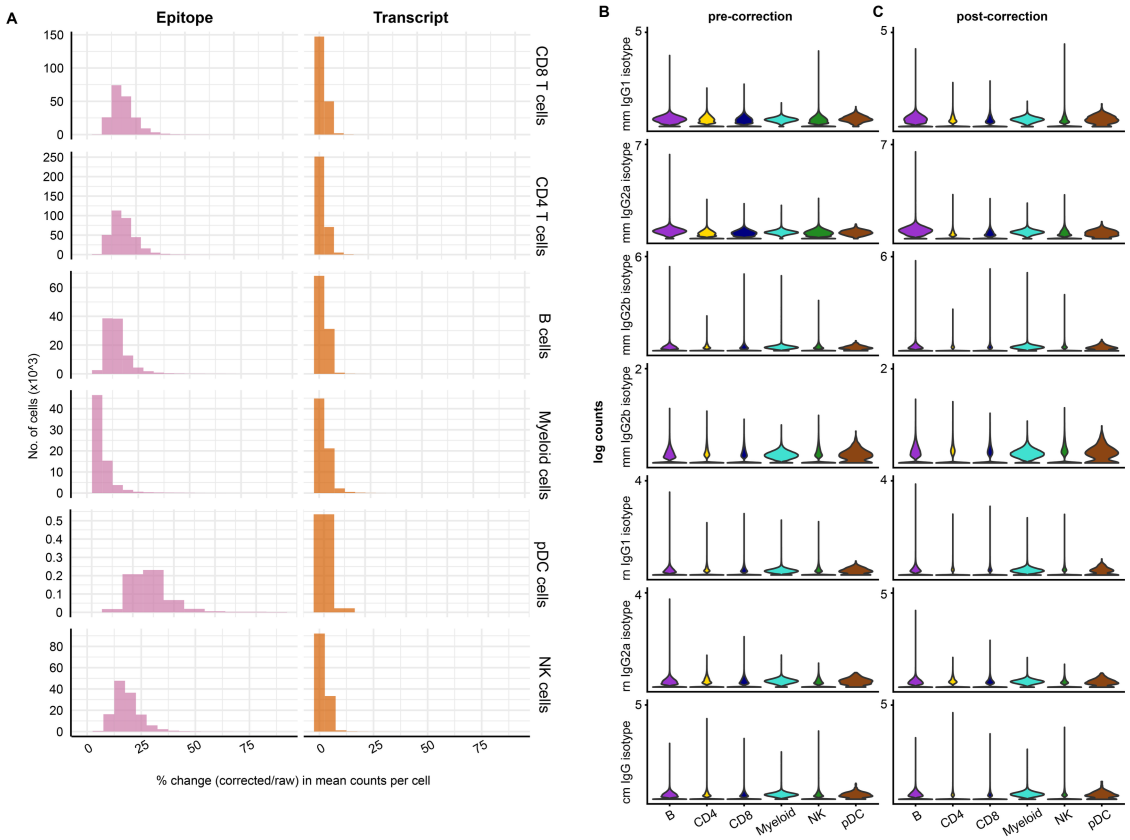

Figure 10: Overview of correction effects across platforms for all cells. (A) Average percentage change in count corrections per cell for both RNA and protein. Counts of isotype control antibodies pre- **(B)** and post-correction **(C)** with *CellBender*. The prefixes before the isotype controls denote the species origin of the antibodies: “mm” - *Mus musculus*, “rn” - *Rattus norvegicus*, and 'cm' - *Cricetulus migratorius.*

A similar pattern was observed in myeloid and NK cells, where Ig gene counts significantly dropped, while core immune cell lineage marker CD45 and specific markers for myeloid (*LYZ*, *CD14, S100A8/9*) and NK cells (*CD56, CD16*) remained unchanged (Supplementary Figure 1). The corrections in B cells was assessed to ensure the changes were cell type-specific and did not result in the unreasonable deletion of Ig genes and B cell markers. In B cells, Ig genes remained largely uncorrected, while lineage markers such as CD79, CD19, and CD20 were only slightly altered-up to 1.6 % at the transcript level and 7.1 % at the protein level (Figure 9C-D). Notably, the most significant changes in B cells involved genes and proteins typically associated with T cells (genes: *CD3E*, *TRDV2* genes; epitopes: CD3, TCR αβ), NK cells (genes: *NKG7* and *GNLY*; epitope: CD56), and myeloid cells (genes: *LYZ* and *S100A12*) (Figure 9A-B).

CITE-seq data is notably susceptible to ambient count contamination, with an average of 15 % of total counts being adjusted post-correction. This number was increased to as much as 50 % in pDCs (Figure 10A). In contrast, transcript-level corrections are more uniform, affecting about 10% of counts across all cell types. To evaluate non-specific antibody binding, isotype controls are incorporated into the experiments. These controls help identify the extent to which specific isotypes contribute to background signal detection. Interestingly, the corrections made to isotype control antibody counts are not as extensive as those for Ig gene counts, with the majority showing no change post-correction (Figure 10B-C). This observation is critical for filtering out weakly expressed epitopes from the analysis. Therefore, before conducting principal component analysis on CITE-seq data, the epitope features were meticulously filtered. The 90th percentile of

counts for epitope features and isotype controls were compared, retaining only those features with expressions surpassing the 90th percentile among the controls. This method effectively eliminates additional noise from the neighborhood calculations and subsequent clustering. Consequently, only ADT signals that are significantly higher than the background noise are included in further analyses, thus increasing the specificity and reliability of the protein expression data.

3.1.3 Myeloid and T cell compartments show significant cell composition changes across severities

To explore variations in immune cell populations and transcriptional changes across different severities of COVID-19, we performed a detailed analysis of major immune cell types. After data correction, we utilized weighted nearest neighbor algorithms, incorporating both RNA and epitope data, to cluster these cells into subgroups. To investigate the cell subtypes the Louvain algorithm clustered the cells into, DGE was performed on all present genes in the dataset without any filtering steps.

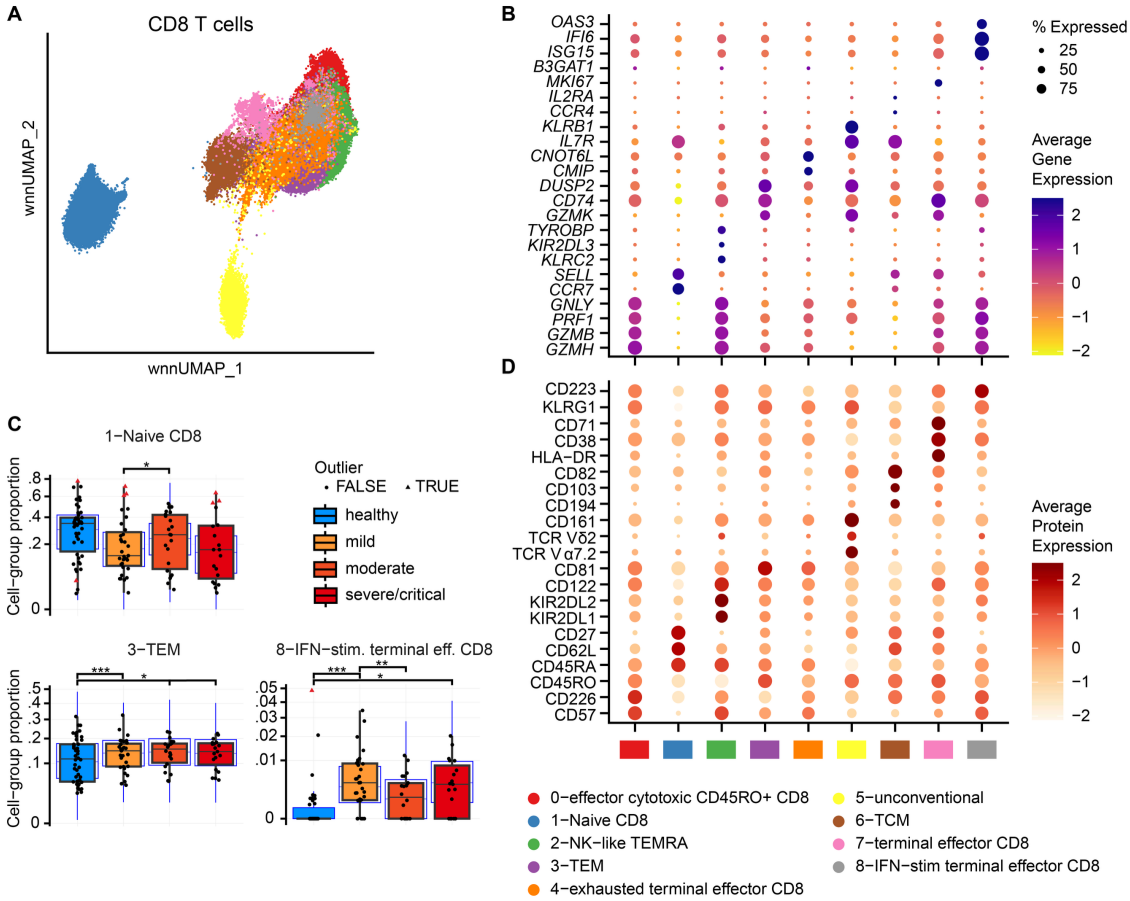

Figure 11: Defined clusters of CD8 T cells and their proportions in different disease severities. (A) UMAP overview of CD8 T cells split into 9 clusters. Expression of markers on gene **(B)** and protein **(D)** level used for annotation of the identified clusters. **(C)** Boxplots indicating significant changes in cell proportions across disease severities within the annotated CD8 T cell clusters. Statistical significance was calculated by *sccomp*. NS, FDR p-value > 0.1; *, FDR p-value < 0.1; **, FDR p-value < 0.05; ***, FDR p-value < 0.01.

CD8 T cells were categorized into nine distinct clusters, with the top 20 differentially expressed genes and proteins identified for each, to investigate their specific functional programming or subtype (Figure 11A-B-D). Cluster 0 is characterized by T cells with high expression of granzymes (*GZMB* and *GZMH*), perforin (*PFR1*), as well as CD226, CD57, and CD45RO proteins, indicating a stage of terminal differentiation, thus this group was designated as “effector cytotoxic CD45+ CD8 T cells.” Cluster 1 includes cells marked by naïve-associated markers *CCR7*, CD45RA, and CD62L on both transcript and protein level, and was therefore labelled “naïve CD8 T cells.” Cluster 2 features a subpopulation that, alongside cytotoxicity and memory CD45RA markers, expresses the killer cell immunoglobulin-like receptor (KIR) at both protein and gene levels, markers typically associated with NK cells. This subgroup was annotated as “NK-like TEMRA.”

Cluster 3 consists of cells expressing CD45RO, lacking CCR7 and *SELL*, and showing partial CD28 expression, classified as T effector memory (TEM). In cluster 4, cells exhibit exhaustion markers such as *CMIP* and *TOX*, alongside a diminished expression of effector molecules, albeit higher than that of naïve T cells, leading to their identification as “exhausted terminal effector CD8.” The unique expression of T cell receptor (TCR) genes in cluster 5, with TCR Vα7.2 indicative of mucosal-associated invariant T (MAIT) cells and TCR Vδ2 specific to γ/δ T cell subsets, marked it as “unconventional.”

Cluster 6, showing expression of *CCR7, SELL, and CCR4* with low cytotoxic gene expression, was identified as having a T central memory (TCM) phenotype.

Cluster 7, denoted as “terminal effector CD8,” expresses cytotoxic markers at levels lower than clusters 0 and 2 but also includes activation markers such as HLA-DR, CD71, and CD38. Finally, cluster 8 is defined by its response to type 1 IFN, crucial during viral infections, expressing genes like *OAS3, IFI6,* and *ISG15* alongside cytotoxic markers, and is annotated as “IFN-stimulated terminal effector CD8.

To investigate shifts in immune cell subpopulations within CD8 T cell clusters, we conducted a compositional analysis (Figure 11C). For enhanced statistical robustness, we combined the severe and critical patient groups. This analysis revealed notable changes in the proportions of naïve CD8 T cells between individuals with mild and moderate COVID-19, with the mild cohort exhibiting a mean proportion of 22 %, in contrast to 26 % in the moderate cohort.

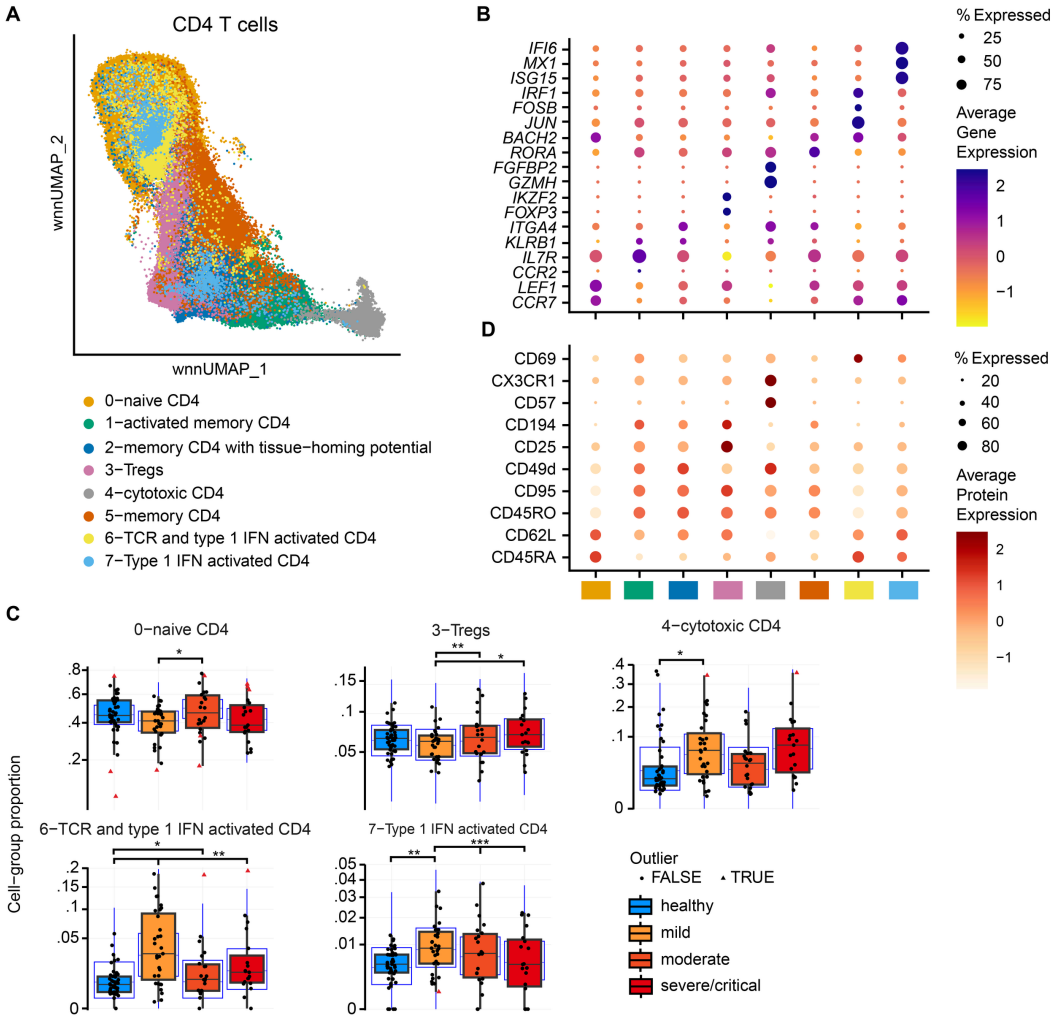

Figure 12: Defined clusters of CD4 T cells and their proportions in different disease severities. (A) UMAP overview of CD4 T cells split into 8 clusters. Expression of markers on gene **(B)** and protein **(D)** level used for annotation of the identified clusters. **(C)** Boxplots indicating significant changes in cell proportions across disease severities within the annotated CD4 T cell clusters. Statistical significance was calculated by *sccomp*. NS, FDR p-value > 0.1; *, FDR p-value < 0.1; **, FDR p-value < 0.05; ***, FDR p-value < 0.01.

Furthermore, healthy individuals demonstrated a lower mean proportion of TEM cells (12 %) compared to all disease-affected cohorts, which showed a consistent mean of approximately 14 %. In addition, both mild and severe/critical patients exhibited higher proportions of IFN-stimulated terminal effector CD8 T cells than seen in healthy controls, with mean proportions of approximately 0.75 % and 0.35 %, respectively. Notably, the mild cohort displayed an increased proportion of this cell type (0.78 %) compared to the moderate disease cohort (0.45 %).

CD4 T cells have been categorized into eight distinct clusters based on their expression profiles (Figure 12A-B-D). Cluster 0 is characterized by the expression of naïve lineage markers *CCR7*, CD62L, and CD45RA, leading to its designation as "naïve CD4." Cluster 1, identified as "activated memory CD4," contains cells that express memory-associated markers CD45RO and *IL7R*, alongside activation markers such as CD95 and CD49d. Cluster 2, termed "memory CD4 with tissue-homing potential," shares a similar marker profile to Cluster 1 but additionally expresses CD62L and *ITGA4*, indicative of cell adhesion and migration capabilities. Cluster 3, comprising cells expressing regulatory T cell markers including CD25, *FOXP3*, and *IKZF2*, thus has been annotated as “Tregs”. Cluster 4 has been labelled as “cytotoxic CD4” as it consists of cells with an enhanced cytotoxic profile, evidenced by markers like *GZMH*, *FGFBP2*, and CD57. The expression of a similar transcriptional profile to clusters 1 and 2 but distinguished by the expression of RORA and absence of activation markers, suggesting a Th17 phenotype of “memory CD4” T cells. Cluster 6 is characterized by its significant expression of transcription factors

IRF1, JUN, and *FOSB*, which are pivotal in the signaling pathways activated by Type 1 IFN response. Additionally, this cluster exhibits upregulation of CD69, a hallmark of immediate early activation, thus identifying these cells as "TCR and Type 1 IFN activated CD4 T cells". Conversely, Cluster 7 is characterized by a distinct transcriptional profile enriched with IFN-stimulated genes, including *IFI6*, *MX1*, and *ISG15*, without concurrent upregulation of TCR engagement-associated genes, marking this subset as "Type 1 IFN activated CD4" T cells.

In the CD4 T cell naïve compartment, a comparative analysis revealed a diminished proportion in mild COVID-19 cases (40.7 %) relative to moderate cases (46.6 %), similar to CD8 T cells (Figure 12C). Moreover, patients with moderate and severe/critical disease exhibited elevated proportions of regulatory T cells (Tregs), accounting for 6.9 % and 7.3 % respectively, in contrast to 5.9 % observed in mild cases. An uptick in the fraction of cytotoxic CD4+ T cells was

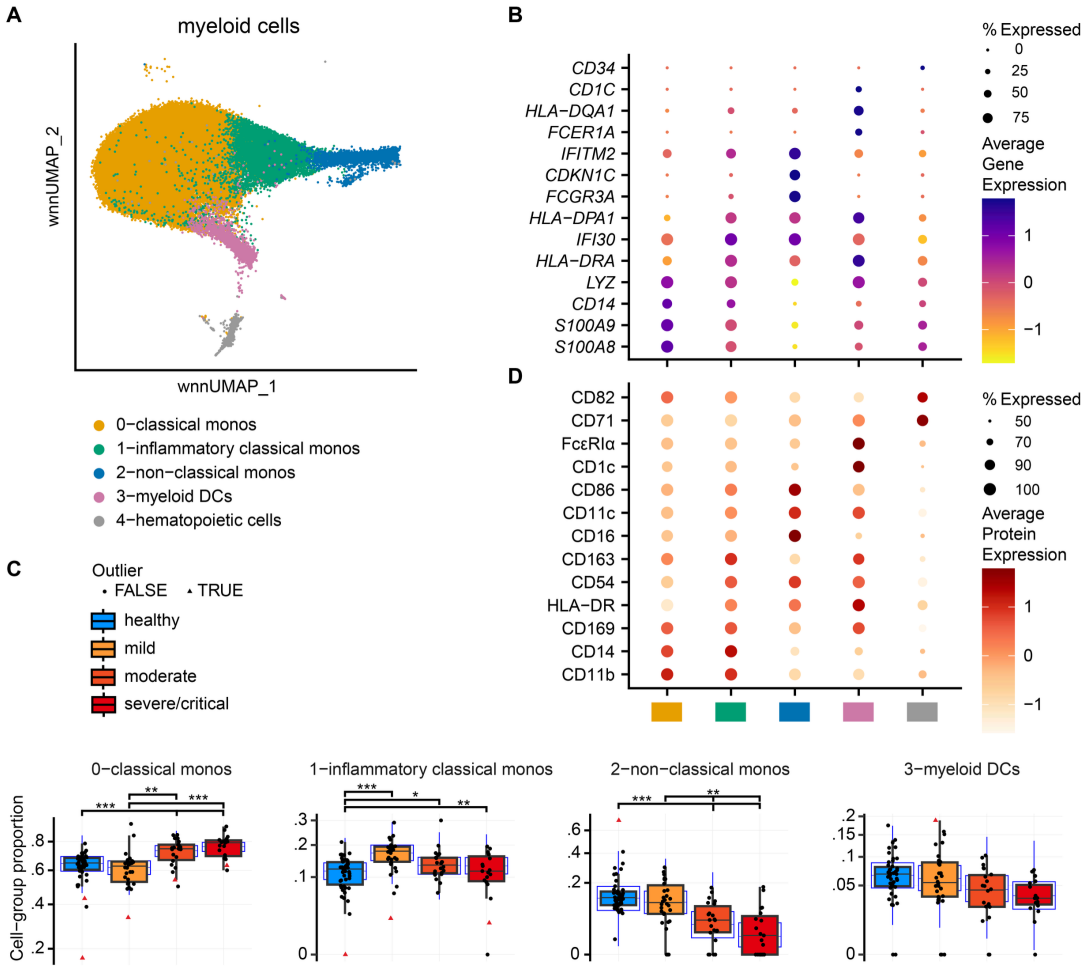

Figure 13: Defined clusters of myeloid cells and their proportions in different disease severities. (A) UMAP overview of myeloid cells split into 5 clusters. Expression of markers on gene **(B)** and protein **(D)** level used for annotation of the identified clusters. **(C)** Boxplots indicating significant changes in cell proportions across disease severities within the annotated myeloid cell clusters. Statistical significance was calculated by *sccomp*. NS, FDR p-value > 0.1; *, FDR p-value < 0.1; **, FDR p-value < 0.05; ***, FDR p-value < 0.01.

noted in mild cases, rising from 4.9 % in healthy individuals to 7.7 %. While a similar increase was noted in the severe/critical cohort, this change did not reach statistical significance. A marked imbalance was noted in the prevalence of TCR and Type 1 IFN activated CD4+ T cells; mild cases demonstrated the highest proportion at 5.1 %, compared to a decreased elevation of 1.4 % in moderate cases and 2.3 % in severe/critical cases, against a baseline of 0.9 % in healthy controls. A parallel trend was observed in Type 1 IFN activated CD4+ T cells, where an augmented proportion was evident in patients across all disease severities compared to healthy controls-1.06 % in mild, 0.97 % in moderate, and 0.95 % in severe/critical cases, relative to 0.57 % in the healthy cohort.

Myeloid cells and DCs play a pivotal role in viral infections by acting as first responders that detect pathogens through pattern recognition receptors and initiate innate immune responses. DCs bridge innate and adaptive immunity by processing and presenting viral antigens to T cells, thereby shaping the quality and magnitude of the antiviral adaptive response. The programming of these cell types was investigated in the context of SARS-CoV-2 severity.

Within the myeloid cell compartment, five distinct clusters were delineated (Figure 13A-B-D). Cluster 0, the largest, consists of classical CD14+ monocytes, characterized by the expression of *LYZ*, *S100A8/9*, and CD11b. Cluster 1 shares a similar profile with cluster 0 but is distinguished by additional markers crucial for responses to infectious diseases, including HLA-DR (noted at both transcript and protein levels), *IFI30*, and CD54. Cluster 2 encompasses non-classical monocytes, marked by CD16 and *CDKN1C* expression alongside inflammatory

markers such as *IFITM2*, CD11c, and CD86. Cluster 3 is identified by its composition of myeloid DCs, expressing CD1c and FCεR1α alongside MHC class II molecules (HLA-DR/DP/DQ), at both protein and transcript levels. Lastly, smallest cluster 4, is recognized as hematopoietic stem and progenitor cells, as indicated by the presence of *CD34*, CD71, and CD82 markers.

Compositionally, an elevated presence of classical monocytes was noted in patients with moderate and severe/critical COVID-19, reaching 73 % and 77 %, respectively, compared to 64 % and 62 % in healthy individuals and mild cases (Figure 13C). Conversely, the fraction of inflammatory classical monocytes surged to 17 % in mild cases, while remaining consistent with healthy control levels at approximately 12 % across moderate, severe, and critical disease cohorts. In the non-classical monocyte subset, a notable reduction was observed among moderate and severe/critical patients, decreasing from approximately 14 % in mild and healthy cohorts to 6.7 % in moderate and 5.1 % in severe/critical cases. The myeloid DC compartment also exhibited a decline from 7 % in mild and healthy groups to 5 % and 3.8 % in moderate and severe/critical patients, respectively, although these differences did not reach statistical significance.

This comprehensive analysis delineates the intricate alterations in immune cell populations across varying severities of COVID-19, by identifying heterogenous populations within major CD8 and CD4 T cell populations, as well as within the myeloid cell compartment. The results underscore the dynamic immune modulation in response to SARS-CoV-2 infection, highlighted by distinct shifts in the prevalence of identified T cell subsets and myeloid cells, particularly noting an increase in classical monocytes and regulatory T cells in more severe cases, alongside modulations in cytotoxic and activated T cell subsets.

3.1.4 Hyperinflammation and Exhaustion of Monocytes and Myeloid Dendritic Cells in Patients with Severe and Critical COVID-19

To investigate the transcriptional landscape of myeloid cells during disease progression, pseudobulk analysis was used to circumvent the limitations commonly encountered in scRNA-seq data. For this data from individual cells

was aggregated on cell type and donor level, significantly enhancing statistical power. By doing so, we aimed to mitigate the impact of dropout events, where the absence of detected gene expression can mask true biological signals. Furthermore, pseudobulk analysis allowed us to tackle the challenge of cellular heterogeneity, providing a more uniform and interpretable dataset to reveal intricate transcriptional variations within myeloid cells in various disease severities to elucidate their roles in disease mechanisms and progression.

DGE analysis of classical monocytes between healthy individuals and mild COVID-19 patients revealed an upregulation of genes linked to the IFN response, including *IFI27*, *IFITM3*, and *OAS2* (Figure 14A). Pathway enrichment analysis confirmed this observation, with the most enriched pathways being “IFN

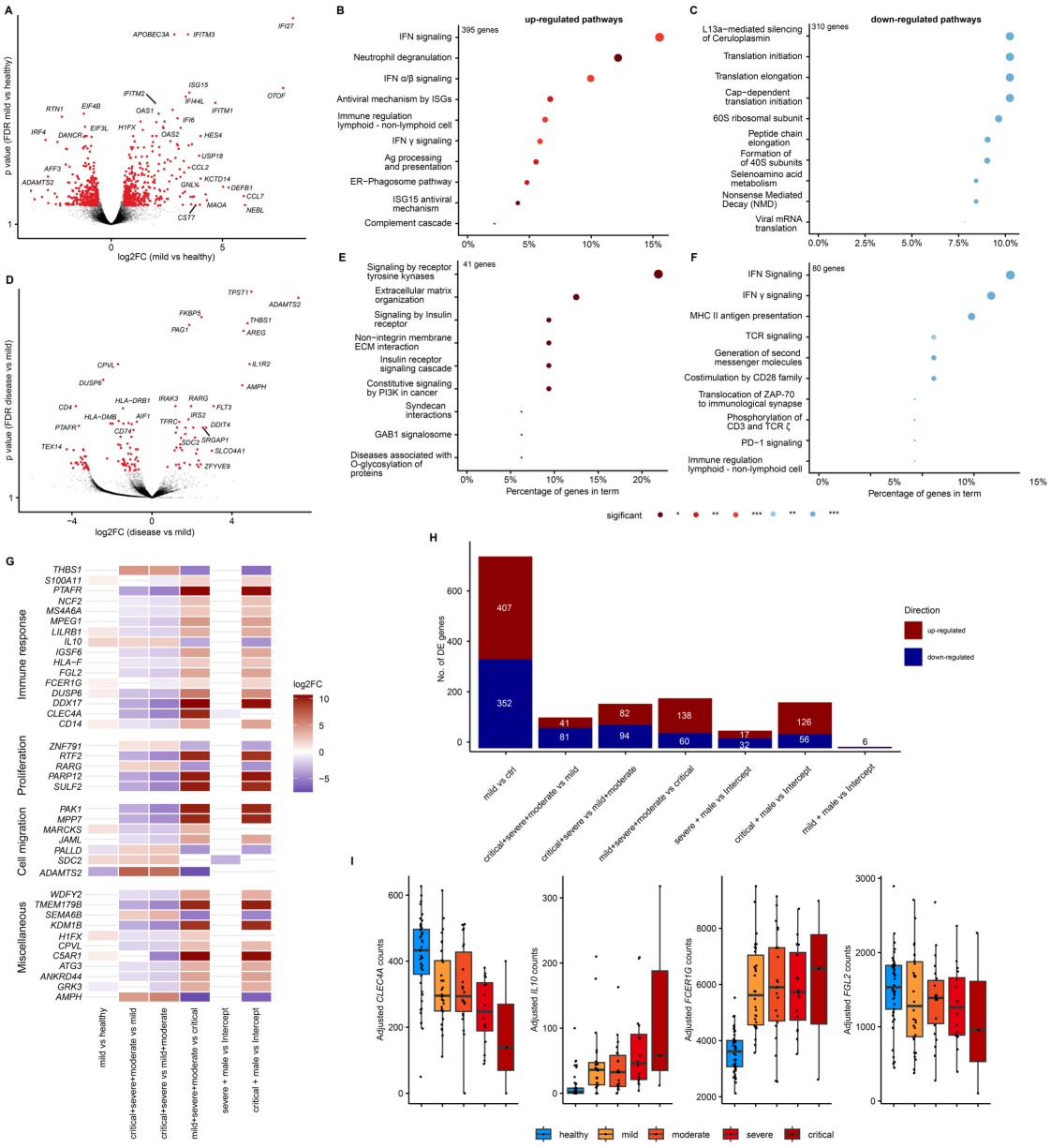

Figure 14: Pseudobulk analysis of classical monocytes across COVID-19 severity levels. (A) Volcano plot displaying significantly upregulated and downregulated genes between mild cases and healthy donors. **(B-C)** Top 10 enriched pathways derived from differentially expressed (DE) genes comparing mild cases to healthy donors. **(D)** Volcano plot highlighting key upregulated and downregulated genes when comparing moderate, severe, and critical cases to mild cases. **(E-F)** Top 10 pathways enriched based on DE genes from comparisons between moderate, severe, and critical cases versus mild cases. **(H)** Overview of the number of DE genes identified across all tested contrasts. **(G)** Heatmap of the log2 fold changes of genes identified as differentially expressed in at least four contrasts, organized by their biological function. **(I)** Boxplots illustrating the expression patterns of selected genes *(CLEC4A, IL10, FCER1G, FGL2*) across different severity levels.

signaling", "antiviral mechanisms by ISGs", and "antigen processing and presentation" (Figure 14B). Conversely, downregulated genes were predominantly associated with transcription and translation processes, such as *IRF4*, *AFF3*, and *EIF4B*, with pathway enrichment highlighting "translation initiation", "peptide chain elongation", and "viral mRNA translation" (Figure 14A,C).

To explore differential expression in more severe disease states relative to mild conditions, a weighted average comparison was employed that integrated the critical, severe, and moderate groups and compared against the mild group. This method allows for a comprehensive analysis that integrates the nuances of disease severity across a spectrum, rather than comparing individual severities in isolation against the mild condition. In more severe COVID-19 cases, a suppression of antigen presentation was noted, evidenced by reduced expression of *HLA-DRB1* and *HLA-DMB*, alongside a diminished expression of genes implicated in the resolution of inflammation, such as *DUSP6*. This analysis also unveiled an upregulation of anti-inflammatory genes associated with the IL-1 receptor, like *IL1R2* and *IRAK3*, and markers of inflammation such as *FKBP5*

(Figure 14D). Enriched pathways in upregulated genes included signaling by receptor tyrosine kinases, extracellular matrix organization, and insulin receptor signaling, whereas downregulated pathways were centered on IFN signaling and MHC class II antigen presentation (Figure 14E-F).

Additionally, a series of weighted comparisons was conducted to dissect transcriptional variations across different COVID-19 severity levels and examine the interplay between disease severity and patient sex (Figure 14H). By

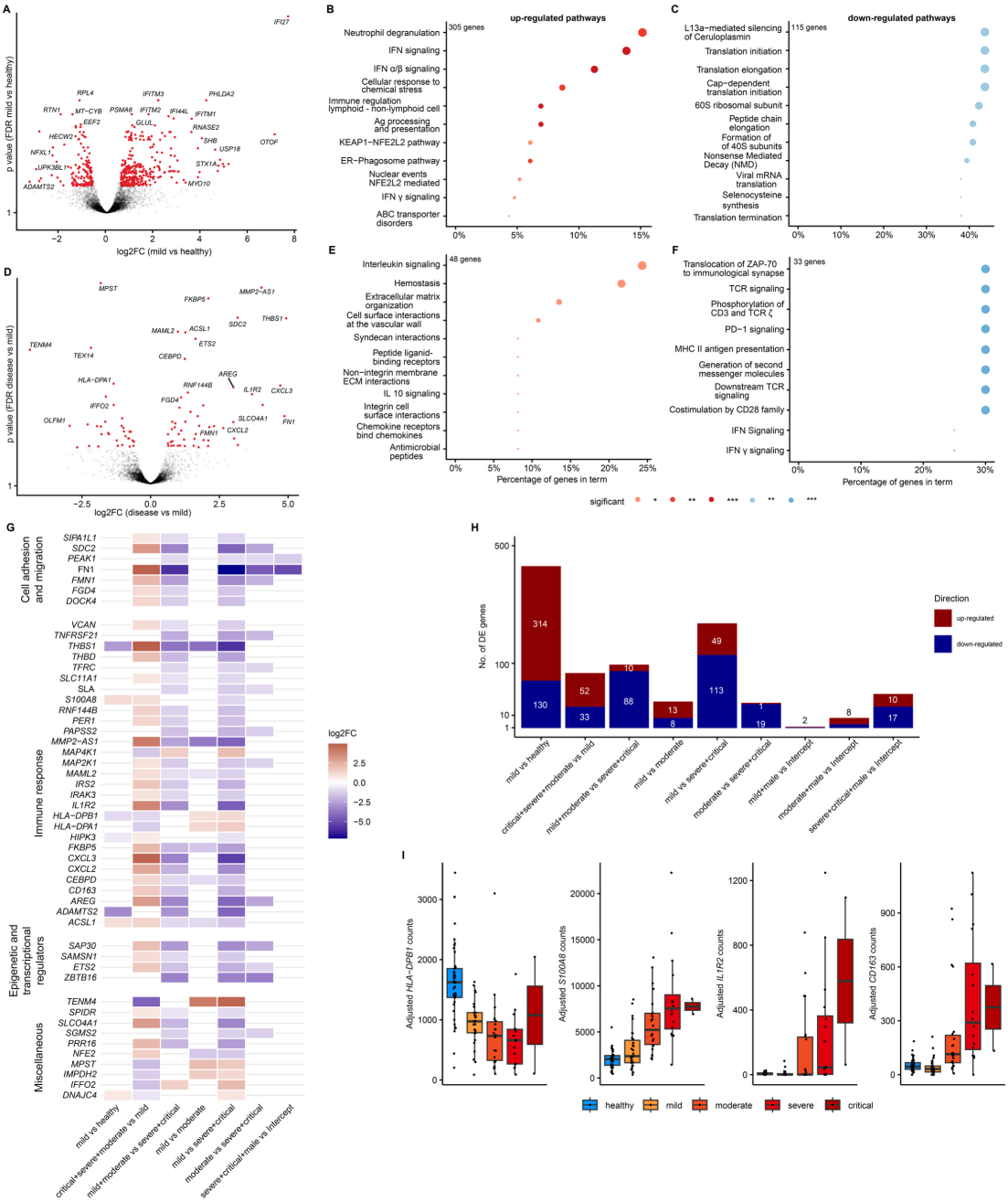

Figure 15: Pseudobulk analysis of inflammatory classical monocytes across COVID-19 severity levels. (A) Volcano plot displaying significantly upregulated and downregulated genes between mild cases and healthy donors. **(B-C)** Top 10 enriched pathways derived from differentially expressed (DE) genes comparing mild cases to healthy donors. **(D)** Volcano plot highlighting key upregulated and downregulated genes when comparing moderate, severe, and critical cases to mild cases. **(E-F)** Top 10 pathways enriched based on DE genes from comparisons between moderate, severe, and critical cases versus mild cases. **(H)** Overview of the number of DE genes identified across all tested contrasts. **(G)** Heatmap of the log2 fold changes of genes identified as differentially expressed in at least four contrasts, organized by their biological function. **(I)** Boxplots illustrating the expression patterns of selected genes *(HLA-DPB1, S100A8, IL1R2, CD163*) across different severity levels.

aggregating gene expression data from various severity conditions, it was sought to identify genes with consistent differential expression patterns across the severity spectrum. These strategic comparisons aimed to delineate biological responses shared among severity groups and evaluate the combined effects of severity and sex on gene expression. The raw counts were aggregated at the donor level. Differential expression testing was performed using a combinatorial design to identify genes associated with COVID-19 severity and by taking into account the age, sex and study influence on the gene expression patterns.

The analysis identified 39 genes overlapping within at least four comparisons, categorized by their biological functions in monocytes into four groups: immune response, proliferation, cell migration, and miscellaneous functions (Figure 14G). Among the immune response genes, we observed an elevation in genes associated with inflammation resolution, such as *IL10*, which progressively increased with severity. Conversely, genes like *CLEC4A* and *FGL2*, which are involved in homeostasis and exhibit anti-inflammatory properties, decreased with severity. Additionally, genes linked to inflammation and cytokine production, such as *FCER1G*, were identified, illustrating the complex interplay of immune

responses in monocytes across different stages of COVID-19 severity (Figure 14I).

In the subset of inflammatory classical monocytes, DGE analysis between healthy individuals and mild COVID-19 patients yielded a gene list characterized by upregulated genes involved in the interferon response and antigen presentation, similar to the previously described cluster, while genes related to translation were found to be downregulated (Figure 15A-C). Conversely, when examining more advanced disease severities compared to mild cases, upregulated genes included chemokines and those involved in chemokine production, such as *CXCL2*, *CXCL3*, and *CEBPD*, as well as anti-inflammatory genes like *IL1R2 (Figure 15D)*. Pathway enrichment analysis of upregulated genes in COVID-19 highlighted “interleukin signaling”, “homeostasis”, and “extracellular matrix (ECM) organization” (Figure 15E). Downregulated genes

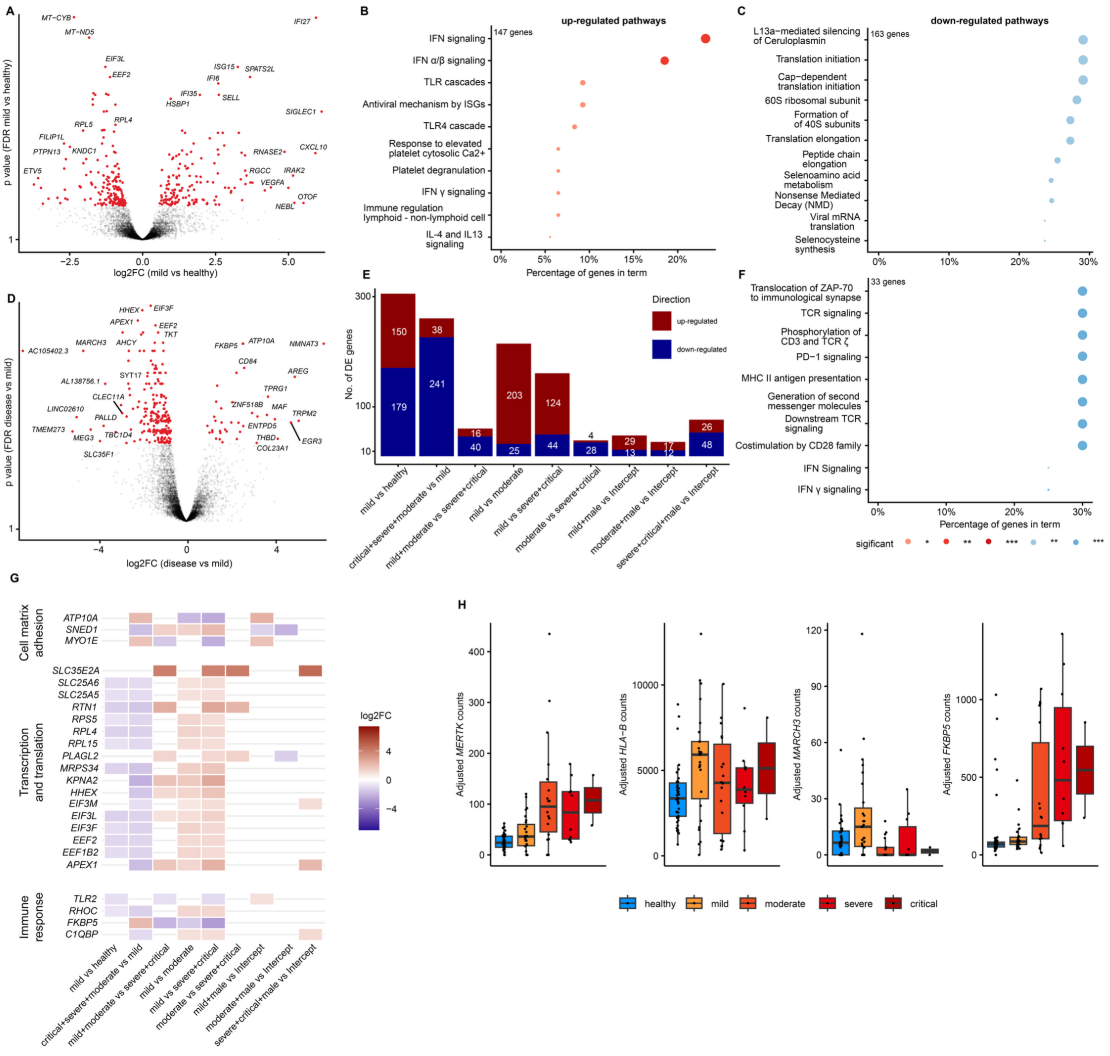

Figure 16: Pseudobulk analysis of non-classical monocytes across COVID-19 severity levels. (A) Volcano plot displaying significantly upregulated and downregulated genes between mild cases and healthy donors. **(B-C)** Top 10 enriched pathways derived from differentially expressed (DE) genes comparing mild cases to healthy donors. **(D)** Volcano plot highlighting key upregulated and downregulated genes when comparing moderate, severe, and critical cases to mild cases. **(F)** Top 10 pathways enriched based on DE genes from comparisons between moderate, severe, and critical cases versus mild cases. **(E)** Overview of the number of DE genes identified across all tested contrasts. **(G)** Heatmap of the log2 fold changes of genes identified as differentially expressed in at least four contrasts, organized by their biological function. **(H)** Boxplots illustrating the expression patterns of selected genes *(MERTK, HLA-B, MARCH3, FKBP5*) across different severity levels.

included *HLA-DPA1* and genes implicated in “cell adhesion and migration”, such as *TENM4* and *OLFM1*, with corresponding pathways showing reductions in “MHC class II antigen presentation” and “interferon signaling” (Figure 15D,F).

Employing a similar methodological approach as described earlier, with a series of comparisons (Figure 15H), 50 genes were identified to be present in at least three contrasts. These were categorized into groups related to immune response, cell adhesion and migration, epigenetic and transcriptional regulation, and miscellaneous functions (Figure 15G). Among the immune response-related genes, those associated with inflammation, such as S100A8, showed increased transcript levels correlating with disease severity (Figure 15I). Conversely, genes related to antigen presentation, including *HLA-DPA1* and *HLA-DPB1*, were diminished in more severe cases. Additionally, genes indicative of an anti-inflammatory phenotype, such as *CD163* and *IL1R2*, were upregulated with increasing disease severity.

These findings suggest that the identified classical and inflammatory classical monocytes, pivotal for mounting an effective immune response against SARS-CoV-2, exhibit reduced antigen presentation capabilities as disease severity

escalates. Simultaneously, there is an enhanced expression of chemokines facilitating the further recruitment of neutrophils and monocytes, alongside a mix of inflammatory and anti-inflammatory genes, indicative of a state of exhaustion within this cell subset.

DGE analysis in the non-classical monocyte subset of myeloid cells comparing healthy individuals to those with mild COVID-19 mirrored the transcriptional response observed in classical monocytes (Figure 16A-C). This included elevated interferon signaling and antigen presentation alongside reduced translation capacity. When examining the gene expression profile contrasting advanced disease states to mild, genes were identified which are implicated in tissue repair, such as *AREG*, and the production of anti-inflammatory cytokines,

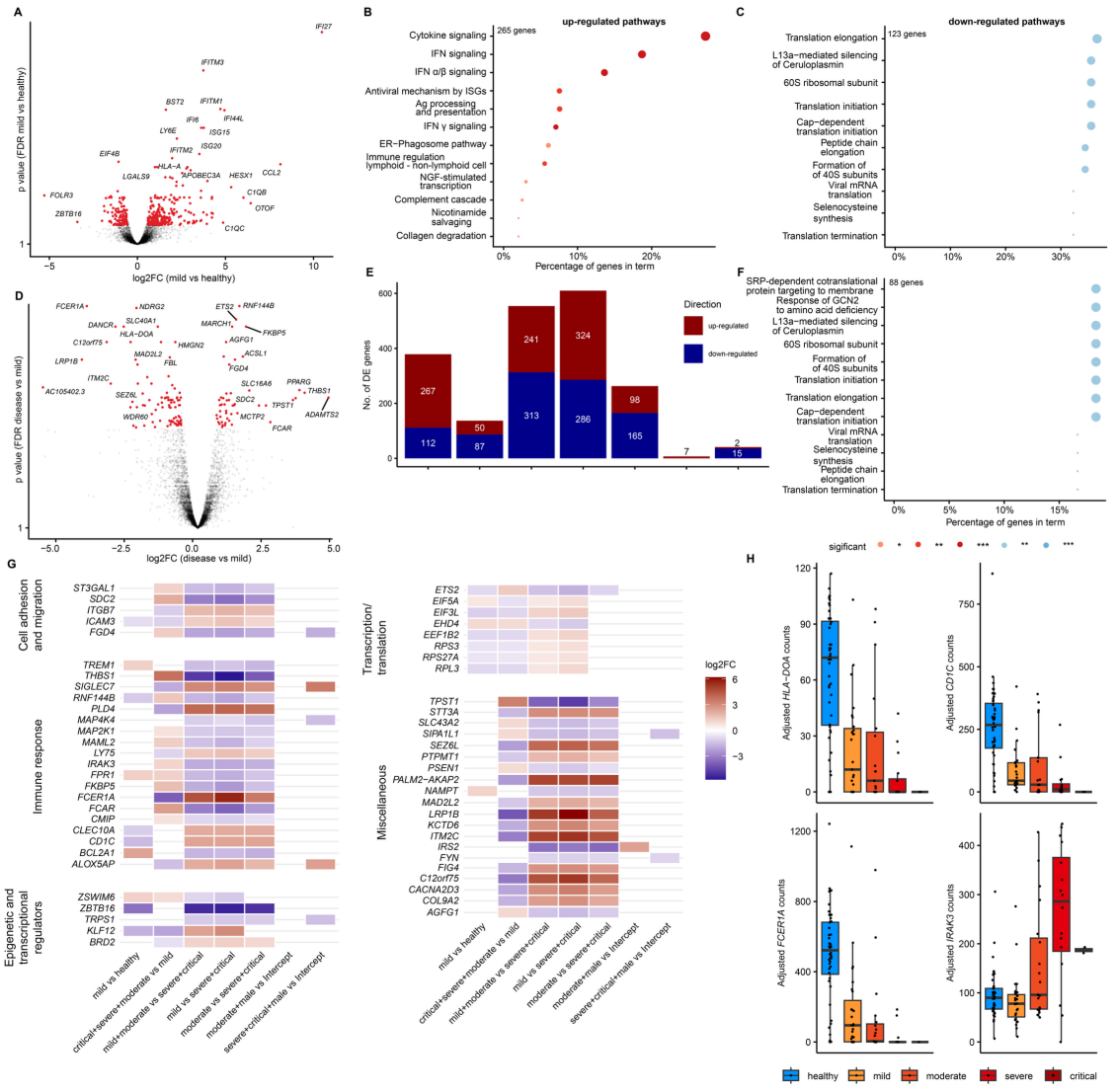

Figure 17: Pseudobulk analysis of myeloid dendritic cells across COVID-19 severity levels. (A) Volcano plot displaying significantly upregulated and downregulated genes between mild cases and healthy donors. **(B-C)** Top 10 enriched pathways derived from differentially expressed (DE) genes comparing mild cases to healthy donors. **(D)** Volcano plot highlighting key upregulated and downregulated genes when comparing moderate, severe, and critical cases to mild cases. **(F)** Top 10 pathways enriched based on DE genes from comparisons between moderate, severe, and critical cases versus mild cases. **(E)** Overview of the number of DE genes identified across all tested contrasts. **(G)** Heatmap of the log2 fold changes of genes identified as differentially expressed in at least four contrasts, organized by their biological function. **(H)** Boxplots illustrating the expression patterns of selected genes *(HLA-DOA, CD1C, FCER1A, IRAK3*) across different severity levels.

notably *MAF (Figure 16D)*. However, with only 38 genes showing significant upregulation, no pathways were markedly enriched.

Analysis of downregulated genes highlighted pathways tied to “MHC class II antigen presentation” and “interferon signaling” (Figure 16F). An extensive comparison across disease severities revealed 21 genes consistently differentially expressed in at least four contrasts, categorized into groups of transcription and translation, cell matrix adhesion, and immune response (Figure 16G). Notably, the majority of these genes are related to ribosomal function and translation factors. Only four genes were directly associated with immune regulation, including *TLR2*, which plays a role in pathogen recognition, and *C1QBP*, involved in the coagulation cascade.

Furthermore, anti-inflammatory markers influencing IL-1 signaling, such as *MARCH3*, and the MHC class I gene *HLA-B* were found to be more prevalent in mild cases compared to more severe disease states (Figure 16H). Conversely, the anti-inflammatory marker *MERTK* and the inflammation-associated *FKBP5* gene exhibited higher expression in severe cases than in mild and healthy groups.

These findings underscore a shared phenotype between non-classical and classical monocytes, characterized by diminished MHC class I/II antigen presentation. The variable regulation of anti-inflammatory markers points towards an exhausted monocyte phenotype within the progression of COVID-19, reflecting a complex interplay of immune responses across different disease severities.

Myeloid DCs exhibited a transcriptional shift from healthy to mild disease conditions reiterated changes observed in other myeloid cell subsets, characterized by an upregulation of IFN signaling, cytokine signaling, and antigen presentation, alongside a suppression of translation processes (Figure 17A-C). In the comparison between complex advanced disease severities and mild cases, genes involved in the ubiquitination of MHC class II molecules, such as *MARCH1*, and markers related to cell adhesion and migration, including *ADAMTS2* and *SDC2*, were upregulated (Figure 17D). However, due to a limited number of DE genes (50 genes), no pathways reached significant enrichment. On the downregulated side, genes that facilitate DC maturation, like *NDRG2*, as well as those involved in antigen presentation and immune response, such as *FCER1A* and *HLA-DOA*, were identified (Figure 17D). These downregulated genes were associated with pathways related to translation (Figure 17F).

Through the series of set contrasts (Figure 17E), 57 genes were identified as differentially expressed in at least four contrasts with a log2 fold change cutoff of ≥ 0.2 and a false discovery rate (FDR)-adjusted p-value threshold of ≤ 0.1 (Figure 17 G). These genes were organized into five categories based on biological function: cell adhesion and migration, immune response, epigenetic and transcriptional regulators, transcription and translation, and miscellaneous. Among these, genes linked to antigen presentation and T cell licensing, such as *HLA-DOA, CD1C*, and *LY75*, were found to be downregulated with increasing disease severity (Figure 17G-H). Conversely, IRAK3, an anti-inflammatory regulator of IL1 receptor signaling, was upregulated in more severe cases (Figure 17H). Additionally, FCER1A, known for its association with anti-inflammatory

properties and inflammation resolution, exhibited decreased expression in more severe disease states.

This analysis highlights a shift towards immature DCs with altered antigen presentation and T cell activation capacity as the COVID-19 disease progresses.

3.2 Comparative analysis of antibody titers against the spike protein of SARS-CoV-2 variants in infected patient cohorts and diverse vaccination regimes

This study presented in this subsection was conducted at the University Hospital of Bonn, where patients and healthy donors were recruited with the goal of capturing a broad representation across different COVID-19 disease severities and immune backgrounds. The inclusion strategy prioritized diversity, aiming to integrate as many distinct patient cohorts as possible to enable meaningful comparisons within and between groups.

The primary objective of this analysis was to assess how antibody titers against the SARS-CoV-2 spike protein vary across these cohorts. Particular emphasis was placed on evaluating how different vaccine formulations induce humoral responses, and how these responses compare to those generated by natural infection. This comparative framework also aimed to reveal the dynamics of antibody waning over time and the immunological benefits of hybrid immunity in convalescent individuals following vaccination.

To explore the nuances of the adaptive immune response across varying disease severities of SARS-CoV-2 infection and their correlation with outcomes, this study delved into the dynamics of α-Spike-Ab titers among SARS-CoV-2-infected patients, encompassing a spectrum of disease outcomes including mild cases, critical illness, recovered, and Long COVID. Additionally, the investigation extended to different vaccination strategies, analyzing both mRNA and vector-based vaccines, over a period of up to one year. Through longitudinal quantification of cytokines, neuroinflammation markers, and B and T cell population phenotypes using flow cytometry, comprehensive insights were

garnered. The findings have been documented in the publication Odainic et al., 2022 and are recapitulated here in chapter 3.2.

3.2.1 α-Spike-Ab titers differ with disease severity of COVID-19 and correlate to elevated numbers of class-switched B and Tfh Cells

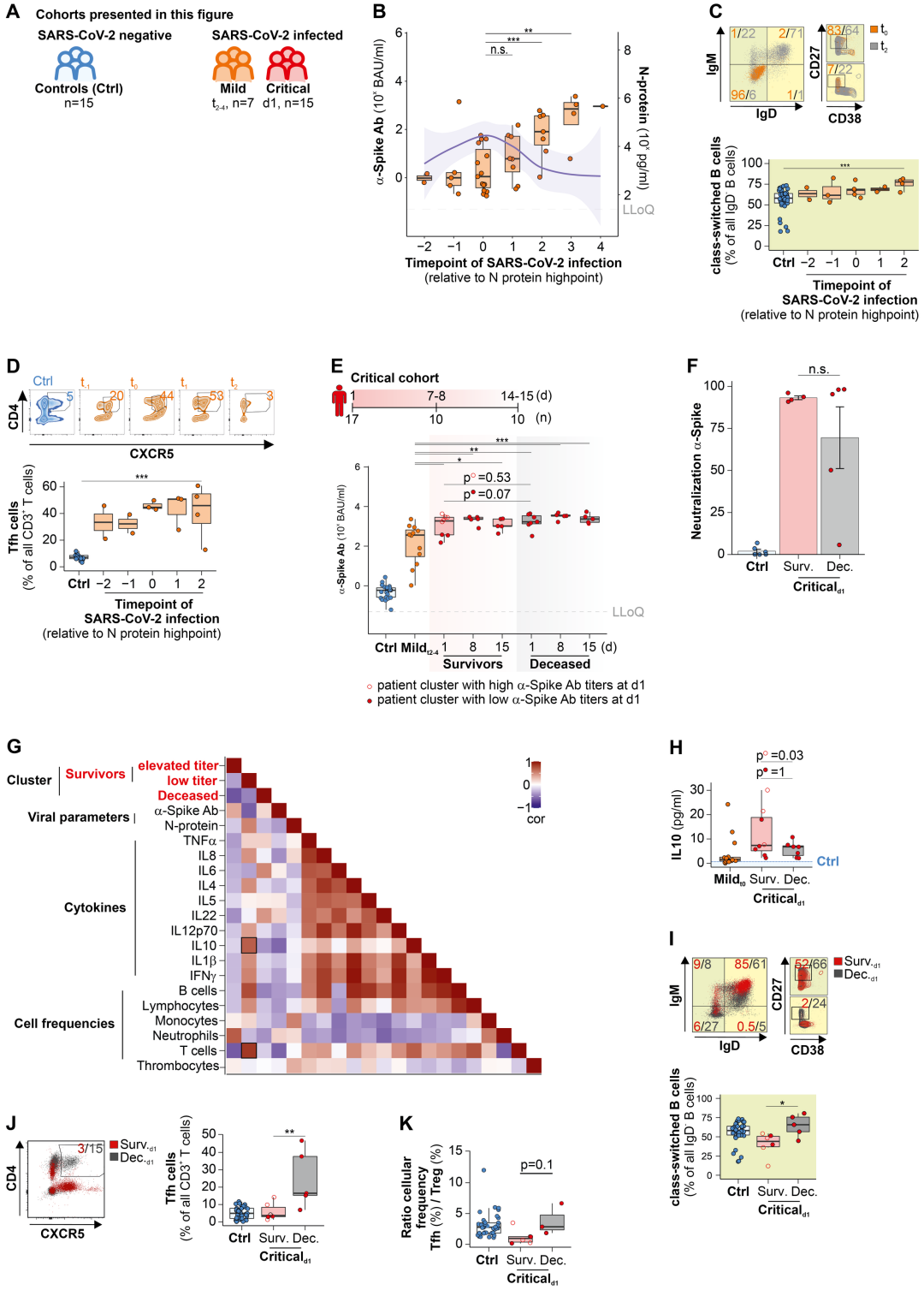

Figure 18: Analysis of Ab titers against the Wuhan SARS-CoV-2 Spike protein across various stages of COVID-19, focusing on the correlation with B and T cell maturation. **(A)** Composition and size of patient cohorts in study. **(B)** Progression of α-Spike-Ab titers in patients with mild COVID-19, aligned to the peak N-protein concentration (t0) in serum, with the shaded area depicting the 95% confidence interval for N-protein levels. **(C)** Representative dot plot (upper panel) and a consolidated box plot (lower panel) illustrating B cell dynamics in patients with a mild course of the disease. **(D)** Contour plots (left panel) and a summarized box plot (right panel) showcasing T follicular helper cell distributions in mildly affected COVID-19 patients. **(E)** α-Spike-Ab levels in sera from critically ill COVID-19 patients, with non-filled points highlighting individuals exhibiting heightened Ab titers. **(F)** Neutralizing capability of antibodies targeting the Spike protein's receptor-binding domain (RBD) between healthy, non-vaccinated controls and critically ill patients. **(G)** Pearson correlation plot for select patient parameters on day 1 of a critical disease phase, with bordered squares indicating statistically significant correlations. **(H)** Boxplot of IL-10 concentrations in the serum of critical patients. **(I)** Contour plots of the critical patient cohort, with non-filled points identifying a subgroup with elevated Ab titers. **(J)** Representative dot plot (left panel) and a quantitative box plot (right panel) for T follicular helper cells in critically ill COVID-19 patients, where non-filled points represent the subgroup with enhanced Ab titers. **(K)** Ratio of T follicular helper cell frequencies to T regulatory cells ($CD3^{+}CD4^{+}CD25^{high}CD127^{-}$), with non-filled points indicating patients with increased Ab titers. "Ctrl" refers to a control group with similar symptoms but negative for SARS-CoV-2. The blue line represents the average concentration in healthy controls; the blue dashed line marks the 95% confidence interval. Lower Level of Quantification (LLoQ) and Mann-Whitney U test results are provided, with unadjusted p-values for panels B, C, E, G, H, I, J; * denotes p value < 0.05, ** denotes p value < 0.01, *** denotes p value < 0.001.

In this study Ab development during the initial phase of SARS-CoV-2 infection

was tracked, monitoring its persistence throughout hospitalization and assessing the longevity of antibody presence for up to 21 days across three distinct cohorts (Figure 18A). The cohorts comprised patients of similar age ranges (average years: Controls = 57, Mild = 54, Critical = 63; Supplementary Figure 2A) and with a comparable prevalence of systemic diseases like hypertension (21-41 %) and diabetes (7–12 %). Notably, the sex distribution was balanced across all groups, with the exception of the critically ill cohort, where males predominated (88 %), a trend identified early in the pandemic's first year.

Focusing on the early infection phase, α-Spike-Ab (specific to the Wuhan variant) development was evaluated in 15 patients with mild COVID-19, who recovered at home without the need for medical intervention. Blood samples were collected on multiple occasions within the first eight days and again on day 15 post-enrollment (Figure 18B). Given the challenge of precisely determining infection onset, we utilized the peak serum level of SARS-CoV-2 Nucleoprotein (N-protein) as a reference point (t0) to standardize the analysis across the cohort. Samples from days preceding and following t0 were labeled accordingly.

We observed α-Spike-Ab concentrations beginning to rise within one to three days post-infection, with a significant increase noted from day seven onwards (t2, Figure 18B). Conversely, N-protein levels decreased, indicative of viral clearance, a phenomenon we have previously documented. Furthermore, we measured α-Spike-Ab titers against the alpha, beta, and gamma SARS-CoV-2 variants (Supplementary Figure 2B, C), noting low titers at t2 (Supplementary Figure 2B). Increased titers of α-Spike-Ab (Wuhan variant) led to noticeable differences in immunity against these variants at subsequent timepoints (t2 and t3, Supplementary Figure 2C). For comparative analysis of antibody responses against various virus strains, we calculated the percentage reduction in antibody concentrations against the alpha (17 %), beta (51 %), and gamma (50 %) variants compared to the Wuhan strain at t2 (Supplementary Figure 2C), facilitating insights into variant-specific immune responses.

To elucidate the roles of B and CD4+ T cells in the humoral response to SARS-CoV-2 infection, we conducted flow cytometry analyses on various B cell subpopulations and Tfh cells within the peripheral blood of study groups. Our findings revealed that, compared to controls, SARS-CoV-2-infected patients exhibited a notable increase in the percentage of pro-B cells at the onset of infection (t0), with mean percentages rising significantly from 33 ± 3 % in controls to 93 ± 1 % in mild cases at t0 (Supplementary Figure 2D). Conversely, the proportion of mature B cells diminished at t0 (from 53 ± 4 % in controls to 3 ± 0 % in mild cases), while immature B cell percentages saw an increase from t0 onwards (from 3 ± 1 % at t0 to 7 ± 2 % at t2 in mild cases).

A significant correlation was observed between the increase in IgD^{-} $CD38^{low}CD27^{+}$ class-switched B cells-from 58 (52–64) % in controls to 78 (73-80) % at t2 in mild cases (Figure 18C)-and elevated α-Spike-Ab concentrations seven days post-infection (t2), suggesting an enhanced humoral response ($p = 0.01$, $r = 0.59$). However, the frequencies of non-class-switched B cells ($IgD^{+}CD38^{low}CD27^{+}$) remained unchanged (median, interquartile range for controls: 10 (6–16) % vs. mild cases at t2: 9 (9–10) %; Supplementary Figure 2E).

Moreover, we observed a substantial increase in the population of $CD4^{+}CXCR5^{+}CD3^{+}$ Tfh cells, which are essential for driving B cell differentiation into antibody-producing plasma cells, in infected patients compared to uninfected controls (median, interquartile range for controls: 7 (6-9) % vs. mild cases from t-2 to t2: 32-51 %; Supplementary Figure 2D). This upsurge underscores the critical engagement of Tfh cells in mounting an effective humoral response during SARS-CoV-2 infection.

The differences in α-Spike-Ab concentrations between mild and critical COVID-19 cases have been explored, assessing their potential to forecast severe disease outcomes. Antibody titers were tracked from ICU admission through to hospital discharge, death, or up to 15 days of hospitalization (Figure 18E). A notable distinction in α-Spike-Ab levels was observed between mildly infected

individuals and critically ill patients who succumbed to the infection (p_{d1} value= 0.005, p_{d8} value = 0.0006, p_{d15} value = 0.001, Figure 18E) as well as those who recovered (p_{d1} value = 0.04, p_{d8} value = 0.004, p_{d15} value = 0.03, Figure 18E). Despite this, the comparison of antibody concentrations between survivors and non-survivors over the study period showed no significant differences (Figure 18E). Similar to mild COVID-19 cases, we noted that antibody titers against the alpha, beta, and gamma variants were lower in critically ill patients compared to those against the original Wuhan strain (Supplementary Figure 2F).

Considering the hypothesis that severe disease outcomes might be associated with low IgG antibody affinity for the Spike protein's RBD, neutralization assays were conducted against the initial strain as well as alpha, beta and gamma variants of concern. These assays measured the competitive interaction between neutralizing antibodies in patient sera and a human ACE2 protein standard for capture SARS-CoV-2 RBD antigens (Figure 18F, Supplementary Figure 2G). Unlike the control group, in which the presence of neutralizing antibodies was minimal (with mean and SEM values for the Wuhan strain at 2 ± 1 %, alpha variant at 3 ± 1 %, beta variant at 3 ± 2 %, and gamma variant at 10 ± 2 %), patients with severe COVID-19 showed detectable levels of neutralizing antibodies. These antibodies had varying effectiveness against the four SARS-CoV-2 variants, as well as between the survivor and deceased patients, yet these differences were found to be not significant (mean and SEM for Wuhan Surv.: 93 ± 1 %, Dec.: 70 ± 18 %; alpha Surv.: 86 ± 3 %, Dec.: 65 ± 18 %; beta Surv.: 45 ± 6 %, Dec.: 36 ± 15 %; gamma Surv.: 59 ± 6 %, Dec.: 47 ± 14 %). Regardless of whether patients survived or died, the antibodies showed the lowest neutralization rates against beta variant among all analyzed strains (Supplementary Figure 2G).

Further analysis identified a split in α-Spike-Ab levels upon ICU admission among survivors, independent of viral load, while all deceased patients consistently showed high α-Spike-Ab levels throughout hospitalization. A Pearson correlation integrating cytokine levels and immune cell frequencies for critically ill patients suggested that lower α-Spike-Ab titers in survivors correlated with deviations in

immune response markers, like elevated IL10 levels and T cell counts (Figures 18G,H).

Without considering specific patient groups, those critically ill COVID-19 patients who survived showed a trend towards higher concentrations of the anti-inflammatory cytokine IL10 (p value = 0.28, Figure 18H). This trend towards elevated IL10 serum levels became statistically significant when survivors were categorized based on their α-Spike-Ab levels, indicating that higher antibody levels were associated with increased IL10 concentrations. In contrast, critically ill patients who succumbed to COVID-19 had a lower count of mature B cells upon their admission to the ICU compared to the control group, but a greater number of pro B cells were observed (mean and SEM for controls: 33 ± 3 %; survivors: 17 ± 3 %; deceased: 58 ± 12 %, as detailed in Supplementary Figure 2I). The proportion of immature B cells in uninfected controls was smaller than in both the deceased and surviving patients, with rates being similar between these last two groups (mean and SEM for controls: 3 ± 0 %; survivors: 15 ± 6 %; deceased: 10 ± 4 %). Notably, patients who died had a higher proportion of class-switched memory B cells than those who recovered from the infection (median, interquartile range for survivors: 44 (37-51) %; deceased: 66 (57-76 %) (Figure 18I). However, no significant variance was detected in the frequency of class-switched memory B cells between survivors with differing levels of α-Spike-Ab (p value = 0.8). Similar trends were noted in the levels of Tfh cells, where survivors showed a median and interquartile range of 4 % (3-10 %), while deceased patients had significantly higher levels at 17 % (15-38 %) (Figure 18J). However, for non-class-switched B cells, both groups had similar proportions, with survivors at a median of 8 % (5-12 %) and deceased patients also at 8 % (4-24 %) (Supplementary Figure 2J). The relationship between the frequencies of Tfh and Treg cells serves as an indicator of an active inflammatory immune reaction and potential autoimmune conditions. In our study, critically ill patients who did not survive exhibited a Tfh/Treg cell ratio that was 3 times higher than that of survivors (Figure 18K), suggesting a complex dysregulated immune response. This dysregulation appeared to occur at multiple levels, including a deficiency in

anti-inflammatory cytokines like IL10 and a disruption in Treg cell function. Despite previous studies linking a low IFNγ to IL10 ratio with viral infections, our analysis showed no significant difference in this ratio between control individuals and critical patients, irrespective of their outcome from SARS-CoV-2 infection. Thus, we determined that using the IFNγ/IL10 ratio as a predictive marker for severe outcomes of SARS-CoV-2 is not effective.

Additionally, this study aimed to understand whether the chronic persistence of a viral reservoir and an ongoing immune response, characterized by continuous antibody production against the Spike protein and cytokine secretion by immune cells, could underlie the pathogenesis of Long COVID. Our Long COVID patient cohort, comprising 20 individuals, experienced persistent symptoms including fatigue, tachycardia or elevated blood pressure ("cardiovascular system"), headaches, and insomnia (Figure 19A, Supplementary Figure 3A, B). These patients, closely age-matched with a control group presenting similar symptoms

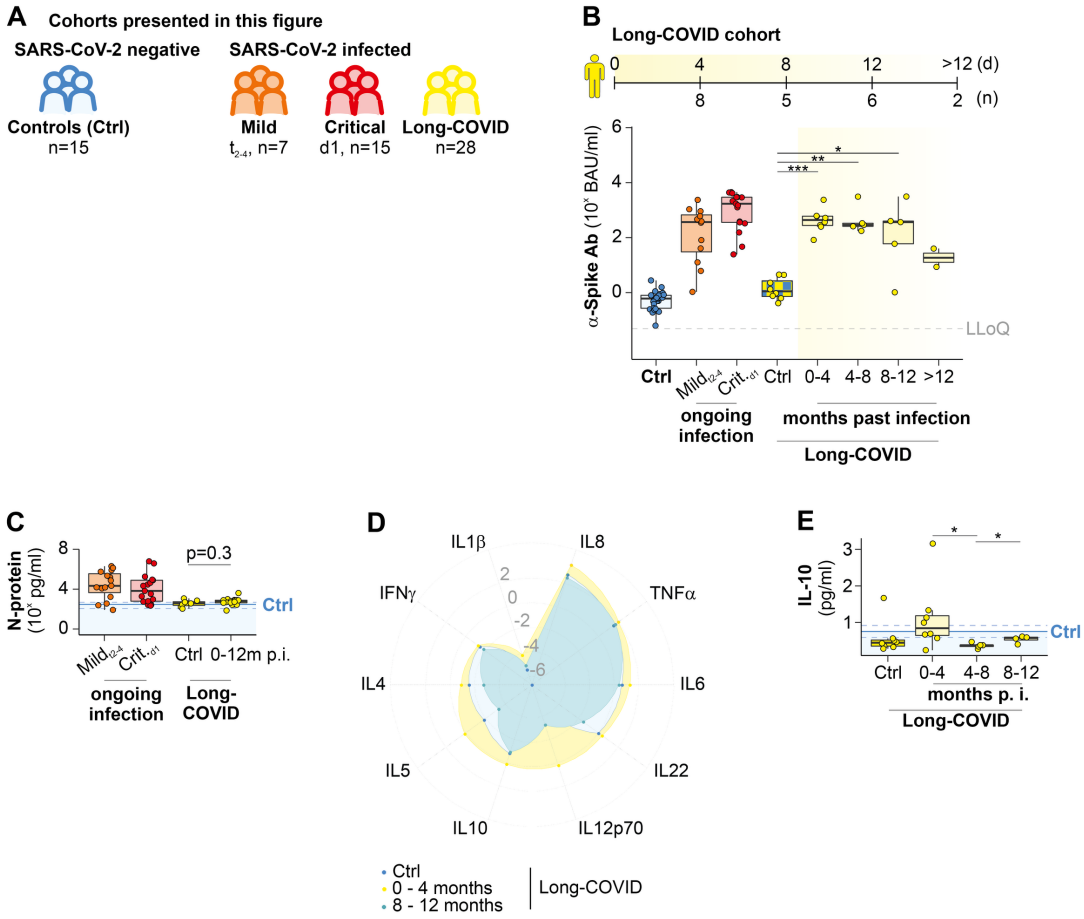

Figure 19: Antibody titers against the Wuhan SARS-CoV-2 Spike protein and cytokine levels in Long COVID patients. (A) Patient cohorts analyzed in the study. **(B)** Comparative analysis of α-Spike-Ab titers in Long COVID participants across different post-infection timepoints, alongside data from healthy controls, and patients with mild and critical COVID-19 disease courses, as well as Long COVID control subjects. **(C)** N-protein levels, **(D)** a radar plot of normalized cytokine titers, and IL10 concentrations **(E)** in LC and LC Ctrl patients. "Ctrl" represents a control group exhibiting similar symptoms but which never experienced SARS-CoV-2 infection. The mean concentration in healthy controls is depicted by a blue line, with the 95% confidence interval shown by a blue dashed line. The Lower Level of Quantification (LLoQ) and Mann-Whitney U test results are provided, with significance levels marked as * p value < 0.05, ** p value < 0.01, *** p value < 0.001.

(LC control, mean years: 40; Long COVID, mean years = 39; Supplementary Figure 3A, B), exhibited sustained elevated antibody (Ab) titers against various SARS-CoV-2 variants for up to eight months post-infection, which then declined over a 12-month observation period (Figure 19B, Supplementary Figure 3C). Conversely, α-Spike-Ab levels in the control group were significantly lower (392-fold reduction) compared to the initial four months in Long COVID patients (median, interquartile range for LC controls: 1 (1-39) BAU/ml; Long COVID0-4 months: 444 (278-600) BAU/ml), aligning with the antibody titers seen in healthy, age-matched controls (median, interquartile range for Ctrl: 1 (0-1) BAU/ml) and confirming the absence of previous SARS-CoV-2 infection in the LC control group (Figure 19B).

Despite these elevated α-Spike-Ab titers, no SARS-CoV-2 N-protein was detected in Long COVID patients (means for Long COVID0-12 months: 594 pg/ml; LC control: 477 pg/ml), differing markedly from acutely infected individuals (means for $Mild_{t2\text{-}4}$: 1072 pg/ml; $Critical_{d1}$: 6927 pg/ml; Figure 19C). Serum samples were analyzed for classical inflammatory and anti-inflammatory cytokines as indicators of a prolonged immune response. An initial four-month

period post-infection showed a slight increase in cytokine levels such as IL8, TNFα, IL6, IL12p70, IL10, IL5, and IL4 (Figure 19D), with IL12p70 significantly elevated in Long COVID patient (means for LC control: 0.00 pg/ml; Long $COVID_{0-4}$ months: 0.13 pg/ml; Supplementary Figure 3D). Notably, IL10 levels were significantly higher in the four to eight-month period post-infection (means for Long $COVID_{0-4}$ months: 0.84 pg/ml; Long $COVID_{4-8}$ months: 0.38 pg/ml; Figure 19E). Additionally, serum markers of neuroinflammation and degeneration were assessed, revealing no significant differences in Aβ40, Aβ42, GFAP, and NF-light concentrations between Long COVID patients and controls (Supplementary Figure 3E), indicating that neuroinflammation could not be directly linked to Long COVID symptoms.

Our findings reveal an increase in class-switched memory B cells and α-Spike-Ab titers starting from the seventh day post-infection. Patients across the disease spectrum-those with mild symptoms, those critically ill, and individuals with Long COVID-exhibited similar α-Spike-Ab levels. Notably, both survivors of critical COVID-19 and Long COVID sufferers had heightened levels of the anti-inflammatory cytokine IL10, irrespective of N-protein levels. In contrast, those who succumbed to the virus had lower IL10 levels but a higher count of class-switched memory B cells and Tfh cells. Furthermore, an increased Tfh/Treg cell ratio was observed, suggesting a potential trigger for an autoimmune response due to multiple organ damage in critically ill patients who did not survive the infection.

3.2.2 mRNA-based COVID-19 vaccines provide time-limited titer of antibodies to SARS-CoV-2

Since December 2020, Europe had access to three COVID-19 vaccines: AstraZeneca's vector-based ChAdOx1nCOV-19 Vaxzevria (AZ), and the mRNA-based vaccines from Pfizer-BioNTech Comirnaty (BT) and Moderna Spikevax (MO). We recruited 76 volunteers across three cohorts, each following a slightly varied vaccination regimen, to evaluate the development and duration of α-Spike-Ab in response to each vaccine type (Figure 20A, Supplementary Figure 4A).

Post-first AZ dose, α-Spike-Ab levels against the Wuhan strain and, to a lesser degree, the alpha, beta, and gamma variants rose to levels seen in ongoing infections (Figure 20B, Supplementary Figure 4B), accompanied by common adverse effects suggesting immune activation. Fourteen days following the first dose of the AZ vaccine, we measured the levels of 10 pro- and anti-inflammatory cytokines in peripheral blood of vaccinated individuals. Among these, IFNγ stood out as the sole cytokine to show a significant 10-fold increase even two weeks post-vaccination (with average levels for controls at 0.04 pg/ml and after the first AZ dose at 0.44 pg/ml; Figure 20C, D).

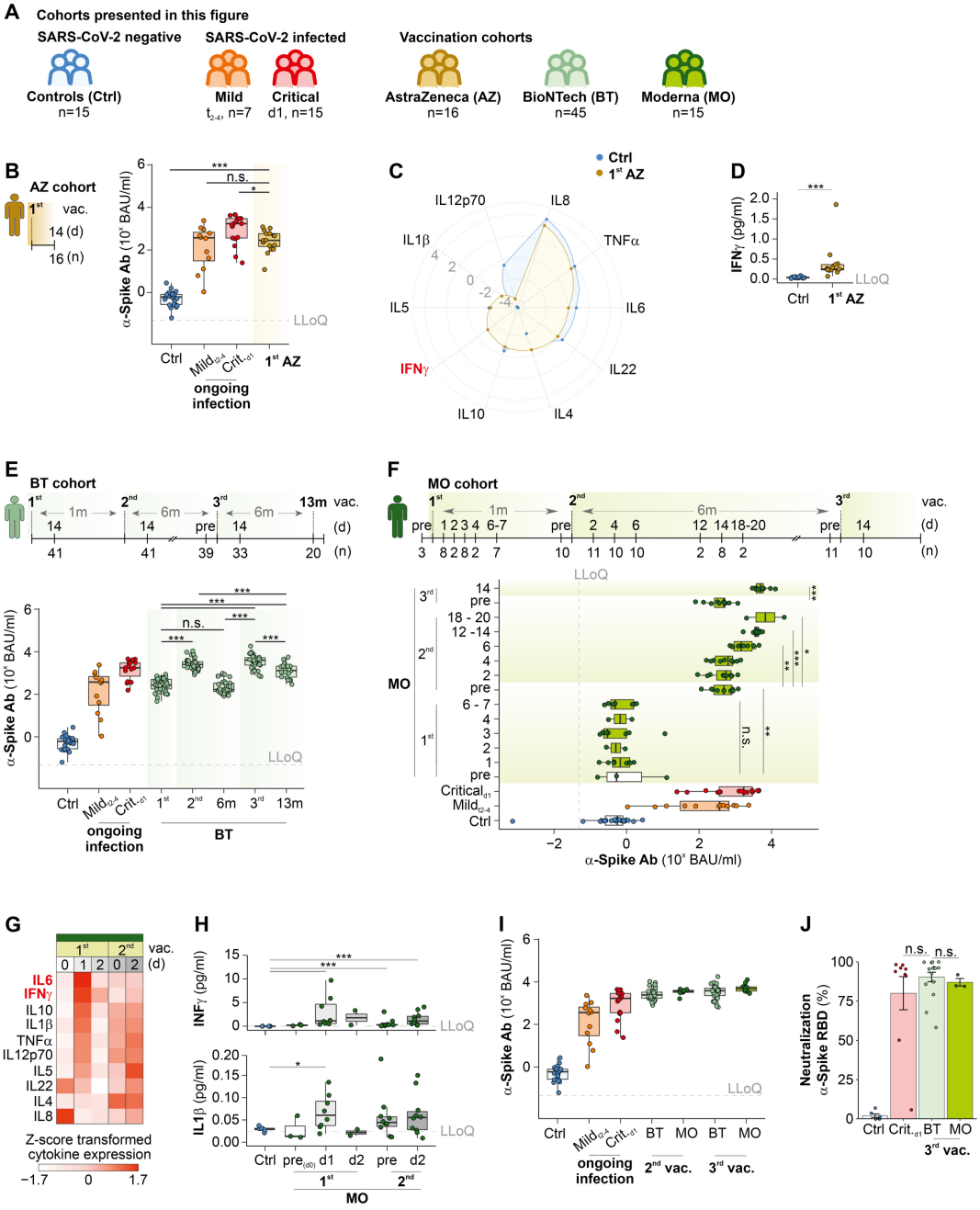

Figure 20: Antibody titers development as response to inoculation with COVID-19 vaccine. (A) Overview of participant cohorts of donors after vaccination and SARS-CoV-2 infected. α-Spike-Ab levels **(B)**, cytokine profiles **(C)**, and specific IFNγ measurements **(D)** in sera of donors 14 days post-AZ vaccination. Depiction of BT **(E)** and MO **(F)** vaccination schedules alongside a time series of α-Spike-Ab titers post-multiple vaccinations. **(G)** Cytokine level heatmap, Z-score normalized, pre- and post-MO vaccination. **(H)** Specific cytokine levels for IFNγ and IL1β pre- and post-MO vaccination. **(I)** α-Spike-Ab titer comparison after various doses of mRNA vaccines. **(J)** Antibody neutralization potential against SARS-CoV-2 Spike-RBD comparing healthy controls, critically ill COVID-19 patients, and BT/MO vaccinated individuals six months post-second booster. Lower Level of Quantification denoted as LLoQ; Mann–Whitney U test applied for statistical analysis, with unadjusted p-values provided for (A) and adjusted for (B, E); Significance levels marked as * p value < 0.05, ** p value < 0.01, *** p value < 0.001.

Administering the first dose of the Pfizer-BioNTech Comirnaty vaccine led to α-Spike-Ab titers in healthy individuals that were equivalent to those seen in COVID-19 patients during the early stages of an active SARS-CoV-2 infection (with median levels for mild cases at days 2-4 being 369 BAU/ml, and after the first Pfizer-BioNTech dose at 272 BAU/ml; Figure 20E). Additionally, a pattern was observed similarly in the AZ vaccination and in those with ongoing SARS-CoV-2 infections, where α-Spike-Ab titers against various SARS-CoV-2 variants decreased by as much as 50 % (Supplementary Figure 4C). The second Pfizer–BioNTech shot significantly boosted α-Spike-Ab levels (with a median of 2488 BAU/ml); however, this heightened response waned over time. By six months post-booster, α-Spike-Ab levels dropped to below what was observed two weeks following the first shot (median at 6 months post-booster: 164 BAU/ml). A third dose successfully reinstated and even surpassed the α-Spike-Ab titers seen 14 days after the second shot (median for the third dose: 3920 BAU/ml). Titers decreased again by the six-month mark following the third vaccination, but

remained at a robust level (median at 13 months post-first vaccination: 1283 BAU/ml).

The dynamics of α-Spike-Ab titers observed with Moderna's Spikevax vaccination mirrored those seen with other vaccines. Six days post-initial MO vaccination, α-Spike-Abs were undetectable (median for days 6-7: 0 BAU/ml; Figure 20F). However, titers against the Wuhan strain of SARS-CoV-2 (and to a smaller extent other variants as shown in Supplementary Figure 4D) rose after four weeks. Following the booster dose, there was a sharp increase in titers after 20 (medians for before the second dose: 483 BAU/ml; days 18–20 after the second dose: 12,221 BAU/ml). Similar to the BT vaccine, α-Spike-Ab levels dropped back to initial immunization levels six months after the booster (median before the third dose: 484 BAU/ml), but a third shot raised the titers to levels seen after the second dose (median 14 days after the third dose: 5001 BAU/ml). Participants receiving the MO vaccine reported flu-like symptoms, akin to those vaccinated with AZ.

To explore whether the MO vaccine side effects are triggered by an excessive inflammatory response, we measured pro- and anti-inflammatory cytokine levels in participants' serum before and after the first and second vaccinations (Figure 20G). Inflammatory cytokines such as IL6, IFNγ, IL1β, and TNFα spiked 24 hours post-first vaccine dose (Supplementary Figure 4E), with only IFNγ (medians for control: 0.03 pg/ml; day 1 post-first dose: 1.16 pg/ml) and IL1β (medians for control: 0.03 pg/ml; day 1 post-first dose: 0.06 pg/ml) showing significant increases (Figure 20H). This increase in pro-inflammatory cytokines was temporary, returning to baseline by day 2 post-vaccination. No significant rise in cytokine levels was observed after the second vaccination compared to levels before the initial vaccination.

Fourteen days following both the second and third doses of the vaccines, there were no notable differences in Ab levels produced by the BT or MO formulations, nor were there differences between the vaccination strategies at this specific time (Figure 20I). Our evaluation of COVID-19 vaccine efficacy extended to analyzing

the neutralizing ability of α-Spike-Abs generated by the BT and MO vaccines six months after the second booster (third vaccination). The antibodies from vaccinated individuals exhibited a level of neutralization against the Spike RBD of both the Wuhan and alpha variants comparable to that observed in critically ill COVID-19 patients (Figure 20J, Supplementary Figure 4F). Although data points for the MO vaccine group were fewer, antibodies from the BT vaccine displayed a notably higher neutralization capacity against the beta and gamma variants of SARS-CoV-2 (Supplementary Figure 4F).

In conclusion, both mRNA-based vaccines demonstrated comparable effectiveness in generating Ab titers against various SARS-CoV-2 variants. Furthermore, a decline in Ab titers targeting the Spike protein was noted across all the mRNA vaccines studied, occurring over a six-month period following vaccination.

3.2.3 Comparative efficacy of mixed-vaccine regimens versus single-vaccine approaches on SARS-CoV-2 Spike Ab titers

Due to vaccine shortages and multiple reports of severe adverse events such as cerebral vein thrombosis following COVID-19 vaccination (Sharifian-Dorche *et al.*, 2021; Perry *et al.*, 2021; Jaiswal *et al.*, 2022), the recommendations for administering AZ, Jcovden Janssen-Cilag (JJ), BT, and MO vaccines were updated. The German Vaccine Committee (STIKO) at the Robert Koch Institute in Berlin recommended using AZ for the initial dose followed by an mRNA-based COVID-19 vaccine for the booster, or two doses of AZ exclusively for individuals over 60 years old. Our study included 3 healthy participants who received two initial doses of AZ followed by a booster dose of BT (Figure 21A, Supplementary Figure 5A). Previous findings confirmed that a single dose of AZ significantly raised α-Spike-Ab levels against the original Wuhan strain and other variants (Figure 21B, Supplementary Figure 5B). Following a booster with BT within 28 days after the second dose of AZ, α-Spike-Ab levels surged 13-fold by day 7 (medians for before BT: 181 BAU/ml; 7 days after BT: 3153 BAU/ml; Figure 21A), matching the antibody levels seen in participants who received two BT doses.

Additionally, we examined α-Spike-Ab titers in 4 participants adhering to another STIKO recommendation: one dose of AZ followed by two doses of BT. Their antibody levels were compared to those in control participants who received three BT doses. The interval between the first and second BT doses was less than 8 weeks, resulting in already elevated α-Spike-Ab levels before the second BT dose (median before the second BT: 2781 BAU/ml), which were on par with levels seen after two or three BT doses (medians for after the second BT: 2488 BAU/ml;

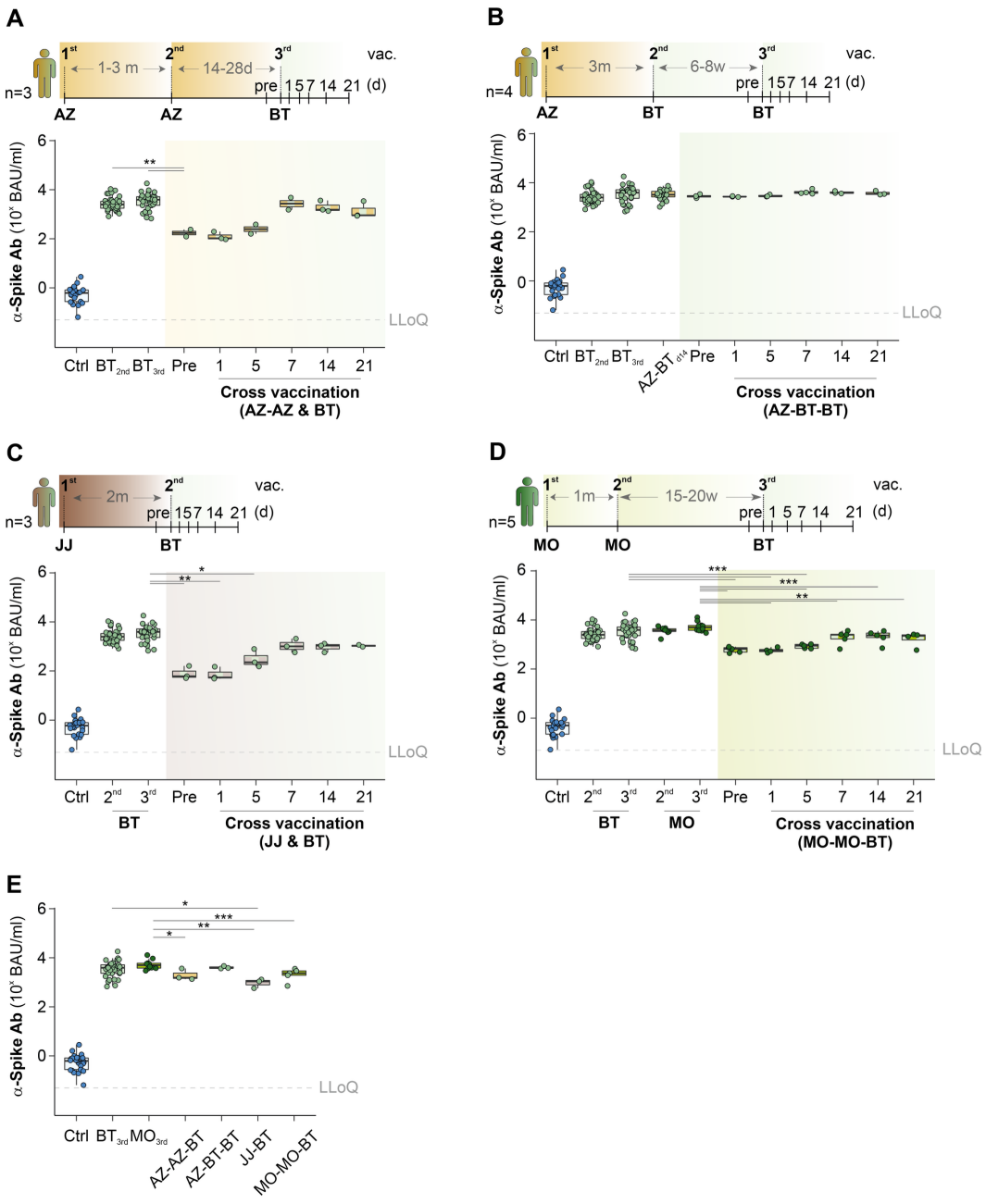

Figure 21: Comparison of antibody levels against the SARS-CoV-2 Wuhan Spike across different vaccination regimes. (A–D) Depicted at the top are the vaccination sequences and timeline, whereas at the bottom are the α-Spike-Ab concentrations over time for groups vaccinated with various combinations as outlined in the sequences of AZ-AZ-BT **(A)**, AZ-BT-BT **(B)**, JJ-BT **(C)**, and MO-MO-BT **(D)**. **(E)** Showcases a comparison across these different vaccination strategies; LLoQ stands for Lower Level of Quantification; the Mann-Whitney U test was used for statistical analysis, with unadjusted p-values in (A) and adjusted p-values in (C-E); significance levels are indicated as follows: * p value < 0.05, ** p value < 0.01, *** p value < 0.001.

after the third BT: 3920 BAU/ml). No significant increase in α-Spike-Ab levels was noted up to 21 days following the second BT dose (21 days after the second BT: 3468 BAU/ml).

Differing from the group that adhered to an AZ-BT-BT vaccination regimen, three individuals who received just a single JJ vaccine exhibited notably lower α-Spike-Ab levels two months post-vaccination (median prior to boost: 61 BAU/ml; Figure 21C). Introducing a booster dose of BT significantly elevated their antibody titers to 1007 BAU/ml within seven days, reaching levels seen in those who had received two or three doses of BT (medians for second BT dose: 2488 BAU/ml; third BT dose: 3920 BAU/ml). Thus, it's evident that individuals initially vaccinated with JJ can significantly benefit from a subsequent BT booster dose.

Ultimately, it was noted that participants initially receiving two doses of the MO vaccine and then switching to BT for their third dose did not see an advantage from this vaccination strategy (Figure 21D). Their α-Spike-Ab levels were half those observed in participants who were administered three doses of MO (medians 14 days after BT: 2347 BAU/ml; after the third MO dose: 5001 BAU/ml).

In conclusion, each of the varied vaccination approaches studied achieved acceptable α-Spike-Ab levels against the Wuhan strain and other variants 14 days following the final booster dose (Figure 21E, Supplementary Figure 5B).

However, it was noted that α-Spike-Ab levels in groups following a mixed vaccination regimen were significantly lower compared to those in the control groups receiving three doses of the same vaccine, either BT or MO.

3.2.4 Cured COVID-19 donors benefit from vaccination after six months post infection

Following infection with SARS-CoV-2, individuals rapidly produced antibodies targeting the virus's Spike protein within the first week (Figure 18B). However, for those experiencing Long COVID, α-Spike-Ab levels began to decline after eight months, continuing to drop through to 12 months (Figure 19B). In an effort to booster immunity against SARS-CoV-2 re-infection, three individuals who had recovered from COVID-19 received two doses of BT vaccine six months post-infection (Figure 22A). These individuals were considered healthy, having no history of hypertension, diabetes, or obesity (Figure 22B). The antibody levels in these recovered patients were notably lower six months post-infection (median before first BT dose: 148 BAU/ml; Figure 22C) compared to healthy individuals who had received two doses of the BT vaccine (median after second BT dose: 3488 BAU/ml). Interestingly, the recovered COVID-19 patients exhibited relatively higher antibody titers against the alpha and gamma variants of SARS-CoV-2, similar to those with an active infection, when compared to vaccinated individuals (Supplementary Figures 2C,F, 4C,D, and 6A). Administering one dose of the BT vaccine resulted in a significant increase in α-Spike-Ab levels seven days later (median after 7 days: 3008 BAU/ml), matching levels seen in controls who also received the BT vaccine. A subsequent dose one month later did not further elevate α-Spike-Ab levels beyond those achieved with the initial BT dose (median after second dose, day 7: 3918 BAU/ml). It is critical to note that recovering from SARS-CoV-2 infection, followed by BT vaccination, did not sustain antibody production against the Spike protein in the long term; antibody levels dropped to a baseline of 544 BAU/ml 183 days post-vaccination (Figure 22C). These findings reinforce the consensus in the scientific community that individuals who have recovered from COVID-19 still benefit from receiving an mRNA-based vaccine six months after their infection. A sole SARS-CoV-2

infection does not produce antibody levels that are either more durable or higher than those generated by vaccination.

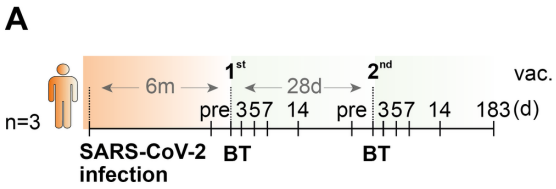

B

Characteristic	vaccination[1], N = 3
Age	
24	1 (33%)
25	2 (67%)
Sex	
f	1 (33%)
m	2 (67%)
Hypertension	0 (0%)
Diabetes	0 (0%)
Overweight	0 (0%)

[1] n (%)

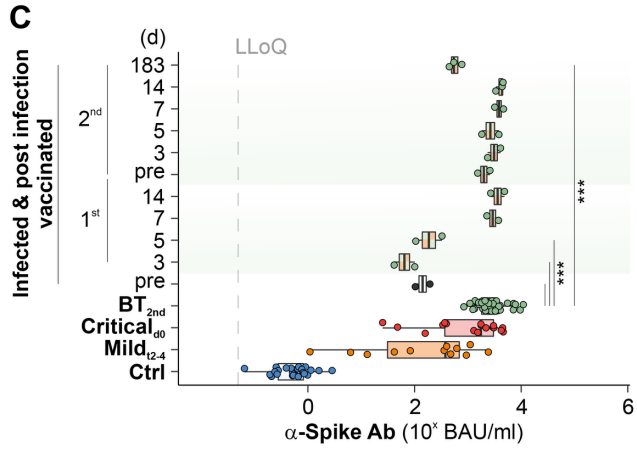

Figure 22: Ab titers targeting the Spike protein of the Wuhan SARS-CoV-2 strain before and after immunization. (A) Graph depicts the vaccination timeline, **(B)** provides a table detailing patient clinical characteristics, and (C) shows the α-Spike-Ab concentrations in patients 6 months after infection shortly before vaccination and subsequent inoculations at specified intervals. LLoQ stands for Lower Level of Quantification; the Mann-Whitney U test was employed for statistical analysis with unadjusted p-values in part (C); a significance level of *** indicates a p value < 0.001.

3.3 Programming of peripheral classical monocytes during COVID-19

Since antigen-presenting cells play a central role in orchestrating immune responses during infection, particularly through antigen presentation and cytokine signaling. The study presented in this subsection of the thesis focused on examining their functional states during COVID-19. Due to the practical and ethical limitations of accessing dendritic cells and tissue-resident macrophages directly from infected human tissues, classical $CD14^+$ monocytes were selected as surrogate immune cells. These cells circulate in peripheral blood, are readily accessible, and can migrate to infection sites where they differentiate into macrophages and contribute significantly to shaping local and systemic immune responses.

To explore the transcriptional and functional programming of monocytes during varying severities of COVID-19, bulk RNA sequencing was performed on $CD14^+$ monocytes isolated from 52 donors recruited at the University Hospital Bonn. Donors with a critical disease course were enrolled upon their first day of admission to the intensive care unit (ICU), while individuals with mild symptoms, along with healthy controls, were sampled at their homes at scheduled timepoints over a period of up to three weeks. This design enabled a detailed comparative analysis of monocyte gene expression patterns across different clinical severities and stages of infection.

3.3.1 Study cohort and clinical parameters

In this study, 37 patients were categorized as "critical," along with ten healthy control donors and five patients with mild symptoms (Table 2). The high mortality rate of 58 % among critical patients resulted in incomplete kinetic analyses of monocytic programming for some donors. However, the death of a patient did not lead to the exclusion from the study. The median age was 60 years for critical patients and 62 years for healthy volunteers, while the mild cohort had a median age of 41 years. Additionally, males constituted 81 % of the ICU cohort, indicating a male prevalence in this critical group. PCR tests were performed on all mild and critical donors at the time of their admission to the study; 89 % of critical donors

demonstrated viral replication in the upper respiratory organs, while all mild donors tested positive for viral RNA.

Variable	Overall, N = 52[1]	healthy, N = 10[1]	mild, N = 5[1]	critical, N = 37[1]
Male sex	36/52 (69%)	5/10 (50%)	1/5 (20%)	30/37 (81%)
Age	61 (54, 65)	62 (59, 68)	41 (38, 53)	60 (54, 65)
Deceased	22/52 (42%)	0/10 (0%)	0/5 (0%)	22/37 (59%)
PCR test on enrollment				
negative	3/33 (9.1%)	0/0 (NA%)	0/5 (0%)	3/28 (11%)
positive	30/33 (91%)	0/0 (NA%)	5/5 (100%)	25/28 (89%)

[1] Frequency (%) or Median (IQR)

Table 2: Demographic and Clinical Characteristics of Study Participants. The table includes age, sex, mortality status during the study, and PCR test results at enrollment for each participant.

Comorbidities were identified among the critical patients, and healthy volunteers were matched accordingly. Within the critical patient group, 57 % suffered from hypertension prior to contracting SARS-CoV-2, compared to 40 % among healthy controls (Table 3). Interestingly, 60 % of the healthy volunteers had Diabetes mellitus type 2, while only 41 % of the critical patients were affected by the same condition. Asthma was present in both groups, with 10 % in the healthy cohort and 30 % in the critical group. In the mild group, only one donor was affected by hypertension, others presenting no comorbidities.

Additionally, two individuals in the healthy cohort were in remission from ovarian carcinoma and prostate carcinoma, respectively. These subjects were included in the study as they were no longer undergoing cancer therapy. Conversely, among the critical patients, one was diagnosed with chronic lymphocytic leukemia (CLL) and was excluded from the study due to the potential for altered immune responses caused by the cancer rather than the infection. Another critical patient with metastatic lung adenocarcinoma was included in the study, as the patient was not receiving cytostatic or immunomodulatory treatment, allowing for

the assumption that his myeloid cell compartment was functional and not compromised.

Comorbidity	**Overall,** N = 52[1]	**healthy,** N = 10[1]	**mild,** N = 5[1]	**critical,** N = 37[1]
Cardiovascular	26/52 (50%)	4/10 (40%)	1/5 (20%)	21/37 (57%)
Metabolic	21/52 (40%)	6/10 (60%)	0/5 (0%)	15/37 (41%)
Respiratory	12/52 (23%)	1/10 (10%)	0/5 (0%)	11/37 (30%)
Viral	4/52 (7.7%)	0/10 (0%)	0/5 (0%)	4/37 (11%)
Renal	2/52 (3.8%)	0/10 (0%)	0/5 (0%)	2/37 (5.4%)
Hepatic	4/52 (7.7%)	1/10 (10%)	0/5 (0%)	3/37 (8.1%)
Endocrine	12/52 (23%)	2/10 (20%)	0/5 (0%)	10/37 (27%)
Autoimmune	4/52 (7.7%)	0/10 (0%)	0/5 (0%)	4/37 (11%)
Cancer	4/52 (7.7%)	2/10 (20%)	0/5 (0%)	2/37 (5.4%)

[1]Frequency (%)

Table 3: Comorbidities of the participants. This table outlines the prevalence of comorbid conditions among the critical patients and the matched healthy volunteers, as well as donors with mild COVID-19 in the study.

Complete blood counts indicated that patients admitted to the ICU were suffering from normocytic normochromic anaemia, with an average of 3.4 T/l cells and a haemoglobin level of 10.8 g/dl upon admission. This condition remained unchanged throughout the study period (Table 4). Moreover, the critically ill patients exhibited neutrophilia and lymphocytopenia even before ICU admission (Table 4). However, there was a notable improvement during the study period, with neutrophil percentages decreasing from 86 % to 77 % and lymphocyte percentages increasing from 7.7 % to 12.7 % of total peripheral immune cells.

Although there was a significant increase in the proportions of monocytes from 4.5 % to 6.2 %, eosinophils from 0.9 % to 3.2 %, and basophils from 0.2 % to 0.4 % among the critical patients, these changes remained within the normal reference ranges for these parameters (Table 4). Thus, while there were shifts in specific cell types, these either remained within clinically normal limits or improved.

Variable (normal range)	**Overall,** N = 68[1]	**The first test,** N = 37[1]	**The last test,** N = 37[1]	**Difference**[2]	**95% CI**[2,3]	**p-value**[2]
Leukocytes (3.9-10.2 G/l)	10.8 (7.5, 14.0)	11.5 (7.3, 15.3)	9.9 (7.5, 13.0)	1.7	-0.43, 3.8	0.12
Erythrocytes (4.3-5.75 T/l)	3.38 (3.10, 3.60)	3.40 (3.10, 3.70)	3.35 (3.20, 3.55)	0.05	-0.16, 0.26	0.7
Haemoglobin (13.5-17.3 g/dl)	9.94 (9.18, 10.40)	10.01 (8.90, 10.80)	9.85 (9.33, 10.20)	0.17	-0.44, 0.78	0.6
MCV (80-99 fl)	89.9 (87.0, 94.0)	89.4 (87.0, 94.0)	90.4 (87.0, 95.0)	-0.95	-3.4, 1.5	0.4
MCH (27-34 fl)	29.54 (29.00, 31.00)	29.54 (28.00, 31.00)	29.55 (29.00, 30.75)	-0.01	-0.83, 0.81	>0.9
Neutrophils (42-77 %)	82 (78, 88)	86 (81, 91)	77 (70, 82)	8.9	5.1, 13	**<0.001**
Neutrophils (1.5-7.7 G/l)	8.7 (5.6, 11.6)	9.9 (6.8, 12.6)	7.0 (5.0, 9.9)	2.9	0.93, 4.9	**0.005**
Lymphocytes (20-44 %)	9.8 (5.7, 12.2)	7.7 (4.6, 9.6)	12.7 (8.6, 16.1)	-5.0	-7.9, -2.1	**<0.001**
Lymphocytes (1.1-4.5 G/l)	0.91 (0.62, 1.15)	0.78 (0.45, 1.01)	1.10 (0.78, 1.36)	-0.32	-0.55, -0.10	**0.006**
Monocytes (2-9.5 %)	5.23 (3.00, 6.85)	4.50 (2.75, 5.58)	6.20 (5.00, 8.00)	-1.7	-3.0, -0.42	**0.010**
Monocytes (0.1-0.9 G/l)	0.55 (0.28, 0.72)	0.54 (0.20, 0.73)	0.56 (0.34, 0.69)	-0.02	-0.19, 0.16	0.8
Eosinophils (0.5-5.5 %)	1.88 (0.10, 2.33)	0.85 (0.00, 1.25)	3.22 (0.95, 4.85)	-2.4	-3.7, -1.1	**<0.001**
Eosinophils (0.02-0.5 G/l)	0.17 (0.01, 0.26)	0.09 (0.00, 0.11)	0.27 (0.08, 0.45)	-0.18	-0.29, -0.08	**0.001**
Basophils (0-1.75 %)	0.30 (0.10, 0.40)	0.20 (0.10, 0.30)	0.42 (0.30, 0.58)	-0.21	-0.33, -0.09	**<0.001**
Basophils (0-0.2 G/l)	0.034 (0.010, 0.048)	0.033 (0.010, 0.035)	0.036 (0.015, 0.050)	0.00	-0.02, 0.02	0.7

[1] Mean (IQR)
[2] Welch Two Sample t-test
[3] CI = Confidence Interval

Table 4: Blood counts of critical donors during the study. This table presents complete blood counts performed at ICU admission and subsequently at the end of the study or shortly before death, detailing shifts in specific cell types by comparing results from the first and last tests conducted. The first column lists each cell type alongside the normal range for healthy individuals, with abbreviations such as G representing Giga (10^9), T for Tera (10^{12}), and fl for femtoliters. Significant changes over time were assessed using the Welch two-sample t-test, with significant findings highlighted by bolding the p-values.

3.3.2 Mild disease course correlates with interferon signature and antigen presentation

Monocytes were isolated and 3' RNA sequencing was conducted to analyze their transcriptomes of critical patients, along with samples of monocytes from mild cases and healthy participants. In total, 131 samples were sequenced across the different groups.

From the ten healthy volunteers, three samples were collected each within a two-

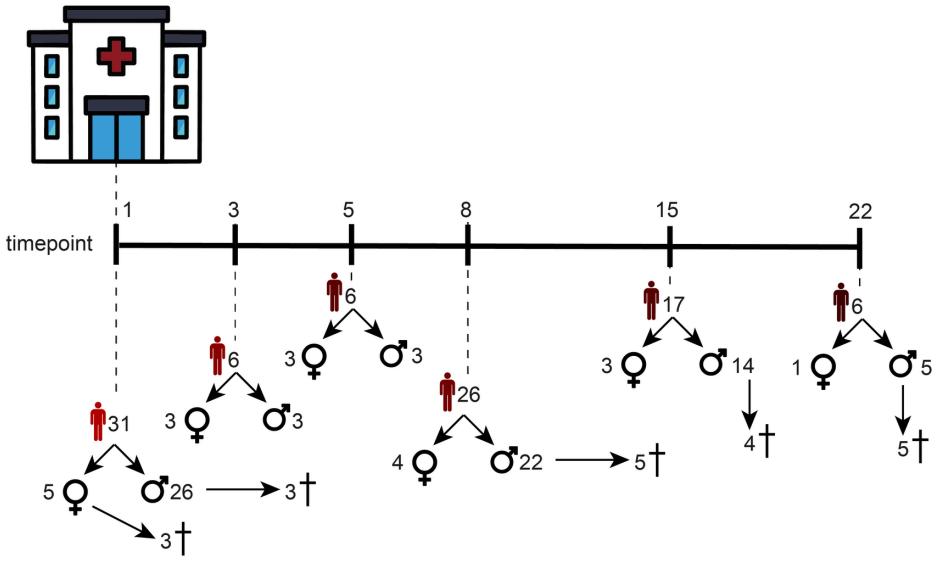

Figure 23: Temporal distribution of monocyte RNA sequencing samples from critical COVID-19 patients. Numbers of sequenced samples for every timepoint of the study. For the days 1, 3, 5, 8, 15 and 22 after enrollment into the study 31, 6, 6, 26, 17 and 6 samples of monocytic RNA from critical patients have been sequenced, respectively. In total 19 patients deceased during the study, leading to incomplete timecourse. Additional 5 patients passed away after completion of the study.

week period, resulting in 30 samples of healthy monocytes. For the critical patients, 31 monocytic RNA samples were sequenced on the first day of their enrollment in the study (Figure 23). However, by the next sampling day, six of these patients had passed away. On days three and five after admission, six samples were collected at each time point from the remaining critical patients. At

the later stages of the study, on days eight and 15, 26 and 17 samples were sequenced, respectively. During the interval between these two points, an additional nine critical patients deceased. At the conclusion of the study, six samples were collected, five of which were from critical patients who passed away shortly thereafter.

The Principal Component Analysis (PCA) was performed on 10,725 genes to reduce the complexity of gene expression data into two principal dimensions, revealing distinct clustering patterns based on patient condition (Figure 24). The

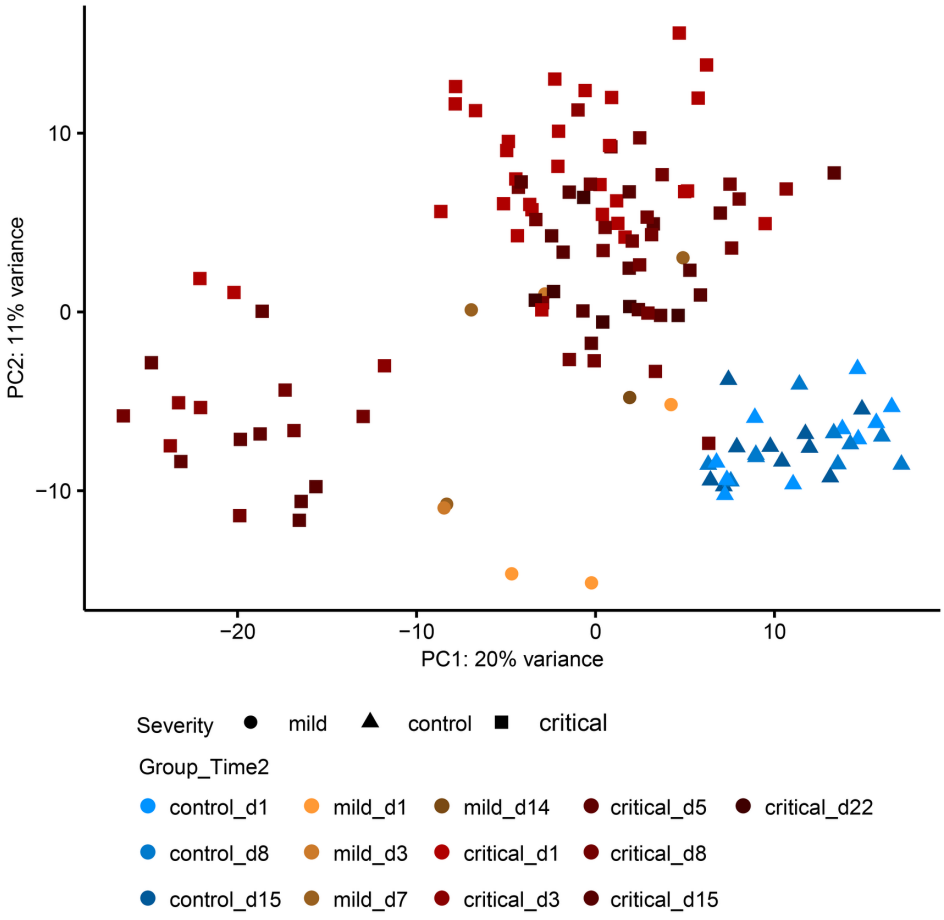

Figure 24: PCA of gene expression from bulk sequenced RNA of monocytes. The principal component analysis includes all present genes (10,725 genes) from 131 sequenced samples of monocytes.

initial analysis shows that monocytes from healthy controls form a tight cluster,

remaining consistent regardless of sampling time, which suggests a stable transcriptomic profile across different time points. Conversely, monocytes from critical patients at early stages of their ICU are clustered distinctly far apart from the healthy control group. Over time, as the patients remain at the ICU, their monocytes undergo transcriptomic changes that make their profiles increasingly resemble those of healthy individuals. This trend may indicate a transcriptomic normalization associated with ongoing treatment. Monocytes from mild COVID-19 cases initially position between the clusters of critical and healthy groups. As time progresses, these mild cases tend to shift closer to the cluster of critical patients.

To further analyze these patterns and explore the relationships between gene expression, patient cohort, and time points in a systematic way, Weighted Correlation Network Analysis (WGCNA) was utilized. WGCNA is a robust data-mining technique suitable for high-dimensional datasets, which constructs weighted correlation networks to identify clusters, or modules, of co-expressed genes. Given that samples from healthy individuals consistently clustered together across all time points, they were aggregated into a single group for comparative purposes to enhance the statistical power of the analysis.

The comprehensive WGCNA, performed on the full set of 10,725 present genes, resulted in the identification of 20 distinct modules, labelled as colours (Figure 25). These modules represent groups of genes that exhibit highly correlated expression patterns across the dataset. Each module's behavior can be summarized by a single representative expression profile, known as an Eigengene.

An Eigengene is defined as the first principal component of a given module, acting as a representative weighted average expression profile for that module. It effectively encapsulates the dominant, collective expression changes within the module across various conditions or over time. By correlating eigengenes with disease severity at different time points, we can gain a deeper understanding of the complex biological changes occurring during the disease progression.

Since Module Eigengenes (ME) represent the overall expression profile of their respective modules, all genes within a module are subsequently associated with the phenotype being studied. This association simplifies the interpretation of large-scale gene expression data, making it easier to discern patterns and insights across different stages of severity and over time.

The resulting modules were selected using the Pearson correlation coefficients with thresholds set at a minimum of 0.3 and a p-value of at least 0.05, calculated using the Student asymptotic test, to identify 17 distinct clusters that characterize the programming of monocytes throughout the study timeline (**Figure 25**).

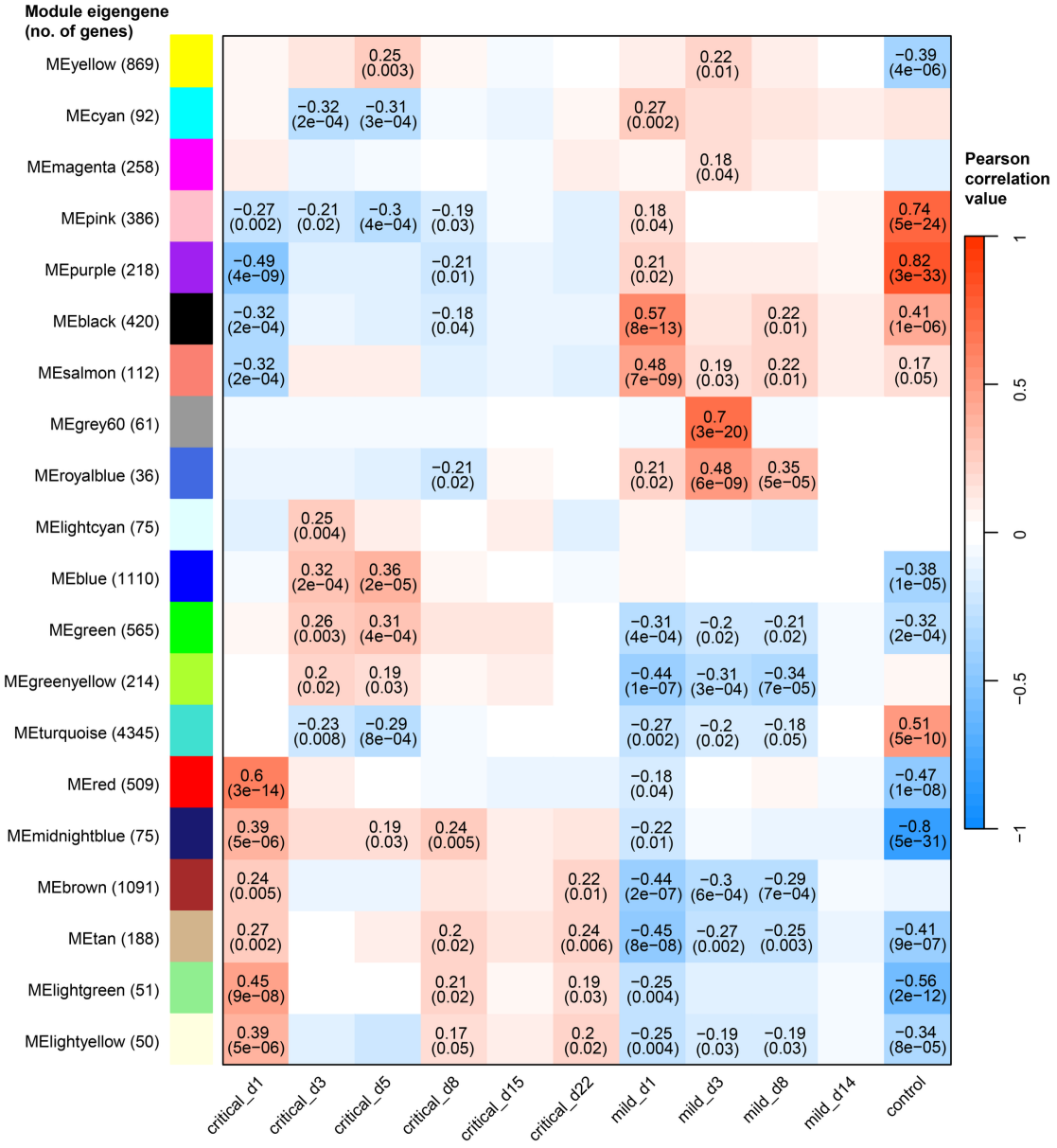

Figure 25: Weighted Correlation Network Analysis (WGCNA) Heatmap. Heatmap was generated from a WGCNA performed on 10,725 genes, identifying 20 distinct clusters with a minimum module size of 30. The y-axis displays the module eigengene for each defined cluster, labeled by color with the number of genes in the module indicated in brackets. The coloring of the tiles corresponds to the Pearson correlation values, and only tiles representing significant correlations (p-value less than 0.05 calculated by the Student asymptotic test) are displayed.

Genes playing a role in the early disease were contained in the 'black' and 'salmon' clusters, showing a strong positive correlation with the mild disease phenotype from the first day of inclusion. These clusters distinctly contrasted with the critical patients admitted to the ICU on the same day, where they showed a significant negative correlation. As the disease progressed, monocyte behavior shifted notably on days three and five. The 'grey60' and 'royalblue' clusters aligned more closely with the mild disease, suggesting adaptive changes in response to the ongoing infection.

In contrast, the 'yellow', 'green', and 'blue' clusters displayed negative correlations with the healthy cohort while showing positive correlations with the critical cohort during the days three to five after admission to the study. The 'green' cluster also showed a negative correlation with the mild cohort within the first week after admission. Additionally, the clusters 'cyan', 'pink', and 'purple' presented a negative correlation with the critical cohort during the initial five days, with the 'pink' and 'purple' clusters also showing a strong positive correlation exceeding 0.7 with the healthy cohort.

During the initial days of inclusion into the study, the 'greenyellow', 'brown', and 'tan' clusters were significantly negatively correlated with the mild cohort. In contrast, the 'red', 'midnightblue', 'lightgreen', and 'lightyellow' clusters showed

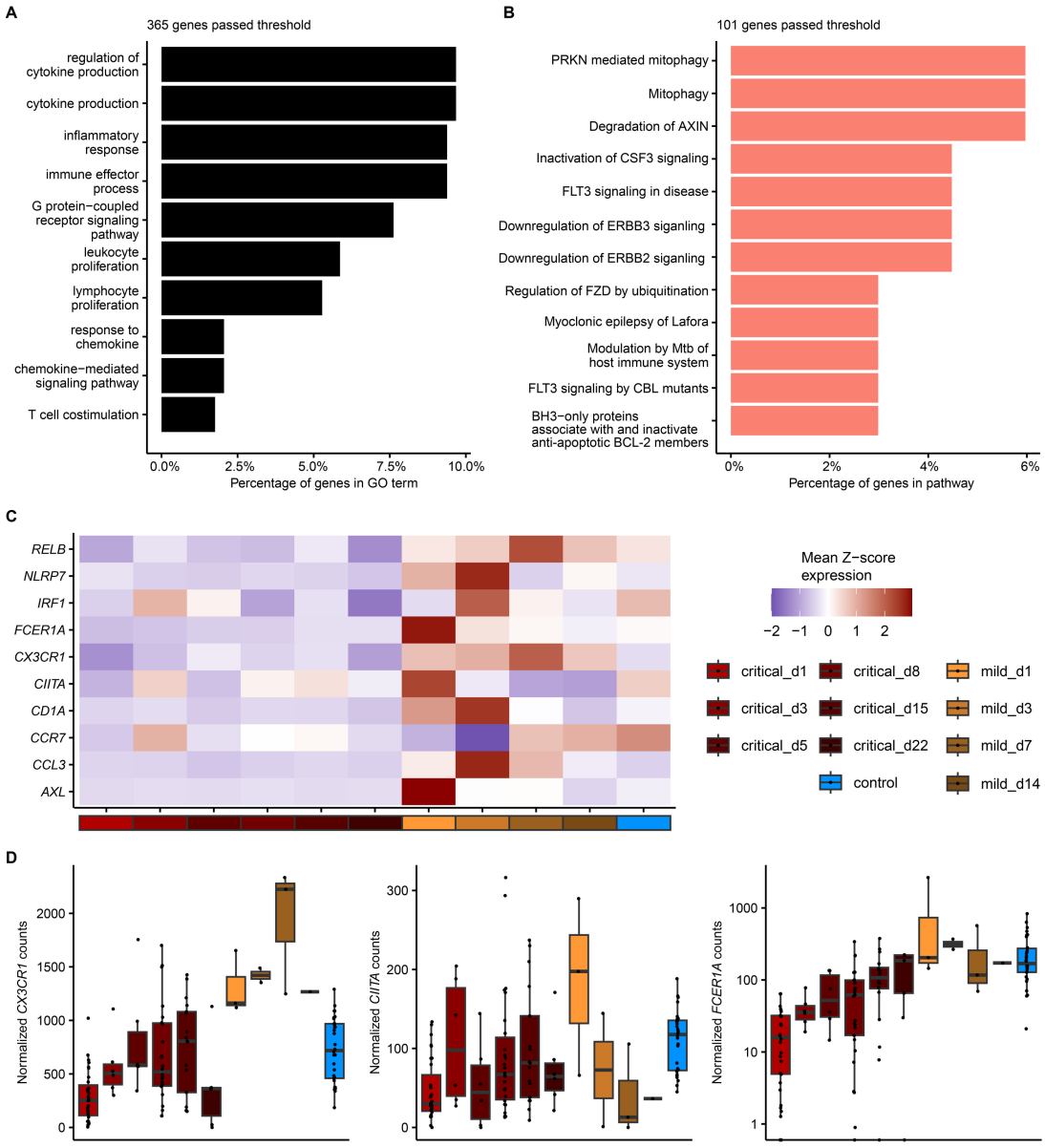

Figure 26: Functional enrichment and gene expression correlating with mild COVID-19 in early stage. GO term enrichment of the 'black' cluster of genes **(A)** and pathway enrichment of the 'salmon' module **(B)**. Heatmap of mean z-score normalized gene expression of selected genes from enriched GO **(C)**. Boxplots indicating normalized gene expression of *CX3CR1, CIITA, FCER1A* **(D)**.

significant negative correlation with healthy donors and a slight negative correlation with the mild, while being strongly correlated with the patients on the first day of admission to the ICU.

To elucidate the genes driving the immune response in the early days during a SARS-CoV-2 infection, Gene ontology (GO) term enrichment analysis was performed on the genes from the 'black' module. Genes within this cluster are involved in “cytokine production”, “inflammatory responses”, and “chemokine responses” (Figure 26A). Notably, genes such as *CIITA, FCER1A,* and *CD1A*, which are essential for antigen presentation, along with *CX3CR1*, *IRF1*, and *CCL3* that enhance the defense response to viral infections, exhibited higher expression levels in patients exhibiting mild symptoms compared to those in critical conditions (Figure 26C-D). A similar pattern was also observed in genes like *CCR7*, crucial for the migration of inflammatory monocytes to infection sites,

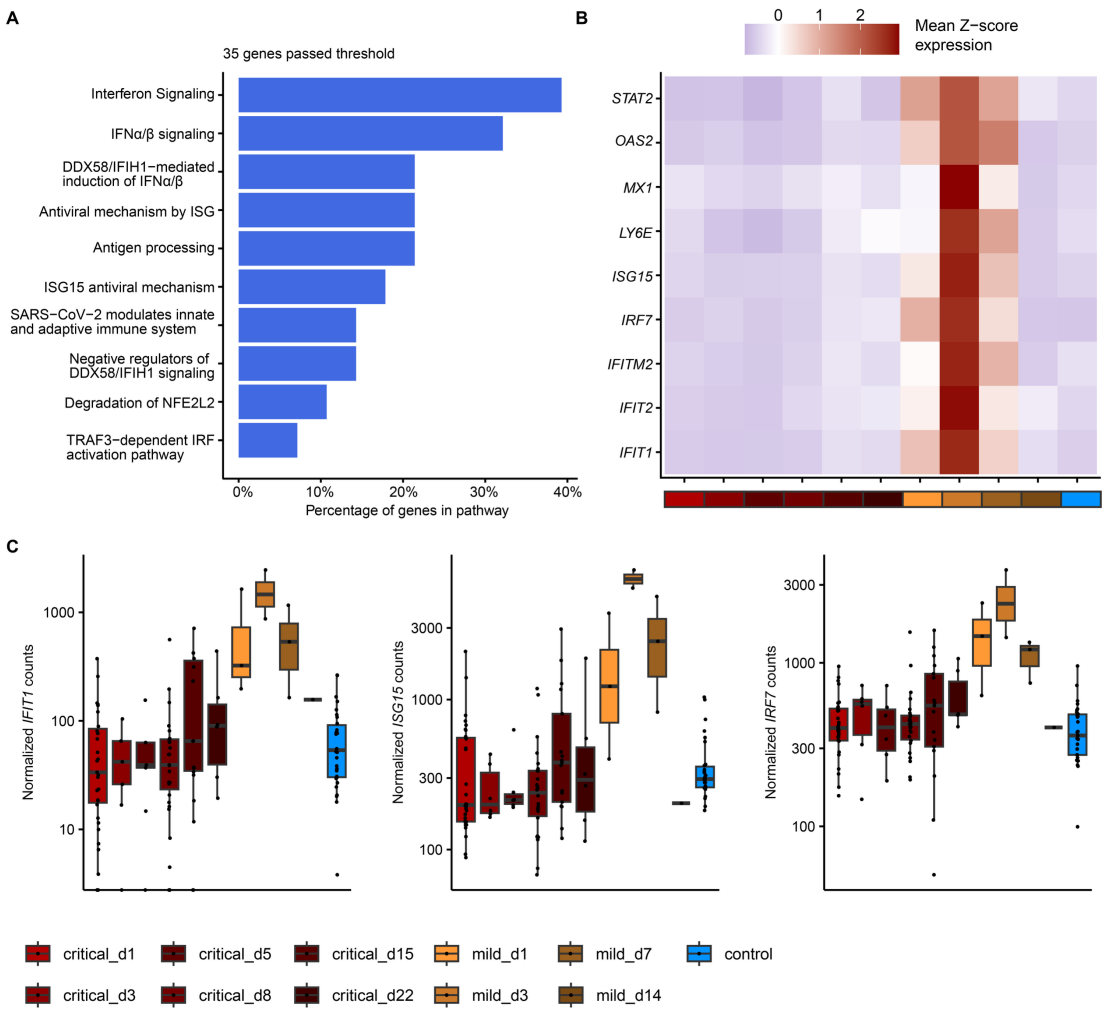

Figure 27: Functional enrichment and gene expression correlating with mild COVID-19 in early disease progression. Pathway enrichment of the 'royalblue' cluster of genes **(A)**. Heatmap of mean z-score normalized gene expression of selected genes from enriched pathway **(B)**. Boxplots indicating normalized gene expression of *IFIT1, ISG15, IRF7* **(C)**.

and *AXL*, which mediates apoptotic cell removal. Additionally, an analysis of the genes belonging to the 'salmon' cluster using pathway enrichment highlighted pathways associated with mitophagy, a key process in “regulating the immune response”, as well as “modulation by Mycobacterium tuberculosis (Mtb) of the host immune system”, a known intracellular pathogen which can also infect monocytes (Figure 26B).

As the disease progresses, significant changes occur in monocyte programming, which were explored by examining gene expression in the 'grey60' and 'royalblue' modules. Although no significant enrichment for GO terms or pathways was observed in the 'grey60' cluster, the 'royalblue' module presented enriched for pathways involved in “type I interferon signaling”, “antigen processing”, and “antiviral mechanisms induced by ISGs” (Figure 27A).

Genes such as *IFIT1/2*, *IFITM2*, *ISG15*, and *OAS2* within these pathways exhibited high expression levels in patients with mild symptoms during the first week after admission to the study (Figure 27B-C). The peak expression of these genes occurred on day three, underscoring the critical role of type I interferon responses in the early stages of infection and suggesting a potential mechanism behind the milder symptoms observed in some patients.

Upon admission to the ICU, the programming of monocytes was characterized through the analysis of the 'red', 'midnightblue', 'lightgreen', and 'lightyellow' modules, which are correlated with this specific phenotype. GO term enrichment

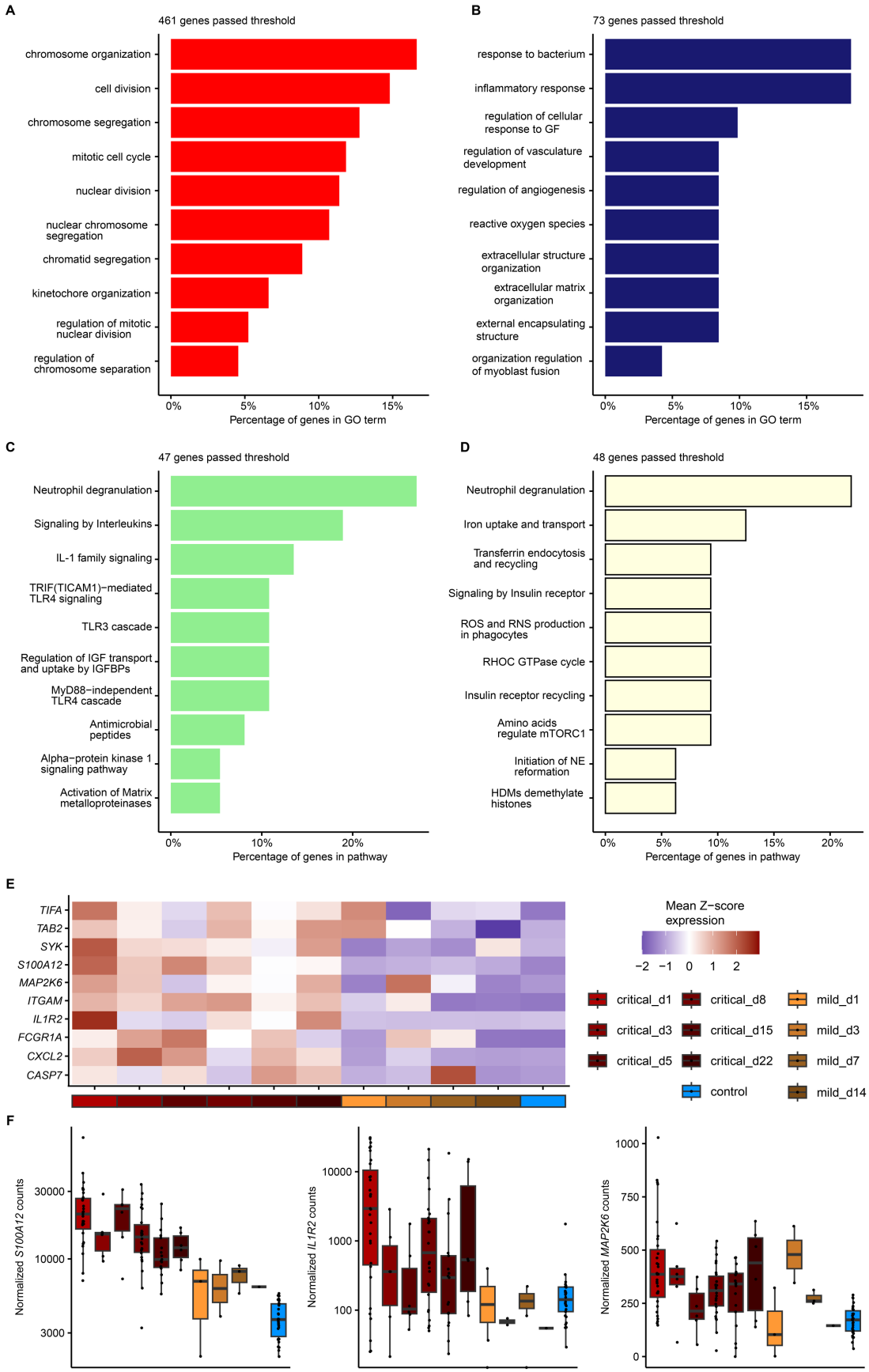

in the 'red' cluster identified an association with “cell division” (Figure 28A). The

Figure 28: Functional enrichment and gene expression correlating with critical COVID-19 upon admission to the study. GO term enrichment of the 'red' **(A)** and 'midnightblue' **(B)** modules. Pathway enrichment of the 'lightgreen' **(C)** and 'lightyellow' cluster of genes **(D)**. Heatmap of mean z-score normalized gene expression of selected genes from enriched GO and pathways **(E)**. Boxplots indicating normalized gene expression of *S100A12, IL1R2, MAP2K6* **(F)**.

'midnightblue' cluster, which encompasses 75 genes, is linked with the response to bacterial presence and inflammatory responses (Figure 28B). Notable genes within this cluster include *S100A12*, *CXCL2*, and *ITGAM*, which are pivotal in coordinating immune cell migration and adhesion (Figure 28E-F). These genes were consistently expressed at higher levels in the critical cohort over time, in comparison to both mild and healthy groups. The 'lightgreen' cluster is characterized by genes involved in TLR4 signaling and IL-1 family signaling, pathways critical for the innate immune response (Figure 28B). Key genes such as *IL1R2*, *MAP2K6*, *TIFA*, *SYK*, and *TAB2* are notably expressed at higher levels in the critical cohort, highlighting their role in exacerbating inflammatory responses (Figure 28E-F). Lastly, the 'lightyellow' cluster includes genes associated with neutrophil degranulation, reactive oxygen species (ROS) production, and the epigenetic regulation of gene expression through histone demethylation (Figure 28D).

The yellow, blue, and green modules consist of genes that correlate across days three and five of the study in the critical cohort. No module shows specific correlation with day three or day five individually, suggesting that there are only minor differences in monocyte programming between these two time points. This leads to a combined signature for these days, likely due to a limited number of samples available for each individual time point.

In the 'green' module, although no pathways or GO terms were significantly enriched, but genes associated with pro-inflammatory immune response, such as *S100A11*, *CD58*, *CD40*, and *C1QA* were identified (Figure 29C). *S100A11*

showed higher expression in critical patients throughout the study compared to mild and healthy patients (Figure 29D). Additionally, markers involved in augmenting T cell activation, such as *CD58* and *CD40*, were also identified in this cluster. *CD58* was initially expressed during the first 3 days in the mild cohort but was subsequently downregulated, whereas *CD40* showed persistent presence in the critical cohort and peaked on day five. *C1QA*, a gene associated with complement-induced phagocytosis, was also noted to increase over time in critical donors, peaking on day 15 post-inclusion in the study.

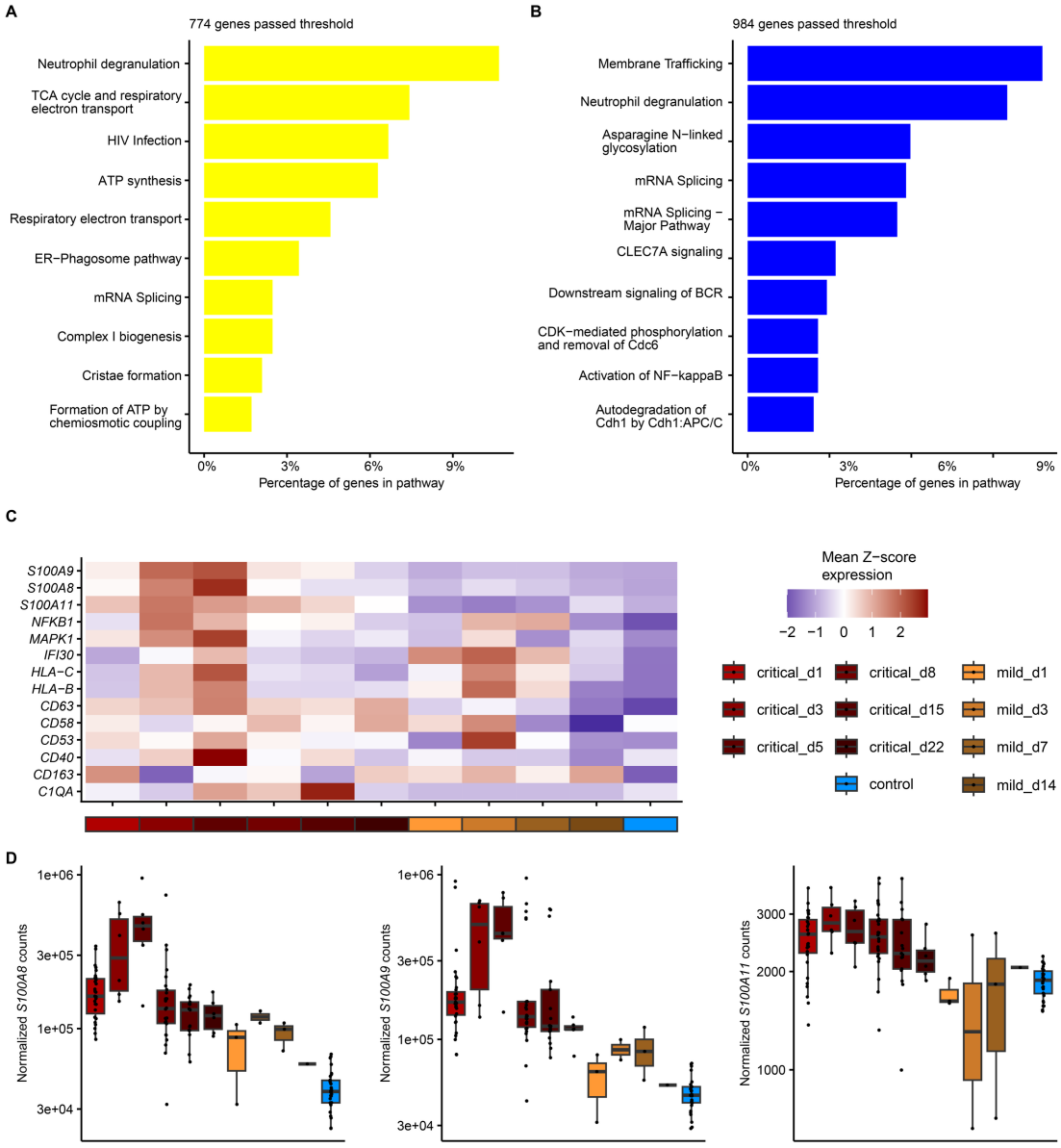

Figure 29: Functional enrichment and gene expression correlating with critical COVID-19 during disease progression. Pathway enrichment of the 'yellow' **(A)** and 'blue' module genes **(B)**. Heatmap of mean z-score normalized gene expression of selected genes from enriched pathways **(C)**. Boxplots indicating normalized gene expression of *S100A8, S100A9, S100A11* **(D)**.

The 'yellow' and 'blue' modules presented significantly enriched pathways involved in neutrophil degranulation and NF-κB activation (Figure 29A-B). Key genes in these pathways include *S100A8/9*, Ca^{2+} binding proteins known as potent pro-inflammatory factors. These proteins are produced by various cells upon stimulation and are responsible for inducing neutrophil migration and degranulation. Their expression increased during the initial 5 days in the ICU and decreased subsequently (Figure 29C-D). A similar trend was observed in genes that promote the pro-inflammatory response, such as *NFKB1* and *MAPK1*. Additionally, genes involved in MHC class I (*HLA-B* and *HLA-C*) were present in these modules, showing elevated expression on days three to five in the critical group and on day three in the mild cohort. Also within the yellow module, the granule release marker *CD63* was identified as being more highly expressed in monocytes from critical patients throughout the study period compared to those from mild and healthy individuals.

To elucidate the functions that are suppressed during the critical progression of the disease, the analysis focused on the modules that negatively correlate with this phenotype: 'cyan', 'pink', and 'purple'. Pathway enrichment analysis on the genes from the 'cyan' module revealed significant enrichment in pathways related to “iron uptake and transport”, as well as “heparan sulfate and heparin metabolism” (Figure 30A). In the 'purple' cluster, genes essential for antigen presentation on MHC class II were identified (Figure 30B). Notably, there was a downregulation of HLA genes, *CD86*, and *CD1C*, as well as genes associated with the macrophage differentiation of monocytes such as *CCL5* in critical patients compared to mild and healthy donors (Figures 30C-D).

While no significant GO terms or pathways were enriched in the genes from the 'pink' module, a manual search identified genes that play roles in modulating the

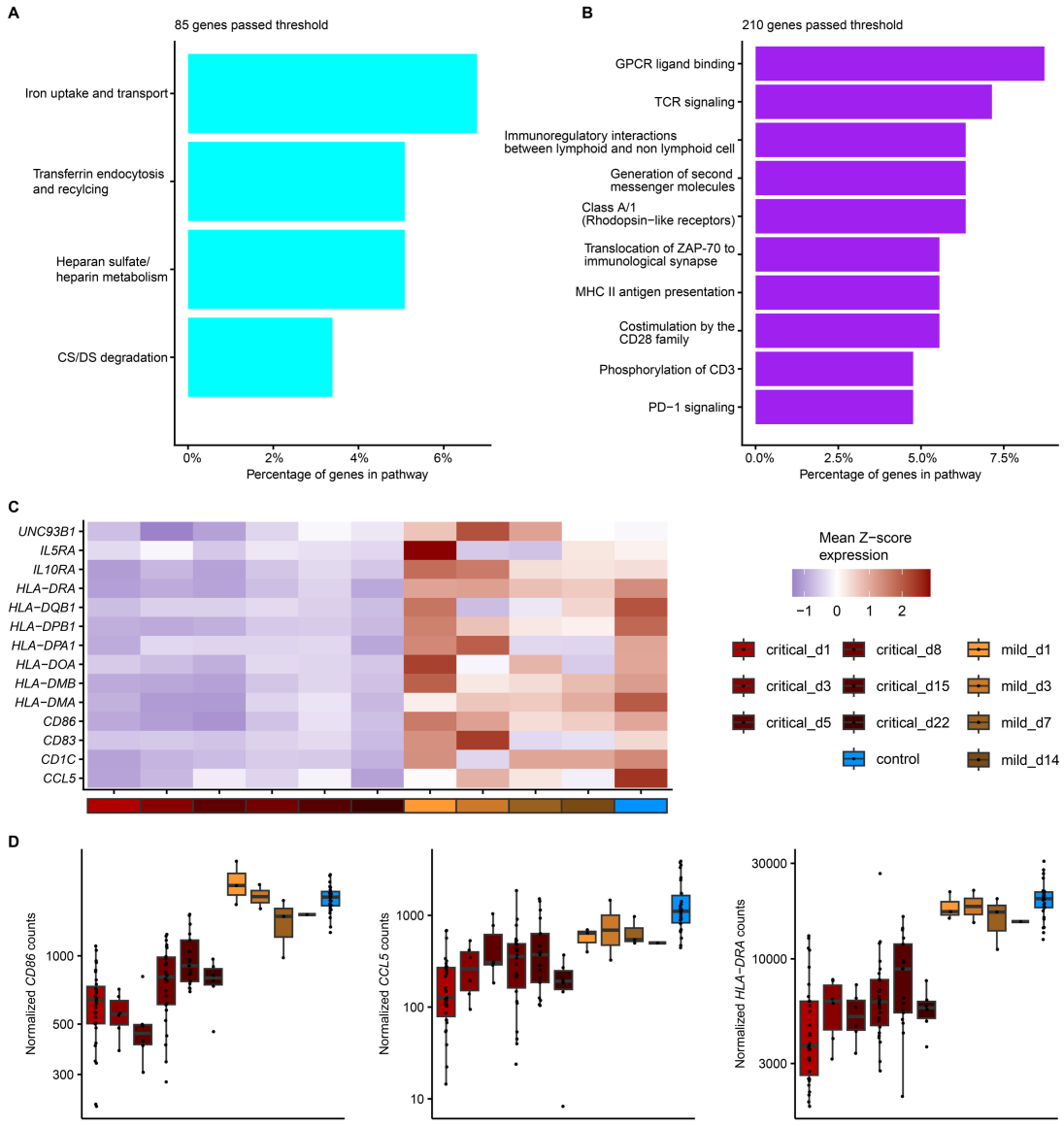

Figure 30: Functional enrichment and gene expression negatively correlating with critical COVID-19. Pathway enrichment of the 'cyan' **(A)** and 'purple' module genes **(B)**. Heatmap of mean z-score normalized gene expression of selected genes from enriched pathways **(C)**. Boxplots indicating normalized gene expression of *CD86, CCL5, HLA-DRA* **(D)**.

immune response, including *UNC93B1*, *IL5RA*, and *IL10RA*. This highlights specific immune functions that are diminished in critically ill patients, providing insight into the mechanisms that may contribute to the severity of the disease.

The WGCNA revealed profound differences in gene expression and functional orientation of classical monocytes that correlate with disease severity of COVID-19. Mild disease course is associated with upregulated genes involved in antigen presentation, such as *CIITA* and *CX3CR1*, and in interferon signaling pathways, including upregulation of genes as *IFIT1*, *ISG15*, and *OAS2*. These findings suggest that in mild COVID-19, monocytes effectively support the adaptive immune system's response against SARS-CoV-2, enhancing virus-targeted elimination. Conversely, in critical disease, there is a marked increase in the expression of genes associated with a pro-inflammatory immune response, including members of the S100 family like *S100A8*, *S100A9*, and *S100A11*, as well as *NFKB1*. This is accompanied by a negative correlation with the expression of MHC class II, *CD1C*, and *CD86*, indicating that although monocytes in severe cases are highly pro-inflammatory, they fail to perform adequately as professional APCs. This dysfunction may contribute to the lack of a targeted adaptive immune response, potentially explaining the cytokine storm, hyperactivation, and subsequent paralysis of T cells observed in severe COVID-19 cases.

4. Discussion

4.1 Assessing the immune response in COVID-19 using single cell RNA sequencing

The first study described in this thesis was conducted in Melbourne, Australia and employed single-cell RNA sequencing to profile the immune landscape of T and myeloid cells across varying severities of COVID-19. By integrating transcriptomic and protein expression data from approximately one million cells, we characterized major shifts in immune cell composition and function during the early stages of infection. Within the investigated immune cell compartments signatures of hyperinflammation, immune exhaustion, and impaired antiviral signaling in severe and critical cases was revealed. These findings provide mechanistic insights into how immune dysregulation contributes to COVID-19 severity and establish a high-resolution resource for future investigations.

Annotating sequenced single-cell datasets containing multiple cell types is a critical initial step before exploring functional changes across conditions of interest (Butler *et al.*, 2018). Manual annotation involves clustering cells using community detection algorithms such as Louvain or Leiden, where each cell is treated as a node in a network and the connections, or edges, between these nodes represent the similarity in their gene expression profiles (Traag *et al.*, 2019; Kiselev *et al.*, 2019). This similarity is often quantified using the Jaccard index, which measures the ratio of the intersection to the union of the genes expressed by the compared cells. By retaining only those edges that surpass a specified similarity threshold, the algorithm ensures the formation of clusters composed of cells that are transcriptionally similar and belong to the same local neighborhood (Stuart *et al.*, 2019). This method facilitates the identification of distinct cellular populations within the heterogeneous mixture, setting the stage for deeper analyses of their biological functions.

After clustering, the defined clusters of cells are analyzed to identify marker genes that distinguish them (Ianevski *et al.*, 2022). These markers can then be used to infer the cell types represented by each cluster or, in finer analyses, to differentiate cells within a type into specific subtypes based on their programming. However, manual annotation is inherently subjective and depends heavily on user-defined parameters such as clustering resolution, the number of neighbors in neighborhood graphs, and similarity thresholds. This variability can lead to irreproducibility across different users unless exact settings are known (Lähnemann *et al.*, 2020; Heumos *et al.*, 2023).

To address these challenges, automated annotation frameworks like *SingleR* and *Azimuth* have been developed (Clarke *et al.*, 2021). These tools use correlation measures, such as the Spearman coefficient, to compare gene expression in a target dataset against a reference dataset of known cell types, typically utilizing the most variable genes. However, these methods rely on reference datasets that may themselves contain sequencing noise, potentially leading to inaccurate annotations. Furthermore, the effectiveness of these tools diminishes when annotating cell types from tissues not represented in the reference datasets, as

cell programming can vary significantly between tissues. In our analysis to mitigate these issues, we have used a consensus annotation approach that combines results from multiple tools and reference datasets. For instance, *SingleR* has been applied using both the BlueprintEncode reference, based on 259 bulk RNA-seq samples, and the Monaco reference, which includes 114 bulk RNA-Seq profiles of sorted PBMCs. Additionally, the *Seurat*-built *Azimuth* pipeline utilizes a reference dataset comprising 24 sequenced single-cell samples from PBMCs. By integrating these diverse sources, we enhance the robustness and accuracy of the annotations.

Future enhancements to the proposed method could involve expanding the number of tools and reference datasets used for consensus annotation, potentially improving accuracy despite increasing computational requirements. Additionally, it would be advantageous to implement a weighting system for datasets and tools, tailoring their use according to their applicability to the specific dataset to study, such as compatibility with the tissue type or sequencing technology used. Moreover, the implementation of advanced machine learning techniques like *scGPT*, a pre-trained deep learning model developed with data from over 33 million single cells which has shown high accuracy and efficiency in cell type annotation.

Once the cells were grouped into major immune populations by consensus annotation, they were further clustered to delineate subtypes. During this analysis, some clusters identified Ig genes as markers for CD8+ T cell subtypes. The detection of Ig genes in about 50% of the total cells, albeit at low expression levels in both RNA and CITE-Seq, suggested these were technical artefacts rather than biological signals. Such occurrences are common in scRNA-seq experiments, particularly when utilizing droplet-based methods like those offered by 10x Genomics (Young and Behjati, 2020).

In a typical scRNA-seq workflow using droplet-based systems, a suspension of single cells is prepared, with each cell encapsulated into an individual oil droplet that contains barcodes and enzymes essential for reverse transcription and PCR

amplification (Kolodziejczyk *et al.*, 2015). Every transcript from a cell within a droplet is tagged with a unique molecular identifier (UMI) barcode, and additionally, each transcript receives a cell-specific barcode (Jovic *et al.*, 2022). This dual-barcoding allows for the precise identification and quantification of transcripts per cell, facilitating clear distinction between cells (Hwang *et al.*, 2018). Ideally, each droplet should encapsulate a single cell, and the cell's mRNA is released into the droplet for barcoding during cell lysis. However, during the passage of cells through the microfluidic channels, these can rupture or degrade and consequently release cell contents into the system (Muskovic and Powell, 2021). This leads to cell-free mRNA molecules being co-encapsulated and barcoded within droplets containing other cells, making them indistinguishable from endogenous transcripts. Consequently, these ambient RNA molecules are incorrectly assigned to a cell's transcriptome, representing artefacts rather than genuine cellular transcripts (Alvarez *et al.*, 2020).

These artefacts can significantly impact downstream analyses, such as cell annotation, clustering, and the interpretation of biological changes, potentially leading to erroneous conclusions (Caglayan *et al.*, 2022). To address these challenges, computational tools like *DecontX* and *CellBender* have been developed to improve data integrity. *DecontX* utilizes a Bayesian approach to estimate and remove artefact contamination from individual cells (Shiyi Yang *et al.*, 2020). However, it depends on pre-existing cell group annotations or performs heuristic clustering to define cell populations. This dependency is problematic because clustering itself is based on the transcriptional profiles of cells, which may be skewed by the very contaminants *DecontX* aims to eliminate. This creates a cyclical issue, the effective decontamination requires accurate cell clustering, but accurate clustering depends on having decontaminated counts.

Conversely, *CellBender* is an unsupervised machine learning model that identifies background noise by analyzing empty droplets within the dataset and subsequently subtracts this background from each cell-containing droplet (Fleming *et al.*, 2023). This method has proven effective in our hands, as *CellBender* was able to specifically and accurately correct counts without

introducing off-target effects. This cell type-specific correction ensures that the clustering and subsequent analyses reflect true biological signals.

Based on the analysis of isotype controls in our CITE-seq panel, it was observed that while *CellBender* effectively corrects for ambient RNA contamination, it does not address the issue of non-specific antibody binding during cell labelling, as the isotype controls ideally should not have counts. This problem is similarly encountered in flow cytometry experiments, where it is typically managed using compensation techniques and isotype controls to assess background signal (Andersen *et al.*, 2016). For normalizing CITE-seq data, a tool known as dsb is available, which adjusts for background signal, however, it does not specifically incorporate isotype control data for each labelled antigen, and instead generalizes background correction without aligning it precisely with corresponding isotype controls (Mulè *et al.*, 2022). Due to this limitation, we opted to refine our approach to influence clustering outcomes more accurately. We decided to filter the markers used to construct the principal components for every cell type based on their expression relative to isotype control background levels, specifically excluding those markers whose expression was below this threshold. In addition, a newly published Bayesian hierarchical model called *DecontPro* shows promise for addressing these complexities, as it is designed to correct for both ambient contamination and non-specific binding (Yin *et al.*, 2024).

Following the correction of counts, the major immune cell types were clustered to identify subgroups, revealing significant changes within the T cell compartment. Notably, there was a marked increase in the proportions of CD8+ TEM and IFN-stimulated terminal effector CD8+ T cells in diseased individuals compared to healthy controls. These IFN-stimulated T cells play a pivotal role in mounting an effective immune response and controlling infections (Unterman *et al.*, 2022). In the CD4+ T cell population, there was a notable rise in the proportions of Tregs in patients with moderate and severe/critical COVID-19 compared to those with mild symptoms. This increase suggests that Tregs may potentially inhibit effector T cells from clearing the viral infection while simultaneously exacerbating inflammatory responses, leading to poorer outcomes (Galván-Peña *et al.*, 2021;

Saheb Sharif-Askari *et al.*, 2023). While Tregs are crucial for preventing excessive inflammation and facilitating the resolution of infection, their premature or excessive activity could compromise viral clearance, thus contributing to more severe disease manifestations (Jovisic *et al.*, 2023). Conversely, an increase in cytotoxic CD4+ T cells was observed in the mild patient group compared to healthy individuals, indicating that these CD4+ T cells might be assisting NK and CD8+ T cells in eliminating MHC class II-presenting infected cells (Devarajan *et al.*, 2023). Although previous studies have correlated highly activated and cytotoxic CD4+ T cells with disease progression and increased hospitalization rates, no significant differences in the proportions of these cells across disease severities were observed in this dataset (Meckiff *et al.*, 2020; Moss, 2022; Baird *et al.*, 2023). Moreover, there was a notably lower proportion of both type I IFN and TCR-activated and type I IFN-activated CD4+ T cells in moderate and severe/critical cases compared to milder cases. This observation suggests an impaired development of T helper type 1 cells, which are crucial in coordinating antiviral immunity (Huber and David Farrar, 2011; Swain *et al.*, 2012) . The deficiency in these cells likely contributes to an ineffective immune response in patients with more severe forms of the disease (Zheng *et al.*, 2020; Gazzinelli-Guimaraes *et al.*, 2022).

In the myeloid cell compartment, a significant increase in the proportion of inflammatory classical monocytes was observed in diseased patients compared to healthy donors. Furthermore, an increase in the proportions of classical monocytes was noted in patients with moderate and severe/critical disease relative to those with mild disease. Given that these populations express pro-inflammatory markers such as *S100A8/9* and *LYZ*, it is suggested that they are substantially involved in the production of pro-inflammatory cytokines during the acute phase of SARS-CoV-2 infection. The elevated levels of highly activated and pro-inflammatory monocytes are implicated in the progression of the disease (Schulte-Schrepping *et al.*, 2020; Rajamanickam *et al.*, 2021; Vanderbeke *et al.*, 2021). Conversely, there was a noticeable decrease in non-classical monocytes across increasing disease severities compared to healthy controls. Non-classical

monocytes, known for their high phagocytic potential, play a critical role in the antiviral immune response and in facilitating disease resolution (Wong *et al.*, 2011; Boyette *et al.*, 2017). The reduction or depletion of these cells may contribute to the development of a severe disease course (Gatti *et al.*, 2020; Vanderbeke *et al.*, 2021). Although not statistically significant, a similar trend was observed in mDCs, which are crucial for bridging the innate and adaptive immune responses through antigen presentation and the licensing of T cells (Pérez-Gómez *et al.*, 2021). Other studies have also noted a correlation between disease severity and reduced numbers of DCs, suggesting that their depletion may delay effective T cell activation (Rajamanickam *et al.*, 2022). This delay can lead to a extended pro-inflammatory immune response that causes extensive tissue damage instead of facilitating viral clearance (R. Zhou *et al.*, 2020; Sánchez-Cerrillo *et al.*, 2020). This changes in the proportion of the myeloid cell compartment underscores the importance of maintaining a balanced myeloid cell response to prevent exacerbated inflammatory reactions and ensure effective viral control.

Transcriptional changes were observed across the myeloid cells in patients with mild COVID-19 compared to healthy individuals. These changes included upregulation of ISGs and downregulation of genes involved in translation, a strategy commonly used to limit viral replication during infections. Such patterns are consistent with the body's typical response to viral infections, including influenza, and have been correlated with non-hospitalization in other studies (Zhai *et al.*, 2015; Shaath *et al.*, 2020; Pekayvaz *et al.*, 2022). Additionally, pathway enrichment analysis revealed enrichment of interferon signaling and MHC II antigen presentation pathways among the downregulated genes in patients with moderate, severe, and critical COVID-19 compared to those with mild symptoms, aligning with findings from other studies (Hadjadj *et al.*, 2020; Liu and Li, 2023). The deficient or delayed interferon response, coupled with reduced antigen presentation by professional APCs may contribute to the severe disease progression observed in COVID-19, underscoring the importance of a robust and

timely immune response in mitigating severe outcomes (Robertson *et al.*, 2023; Gressier *et al.*, 2023; Lin *et al.*, 2024).

In classical monocytes, a gradual downregulation of *CLEC4A* was observed with increasing severity of COVID-19. CLEC4A, is a PRR that possesses an intracellular immunoreceptor tyrosine-based inhibitory motif (ITIM), and plays a crucial role in regulating immune responses by negative regulation of TLR signaling upon activation (Uto *et al.*, 2016). The absence of CLEC4A has been demonstrated to enhance the activation of DCs and macrophages upon TLR stimulation (Nasu *et al.*, 2020; Park *et al.*, 2022). In the context of COVID-19, the downregulation of CLEC4A may lead to an hyperactivation of monocytes through TLR signaling by viral-induced cell death DAMPs, leading to an overdrive of pro-inflammatory pathways. Additionally, classical monocytes in more severe cases of COVID-19 exhibited higher levels of *IL10* transcripts, which is critical for resolving inflammation and maintaining homeostasis (Iyer and Cheng, 2012). However, a premature increase in IL10 has been linked to the induction of exhausted T cell phenotypes and an increased likelihood of hospitalization in COVID-19 patients (Hadjadj *et al.*, 2020; Han *et al.*, 2020; L. Yang *et al.*, 2021). This suggests that while IL10 is generally beneficial, its early and elevated expression during acute COVID-19 may interfere with effective immune responses, ultimately affecting the disease outcome.

Inflammatory classical monocytes in severe cases of COVID-19 showed an upregulation of the IL10 signaling pathway, alongside the expression of pro-fibrotic markers such as *CD163*, which suggests an enhanced pro-fibrotic response that may contribute to the severity of lung pathology observed in ARDS in severely ill patients (Schulte-Schrepping *et al.*, 2020; Wendisch *et al.*, 2021; Kvedaraite *et al.*, 2021). Furthermore, these monocytes exhibited high levels of transcripts for the pro-inflammatory gene *S100A8* increasing with each severity, a potent chemoattractant and activator of neutrophils. S100A8 also activates other cell types through TLR4 signaling, playing a significant role in the pro-inflammatory cascade (Chakraborty *et al.*, 2017; Tan *et al.*, 2017). The involvement of neutrophils is notable in the pathology of both COVID-19 and

influenza infections, underscoring the common inflammatory mechanisms these respiratory viruses induce leading to ARDS (Camp and Jonsson, 2017; Zuo *et al.*, 2020; Cavalcante-Silva *et al.*, 2021; Guo *et al.*, 2021).

The non-classical monocytes have been identified to present an anti-inflammatory phenotype, displaying low antigen presentation capacity while expressing markers like *MERTK*, crucial for the efficient phagocytosis of apoptotic cells and the resolution of inflammation (Rothlin *et al.*, 2007; Lemke, 2013). In severe cases of disease, however, these monocytes are significantly underrepresented, emphasizing the importance of a balanced immune response in managing inflammation effectively. The scarcity of non-classical monocytes in severe conditions highlights their vital role in controlling inflammatory processes and clearing dead cells, which, if accumulated, may trigger hyperinflammation through the release of DAMPs.

In more severe cases of COVID-19, mDCs showed a significant transcriptional shift characterized by pro-inflammatory activation coupled with a decrease in antigen presentation capabilities, marked by the downregulation of genes associated with MHC class II and *CD1C*. Such changes suggest the predominance of immature dendritic cells in the periphery or the presence of exhausted and dysfunctional DCs (Jin *et al.*, 2010). This impaired dendritic cell function can critically hinder the activation of CD8 T cells and their subsequent induction of IFN-γ, a key cytokine in mounting an effective antiviral response (Saichi *et al.*, 2021). Consequently, the compromised ability of these dendritic cells to properly present antigens and activate T cells may be a contributing factor to the exacerbated severity observed in patients with severe COVID-19, reflecting a disrupted immune mechanism crucial for controlling viral infections.

In summary, this study highlighted that severe COVID-19 is characterized not only by a shift towards increased pro-inflammatory cell populations but also by reduced populations of IFN-activated cells. Additionally, cells within the myeloid compartment exhibited diminished IFN signaling and antigen presentation capabilities while displaying enhanced pro-inflammatory activation. These

findings underscore the complex immunological dysregulation that contributes to the severity of the disease, pointing to critical areas for potential therapeutic intervention.

4.2 Comparative analysis of antibody titers against the spike protein of SARS-CoV-2 variants in infected patient cohorts and diverse vaccination regimes

The second study presented in this thesis was conducted independently from the single-cell RNA-seq analysis and focuses on the humoral immune response to SARS-CoV-2. Performed at the University Hospital Bonn, this investigation aimed to quantify and compare antibody titers against the spike protein across various patient cohorts, including naturally infected individuals and those receiving different vaccination regimens. By evaluating how antibody levels vary with disease severity and vaccine type, this study provides important insights into the dynamics and durability of vaccine-induced and infection-induced immunity.

At the outset of the SARS-CoV-2 pandemic, there was a critical need to reduce the number of severely ill COVID-19 patients as healthcare systems worldwide were overwhelmed with demands for beds in the ICU, with patients overflowing into hospital corridors. The crisis intensified when healthcare workers contracted the SARS-CoV-2, leading to a substantial reduction in medical staff. In response, pharmaceutical companies and governmental agencies rapidly mobilized to create an effective vaccine as fast as possible against SARS-CoV-2, designed to elicit a robust humoral response by generating neutralizing antibodies targeting the S protein.

In March 2020, the U.S. Food and Drug Administration (FDA) and the EMA hosted the initial global regulatory meeting to strategize on expediting the development of vaccines against SARS-CoV-2 (The United States Food and Drug Administration, 2020). To speed up the testing and approval of the vaccines, there was an exception made and the traditional sequential conduct of clinical trial phases (1-3) was altered to a parallel execution (Kim *et al.*, 2021). By December 2020, the safety and efficacy of the first COVID-19 vaccine Comirnaty was published and shortly afterwards the FDA and EMA granted an emergency

use authorization (EUA) for Comirnaty, targeting the prevention of COVID-19 in individuals older than 16 (Polack *et al.*, 2020; Fortner and Schumacher, 2021). Following this, vaccines developed by Moderna, AstraZeneca, and Janssen-Cilag were approved in that sequence, ensuring that by the year's end-merely one year from the pandemic's start, a number of vaccines had been authorized for use in the US and Europe (Hotez *et al.*, 2021). The follow-up period for these approval studies was only about two months, leaving many questions about antibody dynamics unanswered. Numerous subsequent studies evaluated the differences among these vaccines (Rotshild *et al.*, 2021; Meo *et al.*, 2021; Fan *et al.*, 2021; Xie *et al.*, 2022). Importantly, the production of neutralizing antibodies against the S protein led to reduced viral loads and hospitalizations in vaccinated individuals, underscoring the effectiveness of vaccination (Favresse *et al.*, 2021; Thompson *et al.*, 2021; Andrews *et al.*, 2022).

Patients with comorbidities such as obesity and diabetes mellitus have been identified to be at risk of developing severe COVID-19 (Tao Chen, Wu, *et al.*, 2020; Brochot *et al.*, 2020). However, in this study no significant correlations were found between these conditions and anti-spike antibody titers across the patient cohorts, which included individuals with obesity, hypertension, or diabetes. Regardless of the vaccine type administered or the stage of COVID-19, the range of maximum IgG anti-Spike antibody titers was consistent and similar to those observed in healthy participants who had received a single dose of any COVID-19 vaccine. These results align with prior research indicating that IgG and IgM antibodies against the S and N proteins of the virus stabilize approximately two weeks after infection (Brochot *et al.*, 2020; Bao *et al.*, 2021; Wei *et al.*, 2021). Additionally, it was documented a decline in anti-Spike antibodies six months post-infection in individuals who have recovered from COVID-19 as well as those suffering from long COVID. This trend overlaps with findings from a cohort study examining long-term health outcomes in COVID-19 patients after hospital discharge (Huang *et al.*, 2021). Importantly, it was observed that administering a single dose of an mRNA vaccine six months post-infection significantly boosted antibody levels to those comparable with fully vaccinated control groups. This

enhancement suggests that vaccination after infection can be beneficial, even months following initial recovery, to sustain adequate antibody levels. These findings reinforce previous recommendations that advocate for the vaccination of individuals who have previously contracted the virus (Hall *et al.*, 2022).

It was observed that administering three doses of the BT vaccine generated long-lasting α-Spike RBD antibodies with robust neutralizing capabilities, effective against not only the initial Wuhan strain but also subsequent VOC, including alpha, beta, and gamma. Notably, the beta variant showed the greatest resistance to neutralization among the initial four VOCs, including the delta variant (Corbett *et al.*, 2021). This resistance was demonstrated by comparatively lower beta-specific antibody titers and neutralization capacity observed in both vaccinated individuals and patients with severe COVID-19, relative to other strains. In contrast, a separate study reported a lack of any neutralizing response against the beta variant in sera from elderly individuals who had received two doses of the BT vaccine (Newman *et al.*, 2022). This discrepancy underscores the influence of factors such as age and vaccination dosage on the immune response, suggesting that vaccine efficacy may vary significantly across different subgroups of the population and SARS-CoV-2 variants. These results emphasize the need of a third vaccination or inoculations with vaccines tailored to newer variants to sustain a robust antibody response against evolving strains of SARS-CoV-2.

Although most COVID-19 vaccines were generally well tolerated, some recipients experienced mild side effects, such as flu-like symptoms (El-Shitany *et al.*, 2021). Serious side effects, such as myocarditis and thrombosis, were also reported (Higgins *et al.*, 2022; Ling *et al.*, 2022). In this study, no participants reported severe side effects. Common mild side effects included pain at the injection site, headache, fatigue, and occasionally fever, all of which resolved within a day. Severe hyperinflammatory reactions are rare but have been documented in other studies following mRNA and vector-based COVID-19 vaccinations (Bindoli *et al.*, 2022). Abnormal cytokine levels might serve as the primary cause of hyperinflammatory reactions (Gustine and Jones, 2021). Previous investigations

of cytokine levels post-BT vaccination revealed a significant increase in IFNγ after the second dose (Arunachalam *et al.*, 2021). This study confirms similar findings for AZ and MO vaccines. Specifically, an increase in the pro-inflammatory cytokine IL1β was observed in participants' sera 24 hours post-MO vaccination. Cytokine levels returned to normal within two days, indicating that mRNA-based COVID-19 vaccines induce a transient inflammatory immune response in healthy individuals. In cases of hyperinflammatory reactions due to COVID-19 vaccination, the IL1 receptor antagonist anakinra effectively mitigated the excessive immune response (Perna *et al.*, 2022; Conte *et al.*, 2022; Bindoli *et al.*, 2022).

COVID-19 vaccination has also been associated with adverse reactions in individuals treated with certain dermal fillers, such as hyaluronic acid, polymethyl-methacrylate, and fluid silicone (Kalantari *et al.*, 2022). In a case study, 20 patients who had received dermal fillers reported swelling, redness, and other inflammatory reactions at the injection site immediately after receiving a COVID-19 vaccine (Alijotas-Reig *et al.*, 2022). It has been hypothesized that dermal fillers may sensitize the body to polyethylene glycol (PEG) particles, which are used as stabilizers in mRNA COVID-19 vaccines and are linked to anaphylaxis (Zerbinati *et al.*, 2020; Sellaturay *et al.*, 2021; Sellaturay *et al.*, 2022; Kelso, 2022; Kozma *et al.*, 2023). Given that PEG is widely used in pharmaceuticals, cosmetics, and food products, the immune system might have been pre-activated and may explain the adverse events following COVID-19 vaccination (Wylon *et al.*, 2016; Cox *et al.*, 2021; Mortz *et al.*, 2022). Another possible source of inflammatory immune reactions to mRNA-based vaccines is the lipid compounds used to encapsulate the mRNA for transfection into human cells. Recent studies have shown that membrane-destabilizing lipids can activate the NLRP3 inflammasome and induce pro-inflammatory cytokine secretion in murine and human immune cells (Tahtinen *et al.*, 2022; Forster *et al.*, 2022).

Notably, we found that patients with critical COVID-19 exhibited significantly elevated levels of IL10 in their blood. Similar findings by other researchers suggest that increased IL10 levels may contribute to the pathogenesis of severe

COVID-19 by exacerbating viral sepsis-related hyperinflammation and exhausting functional T cells (Diao *et al.*, 2020; L. Lu *et al.*, 2021). IL10 is produced by various immune cells to help re-establish immune homeostasis after an infection (Rojas *et al.*, 2017). While this study did not pinpoint the exact source of IL10, it is plausible that Tregs (Neumann *et al.*, 2020; Galván-Peña *et al.*, 2021), or monocytes, as discussed in a previous chapter, are responsible for the elevated IL10 levels observed in critically ill COVID-19 patients (Q. Yang *et al.*, 2021).

Additionally, our study focused on examining the dynamics and expansion of class-switched memory B cells and circulating Tfh cells, which are crucial for establishing immunity against pathogens (Akkaya *et al.*, 2020). Consistent with previous research, we observed that class-switched B cells expanded rapidly following the onset of symptoms (Hartley *et al.*, 2020). This expansion correlated with increasing α-Spike-Abs titers and the number of Tfh cells during the initial stage of infection. At later stages of unresolved SARS-CoV-2 infections, higher frequencies of class-switched memory B cells and Tfh cells were noted in deceased critically ill patients compared to survivors, resulting in an increased Tfh/Treg ratio. An elevated Tfh/Treg ratio has previously been linked to autoimmune diseases such as systemic lupus erythematosus (Xu *et al.*, 2017). Additionally, IL10-producing Tfh cells have been shown to contribute to impaired immune responses with age, potentially explaining the severe progression and increased mortality of COVID-19 in older patients (Almanan *et al.*, 2020).

The objective of this study was to investigate the dynamics of Ab development against SARS-CoV-2 Spike across various vaccination cohorts and SARS-CoV-2 infected individuals. Since the precise infection-preventing Ab titers are still undetermined, the produced Ab titers by probands from different vaccination regimens were compared. Cytokine levels were assessed to evaluate potential inflammatory responses to the vaccines. In spite of the small sample size, a broad perspective on multiple vaccination strategies was created, demonstrating that even individuals who have recovered from COVID-19 benefit from vaccination. Regarding side effects, findings indicated that COVID-19 vaccination triggered a

low-grade, barely detectable systemic inflammatory response, which was quickly contained and reversed.

4.3 Programming of peripheral classical monocytes during COVID-19

The third study described in this thesis was independently conducted to investigate the transcriptional programming of peripheral classical monocytes during SARS-CoV-2 infection. Focusing on $CD14^{+}$ monocytes as accessible surrogates for tissue-resident antigen-presenting cells, this analysis aimed to uncover how monocyte function varies with disease severity. Using bulk RNA sequencing of samples from donors with mild, critical, and no infection, the study revealed distinct gene expression patterns associated with antiviral responses, inflammation, and immune dysregulation. These results offer valuable insights into how early innate immune programming may influence disease progression and severity in COVID-19.

The monocytes of patients hospitalized in the ICU due to severe COVID-19 symptoms were isolated and their transcriptomes were analyzed to identify gene expression profiles differing from those of healthy individuals and patients with mild disease. This analysis aimed to uncover the transcriptomic programming of monocytes that may contribute to the severity of SARS-CoV-2 infection. A higher prevalence of males in the ICU with COVID-19 was observed in the study, a finding also reported by other studies that a greater proportion of males are admitted to the ICU and a three times higher mortality rate of men from COVID-19 (Gebhard *et al.*, 2020; Jin *et al.*, 2020).

Strong evidence suggests that sexual dichotomy plays a key role in the epigenetic and hormonal regulation of both the innate and adaptive immune systems during viral infections, potentially explaining the higher COVID-19 mortality in males (Bienvenu *et al.*, 2020; Mangiola *et al.*, 2024). In mouse models, estrogens have been shown to mitigate the severity of infections with influenza by reducing pro-inflammatory cytokine secretion (Nguyen *et al.*, 2011; Pazos *et al.*, 2012; Vermillion *et al.*, 2018). The removal of ovaries in female mice increased mortality due to infection with SARS-CoV to levels similar to those observed in male mice,

indicating that hormonal balance directly influences the antiviral response in infections with coronaviruses (Channappanavar *et al.*, 2017). In humans, the mortality and intubation rate of males due to COVID-19 with prostate cancer was higher than in the males with any other oncological disease (Chakravarty *et al.*, 2020; Montopoli *et al.*, 2020).

Further reports indicate that macrophages from female mice exhibit higher expression of interferon-stimulated genes such as Irf7 compared to male mice, suggesting a potential for a stronger innate immune response to viral pathogens (Gal-Oz *et al.*, 2019). Sex-related epigenomic changes have also been observed in PBMCs, with monocytes from males showing enrichment of several inflammation-related gene modules, with genes from these modules presenting enhanced gene expression, and increased chromatin accessibility (Márquez *et al.*, 2020). This suggests that males may be predisposed to a higher baseline level of pro-inflammatory activity, which could contribute to the cytokine storm and increased likelihood of severe COVID-19 outcomes (Hadjadj *et al.*, 2020; Blanco-Melo *et al.*, 2020).

The most frequently reported comorbidity among ICU-admitted COVID-19 patients in this study was hypertension, affecting more than half of the patients. Early in the pandemic, it was reported that patients requiring hospitalization often had a history of hypertension, which was also associated with higher mortality rates (S. Huang *et al.*, 2020; Sardu *et al.*, 2020; Trump *et al.*, 2021). While a direct causal relationship is fully established, older individuals, who have a higher incidence of hypertension, are more likely to develop severe COVID-19 (F. Zhou *et al.*, 2020). On the other hand, multiple studies have demonstrated that hypertension is linked to hyperinflammation and oxidative stress (Patrick *et al.*, 2021). This pre-existing inflammation can be exacerbated during SARS-CoV-2 infection, contributing to the cytokine storm during COVID-19 that leads to endotheliitis and increased vascular permeability (Gallo *et al.*, 2022). Vascular inflammation also activates platelets and disrupts the clotting cascades, resulting in microthrombosis and potentially causing vascular events such as stroke,

myocardial damage, severe hypoxia, and respiratory distress (Gattinoni *et al.*, 2020; Lindner *et al.*, 2020; Nannoni *et al.*, 2021).

The second most frequent comorbidity identified in this study in patitents at the ICU was Diabetes mellitus type 2. Earlier studies reported that underlying diabetes mellitus is common amont the patients admitted to the ICU, but since diabetes is typically a disease frequent in elderly it is not known whether diabetes is a risk factors for COVID-19 above the advanced age. Furthermore, usual complications of diabetes such as cardiovascular disease and chronic kidney disease also were shown to increase the COVID-19 mortality and severity rate. One potential explanation might be that hyperglycaemia sustains viral replication of SARS-CoV-2. Via ROS production and activation of hypoxia-inducible factor 1α, and patients with poor glycaemic control were shown to have an increased need for medication, hospitalization and mortality. Additionally, it was previously shown that individuals with impaired glucose tolerance or diabetes mellitus have reduced NK cell activity, which might help to explain why patients with diabetes mellitus are more susceptible to COVID-19 and have a worse prognosis than those without diabetes mellitus.

The second most frequent comorbidity identified in ICU patients in this study was Type 2 Diabetes Mellitus. Earlier studies have reported that underlying diabetes mellitus is common among patients admitted to the ICU (Piva *et al.*, 2020; Myers *et al.*, 2020). However, since diabetes is typically more prevalent in the elderly, it is unclear whether diabetes itself is an independent risk factor for severe COVID-19 beyond the risks associated with advanced age (Lim *et al.*, 2021). Additionally, common complications of diabetes, such as cardiovascular disease and chronic kidney disease, have been shown to increase COVID-19 mortality and severity rates (Goyal *et al.*, 2020; Holman *et al.*, 2020). One potential explanation is that hyperglycemia supports SARS-CoV-2 viral replication in infected monocytes, thus inducing ROS production and activation of hypoxia-inducible factor 1α, which further promotes glycolysis and viral transcription and translation (Codo *et al.*, 2020). Patients on insulin required increasingly higher doses during SARS-CoV-2 infection and those with poor glycemic control have been shown to have

an increased need for medication, higher rates of hospitalization, and greater mortality (Critchley *et al.*, 2018; Zhu *et al.*, 2020; L. Wu *et al.*, 2020). Additionally, previous studies have shown that individuals with impaired glucose tolerance or diabetes mellitus exhibit decreased NK cell activity, suggesting that the ineffective clearing of infected cells may contribute to the development of severe disease (Kim *et al.*, 2019).

From the beginning of the pandemic, physicians have sought laboratory markers to identify patients at high risk of developing severe COVID-19, enabling timely supportive care and ensuring ICU access if necessary. One of the earliest identified indicators was lymphocytopenia and neutrophilia (Anurag *et al.*, 2020; J. Liu *et al.*, 2020). The neutrophil-to-lymphocyte ratio, a widely used parameter to assess systemic infection and inflammation, quickly became a predictive marker for COVID-19 severity, similar to its use in assessing pneumonia prognosis during bacterial infections (Curbelo *et al.*, 2017; Kong *et al.*, 2020). Consistent with other research, this study found that severe COVID-19 patients had a higher neutrophil-to-lymphocyte ratio which improved over the time on the ICU, reflecting the imbalance between inflammatory and immune responses (Y. Liu *et al.*, 2020; Peñaloza *et al.*, 2021). The neutrophil-to-lymphocyte ratio was previously shown to correlate with age, inflammatory markers such as C-reactive protein (CRP) and higher mortality rates (Jimeno *et al.*, 2021). One potential explanation for the association between high neutrophil-to-lymphocyte ratio and severe COVID-19 is that a balanced immune response is crucial for clearing a viral infection such as SARS-CoV-2 (Li *et al.*, 2022). A high number of neutrophils infiltrating the lungs can secrete pro-inflammatory cytokines directly and induce further cytokine secretion through NETosis (Zuo *et al.*, 2020; Yaykasli *et al.*, 2021). The resultant high cell death rate caused by neutrophil-induced damage disrupts the microvasculature in the lungs, thus impairing its function and leading to thrombosis (Arcanjo *et al.*, 2020; Veras *et al.*, 2020; Middleton *et al.*, 2020). Additionally, studies have shown that a robust CD8+ T cell response aided by helper CD4+ T cells is vital for clearing viral infections such as SARS-CoV-2 (Janssen *et al.*, 2005; Hamilton *et al.*, 2006; Mazzoni *et al.*, 2020; Kusnadi *et al.*,

2021; Mallajosyula *et al.*, 2021). Therefore, insufficient cellular immune response due to lymphopenia could be a key factor leading to severe COVID-19 (André *et al.*, 2022). This supports the idea that a high neutrophil-to-lymphocyte ratio might contribute to severe disease by indicating an imbalanced immune response (Higaki *et al.*, 2022).

The WGCNA performed on the transcriptional profiles of monocytes isolated from patients with mild or severe COVID-19, as well as from healthy controls, over a two-week period identified various gene expression patterns in monocytes linked to immunological processes. These gene expressions correlated with the days following inclusion in the study, potentially providing insights into the development of critical COVID-19. This longitudinal analysis helps to identify specific immunological changes over time that may contribute to disease severity.

In the early days following inclusion in the study, and potentially soon after the onset of symptoms, genes from two major pathways: interferon-stimulated genes and antigen presentation, were identified as correlating with mild disease and inversely correlating with critical COVID-19. The genes involved in antigen presentation that showed positive correlation and expression in SARS-CoV-2 infected donors with mild symptoms compared to those with severe symptoms included CIITA, IRF1, and CCR7. CIITA, induced by IFNγ through the JAK-STAT-IRF1 signaling pathway, is the master transcriptional regulator of MHC molecules. It induces the expression of MHC II and enhances the constitutive expression of MHC I, initiating antigen presentation to CD4 and CD8 T cells. Viruses have evolved mechanisms to interfere with the JAK-STAT pathway, thereby inhibiting the antiviral immune response by blocking ISGs and indirectly downregulating MHC through CIITA and antigen presentation. SARS-CoV-2's main protease, NSP5, has been shown to use HDAC2 to inactivate CIITA through deacetylation. Similar to the findings of this study, low CIITA expression has been shown to indicate severe disease, confirming that SARS-CoV-2 manipulates the antigen presentation pathway to evade the immune response by inhibiting the master regulator. CCR7 upregulation and expression, as a consequence of antigen encounter, leads to monocyte migration to the draining lymph nodes for antigen

presentation to T cells. This further suggests an impairment of antigen presentation and an inability to specifically activate T cells in critically ill COVID-19 patients.

Correlating with the mild disease within the first days after inclusion into the study and potentially not long after the onset of symptoms were identified genes from two major pathways, interferon stimulated genes and antigen presentation correlating with mild disease and inversely correlating with critical COVID-19 phenotype.

The genes involved in antigen presentation that showed positive correlation and expression in SARS-CoV-2 infected donors with mild symptoms, compared to those with severe symptoms, included *CIITA, IRF1, CCR7, CD86*, and *HLA* class II genes. CIITA, induced by IFNγ through the JAK-STAT-IRF1 signaling pathway, is the master transcriptional regulator of MHC molecules. It induces the expression of MHC II and enhances the constitutive expression of MHC I, initiating antigen presentation to CD4 and CD8 T cells (Chang *et al.*, 2002). Viruses, including SARS-CoV-2, have developed mechanisms to interfere with the JAK-STAT pathway, thereby inhibiting the antiviral immune response by blocking ISGs and downregulating MHC through CIITA (Hegde *et al.*, 2003; Da-Yuan *et al.*, 2021). SARS-CoV-2's main protease, NSP5, has been shown to use HDAC2 to inactivate CIITA through deacetylation (Taefehshokr *et al.*, 2024). Additionally, low CIITA expression in monocytes and dendritic cells is indicative of severe disease, confirming that SARS-CoV-2 manipulates the antigen presentation pathway to evade the immune response by inhibiting this master regulator (Cai *et al.*, 2021; Argüello González *et al.*, 2022). This disruption of CIITA function is observed in this study due to the downregulation of HLA class II genes, such as *HLA-DRA, HLA-DQB1, HLA-DPB1, HLA-DPA, HLA-DOA, HLA-DMB*, and *HLA-DMA*, aligning with findings from other studies indicating low expression in severe COVID-19 cases (Giamarellos-Bourboulis *et al.*, 2020; Schulte-Schrepping *et al.*, 2020; Hasan *et al.*, 2022; Dobi *et al.*, 2022; Henao-Agudelo *et al.*, 2024). Additionally, the co-stimulatory molecule CD86, necessary for efficient T cell activation after antigen presentation, was also identified to

negatively correlate with disease severity (Kreutmair *et al.*, 2021). SARS-CoV has been shown to infect DCs to impede their maturation and maintain low levels of CD86, suggesting a similar strategy used by SARS-CoV-2 (Borcherding *et al.*, 2021). CCR7 upregulation and expression, following antigen encounter, lead to monocyte migration to draining lymph nodes for antigen presentation to T cells (Winkler *et al.*, 2024). This indicates that in donors with mild symptoms, inflammatory monocytes capable of antigen presentation successfully relocate to the lymph nodes. In contrast, critically ill patients experience not only impaired antigen presentation but also limited access of monocytes to the lymph nodes (Hopkins *et al.*, 2023). Overall, these results suggest that SARS-CoV-2 employs potential viral escape mechanisms by impeding antigen presentation, thus evading the immune response.

Genes associated with the interferon signaling pathway identified in this study included *AXL, IFIT1, IFIT2, IFITM2, IRF7, ISG15,* and *OAS2*, which strongly correlated with donors experiencing mild COVID-19 in the initial days following their inclusion in the study. The IFIT gene family, a well-characterized group of ISGs, is induced shortly after infection (Sen and Sarkar, 2007), functioning to limit viral replication by inhibiting the translation of viral proteins from RNA through eIF3 and by directly binding to viral proteins essential for replication (Guo *et al.*, 2000; Wang *et al.*, 2003; Hui *et al.*, 2003; Saikia *et al.*, 2010). Studies indicate that the IFIT family proteins can also limit the replication of SARS-CoV-2 by sequestering single-stranded 5′-ppp or 2′-O-unmethylated RNA, suggesting a critical host defense mechanism at the onset of COVID-19 infection (Martin-Sancho *et al.*, 2021; X. Zhao *et al.*, 2022). Additionally, IFITM2, which is constitutively expressed in all cells and robustly induced upon interferon signaling, inhibits the entry of various viruses into the host cytoplasm, including Influenza, Ebola virus, and both SARS-CoV-1 and SARS-CoV-2 (Diamond and Farzan, 2013; Winstone *et al.*, 2021). The interferon regulatory factor IRF7, involved in the positive regulation of type I interferon production, has been linked with severe COVID-19, as inborn deficiencies of the IRF7 gene have been identified in patients with life-threatening pneumonia due to COVID-19 (Zhang *et*

al., 2020). The SARS-CoV-2 papain-like protease was demonstrated to alter the interferon-induced ubiquitin-like modifier ISG15, known to limit the replication and egress of pathogens, thereby driving the aberrant macrophage immune response (Munnur *et al.*, 2021). Mutations in the protein OAS2, which binds dsRNA products and marks them for degradation to limit viral replication, have been shown to be linked to MIS-C in children and to high-risk patients for developing severe COVID-19 (Schmiedel *et al.*, 2021; Lee *et al.*, 2022). The TAM family member protein AXL, primarily functioning to limit TLR signaling and induce apoptotic cell removal, was found to correlate with mild disease in this study (Lemke and Rothlin, 2008). Although other studies indicate that AXL expression is linked with increased infection of lung epithelial cells, with its soluble part in the serum correlating with disease severity and proposed as an indicator of deterioration and disease progression, it is important to note the identification of its expression in CD14+ monocytes in this study (S. Wang *et al.*, 2021; You *et al.*, 2024). This suggests that the timing and the specific cell type expressing AXL might play a decisive role in COVID-19 disease severity. Taken together, these findings underscore the critical role of interferon pathways and the involved genes during the initial phase of the disease in controlling SARS-CoV-2 infection.

Highly correlative with critical cohort were found genes involved in the pro-inflammatory pathways. Genes from the S100 family of alarmins were strongly upregulated in the critical cohort compared to the mild ones including S100A8, S100A9, S100A11, S100A12. The primary role of the proteins is to modulate the immune response towards secretion of proinflammatory cytokines, reactive oxygen species and nitric oxide (Wang *et al.*, 2018). Both S100A8 and S100A9 proteins can be secreted by either macrophages or through the release of NETs by the neutrophils. It has been documented that S100A8/9 can serve as ligands for TLR4 to induce the pro-inflammatory cytokine secretion (Vogl *et al.*, 2007; El Gazzar, 2015; Narumi *et al.*, 2015). Taken into account the high correlation of the TLR4 signaling pathway genes as MAP2k6, TIFA, SYK, TAB2, NFKB1 with the critical cohort, confirms the interaction of this mechanism. The contained overexpression of S100 protein family, with high invading numbers of neutrophils

in the lung by high expression and potential secretion of the neutrophil chemoattractant CXCL2, their NET release in the lung, contribute to the to uncontrolled inflammation and cytokine storm, as has been observed in this and previous studies on COVID-19 cases (Kuipers *et al.*, 2013; Freise *et al.*, 2019; Liting Chen *et al.*, 2020; Guo *et al.*, 2021). Interestingly, infection of interferon-gamma alpha receptor (IFNAR)-deficient mice were infected with murine coronavirus mouse hepatitis virus A-59 (MHV-59), showed a similar phenotype as in severe COVID-19 patients, with strongly upregulated S100a8 and neutrophil recruitment, suggesting that the exaggerated proinflammatory response in critically ill patients is linked with the dampened interferon response (Guo *et al.*, 2021). Additionally, high expression and correlation of T cell stimulation CD58, CD40 together with MHC I genes HLA-B and HLA-C suggest a delayed attempt to boost the CD8 T cell response, but coupled with already present tissue damage, high viral titers and low interferon response might be the cause for the unbalanced immune response, deteriorating health and fatal outcomes (Su *et al.*, 2020; Melms *et al.*, 2021). Moreover, the monocytes in critical donors expressed high levels of the decoy receptor for interleukin1 IL1R2, overlapping with findings from other studies on fatal COVID-19 and sepsis cases, indicating a potential attempt to limit the inflammation leading to dynsfunctional monocytes (Reyes *et al.*, 2020; Bost *et al.*, 2021).

In the critical cohort, genes involved in pro-inflammatory pathways were highly correlative. The S100 family of alarmins, including *S100A8*, *S100A9*, *S100A11*, and *S100A12*, were strongly upregulated compared to the mild cohort. These proteins primarily modulate the immune response by promoting the secretion of pro-inflammatory cytokines, reactive oxygen species, and nitric oxide (Wang *et al.*, 2018). S100A8 and S100A9 can be secreted by macrophages or through the release of NETs by neutrophils and it has been documented that S100A8/9 act as ligands for TLR4, inducing pro-inflammatory cytokine secretion (Vogl *et al.*, 2007; El Gazzar, 2015; Narumi *et al.*, 2015). The high correlation of TLR4 signaling pathway genes such as *MAP2K6*, *TIFA*, *SYK*, *TAB2*, and *NFKB1* with the critical cohort supports the interaction of this mechanism. The overexpression

of the S100 protein family, coupled with high numbers of neutrophils infiltrating the lungs and the secretion of the neutrophil chemoattractant *CXCL2*, leads to NET release and even higher alarmin secretion in the lungs, contributing to uncontrolled inflammation and cytokine storms observed in COVID-19 cases (Kuipers *et al.*, 2013; Freise *et al.*, 2019; Liting Chen *et al.*, 2020; Guo *et al.*, 2021). Interestingly, studies on interferon-gamma alpha receptor (IFNAR)-deficient mice infected with murine coronavirus mouse hepatitis virus A-59 (MHV-59) showed a similar phenotype to severe COVID-19 patients, with strongly upregulated *S100a8* and significant neutrophil recruitment, suggesting that the exaggerated pro-inflammatory response in critically ill patients is linked to a dampened interferon response (Guo *et al.*, 2021). Additionally, high expression and correlation of T cell stimulation markers *CD58* and *CD40*, along with MHC I genes *HLA-B* and *HLA-C*, suggest a delayed attempt to boost the CD8 T cell response. However, this response, combined with existing tissue damage, high viral titers, and a low interferon response, likely contributes to the unbalanced immune response, deteriorating health, and fatal outcomes (Su *et al.*, 2020; Melms *et al.*, 2021). Furthermore, monocytes in critical donors expressed high levels of the decoy receptor for interleukin-1, *IL1R2*, which overlaps with findings from other studies on fatal COVID-19 and sepsis cases, indicating a potential attempt to limit inflammation, leading to dysfunctional monocytes (Reyes *et al.*, 2020; Bost *et al.*, 2021). Overall, these findings highlight the complex interplay of immune responses in critically ill COVID-19 patients, contributing to severe disease progression.

In conclusion, this study highlights the multifaceted immune dysregulation in critically ill COVID-19 patients. The transcriptomic analysis of monocytes revealed distinct gene expression profiles associated with severe disease, emphasizing the role of immune pathways such as interferon signaling and antigen presentation. A higher prevalence of severe outcomes in males was noted, likely due to epigenetic and hormonal influences that exacerbate the inflammatory response. Comorbidities like hypertension and Type 2 Diabetes Mellitus further compounded the risk, contributing to hyperinflammation and

impaired immune function. The identification of key regulatory genes and pathways, including the JAK-STAT-IRF1 signaling pathway and the role of S100 family proteins, underscores the importance of targeted therapeutic strategies to modulate the immune response. These findings provide valuable insights into the mechanisms driving severe COVID-19 and highlight potential avenues for improving patient outcomes through personalized medicine.

5. **Conclusion**

This thesis uses a multi-omics investigation into the immune responses to SARS-CoV-2, presenting data from multiple patient cohorts, including those with varying disease severities, vaccine regimens, and individuals experiencing Long COVID. The main objective converges on the unified goal to investigate the outcome of SARS-CoV-2 infection. The presented results indicate a dynamic interplay between pro-inflammatory responses and effective antigen presentation being the key culprits in COVID-19 disease severity.

In severe and critical COVID-19 cases, the innate immune system becomes dysregulated, marked by an accumulation of pro-inflammatory monocytes and dendritic cells that exhibit diminished interferon signaling and antigen-presenting capacity. This skewed activation leads to hyperinflammation and impairs the initiation of a protective adaptive immune response. Conversely, mild cases are associated with a stronger interferon signature and more functional antigen presentation, allowing for effective viral control.

The adaptive immune response, particularly the development of antibodies against the SARS-CoV-2 spike protein, also varies significantly by disease severity and vaccination status. While both mild and critical patients generate high antibody titers, the immune quality differs. In mild cases, robust antibody responses are supported by coordinated T follicular helper and class-switched B cell activity. In contrast, critical cases, though capable of producing high antibody levels, show signs of immune imbalance, with increased Tfh/Treg ratios and potential immune exhaustion.

Vaccination induces a strong humoral response, particularly with mRNA vaccines, although the antibody titer diminishes over time. Notably, individuals who recovered from COVID-19 benefit substantially from vaccination, supporting the concept of hybrid immunity as a superior protective strategy. Additionally, as SARS-CoV-2 continues to mutate to evade antibody responses by altering the amino acid sequence of the spike protein, updated booster vaccinations targeting emerging variants are recommended to maintain effective immune protection.

Together, these findings underscore the importance of a balanced immune response in achieving favorable outcomes during SARS-CoV-2 infection. The work highlights how both insufficient antiviral signaling and excessive inflammation can drive pathology, offering valuable insights for guiding future therapeutic interventions, vaccine strategies, and management of long-term COVID-related complications.

While the multi-omics approach employed in this thesis enabled a comprehensive and integrative view of immune responses to SARS-CoV-2, several methodologies were not ideal and should be thus the results should be taken with a grain of salt. The single-cell RNA sequencing dataset, although large and informative, was limited by sparse clinical metadata and potential batch effects, which may have influenced the resolution of certain immune signatures despite harmonization efforts. In the antibody profiling study, the inclusion of diverse patient cohorts introduced biological richness but also confounding factors, such as differences in sampling time points and imbalance between numbers of participants in each cohort. The bulk RNA sequencing of peripheral monocytes provided valuable insights into systemic innate immunity, yet lacks spatial context and cellular heterogeneity, which would be better captured by single-cell or spatial transcriptomics. Nonetheless, by combining complementary methodologies and diverse clinical cohorts, this thesis offers a robust and multifaceted exploration of COVID-19 immunity, while also identifying key areas for future investigation, particularly in longitudinal and tissue-specific studies.

6. Abstract

This thesis explores the immune mechanisms activated during SARS-CoV-2 infection across different disease severities through a comprehensive multi-omics approach. It specifically emphasizes the role of peripheral monocytes, investigating their programming during infection using bulk RNA-Sequencing. Additionally, the study delves into the development of antibodies in response to both infection and vaccination against the virus. Through single-cell RNA sequencing, it further deciphers the immune pathways activated in various immune cells within peripheral blood. This research provides valuable insights into the complex immune responses to SARS-CoV-2, connected to low interferon response, antigen presentation and highly pro-inflammatory state of severe COVID-19 patients.

7. List of figures

8. List of tables

9. References

Ackermann, M. *et al.* (2020) ‘Pulmonary Vascular Endothelialitis, Thrombosis, and Angiogenesis in Covid-19’. *New England Journal of Medicine*, 383(2), pp. 120–128.

Ahn, J.H. *et al.* (2021) ‘Nasal Ciliated Cells Are Primary Targets for SARS-CoV-2 Replication in the Early Stage of COVID-19’. *The Journal of Clinical Investigation*, 131(13).

Akkaya, M., Kwak, K. and Pierce, S.K. (2020) ‘B Cell Memory: Building Two Walls of Protection against Pathogens’. *Nature Reviews Immunology*, 20(4), pp. 229–238.

Alijotas-Reig, J. *et al.* (2022) ‘Inflammatory Immune-mediated Adverse Reactions Induced by COVID-19 Vaccines in Previously Injected Patients with Soft Tissue Fillers: A Case-series of 20 Patients’. *Journal of Cosmetic Dermatology*.

Almanan, M. *et al.* (2020) ‘IL-10–Producing Tfh Cells Accumulate with Age and Link Inflammation with Age-Related Immune Suppression’. *Science Advances*, 6(31), p. eabb0806.

Altmann, D.M. *et al.* (2023) ‘The Immunology of Long COVID’. *Nature Reviews Immunology*, 23(10), pp. 618–634.

Alvarez, M. *et al.* (2020) ‘Enhancing Droplet-Based Single-Nucleus RNA-Seq Resolution Using the Semi-Supervised Machine Learning Classifier DIEM’. *Scientific Reports*, 10(1), p. 11019.

Amraei, R. *et al.* (2021) ‘CD209L/L-SIGN and CD209/DC-SIGN Act as Receptors for SARS-CoV-2’. *ACS Central Science*, 7(7), pp. 1156–1165.

Andersen, K.G. *et al.* (2020) ‘The Proximal Origin of SARS-CoV-2’. *Nature Medicine*, 26(4), pp. 450–452.

Andersen, M.N. *et al.* (2016) ‘Elimination of Erroneous Results in Flow Cytometry Caused by Antibody Binding to Fc Receptors on Human Monocytes and Macrophages’. *Cytometry Part A*, 89(11), pp. 1001–1009.

André, S. *et al.* (2022) ‘T Cell Apoptosis Characterizes Severe Covid-19 Disease’. *Cell Death & Differentiation*, 29(8), pp. 1486–1499.

Andrews, N. *et al.* (2022) ‘Effectiveness of COVID-19 Booster Vaccines against COVID-19-Related Symptoms, Hospitalization and Death in England’. *Nature Medicine*, 28(4), pp. 831–837.

Andrews, S. *et al.* (2012) Available at: https://www.bioinformatics.babraham.ac.uk/projects/fastqc/.

Anurag, A., Jha, P.K. and Kumar, A. (2020) ‘Differential White Blood Cell Count in the COVID-19: A Cross-Sectional Study of 148 Patients’. *Diabetes & Metabolic Syndrome: Clinical Research & Reviews*, 14(6), pp. 2099–2102.

Apostolidis, S.A. *et al.* (2021) ‘Cellular and Humoral Immune Responses Following SARS-CoV-2 MRNA Vaccination in Patients with Multiple Sclerosis on Anti-CD20 Therapy’. *Nature Medicine*, 27(11), pp. 1990–2001.

Arcanjo, A. *et al.* (2020) ‘The Emerging Role of Neutrophil Extracellular Traps in Severe Acute Respiratory Syndrome Coronavirus 2 (COVID-19)’. *Scientific Reports*, 10(1), p. 19630.

Argüello González, G. *et al.* (2022) ‘Low Levels of CIITA and High Levels of SOCS1 Predict COVID-19 Disease Severity in Children and Adults’. *IScience, 2022, 25 (1).*

Arunachalam, P.S. *et al.* (2021) ‘Systems Vaccinology of the BNT162b2 MRNA Vaccine in Humans’. *Nature*, 596(7872), pp. 410–416.

Atyeo, C. *et al.* (2020) ‘Distinct Early Serological Signatures Track with SARS-CoV-2 Survival’. *Immunity*, 53(3), pp. 524–532.

Baird, S. *et al.* (2023) ‘A Unique Cytotoxic CD4+ T Cell-signature Defines Critical COVID-19’. *Clinical & Translational Immunology*, 12(8), p. e1463.

Bao, Y. *et al.* (2021) ‘Dynamic Anti-Spike Protein Antibody Profiles in COVID-19 Patients’. *International Journal of Infectious Diseases*, 103, pp. 540–548.

Barrat, F.J., Crow, M.K. and Ivashkiv, L.B. (2019) ‘Interferon Target-Gene Expression and Epigenomic Signatures in Health and Disease’. *Nature Immunology*, 20(12), pp. 1574–1583.

Bianchi, M.E. (2007) ‘DAMPs, PAMPs and Alarmins: All We Need to Know about Danger’. *Journal of Leucocyte Biology*, 81(1), pp. 1–5.

Bienvenu, L.A. *et al.* (2020) ‘Higher Mortality of COVID-19 in Males: Sex Differences in Immune Response and Cardiovascular Comorbidities’. *Cardiovascular Research*, 116(14), pp. 2197–2206.

Bindoli, S. *et al.* (2022) ‘Hyperinflammation after Anti-SARS-CoV-2 MRNA/DNA Vaccines Successfully Treated with Anakinra: Case Series and Literature Review’. *Experimental Biology and Medicine*, 247(4), pp. 338–344.

Blanco-Melo, D. *et al.* (2020) ‘Imbalanced Host Response to SARS-CoV-2 Drives Development of COVID-19’. *Cell*, 181(5), pp. 1036–1045.

Borcherding, L. *et al.* (2021) ‘Impaired Dendritic Cell Homing in COVID-19’. *Frontiers in Medicine*, 8, p. 761372.

Bost, P. *et al.* (2021) ‘Deciphering the State of Immune Silence in Fatal COVID-19 Patients’. *Nature Communications*, 12(1), p. 1428.

Bowe, B., Xie, Y. and Al-Aly, Z. (2023) ‘Postacute Sequelae of COVID-19 at 2 Years’. *Nature Medicine*, 29(9), pp. 2347–2357.

Boyette, L.B. *et al.* (2017) ‘Phenotype, Function, and Differentiation Potential of Human Monocyte Subsets’. *PloS One*, 12(4), p. e0176460.

Braun, J. *et al.* (2020) ‘SARS-CoV-2-Reactive T Cells in Healthy Donors and Patients with COVID-19’. *Nature*, 587(7833), pp. 270–274. DOI: 10.1038/s41586-020-2598-9.

Brochot, E. *et al.* (2020) ‘Anti-Spike, Anti-Nucleocapsid and Neutralizing Antibodies in SARS-CoV-2 Inpatients and Asymptomatic Individuals’. *Frontiers in Microbiology*, p. 2468.

Bruchez, A. *et al.* (2020) ‘MHC Class II Transactivator CIITA Induces Cell Resistance to Ebola Virus and SARS-like Coronaviruses’. *Science*, 370(6513), pp. 241–247.

Burrell, C.J., Howard, C.R. and Murphy, F.A. (2017) ‘Coronaviruses’. *Fenner and White’s Medical Virology*, p. 437.

Butler, A. *et al.* (2018) ‘Integrating Single-Cell Transcriptomic Data across Different Conditions, Technologies, and Species’. *Nature Biotechnology*, 36(5), pp. 411–420. DOI: 10.1038/nbt.4096.

Caglayan, E., Liu, Y. and Konopka, G. (2022) ‘Neuronal Ambient RNA Contamination Causes Misinterpreted and Masked Cell Types in Brain Single-Nuclei Datasets’. *Neuron*, 110(24), pp. 4043–4056.

Cai, G. *et al.* (2021) ‘SARS-CoV-2 Impairs Dendritic Cells and Regulates DC-SIGN Gene Expression in Tissues’. *International Journal of Molecular Sciences*, 22(17), p. 9228.

Camp, J. V. and Jonsson, C.B. (2017) ‘A Role for Neutrophils in Viral Respiratory Disease’. *Frontiers in Immunology*, 8, p. 246628.

Campbell, G.R. *et al.* (2021) ‘SARS-CoV-2, SARS-CoV-1, and HIV-1 Derived SsRNA Sequences Activate the NLRP3 Inflammasome in Human Macrophages through a Non-Classical Pathway’. *Iscience*, 24(4).

Cantuti-Castelvetri, L. *et al.* (2020) ‘Neuropilin-1 Facilitates SARS-CoV-2 Cell Entry and Infectivity’. *Science*, 370(6518), pp. 856–860.

Cao, Y. *et al.* (2022) ‘Omicron Escapes the Majority of Existing SARS-CoV-2 Neutralizing Antibodies’. *Nature*, 602(7898), pp. 657–663. DOI: 10.1038/s41586-021-04385-3.

Carfì, A., Bernabei, R. and Landi, F. (2020) ‘Persistent Symptoms in Patients after Acute COVID-19’. *Jama*, 324(6), pp. 603–605.

Cascella, M. *et al.* (2022) ‘Features, Evaluation, and Treatment of Coronavirus (COVID-19)’. *Statpearls [Internet]*.

Cavalcante-Silva, L.H.A. *et al.* (2021) ‘Neutrophils and COVID-19: The Road so Far’. *International Immunopharmacology*, 90, p. 107233.

Cavanagh, D. *et al.* (1994) ‘Revision of the Taxonomy of the Coronavirus, Torovirus and Arterivirus Genera’. *Archives of Virology*, 135(1), p. 227.

Chakraborty, D. *et al.* (2017) ‘Alarmin S100A8 Activates Alveolar Epithelial Cells in the Context of Acute Lung Injury in a TLR4-Dependent Manner’. *Frontiers in Immunology*, 8, p. 1493.

Chakravarty, D. *et al.* (2020) ‘Sex Differences in SARS-CoV-2 Infection Rates and the Potential Link to Prostate Cancer’. *Communications Biology*, 3(1), p. 374. DOI: 10.1038/s42003-020-1088-9.

Chandrashekar, A. *et al.* (2020) ‘SARS-CoV-2 Infection Protects against Rechallenge in Rhesus Macaques’. *Science*, 369(6505), pp. 812–817.

Chang, C.-H., Gourley, T.S. and Sisk, T.J. (2002) ‘Function and Regulation of Class II Transactivator in the Immune System’. *Immunologic Research*, 25, pp. 131–142.

Chang, L., Yan, Y. and Wang, L. (2020) ‘Coronavirus Disease 2019: Coronaviruses and Blood Safety’. *Transfusion Medicine Reviews*, 34(2), pp. 75–80.

Channappanavar, R. *et al.* (2017) ‘Sex-Based Differences in Susceptibility to Severe Acute Respiratory Syndrome Coronavirus Infection’. *The Journal of Immunology*, 198(10), pp. 4046–4053.

Chan-Yeung, M. and Xu, R. (2003) ‘SARS: Epidemiology’. *Respirology*, 8, pp. S9–S14.

Chaplin, D.D. (2010) ‘Overview of the Immune Response’. *Journal of Allergy and Clinical Immunology*, 125(2), pp. S3–S23.

Charfeddine, S. *et al.* (2021) ‘Long COVID 19 Syndrome: Is It Related to Microcirculation and Endothelial Dysfunction? Insights from TUN-EndCOV Study’. *Frontiers in Cardiovascular Medicine*, 8, p. 745758.

Chen, Guang., Wu, D.I., *et al.* (2020) ‘Clinical and Immunological Features of Severe and Moderate Coronavirus Disease 2019’. *The Journal of Clinical Investigation*, 130(5), pp. 2620–2629.

Chen, Jiahui., Wang, R., *et al.* (2020) ‘Mutations Strengthened SARS-CoV-2 Infectivity’. *Journal of Molecular Biology*, 432(19), pp. 5212–5226.

Chen, Liting. *et al.* (2020) ‘Elevated Serum Levels of S100A8/A9 and HMGB1 at Hospital Admission Are Correlated with Inferior Clinical Outcomes in COVID-19 Patients’. *Cellular & Molecular Immunology*, 17(9), pp. 992–994.

Chen, Liang. *et al.* (2020) ‘The ACE2 Expression in Human Heart Indicates New Potential Mechanism of Heart Injury among Patients Infected with SARS-CoV-2’. *Cardiovascular Research*, 116(6), pp. 1097–1100.

Chen, Tao., Wu, D.I., *et al.* (2020) ‘Clinical Characteristics of 113 Deceased Patients with Coronavirus Disease 2019: Retrospective Study’. *Bmj*, 368.

Chen, Yu., Liu, Q. and Guo, D. (2020) ‘Emerging Coronaviruses: Genome Structure, Replication, and Pathogenesis’. *Journal of Medical Virology*, 92(4), pp. 418–423.

Cheng, L. *et al.* (2021) ‘Dynamic Landscape Mapping of Humoral Immunity to SARS-CoV-2 Identifies Non-Structural Protein Antibodies Associated with the Survival of Critical COVID-19 Patients’. *Signal Transduction and Targeted Therapy*, 6(1), p. 304. DOI: 10.1038/s41392-021-00718-w.

Cheng, V.C.C. *et al.* (2007) ‘Severe Acute Respiratory Syndrome Coronavirus as an Agent of Emerging and Reemerging Infection’. *Clinical Microbiology Reviews*, 20(4), pp. 660–694.

Christgen, S. *et al.* (2020) ‘Identification of the PANoptosome: A Molecular Platform Triggering Pyroptosis, Apoptosis, and Necroptosis (PANoptosis)’. *Frontiers in Cellular and Infection Microbiology*, 10, p. 237.

Chua, R.L. *et al.* (2020) ‘COVID-19 Severity Correlates with Airway Epithelium–Immune Cell Interactions Identified by Single-Cell Analysis’. *Nature Biotechnology*, 38(8), pp. 970–979.

Clarke, Z.A. *et al.* (2021) ‘Tutorial: Guidelines for Annotating Single-Cell Transcriptomic Maps Using Automated and Manual Methods’. *Nature Protocols*, 16(6), pp. 2749–2764. DOI: 10.1038/s41596-021-00534-0.

Clausen, T.M. *et al.* (2020) ‘SARS-CoV-2 Infection Depends on Cellular Heparan Sulfate and ACE2’. *Cell*, 183(4), pp. 1043–1057.

Codo, A.C. *et al.* (2020) ‘Elevated Glucose Levels Favor SARS-CoV-2 Infection and Monocyte Response through a HIF-1α/Glycolysis-Dependent Axis’. *Cell Metabolism*, 32(3), pp. 437–446.

Conte, C. *et al.* (2022) ‘Incessant Pericarditis Following the Second Dose of SARS-CoV-2 MRNA Vaccine Successfully Treated with Anakinra: A Case Report’. *European Heart Journal-Case Reports*, 6(9), p. ytac357.

Corbett, K.S. *et al.* (2021) ‘Protection against SARS-CoV-2 Beta Variant in MRNA-1273 Vaccine–Boosted Nonhuman Primates’. *Science*, 374(6573), pp. 1343–1353.

Cox, F., Khalib, K. and Conlon, N. (2021) ‘PEG That Reaction: A Case Series of Allergy to Polyethylene Glycol’. *The Journal of Clinical Pharmacology*, 61(6), pp. 832–835.

Critchley, J.A. *et al.* (2018) ‘Glycemic Control and Risk of Infections among People with Type 1 or Type 2 Diabetes in a Large Primary Care Cohort Study’. *Diabetes Care*, 41(10), pp. 2127–2135.

Crotty, S. (2014) ‘T Follicular Helper Cell Differentiation, Function, and Roles in Disease’. *Immunity*, 41(4), pp. 529–542.

Cui, J., Li, F. and Shi, Z.-L. (2019) ‘Origin and Evolution of Pathogenic Coronaviruses’. *Nature Reviews Microbiology*, 17(3), pp. 181–192.

Cui, X. *et al.* (2021) ‘Pulmonary Edema in COVID-19 Patients: Mechanisms and Treatment Potential’. *Frontiers in Pharmacology*, 12, p. 664349.

Curbelo, J. *et al.* (2017) ‘Inflammation Biomarkers in Blood as Mortality Predictors in Community-Acquired Pneumonia Admitted Patients: Importance of Comparison with Neutrophil Count Percentage or Neutrophil-Lymphocyte Ratio’. *PloS One*, 12(3), p. e0173947.

Daly, J.L. *et al.* (2020) ‘Neuropilin-1 Is a Host Factor for SARS-CoV-2 Infection’. *Science*, 370(6518), pp. 861–865.

Davis, H.E. *et al.* (2023) ‘Long COVID: Major Findings, Mechanisms and Recommendations’. *Nature Reviews Microbiology*, 21(3), pp. 133–146.

Da-Yuan, C. *et al.* (2021) ‘SARS-CoV-2 Disrupts Proximal Elements in the JAK-STAT Pathway’. *Journal of Virology*, 95(19), pp. 10.1128/jvi.00862-21. DOI: 10.1128/jvi.00862-21.

Deng, Z. *et al.* (2022) ‘MRNA Vaccines: The Dawn of a New Era of Cancer Immunotherapy’. *Frontiers in Immunology*, 13, p. 887125.

Devarajan, P. *et al.* (2023) ‘Cytotoxic CD4 Development Requires CD4 Effectors to Concurrently Recognize Local Antigen and Encounter Type I IFN-Induced IL-15’. *Cell Reports*, 42(10).

Diamond, M.S. and Farzan, M. (2013) ‘The Broad-Spectrum Antiviral Functions of IFIT and IFITM Proteins’. *Nature Reviews Immunology*, 13(1), pp. 46–57.

Diamond, M.S. and Kanneganti, T.-D. (2022) ‘Innate Immunity: The First Line of Defense against SARS-CoV-2’. *Nature Immunology*, 23(2), pp. 165–176.

Diao, B. *et al.* (2020) ‘Reduction and Functional Exhaustion of T Cells in Patients with Coronavirus Disease 2019 (COVID-19)’. *Frontiers in Immunology*, 11, p. 827.

Dobi, A. *et al.* (2022) ‘Low Levels of the Key B Cell Activation Marker, HLA-DR, in COVID-19 Hospitalized Cases Are Associated with Disease Severity, Dexamethasone Treatment, and Circulating IL-6 Levels’. *Immunologic Research*, 70(5), pp. 714–719.

Dorothy, H., A, K.D. and Judith, M. (1967) ‘Growth and Intracellular Development of a New Respiratory Virus’. *Journal of Virology*, 1(4), pp. 810–816. DOI: 10.1128/jvi.1.4.810-816.1967.

Du, M. *et al.* (2020) ‘Multiomics Evaluation of Gastrointestinal and Other Clinical Characteristics of COVID-19’. *Gastroenterology*, 158(8), pp. 2298–2301.

Du, S.Q. and Yuan, W. (2020) ‘Mathematical Modeling of Interaction between Innate and Adaptive Immune Responses in COVID-19 and Implications for Viral Pathogenesis’. *Journal of Medical Virology*, 92(9), pp. 1615–1628.

El-Shitany, N.A. *et al.* (2021) ‘Minor to Moderate Side Effects of Pfizer-BioNTech COVID-19 Vaccine among Saudi Residents: A Retrospective Cross-Sectional Study’. *International Journal of General Medicine*, 14, p. 1389.

Essalmani, R. *et al.* (2022) ‘Distinctive Roles of Furin and TMPRSS2 in SARS-CoV-2 Infectivity’. *Journal of Virology*, 96(8), pp. e00128-22.

European Medicines Agency. (2024) *European Medicines Agency: COVID-19 Medicines*. Available at: https://www.ema.europa.eu/en/human-regulatory-overview/public-health-threats/coronavirus-disease-covid-19/covid-19-medicines (Accessed: 24 April 2024).

Ewels, P. *et al.* (2016) ‘MultiQC: Summarize Analysis Results for Multiple Tools and Samples in a Single Report’. *Bioinformatics*, 32(19), pp. 3047–3048.

Fan, Y.-J., Chan, K.-H. and Hung, I.F.-N. (2021) ‘Safety and Efficacy of COVID-19 Vaccines: A Systematic Review and Meta-Analysis of Different Vaccines at Phase 3’. *Vaccines*, 9(9), p. 989.

Favresse, J. *et al.* (2021) ‘Neutralizing Antibodies in COVID-19 Patients and Vaccine Recipients after Two Doses of BNT162b2’. *Viruses*, 13(7), p. 1364.

Fehr, A.R. and Perlman, S. (2015) ‘Coronaviruses: An Overview of Their Replication and Pathogenesis’. *Coronaviruses: Methods and Protocols*, pp. 1–23.

Feldstein, L.R. *et al.* (2020) ‘Multisystem Inflammatory Syndrome in US Children and Adolescents’. *New England Journal of Medicine*, 383(4), pp. 334–346.

Feng, Z. *et al.* (2020) ‘Early Prediction of Disease Progression in COVID-19 Pneumonia Patients with Chest CT and Clinical Characteristics’. *Nature Communications*, 11(1), p. 4968.

Fernandes, C.J. *et al.* (2019) ‘Pulmonary Embolism and Gas Exchange’. *Respiration*, 98(3), pp. 253–262.

Fernández-de-Las-Peñas, C. (2022) ‘Long COVID: Current Definition’. *Infection*, 50(1), pp. 285–286.

Ferrando, C. *et al.* (2020) ‘Clinical Features, Ventilatory Management, and Outcome of ARDS Caused by COVID-19 Are Similar to Other Causes of ARDS’. *Intensive Care Medicine*, 46, pp. 2200–2211.

Fleming, S.J. *et al.* (2023) ‘Unsupervised Removal of Systematic Background Noise from Droplet-Based Single-Cell Experiments Using CellBender’. *Nature Methods*, 20(9), pp. 1323–1335.

Forni, D. *et al.* (2017) ‘Molecular Evolution of Human Coronavirus Genomes’. *Trends in Microbiology*, 25(1), pp. 35–48.

Forster, J., Nandi, D. and Kulkarni, A. (2022) ‘MRNA-Carrying Lipid Nanoparticles That Induce Lysosomal Rupture Activate NLRP3 Inflammasome and Reduce MRNA Transfection Efficiency’. *Biomaterials Science*.

Fortner, A. and Schumacher, D. (2021) ‘First COVID-19 Vaccines Receiving the US FDA and EMA Emergency Use Authorization’. *Discoveries*, 9(1).

Franz, K.M. *et al.* (2018) ‘STING-Dependent Translation Inhibition Restricts RNA Virus Replication’. *Proceedings of the National Academy of Sciences*, 115(9), pp. E2058–E2067.

Fraser, B.J. *et al.* (2022) ‘Structure and Activity of Human TMPRSS2 Protease Implicated in SARS-CoV-2 Activation’. *Nature Chemical Biology*, 18(9), pp. 963–971.

Freise, N. *et al.* (2019) ‘Signaling Mechanisms Inducing Hyporesponsiveness of Phagocytes during Systemic Inflammation’. *Blood, The Journal of the American Society of Hematology*, 134(2), pp. 134–146.

Fung, T.S., Huang, M. and Liu, D.X. (2014) ‘Coronavirus-Induced ER Stress Response and Its Involvement in Regulation of Coronavirus–Host Interactions’. *Virus Research*, 194, pp. 110–123.

Fung, T.S. and Liu, D.X. (2019) ‘Human Coronavirus: Host-Pathogen Interaction’. *Annual Review of Microbiology*, 73, pp. 529–557.

Galani, I.-E. *et al.* (2021) ‘Untuned Antiviral Immunity in COVID-19 Revealed by Temporal Type I/III Interferon Patterns and Flu Comparison’. *Nature Immunology*, 22(1), pp. 32–40.

Gallo, G., Calvez, V. and Savoia, C. (2022) ‘Hypertension and COVID-19: Current Evidence and Perspectives’. *High Blood Pressure & Cardiovascular Prevention*, 29(2), pp. 115–123.

Gal-Oz, S.T. *et al.* (2019) ‘ImmGen Report: Sexual Dimorphism in the Immune System Transcriptome’. *Nature Communications*, 10(1), p. 4295. DOI: 10.1038/s41467-019-12348-6.

Galván-Peña, S. *et al.* (2021) ‘Profound Treg Perturbations Correlate with COVID-19 Severity’. *Proceedings of the National Academy of Sciences*, 118(37), p. e2111315118. DOI: 10.1073/pnas.2111315118.

Gatti, A. *et al.* (2020) ‘Decrease of Non-classical and Intermediate Monocyte Subsets in Severe Acute SARS-CoV-2 Infection’. *Cytometry Part A*, 97(9), pp. 887–890.

Gattinoni, L. *et al.* (2020) ‘COVID-19 Does Not Lead to a “Typical” Acute Respiratory Distress Syndrome’. *American Journal of Respiratory and Critical Care Medicine*, 201(10), pp. 1299–1300.

El Gazzar, M. (2015) ‘Immunobiology of S100A8 and S100A9 Proteins and Their Role in Acute Inflammation and Sepsis’. *Int J Immunol Immunother*, 2(2).

Gazzinelli-Guimaraes, P.H. *et al.* (2022) ‘Antigenic Determinants of SARS-CoV-2-Specific CD4+ T Cell Lines Reveals M Protein-Driven Dysregulation of Interferon Signaling’. *Frontiers in Immunology*, 13, p. 883159.

Gebhard, C. *et al.* (2020) ‘Impact of Sex and Gender on COVID-19 Outcomes in Europe’. *Biology of Sex Differences*, 11, pp. 1–13.

Gholami, M. *et al.* (2022) ‘Increased Risk of COVID-19 Mortality Rate in IFITM3 Rs6598045 G Allele Carriers Infected by SARS-CoV-2 Delta Variant’. *Human Genomics*, 16(1), pp. 1–9.

Giamarellos-Bourboulis, E.J. *et al.* (2020) ‘Complex Immune Dysregulation in COVID-19 Patients with Severe Respiratory Failure’. *Cell Host & Microbe*, 27(6), pp. 992–1000.

Gibson, P.G., Qin, L. and Puah, S.H. (2020) ‘COVID-19 Acute Respiratory Distress Syndrome (ARDS): Clinical Features and Differences from Typical Pre-COVID-19 ARDS’. *Medical Journal of Australia*, 213(2), pp. 54–56.

Glynne, P. *et al.* (2022) ‘Long COVID Following Mild SARS-CoV-2 Infection: Characteristic T Cell Alterations and Response to Antihistamines’. *Journal of Investigative Medicine*, 70(1), pp. 61–67.

Gold, J.E. *et al.* (2021) ‘Investigation of Long COVID Prevalence and Its Relationship to Epstein-Barr Virus Reactivation’. *Pathogens*, 10(6), p. 763.

Gordon, D.E. *et al.* (2020) ‘Comparative Host-Coronavirus Protein Interaction Networks Reveal Pan-Viral Disease Mechanisms’. *Science*, 370(6521), p. eabe9403.

Goyal, P. *et al.* (2020) ‘Clinical Characteristics of Covid-19 in New York City’. *New England Journal of Medicine*, 382(24), pp. 2372–2374.

Grant, R.A. *et al.* (2021) ‘Circuits between Infected Macrophages and T Cells in SARS-CoV-2 Pneumonia’. *Nature*, 590(7847), pp. 635–641.

Gressier, E. *et al.* (2023) ‘CD4+ T Cell Calibration of Antigen-Presenting Cells Optimizes Antiviral CD8+ T Cell Immunity’. *Nature Immunology*, pp. 1–12.

Gu, S.X. *et al.* (2021) ‘Thrombocytopathy and Endotheliopathy: Crucial Contributors to COVID-19 Thromboinflammation’. *Nature Reviews Cardiology*, 18(3), pp. 194–209. DOI: 10.1038/s41569-020-00469-1.

Guo, J., Peters, K.L. and Sen, G.C. (2000) ‘Induction of the Human Protein P56 by Interferon, Double-Stranded RNA, or Virus Infection’. *Virology*, 267(2), pp. 209–219.

Guo, Q. *et al.* (2021) ‘Induction of Alarmin S100A8/A9 Mediates Activation of Aberrant Neutrophils in the Pathogenesis of COVID-19’. *Cell Host & Microbe*, 29(2), pp. 222–235.

Gustine, J.N. and Jones, D. (2021) ‘Immunopathology of Hyperinflammation in COVID-19’. *The American Journal of Pathology*, 191(1), pp. 4–17.

de Haan, C.A.M., Vennema, H. and Rottier, P.J.M. (2000) ‘Assembly of the Coronavirus Envelope: Homotypic Interactions between the M Proteins’. *Journal of Virology*, 74(11), pp. 4967–4978.

Hadjadj, J. *et al.* (2020) ‘Impaired Type I Interferon Activity and Inflammatory Responses in Severe COVID-19 Patients’. *Science*, 369(6504), pp. 718–724.

Hafemeister, C. and Satija, R. (2019) ‘Normalization and Variance Stabilization of Single-Cell RNA-Seq Data Using Regularized Negative Binomial Regression’. *Genome Biology*, 20(1), p. 296.

Haffke, M. *et al.* (2022) ‘Endothelial Dysfunction and Altered Endothelial Biomarkers in Patients with Post-COVID-19 Syndrome and Chronic Fatigue Syndrome (ME/CFS)’. *Journal of Translational Medicine*, 20(1), p. 138.

Hall, V. *et al.* (2022) ‘Protection against SARS-CoV-2 after Covid-19 Vaccination and Previous Infection’. *New England Journal of Medicine*, 386(13), pp. 1207–1220.

Hamilton, S.E. *et al.* (2006) ‘The Generation of Protective Memory-like CD8+ T Cells during Homeostatic Proliferation Requires CD4+ T Cells’. *Nature Immunology*, 7(5), pp. 475–481.

Hamre, D. and Procknow, J.J. (1966) ‘A New Virus Isolated from the Human Respiratory Tract.’ *Proceedings of the Society for Experimental Biology and Medicine*, 121(1), pp. 190–193.

Han, H. *et al.* (2020) ‘Profiling Serum Cytokines in COVID-19 Patients Reveals IL-6 and IL-10 Are Disease Severity Predictors’. *Emerging Microbes & Infections*, 9(1), pp. 1123–1130.

Hao, Y. *et al.* (2021) ‘Integrated Analysis of Multimodal Single-Cell Data’. *Cell*, 184(13), pp. 3573–3587.

Hartley, G.E. *et al.* (2020) ‘Rapid Generation of Durable B Cell Memory to SARS-CoV-2 Spike and Nucleocapsid Proteins in COVID-19 and Convalescence’. *Science Immunology*, 5(54), p. eabf8891.

Harvey, W.T. *et al.* (2021) ‘SARS-CoV-2 Variants, Spike Mutations and Immune Escape’. *Nature Reviews Microbiology*, 19(7), pp. 409–424.

Hasan, A. *et al.* (2022) ‘Fatal COVID-19 Is Associated with Reduced HLA-DR, CD123 or CD11c Expression on Circulating Dendritic Cells’. *Journal of Inflammation Research*, pp. 5665–5675.

Hastie, C.E. *et al.* (2022) ‘Outcomes among Confirmed Cases and a Matched Comparison Group in the Long-COVID in Scotland Study’. *Nature Communications*, 13(1), p. 5663.

Hegde, N.R., Chevalier, M.S. and Johnson, D.C. (2003) ‘Viral Inhibition of MHC Class II Antigen Presentation’. *Trends in Immunology*, 24(5), pp. 278–285.

Henao-Agudelo, J.S. *et al.* (2024) ‘Classical Monocytes-Low Expressing HLA-DR Is Associated with Higher Mortality Rate in SARS-CoV-2+ Young Patients with Severe Pneumonia’. *Heliyon*, 10(2).

Heumos, L. *et al.* (2023) ‘Best Practices for Single-Cell Analysis across Modalities’. *Nature Reviews Genetics*, 24(8), pp. 550–572. DOI: 10.1038/s41576-023-00586-w.

Higaki, A. *et al.* (2022) ‘Predictive Value of Neutrophil-to-Lymphocyte Ratio for the Fatality of COVID-19 Patients Complicated with Cardiovascular Diseases and/or Risk Factors’. *Scientific Reports*, 12(1), p. 13606.

Higgins, H. *et al.* (2022) ‘Risk of Thrombosis with Thrombocytopenia Syndrome after COVID-19 Vaccination Prior to the Recognition of Vaccine-induced Thrombocytopenia and Thrombosis: A Self-controlled Case Series Study in England’. *Research and Practice in Thrombosis and Haemostasis*, 6(3), p. e12698.

Hoffmann, M. *et al.* (2020) ‘SARS-CoV-2 Cell Entry Depends on ACE2 and TMPRSS2 and Is Blocked by a Clinically Proven Protease Inhibitor’. *Cell*, 181(2), pp. 271–280.

Holman, N. *et al.* (2020) ‘Risk Factors for COVID-19-Related Mortality in People with Type 1 and Type 2 Diabetes in England: A Population-Based Cohort Study’. *The Lancet Diabetes & Endocrinology*, 8(10), pp. 823–833.

Hopkins, F.R. *et al.* (2023) ‘Major Alterations to Monocyte and Dendritic Cell Subsets Lasting More than 6 Months after Hospitalization for COVID-19’. *Frontiers in Immunology*, 13, p. 1082912.

Hornung, V. *et al.* (2006) ‘5’-Triphosphate RNA Is the Ligand for RIG-I’. *Science*, 314(5801), pp. 994–997.

Hornung, V. *et al.* (2014) ‘OAS Proteins and CGAS: Unifying Concepts in Sensing and Responding to Cytosolic Nucleic Acids’. *Nature Reviews Immunology*, 14(8), pp. 521–528.

Hotez, P.J. *et al.* (2021) ‘COVID-19 Vaccine Decisions: Considering the Choices and Opportunities’. *Microbes and Infection*, 23(4–5), p. 104811. DOI: 10.1016/J.MICINF.2021.104811.

Hou, Y.J. *et al.* (2020) ‘SARS-CoV-2 Reverse Genetics Reveals a Variable Infection Gradient in the Respiratory Tract’. *Cell*, 182(2), pp. 429–446.

Hu, B. *et al.* (2021) ‘Characteristics of SARS-CoV-2 and COVID-19’. *Nature Reviews Microbiology*, 19(3), pp. 141–154.

Huang, C. *et al.* (2021) ‘6-Month Consequences of COVID-19 in Patients Discharged from Hospital: A Cohort Study’. *The Lancet*, 397(10270), pp. 220–232.

Huang, C. *et al.* (2020) ‘Clinical Features of Patients Infected with 2019 Novel Coronavirus in Wuhan, China’. *The Lancet*, 395(10223), pp. 497–506.

Huang, I.-C. *et al.* (2011) ‘Distinct Patterns of IFITM-Mediated Restriction of Filoviruses, SARS Coronavirus, and Influenza A Virus’. *PLoS Pathogens*, 7(1), p. e1001258.

Huang, S. *et al.* (2020) ‘COVID-19 Patients with Hypertension Have More Severe Disease: A Multicenter Retrospective Observational Study’. *Hypertension Research*, 43(8), pp. 824–831.

Huber, J.P. and David Farrar, J. (2011) ‘Regulation of Effector and Memory T-cell Functions by Type I Interferon’. *Immunology*, 132(4), pp. 466–474.

Huffman, J.E. *et al.* (2022) ‘Multi-Ancestry Fine Mapping Implicates OAS1 Splicing in Risk of Severe COVID-19’. *Nature Genetics*, 54(2), pp. 125–127.

Hui, D.J. *et al.* (2003) ‘Viral Stress-Inducible Protein P56 Inhibits Translation by Blocking the Interaction of EIF3 with the Ternary Complex EIF2· GTP· Met-TRNAi’. *Journal of Biological Chemistry*, 278(41), pp. 39477–39482.

Humphries, F. *et al.* (2021) ‘A Diamidobenzimidazole STING Agonist Protects against SARS-CoV-2 Infection’. *Science Immunology*, 6(59), p. eabi9002.

Hung, I.F.N. and Poland, G.A. (2021) ‘Single-Dose Oxford–AstraZeneca COVID-19 Vaccine Followed by a 12-Week Booster’. *The Lancet*, 397(10277), pp. 854–855.

Hwang, B., Lee, J.H. and Bang, D. (2018) ‘Single-Cell RNA Sequencing Technologies and Bioinformatics Pipelines’. *Experimental & Molecular Medicine*, 50(8), pp. 1–14.

Ianevski, A., Giri, A.K. and Aittokallio, T. (2022) ‘Fully-Automated and Ultra-Fast Cell-Type Identification Using Specific Marker Combinations from Single-Cell Transcriptomic Data’. *Nature Communications*, 13(1), p. 1246. DOI: 10.1038/s41467-022-28803-w.

Ivashkiv, L.B. and Donlin, L.T. (2014) ‘Regulation of Type I Interferon Responses’. *Nature Reviews Immunology*, 14(1), pp. 36–49.

Iwasaki, A. and Medzhitov, R. (2015) ‘Control of Adaptive Immunity by the Innate Immune System’. *Nature Immunology*, 16(4), pp. 343–353.

Iyer, S.S. and Cheng, G. (2012) ‘Role of Interleukin 10 Transcriptional Regulation in Inflammation and Autoimmune Disease’. *Critical Reviews™ in Immunology*, 32(1).

Jackson, C.B. *et al.* (2022) ‘Mechanisms of SARS-CoV-2 Entry into Cells’. *Nature Reviews Molecular Cell Biology*, 23(1), pp. 3–20.

Jackson, L.A. *et al.* (2020) ‘An MRNA Vaccine against SARS-CoV-2—Preliminary Report’. *New England Journal of Medicine*.

Jaiswal, V. *et al.* (2022) ‘Cerebral Venous Sinus Thrombosis Following COVID-19 Vaccination: A Systematic Review’. *Journal of Primary Care & Community Health*, 13, p. 21501319221074450.

Janssen, E.M. *et al.* (2005) ‘CD4+ T-Cell Help Controls CD8+ T-Cell Memory via TRAIL-Mediated Activation-Induced Cell Death’. *Nature*, 434(7029), pp. 88–93.

Ji, W. *et al.* (2022) ‘Structures of a Deltacoronavirus Spike Protein Bound to Porcine and Human Receptors’. *Nature Communications*, 13(1), p. 1467.

Jimeno, S. *et al.* (2021) ‘Prognostic Implications of Neutrophil-lymphocyte Ratio in COVID-19’. *European Journal of Clinical Investigation*, 51(1), p. e13404.

Jin, J.-M. *et al.* (2020) ‘Gender Differences in Patients with COVID-19: Focus on Severity and Mortality’. *Frontiers in Public Health*, 8, p. 545030.

Jin, P. *et al.* (2010) ‘Molecular Signatures of Maturing Dendritic Cells: Implications for Testing the Quality of Dendritic Cell Therapies’. *Journal of Translational Medicine*, 8, pp. 1–15.

Johnson, B.A. *et al.* (2021) ‘Loss of Furin Cleavage Site Attenuates SARS-CoV-2 Pathogenesis’. *Nature*, 591(7849), pp. 293–299.

Jovic, D. *et al.* (2022) ‘Single-cell RNA Sequencing Technologies and Applications: A Brief Overview’. *Clinical and Translational Medicine*, 12(3), p. e694.

Jovisic, M. *et al.* (2023) ‘Differential Roles of Regulatory T Cells in Acute Respiratory Infections’. *The Journal of Clinical Investigation*, 133(14).

Kalantari, Y. *et al.* (2022) ‘A Systematic Review on COVID-19 Vaccination and Cosmetic Filler Reactions: A Focus on Case Studies and Original Articles’. *Journal of Cosmetic Dermatology*, 21(7).

Karki, R. *et al.* (2021) ‘Synergism of TNF-α and IFN-γ Triggers Inflammatory Cell Death, Tissue Damage, and Mortality in SARS-CoV-2 Infection and Cytokine Shock Syndromes’. *Cell*, 184(1), pp. 149–168.

Kasuga, Y. *et al.* (2021) ‘Innate Immune Sensing of Coronavirus and Viral Evasion Strategies’. *Experimental & Molecular Medicine*, 53(5), pp. 723–736.

Katsura, H. *et al.* (2020) ‘Human Lung Stem Cell-Based Alveolospheres Provide Insights into SARS-CoV-2-Mediated Interferon Responses and Pneumocyte Dysfunction’. *Cell Stem Cell*, 27(6), pp. 890–904.

Katze, M.G., He, Y. and Gale, M. (2002) ‘Viruses and Interferon: A Fight for Supremacy’. *Nature Reviews Immunology*, 2(9), pp. 675–687.

Kawai, T. and Akira, S. (2011) ‘Toll-like Receptors and Their Crosstalk with Other Innate Receptors in Infection and Immunity’. *Immunity*, 34(5), pp. 637–650.

Keidar, S., Kaplan, M. and Gamliel-Lazarovich, A. (2007) ‘ACE2 of the Heart: From Angiotensin I to Angiotensin (1–7)’. *Cardiovascular Research*, 73(3), pp. 463–469.

Kelso, J.M. (2022) ‘IgE-mediated Allergy to Polyethylene Glycol (PEG) as a Cause of Anaphylaxis to MRNA COVID-19 Vaccines’. *Clinical and Experimental Allergy*, 52(1), p. 10.

Khoury, D.S. *et al.* (2023) ‘Predicting the Efficacy of Variant-Modified COVID-19 Vaccine Boosters’. *Nature Medicine*, 29(3), pp. 574–578. DOI: 10.1038/s41591-023-02228-4.

Kim, J.H. *et al.* (2021) ‘Operation Warp Speed: Implications for Global Vaccine Security’. *The Lancet Global Health*, 9(7), pp. e1017–e1021.

Kim, J.H. *et al.* (2019) ‘Relationship between Natural Killer Cell Activity and Glucose Control in Patients with Type 2 Diabetes and Prediabetes’. *Journal of Diabetes Investigation*, 10(5), pp. 1223–1228.

Kiselev, V.Y., Andrews, T.S. and Hemberg, M. (2019) ‘Challenges in Unsupervised Clustering of Single-Cell RNA-Seq Data’. *Nature Reviews Genetics*, 20(5), pp. 273–282. DOI: 10.1038/s41576-018-0088-9.

Klein, J. *et al.* (2023) ‘Distinguishing Features of Long COVID Identified through Immune Profiling’. *Nature*, 623(7985), pp. 139–148.

Kolodziejczyk, A.A. *et al.* (2015) ‘The Technology and Biology of Single-Cell RNA Sequencing’. *Molecular Cell*, 58(4), pp. 610–620.

Kong, M. *et al.* (2020) ‘Higher Level of Neutrophil-to-Lymphocyte Is Associated with Severe COVID-19’. *Epidemiology & Infection*, 148, p. e139.

Korsunsky, I. *et al.* (2019) ‘Fast, Sensitive and Accurate Integration of Single-Cell Data with Harmony’. *Nature Methods*, 16(12), pp. 1289–1296.

Kozma, G.T. *et al.* (2023) ‘Role of Anti-Polyethylene Glycol (PEG) Antibodies in the Allergic Reactions to PEG-Containing Covid-19 Vaccines: Evidence for Immunogenicity of PEG’. *Vaccine*, 41(31), pp. 4561–4570.

Kreutmair, S. *et al.* (2021) ‘Distinct Immunological Signatures Discriminate Severe COVID-19 from Non-SARS-CoV-2-Driven Critical Pneumonia’. *Immunity*, 54(7), pp. 1578–1593.

Kroll, M.-K. *et al.* (2023) ‘Importance of ACE2 for SARS-CoV-2 Infection of Kidney Cells’. *Biomolecules*, 13(3), p. 472.

Krueger, F. (2015) ‘Trim Galore!: A Wrapper around Cutadapt and FastQC to Consistently Apply Adapter and Quality Trimming to FastQ Files, with Extra Functionality for RRBS Data’. *Babraham Institute*.

Kuba, K. *et al.* (2005) ‘A Crucial Role of Angiotensin Converting Enzyme 2 (ACE2) in SARS Coronavirus–Induced Lung Injury’. *Nature Medicine*, 11(8), pp. 875–879.

Kuipers, M.T. *et al.* (2013) ‘High Levels of S100A8/A9 Proteins Aggravate Ventilator-Induced Lung Injury via TLR4 Signaling’. *PloS One*, 8(7), p. e68694.

Kusnadi, A. *et al.* (2021) ‘Severely Ill Patients with COVID-19 Display Impaired Exhaustion Features in SARS-CoV-2–Reactive CD8+ T Cells’. *Science Immunology*, 6(55), p. eabe4782.

Kvedaraite, E. *et al.* (2021) ‘Major Alterations in the Mononuclear Phagocyte Landscape Associated with COVID-19 Severity’. *Proceedings of the National Academy of Sciences*, 118(6), p. e2018587118.

Lähnemann, D. *et al.* (2020) ‘Eleven Grand Challenges in Single-Cell Data Science’. *Genome Biology*, 21(1), p. 31. DOI: 10.1186/s13059-020-1926-6.

Laidlaw, B.J., Craft, J.E. and Kaech, S.M. (2016) ‘The Multifaceted Role of CD4+ T Cells in CD8+ T Cell Memory’. *Nature Reviews Immunology*, 16(2), pp. 102–111. DOI: 10.1038/nri.2015.10.

Lamers, M.M. *et al.* (2020) ‘SARS-CoV-2 Productively Infects Human Gut Enterocytes’. *Science*, 369(6499), pp. 50–54.

Langfelder, P. and Horvath, S. (2008) ‘WGCNA: An R Package for Weighted Correlation Network Analysis’. *BMC Bioinformatics*, 9, pp. 1–13.

Lapuente, D., Winkler, T.H. and Tenbusch, M. (2024) ‘B-Cell and Antibody Responses to SARS-CoV-2: Infection, Vaccination, and Hybrid Immunity’. *Cellular & Molecular Immunology*, 21(2), pp. 144–158. DOI: 10.1038/s41423-023-01095-w.

Latz, E., Xiao, T.S. and Stutz, A. (2013) ‘Activation and Regulation of the Inflammasomes’. *Nature Reviews Immunology*, 13(6), pp. 397–411.

Lee, A.J. and Ashkar, A.A. (2018) ‘The Dual Nature of Type I and Type II Interferons’. *Frontiers in Immunology*, p. 2061.

Lee, D. *et al.* (2022) ‘Inborn Errors of OAS–RNase L in SARS-CoV-2–Related Multisystem Inflammatory Syndrome in Children’. *Science*, 379(6632), p. eabo3627.

Lee, P.Y. *et al.* (2009) ‘Type I Interferon Modulates Monocyte Recruitment and Maturation in Chronic Inflammation’. *The American Journal of Pathology*, 175(5), pp. 2023–2033.

Lemke, G. (2013) ‘Biology of the TAM Receptors’. *Cold Spring Harbor Perspectives in Biology*, 5(11), p. a009076.

Lemke, G. and Rothlin, C. V. (2008) ‘Immunobiology of the TAM Receptors’. *Nature Reviews Immunology*, 8(5), pp. 327–336.

Lempp, F.A. *et al.* (2021) ‘Lectins Enhance SARS-CoV-2 Infection and Influence Neutralizing Antibodies’. *Nature*, 598(7880), pp. 342–347.

Letko, M. *et al.* (2020) ‘Bat-Borne Virus Diversity, Spillover and Emergence’. *Nature Reviews Microbiology*, 18(8), pp. 461–471.

Li, D. and Wu, M. (2021) ‘Pattern Recognition Receptors in Health and Diseases’. *Signal Transduction and Targeted Therapy*, 6(1), p. 291.

Li, F. (2016) ‘Structure, Function, and Evolution of Coronavirus Spike Proteins’. *Annual Review of Virology*, 3, pp. 237–261.

Li, H. *et al.* (2020) ‘SARS-CoV-2 and Viral Sepsis: Observations and Hypotheses’. *The Lancet*, 395(10235), pp. 1517–1520.

Li, M. *et al.* (2021) ‘Pharmacological Activation of STING Blocks SARS-CoV-2 Infection’. *Science Immunology*, 6(59), p. eabi9007.

Li, Q. *et al.* (2022) ‘Immune Response in COVID-19: What Is Next?’ *Cell Death & Differentiation*, 29(6), pp. 1107–1122.

Li, W. *et al.* (2003) ‘Angiotensin-Converting Enzyme 2 Is a Functional Receptor for the SARS Coronavirus’. *Nature*, 426(6965), pp. 450–454.

Liao, M. *et al.* (2020) ‘Single-Cell Landscape of Bronchoalveolar Immune Cells in Patients with COVID-19’. *Nature Medicine*, 26(6), pp. 842–844.

Lim, S. *et al.* (2021) ‘COVID-19 and Diabetes Mellitus: From Pathophysiology to Clinical Management’. *Nature Reviews Endocrinology*, 17(1), pp. 11–30.

Lin, Q.X.X. *et al.* (2024) ‘Longitudinal Single Cell Atlas Identifies Complex Temporal Relationship between Type I Interferon Response and COVID-19 Severity’. *Nature Communications*, 15(1), p. 567.

Lindner, D. *et al.* (2020) ‘Association of Cardiac Infection With SARS-CoV-2 in Confirmed COVID-19 Autopsy Cases’. *JAMA Cardiology*, 5(11), pp. 1281–1285. DOI: 10.1001/jamacardio.2020.3551.

Ling, R.R. *et al.* (2022) ‘Myopericarditis Following COVID-19 Vaccination and Non-COVID-19 Vaccination: A Systematic Review and Meta-Analysis’. *The Lancet Respiratory Medicine*.

Liu, J. *et al.* (2020) ‘Neutrophil-to-Lymphocyte Ratio Predicts Critical Illness Patients with 2019 Coronavirus Disease in the Early Stage’. *Journal of Translational Medicine*, 18, pp. 1–12.

Liu, W. and Li, H. (2023) ‘COVID-19: Attacks Immune Cells and Interferences with Antigen Presentation through MHC-like Decoy System’. *Journal of Immunotherapy*, 46(3), pp. 75–88.

Liu, Y. *et al.* (2020) ‘Neutrophil-to-Lymphocyte Ratio as an Independent Risk Factor for Mortality in Hospitalized Patients with COVID-19’. *Journal of Infection*, 81(1), pp. e6–e12.

Liu, Y. and Rocklöv, J. (2021) ‘The Reproductive Number of the Delta Variant of SARS-CoV-2 Is Far Higher Compared to the Ancestral SARS-CoV-2 Virus’. *Journal of Travel Medicine*, 28(7), p. taab124.

Lorentzen, C.L. *et al.* (2022) ‘Clinical Advances and Ongoing Trials of MRNA Vaccines for Cancer Treatment’. *The Lancet Oncology*, 23(10), pp. e450–e458.

Love, M.I. *et al.* (2020) ‘Tximeta: Reference Sequence Checksums for Provenance Identification in RNA-Seq’. *PLoS Computational Biology*, 16(2), p. e1007664.

Love, M.I., Huber, W. and Anders, S. (2014) ‘Moderated Estimation of Fold Change and Dispersion for RNA-Seq Data with DESeq2’. *Genome Biology*, 15, pp. 1–21.

Lu, L. *et al.* (2021) ‘A Potential Role of Interleukin 10 in COVID-19 Pathogenesis’. *Trends in Immunology*, 42(1), pp. 3–5.

Lu, Q. *et al.* (2021) ‘SARS-CoV-2 Exacerbates Proinflammatory Responses in Myeloid Cells through C-Type Lectin Receptors and Tweety Family Member 2’. *Immunity*, 54(6), pp. 1304–1319.

Lu, R. *et al.* (2020) ‘Genomic Characterisation and Epidemiology of 2019 Novel Coronavirus: Implications for Virus Origins and Receptor Binding’. *The Lancet*, 395(10224), pp. 565–574.

Lui, G. *et al.* (2020) ‘Viral Dynamics of SARS-CoV-2 across a Spectrum of Disease Severity in COVID-19’. *Journal of Infection*, 81(2), pp. 318–356.

Van Der Made, C.I. *et al.* (2020) ‘Presence of Genetic Variants among Young Men with Severe COVID-19’. *Jama*, 324(7), pp. 663–673.

Mallajosyula, V. *et al.* (2021) ‘CD8+ T Cells Specific for Conserved Coronavirus Epitopes Correlate with Milder Disease in Patients with COVID-19’. *Science Immunology*, 6(61), p. eabg5669.

Mangiola, S. *et al.* (2024) ‘A Multi-Organ Map of the Human Immune System across Age, Sex and Ethnicity’. *BioRxiv*.

Mangiola, S. *et al.* (2023) ‘Sccomp: Robust Differential Composition and Variability Analysis for Single-Cell Data’. *Proceedings of the National Academy of Sciences*, 120(33), p. e2203828120.

Mangiola, S., Molania, R., *et al.* (2021) ‘Tidybulk: An R Tidy Framework for Modular Transcriptomic Data Analysis’. *Genome Biology*, 22, pp. 1–15.

Mangiola, S., Doyle, M.A. and Papenfuss, A.T. (2021) ‘Interfacing Seurat with the R Tidy Universe’. *Bioinformatics*, 37(22), pp. 4100–4107.

Márquez, E.J. *et al.* (2020) ‘Sexual-Dimorphism in Human Immune System Aging’. *Nature Communications*, 11(1), p. 751. DOI: 10.1038/s41467-020-14396-9.

Marsh, S. (2022) *ScCustomize Package*. Available at: https://github.com/samuel-marsh/scCustomize.

Marshall, J.S. *et al.* (2018) ‘An Introduction to Immunology and Immunopathology’. *Allergy, Asthma & Clinical Immunology*, 14(2), pp. 1–10.

Martin-Sancho, L. *et al.* (2021) ‘Functional Landscape of SARS-CoV-2 Cellular Restriction’. *Molecular Cell*, 81(12), pp. 2656–2668.

Mazzoni, A. *et al.* (2020) ‘Impaired Immune Cell Cytotoxicity in Severe COVID-19 Is IL-6 Dependent’. *The Journal of Clinical Investigation*, 130(9), pp. 4694–4703.

McBride, R., Van Zyl, M. and Fielding, B.C. (2014) ‘The Coronavirus Nucleocapsid Is a Multifunctional Protein’. *Viruses*, 6(8), pp. 2991–3018.

McCallum, M. *et al.* (2020) ‘Structure-Guided Covalent Stabilization of Coronavirus Spike Glycoprotein Trimers in the Closed Conformation’. *Nature Structural & Molecular Biology*, 27(10), pp. 942–949.

McIntosh, K. *et al.* (1967) ‘Recovery in Tracheal Organ Cultures of Novel Viruses from Patients with Respiratory Disease.’ *Proceedings of the National Academy of Sciences*, 57(4), pp. 933–940. DOI: 10.1073/pnas.57.4.933.

McMahan, K. *et al.* (2021) ‘Correlates of Protection against SARS-CoV-2 in Rhesus Macaques’. *Nature*, 590(7847), pp. 630–634.

McNab, F. *et al.* (2015) ‘Type I Interferons in Infectious Disease’. *Nature Reviews Immunology*, 15(2), pp. 87–103. DOI: 10.1038/nri3787.

Meckiff, B.J. *et al.* (2020) ‘Imbalance of Regulatory and Cytotoxic SARS-CoV-2-Reactive CD4+ T Cells in COVID-19’. *Cell*, 183(5), pp. 1340–1353.

Melms, J.C. *et al.* (2021) ‘A Molecular Single-Cell Lung Atlas of Lethal COVID-19’. *Nature*, 595(7865), pp. 114–119.

Meo, S.A. *et al.* (2021) ‘COVID-19 Vaccines: Comparison of Biological, Pharmacological Characteristics and Adverse Effects of Pfizer/BioNTech and Moderna Vaccines.’ *European Review for Medical & Pharmacological Sciences*, 25(3).

Merad, M. *et al.* (2022) ‘The Immunology and Immunopathology of COVID-19’. *Science*, 375(6585), pp. 1122–1127.

Mercado, N.B. *et al.* (2020) ‘Single-Shot Ad26 Vaccine Protects against SARS-CoV-2 in Rhesus Macaques’. *Nature*, 586(7830), pp. 583–588.

Mesev, E. V., LeDesma, R.A. and Ploss, A. (2019) ‘Decoding Type I and III Interferon Signalling during Viral Infection’. *Nature Microbiology*, 4(6), pp. 914–924.

Meyerholz, D.K., Lambertz, A.M. and McCray Jr, P.B. (2016) 'Dipeptidyl Peptidase 4 Distribution in the Human Respiratory Tract: Implications for the Middle East Respiratory Syndrome'. *The American Journal of Pathology*, 186(1), pp. 78–86.

Middleton, E.A. *et al.* (2020) 'Neutrophil Extracellular Traps Contribute to Immunothrombosis in COVID-19 Acute Respiratory Distress Syndrome'. *Blood, The Journal of the American Society of Hematology*, 136(10), pp. 1169–1179.

Moderbacher, C.R. *et al.* (2020) 'Antigen-Specific Adaptive Immunity to SARS-CoV-2 in Acute COVID-19 and Associations with Age and Disease Severity'. *Cell*, 183(4), pp. 996–1012.

Montezano, A.C. *et al.* (2023) 'SARS-CoV-2 Spike Protein Induces Endothelial Inflammation via ACE2 Independently of Viral Replication'. *Scientific Reports*, 13(1), p. 14086.

Montopoli, M. *et al.* (2020) 'Androgen-Deprivation Therapies for Prostate Cancer and Risk of Infection by SARS-CoV-2: A Population-Based Study (N= 4532)'. *Annals of Oncology*, 31(8), pp. 1040–1045.

Morgan, M. *et al.* (2023) (1.32.0) *SummarizedExperiment: A Container (S4 Class) for Matrix-like Assays*. DOI: 10.18129/B9.bioc.SummarizedExperiment.

Mortz, C.G. *et al.* (2022) 'Allergy to Polyethylene Glycol and Polysorbates in a Patient Cohort: Diagnostic Work-up and Decision Points for Vaccination during the COVID-19 Pandemic'. *Clinical and Translational Allergy*, 12(1), p. e12111.

Moss, P. (2022) 'The T Cell Immune Response against SARS-CoV-2'. *Nature Immunology*, 23(2), pp. 186–193. DOI: 10.1038/s41590-021-01122-w.

Mulè, M.P., Martins, A.J. and Tsang, J.S. (2022) 'Normalizing and Denoising Protein Expression Data from Droplet-Based Single Cell Profiling'. *Nature Communications*, 13(1), p. 2099.

Munnur, D. *et al.* (2021) ‘Altered ISGylation Drives Aberrant Macrophage-Dependent Immune Responses during SARS-CoV-2 Infection’. *Nature Immunology*, 22(11), pp. 1416–1427. DOI: 10.1038/s41590-021-01035-8.

Muskovic, W. and Powell, J.E. (2021) ‘DropletQC: Improved Identification of Empty Droplets and Damaged Cells in Single-Cell RNA-Seq Data’. *Genome Biology*, 22, pp. 1–9.

Myers, L.C. *et al.* (2020) ‘Characteristics of Hospitalized Adults with COVID-19 in an Integrated Health Care System in California’. *Jama*, 323(21), pp. 2195–2198.

Nakazawa, D. *et al.* (2023) ‘Inhibition of Toll-like Receptor 4 and Interleukin-1 Receptor Prevent SARS-CoV-2 Mediated Kidney Injury’. *Cell Death Discovery*, 9(1), p. 293.

Nannoni, S. *et al.* (2021) ‘Stroke in COVID-19: A Systematic Review and Meta-Analysis’. *International Journal of Stroke*, 16(2), pp. 137–149.

Narumi, K. *et al.* (2015) ‘Proinflammatory Proteins S100A8/S100A9 Activate NK Cells via Interaction with RAGE’. *The Journal of Immunology*, 194(11), pp. 5539–5548.

Nasu, J. *et al.* (2020) ‘Pivotal Role of the Carbohydrate Recognition Domain in Self-Interaction of CLEC4A to Elicit the ITIM-Mediated Inhibitory Function in Murine Conventional Dendritic Cells in Vitro’. *International Immunology*, 32(10), pp. 673–682.

Nchioua, R. *et al.* (2022) ‘SARS-CoV-2 Variants of Concern Hijack IFITM2 for Efficient Replication in Human Lung Cells’. *Journal of Virology*, 96(11), pp. e00594-22.

Neuman, B.W. *et al.* (2011) ‘A Structural Analysis of M Protein in Coronavirus Assembly and Morphology’. *Journal of Structural Biology*, 174(1), pp. 11–22.

Neumann, J. *et al.* (2020) ‘Increased IL-10-producing Regulatory T Cells Are Characteristic of Severe Cases of COVID-19’. *Clinical & Translational Immunology*, 9(11), p. e1204.

Newman, J. *et al.* (2022) ‘Neutralizing Antibody Activity against 21 SARS-CoV-2 Variants in Older Adults Vaccinated with BNT162b2’. *Nature Microbiology*, 7(8), pp. 1180–1188.

Nguyen, D.C. *et al.* (2011) ‘17β-Estradiol Restores Antibody Responses to an Influenza Vaccine in a Postmenopausal Mouse Model’. *Vaccine*, 29(14), pp. 2515–2518.

Notarte, K.I. *et al.* (2022) ‘Impact of COVID-19 Vaccination on the Risk of Developing Long-COVID and on Existing Long-COVID Symptoms: A Systematic Review’. *EClinicalMedicine*, 53.

Odainic, A. *et al.* (2022) ‘Comparative Analysis of Antibody Titers against the Spike Protein of SARS-CoV-2 Variants in Infected Patient Cohorts and Diverse Vaccination Regimes’. *International Journal of Molecular Sciences*, 23(20), p. 12231.

Ortego, J. *et al.* (2007) ‘Absence of E Protein Arrests Transmissible Gastroenteritis Coronavirus Maturation in the Secretory Pathway’. *Virology*, 368(2), pp. 296–308.

Pak, A. *et al.* (2020) ‘Economic Consequences of the COVID-19 Outbreak: The Need for Epidemic Preparedness’. *Frontiers in Public Health*, 8, p. 241.

Paludan, S.R. and Mogensen, T.H. (2022) ‘Innate Immunological Pathways in COVID-19 Pathogenesis’. *Science Immunology*, 7(67), p. eabm5505.

Park, I. *et al.* (2022) ‘C-Type Lectin Receptor CLEC4A2 Promotes Tissue Adaptation of Macrophages and Protects against Atherosclerosis’. *Nature Communications*, 13(1), p. 215.

Patrick, D.M., Van Beusecum, J.P. and Kirabo, A. (2021) ‘The Role of Inflammation in Hypertension: Novel Concepts’. *Current Opinion in Physiology*, 19, pp. 92–98.

Patro, R. *et al.* (2017) ‘Salmon Provides Fast and Bias-Aware Quantification of Transcript Expression’. *Nature Methods*, 14(4), pp. 417–419.

Pazos, M.A. *et al.* (2012) ‘Estrogen Mediates Innate and Adaptive Immune Alterations to Influenza Infection in Pregnant Mice’. *PloS One*, 7(7), p. e40502.

Pekayvaz, K. *et al.* (2022) ‘Protective Immune Trajectories in Early Viral Containment of Non-Pneumonic SARS-CoV-2 Infection’. *Nature Communications*, 13(1), p. 1018.

Peñaloza, H.F., Lee, J.S. and Ray, P. (2021) ‘Neutrophils and Lymphopenia, an Unknown Axis in Severe COVID-19 Disease’. *PLoS Pathogens*, 17(9), p. e1009850.

Peng, Y. *et al.* (2020) ‘Broad and Strong Memory CD4+ and CD8+ T Cells Induced by SARS-CoV-2 in UK Convalescent Individuals Following COVID-19’. *Nature Immunology*, 21(11), pp. 1336–1345. DOI: 10.1038/s41590-020-0782-6.

Pérez-Gómez, A. *et al.* (2021) ‘Dendritic Cell Deficiencies Persist Seven Months after SARS-CoV-2 Infection’. *Cellular & Molecular Immunology*, 18(9), pp. 2128–2139.

Perna, F. *et al.* (2022) ‘Rapid Resolution of Severe Pericardial Effusion Using Anakinra in a Patient with COVID-19 Vaccine-Related Acute Pericarditis Relapse: A Case Report’. *European Heart Journal-Case Reports*, 6(4), p. ytac123.

Perry, R.J. *et al.* (2021) ‘Cerebral Venous Thrombosis after Vaccination against COVID-19 in the UK: A Multicentre Cohort Study’. *The Lancet*, 398(10306), pp. 1147–1156.

Pinto, P.B.A. *et al.* (2024) ‘Co-Immunization with Spike and Nucleocapsid Based DNA Vaccines for Long-Term Protective Immunity against SARS-CoV-2 Omicron’. *Npj Vaccines*, 9(1), p. 252. DOI: 10.1038/s41541-024-01043-3.

Piva, S. *et al.* (2020) ‘Clinical Presentation and Initial Management Critically Ill Patients with Severe Acute Respiratory Syndrome Coronavirus 2 (SARS-CoV-2) Infection in Brescia, Italy’. *Journal of Critical Care*, 58, pp. 29–33.

Pizzato, M. *et al.* (2022) ‘SARS-CoV-2 and the Host Cell: A Tale of Interactions’. *Frontiers in Virology*, 1.

Polack, F.P. *et al.* (2020) ‘Safety and Efficacy of the BNT162b2 MRNA Covid-19 Vaccine’. *New England Journal of Medicine*, 383(27), pp. 2603–2615.

Prelli Bozzo, C. *et al.* (2021) ‘IFITM Proteins Promote SARS-CoV-2 Infection and Are Targets for Virus Inhibition in Vitro’. *Nature Communications*, 12(1), p. 4584.

Proal, A.D. and VanElzakker, M.B. (2021) ‘Long COVID or Post-Acute Sequelae of COVID-19 (PASC): An Overview of Biological Factors That May Contribute to Persistent Symptoms’. *Frontiers in Microbiology*, 12, p. 698169.

Rajamanickam, A. *et al.* (2021) ‘Dynamic Alterations in Monocyte Numbers, Subset Frequencies and Activation Markers in Acute and Convalescent COVID-19 Individuals’. *Scientific Reports*, 11(1), p. 20254.

Rajamanickam, A. *et al.* (2022) ‘Restoration of Dendritic Cell Homeostasis and Type I/Type III Interferon Levels in Convalescent COVID-19 Individuals’. *BMC Immunology*, 23(1), p. 51.

Ramaswamy, A. *et al.* (2021) ‘Immune Dysregulation and Autoreactivity Correlate with Disease Severity in SARS-CoV-2-Associated Multisystem Inflammatory Syndrome in Children’. *Immunity*, 54(5), pp. 1083–1095.

Rebendenne, A. *et al.* (2021) ‘SARS-CoV-2 Triggers an MDA-5-Dependent Interferon Response Which Is Unable to Control Replication in Lung Epithelial Cells’. *Journal of Virology*, 95(8), pp. 10–1128.

Ren, X. *et al.* (2021) ‘COVID-19 Immune Features Revealed by a Large-Scale Single-Cell Transcriptome Atlas’. *Cell*, 184(7), pp. 1895–1913.

Reyes, M. *et al.* (2020) ‘An Immune-Cell Signature of Bacterial Sepsis’. *Nature Medicine*, 26(3), pp. 333–340.

Rieke, G.J. *et al.* (2022) ‘Natural Killer Cell-Mediated Antibody-Dependent Cellular Cytotoxicity against SARS-CoV-2 after Natural Infection Is More Potent than after Vaccination’. *The Journal of Infectious Diseases*, 225(10), pp. 1688–1693.

Riphagen, S. *et al.* (2020) ‘Hyperinflammatory Shock in Children during COVID-19 Pandemic’. *The Lancet*, 395(10237), pp. 1607–1608.

Robertson, S.J. *et al.* (2023) ‘Genetically Diverse Mouse Models of SARS-CoV-2 Infection Reproduce Clinical Variation in Type I Interferon and Cytokine Responses in COVID-19’. *Nature Communications*, 14(1), p. 4481.

Rojas, J.M. *et al.* (2017) ‘IL-10: A Multifunctional Cytokine in Viral Infections’. *Journal of Immunology Research*, 2017.

Rothlin, C. V. *et al.* (2007) ‘TAM Receptors Are Pleiotropic Inhibitors of the Innate Immune Response’. *Cell*, 131(6), pp. 1124–1136.

Rotshild, V. *et al.* (2021) ‘Comparing the Clinical Efficacy of COVID-19 Vaccines: A Systematic Review and Network Meta-Analysis’. *Scientific Reports*, 11(1), p. 22777. DOI: 10.1038/s41598-021-02321-z.

Rui, Y. *et al.* (2021) ‘Unique and Complementary Suppression of CGAS-STING and RNA Sensing-Triggered Innate Immune Responses by SARS-CoV-2 Proteins’. *Signal Transduction and Targeted Therapy*, 6(1), p. 123.

Sadarangani, M., Marchant, A. and Kollmann, T.R. (2021) ‘Immunological Mechanisms of Vaccine-Induced Protection against COVID-19 in Humans’. *Nature Reviews Immunology*, 21(8), pp. 475–484.

Sadoff, J. *et al.* (2021) ‘Safety and Efficacy of Single-Dose Ad26. COV2. S Vaccine against Covid-19’. *New England Journal of Medicine*, 384(23), pp. 2187–2201.

Sahanic, S. *et al.* (2023) ‘SARS-CoV-2 Activates the TLR4/MyD88 Pathway in Human Macrophages: A Possible Correlation with Strong pro-Inflammatory Responses in Severe COVID-19’. *Heliyon*, 9(11).

Saheb Sharif-Askari, F. *et al.* (2023) ‘Increased Blood Immune Regulatory Cells in Severe COVID-19 with Autoantibodies to Type I Interferons’. *Scientific Reports*, 13(1), p. 17344.

Saichi, M. *et al.* (2021) ‘Single-Cell RNA Sequencing of Blood Antigen-Presenting Cells in Severe COVID-19 Reveals Multi-Process Defects in Antiviral Immunity’. *Nature Cell Biology*, 23(5), pp. 538–551.

Saikia, P., Fensterl, V. and Sen, G.C. (2010) ‘The Inhibitory Action of P56 on Select Functions of E1 Mediates Interferon’s Effect on Human Papillomavirus DNA Replication’. *Journal of Virology*, 84(24), pp. 13036–13039.

Sánchez-Cerrillo, I. *et al.* (2020) ‘COVID-19 Severity Associates with Pulmonary Redistribution of CD1c+ DCs and Inflammatory Transitional and Nonclassical Monocytes’. *The Journal of Clinical Investigation*, 130(12), pp. 6290–6300.

Sardu, C. *et al.* (2020) ‘Hypertension, Thrombosis, Kidney Failure, and Diabetes: Is COVID-19 an Endothelial Disease? A Comprehensive Evaluation of Clinical and Basic Evidence’. *Journal of Clinical Medicine*, 9(5), p. 1417.

Schindewolf, C. *et al.* (2023) ‘SARS-CoV-2 Uses Nonstructural Protein 16 to Evade Restriction by IFIT1 and IFIT3’. *Journal of Virology*, 97(2), pp. e01532-22.

Schmiedel, B.J. *et al.* (2021) 'COVID-19 Genetic Risk Variants Are Associated with Expression of Multiple Genes in Diverse Immune Cell Types'. *Nature Communications*, 12(1), p. 6760.

Schoeman, D. and Fielding, B.C. (2019) 'Coronavirus Envelope Protein: Current Knowledge'. *Virology Journal*, 16(1), pp. 1–22.

Schoggins, J.W. (2019) 'Interferon-Stimulated Genes: What Do They All Do?' *Annual Review of Virology*, 6, pp. 567–584.

Schoggins, J.W. *et al.* (2014) 'Pan-Viral Specificity of IFN-Induced Genes Reveals New Roles for CGAS in Innate Immunity'. *Nature*, 505(7485), pp. 691–695.

Schulien, I. *et al.* (2021) 'Characterization of Pre-Existing and Induced SARS-CoV-2-Specific CD8+ T Cells'. *Nature Medicine*, 27(1), pp. 78–85.

Schulte-Schrepping, J. *et al.* (2020) 'Severe COVID-19 Is Marked by a Dysregulated Myeloid Cell Compartment'. *Cell*, 182(6), pp. 1419–1440.

Sekine, T. *et al.* (2020) 'Robust T Cell Immunity in Convalescent Individuals with Asymptomatic or Mild COVID-19'. *Cell*, 183(1), pp. 158–168.

Sellaturay, P. *et al.* (2021) 'Polyethylene Glycol (PEG) Is a Cause of Anaphylaxis to the Pfizer/BioNTech MRNA COVID-19 Vaccine'. *Clinical and Experimental Allergy*, 51(6), p. 861.

Sellaturay, P. *et al.* (2022) 'The Polysorbate Containing AstraZeneca COVID-19 Vaccine Is Tolerated by Polyethylene Glycol (PEG) Allergic Patients'. *Clinical & Experimental Allergy*, 52(1), pp. 12–17.

Sen, G.C. and Sarkar, S.N. (2007) 'The Interferon-Stimulated Genes: Targets of Direct Signaling by Interferons, Double-Stranded RNA, and Viruses'. *Interferon: The 50th Anniversary*, pp. 233–250.

Shaath, H. *et al.* (2020) ‘Single-Cell Transcriptome Analysis Highlights a Role for Neutrophils and Inflammatory Macrophages in the Pathogenesis of Severe COVID-19’. *Cells*, 9(11), p. 2374.

Sharifian-Dorche, M. *et al.* (2021) ‘Vaccine-Induced Immune Thrombotic Thrombocytopenia and Cerebral Venous Sinus Thrombosis Post COVID-19 Vaccination; a Systematic Review’. *Journal of the Neurological Sciences*, 428, p. 117607.

Shen, J. *et al.* (2023) ‘Innate and Adaptive Immunity to SARS-CoV-2 and Predisposing Factors’. *Frontiers in Immunology*, 14, p. 1159326.

Shi, Y. *et al.* (2024) ‘Mutations Accumulated in the Spike of SARS-CoV-2 Omicron Allow for More Efficient Counteraction of the Restriction Factor BST2/Tetherin’. *Plos Pathogens*, 20(1), p. e1011912.

Singh, K.K. *et al.* (2020) ‘Decoding SARS-CoV-2 Hijacking of Host Mitochondria in COVID-19 Pathogenesis’. *American Journal of Physiology-Cell Physiology*, 319(2), pp. C258–C267.

Soneson, C., Love, M.I. and Robinson, M.D. (2015) ‘Differential Analyses for RNA-Seq: Transcript-Level Estimates Improve Gene-Level Inferences’. *F1000Research*, 4.

Soriano, J.B. *et al.* (2022) ‘A Clinical Case Definition of Post-COVID-19 Condition by a Delphi Consensus’. *The Lancet Infectious Diseases*, 22(4), pp. e102–e107.

Soveg, F.W. *et al.* (2021) ‘Endomembrane Targeting of Human OAS1 P46 Augments Antiviral Activity’. *Elife*, 10, p. e71047.

Spelios, M.G., Capanelli, J.M. and Li, A.W. (2022) ‘A Novel Antibody against the Furin Cleavage Site of SARS-CoV-2 Spike Protein: Effects on Proteolytic Cleavage and ACE2 Binding’. *Immunology Letters*, 242, pp. 1–7.

Stoeckius, M. *et al.* (2017) ‘Simultaneous Epitope and Transcriptome Measurement in Single Cells’. *Nature Methods*, 14(9), pp. 865–868.

Stuart, T. *et al.* (2019) ‘Comprehensive Integration of Single-Cell Data’. *Cell*, 177(7), pp. 1888–1902.

Su, S. *et al.* (2016) ‘Epidemiology, Genetic Recombination, and Pathogenesis of Coronaviruses’. *Trends in Microbiology*, 24(6), pp. 490–502.

Su, Y. *et al.* (2020) ‘Multi-Omics Resolves a Sharp Disease-State Shift between Mild and Moderate COVID-19’. *Cell*, 183(6), pp. 1479–1495.

Su, Y. *et al.* (2022) ‘Multiple Early Factors Anticipate Post-Acute COVID-19 Sequelae’. *Cell*, 185(5), pp. 881–895.

Sun, B. *et al.* (2017) ‘Dengue Virus Activates CGAS through the Release of Mitochondrial DNA’. *Scientific Reports*, 7(1), p. 3594.

Sun, L. *et al.* (2013) ‘Cyclic GMP-AMP Synthase Is a Cytosolic DNA Sensor That Activates the Type I Interferon Pathway’. *Science*, 339(6121), pp. 786–791.

Sun, L. *et al.* (2023) ‘T Cells in Health and Disease’. *Signal Transduction and Targeted Therapy*, 8(1), p. 235. DOI: 10.1038/s41392-023-01471-y.

Swadling, L. *et al.* (2022) ‘Pre-Existing Polymerase-Specific T Cells Expand in Abortive Seronegative SARS-CoV-2’. *Nature*, 601(7891), pp. 110–117. DOI: 10.1038/s41586-021-04186-8.

Swain, S.L., McKinstry, K.K. and Strutt, T.M. (2012) ‘Expanding Roles for CD4+ T Cells in Immunity to Viruses’. *Nature Reviews Immunology*, 12(2), pp. 136–148. DOI: 10.1038/nri3152.

Swank, Z. *et al.* (2023) ‘Persistent Circulating Severe Acute Respiratory Syndrome Coronavirus 2 Spike Is Associated with Post-Acute Coronavirus Disease 2019 Sequelae’. *Clinical Infectious Diseases*, 76(3), pp. e487–e490.

Taefehshokr, N. *et al.* (2024) ‘SARS-CoV-2 NSP5 Antagonizes MHC II Expression by Subverting Histone Deacetylase 2’. *Journal of Cell Science*, 137(10).

Tahtinen, S. *et al.* (2022) ‘IL-1 and IL-1ra Are Key Regulators of the Inflammatory Response to RNA Vaccines’. *Nature Immunology*, 23(4), pp. 532–542.

Tan, A.T. *et al.* (2021) ‘Early Induction of Functional SARS-CoV-2-Specific T Cells Associates with Rapid Viral Clearance and Mild Disease in COVID-19 Patients’. *Cell Reports*, 34(6).

Tan, X. *et al.* (2017) ‘Involvement of S100A8/A9-TLR4-NLRP3 Inflammasome Pathway in Contrast-Induced Acute Kidney Injury’. *Cellular Physiology and Biochemistry*, 43(1), pp. 209–222.

The United States Food and Drug Administration. (2020) *FDA and EMA Collaborate to Facilitate SARS-CoV-2 Vaccine Development*. Available at: https://www.fda.gov/news-events/fda-voices/fda-and-ema-collaborate-facilitate-sars-cov-2-vaccine-development (Accessed: 1 May 2024).

Thomas, S.J. *et al.* (2021) ‘Safety and Efficacy of the BNT162b2 MRNA Covid-19 Vaccine through 6 Months’. *New England Journal of Medicine*, 385(19), pp. 1761–1773.

Thompson, E.J. *et al.* (2022) ‘Long COVID Burden and Risk Factors in 10 UK Longitudinal Studies and Electronic Health Records’. *Nature Communications*, 13(1), p. 3528.

Thompson, M.G. *et al.* (2021) ‘Prevention and Attenuation of Covid-19 with the BNT162b2 and MRNA-1273 Vaccines’. *New England Journal of Medicine*, 385(4), pp. 320–329.

Tian, J. *et al.* (2022) ‘Emerging Viruses: Cross-Species Transmission of Coronaviruses, Filoviruses, Henipaviruses and Rotaviruses from Bats’. *Cell Reports*.

Traag, V.A., Waltman, L. and van Eck, N.J. (2019) ‘From Louvain to Leiden: Guaranteeing Well-Connected Communities’. *Scientific Reports*, 9(1), p. 5233. DOI: 10.1038/s41598-019-41695-z.

Trump, S. *et al.* (2021) ‘Hypertension Delays Viral Clearance and Exacerbates Airway Hyperinflammation in Patients with COVID-19’. *Nature Biotechnology*, 39(6), pp. 705–716.

Tye, E.X.C. *et al.* (2022) ‘Mutations in SARS-CoV-2 Spike Protein Impair Epitope-Specific CD4+ T Cell Recognition’. *Nature Immunology*, 23(12), pp. 1726–1734. DOI: 10.1038/s41590-022-01351-7.

Tyrrell, D.A.J. and Bynoe, M.L. (1965) ‘Cultivation of a Novel Type of Common-Cold Virus in Organ Cultures’. *British Medical Journal*, 1(5448), p. 1467. DOI: 10.1136/bmj.1.5448.1467.

Unterman, A. *et al.* (2022) ‘Single-Cell Multi-Omics Reveals Dyssynchrony of the Innate and Adaptive Immune System in Progressive COVID-19’. *Nature Communications*, 13(1), p. 440.

Uto, T. *et al.* (2016) ‘Clec4A4 Is a Regulatory Receptor for Dendritic Cells That Impairs Inflammation and T-Cell Immunity’. *Nature Communications*, 7(1), p. 11273.

Vabret, N. *et al.* (2020) ‘Immunology of COVID-19: Current State of the Science’. *Immunity*, 52(6), pp. 910–941.

Del Valle, D.M. *et al.* (2020) ‘An Inflammatory Cytokine Signature Predicts COVID-19 Severity and Survival’. *Nature Medicine*, 26(10), pp. 1636–1643.

Vanderbeke, L. *et al.* (2021) ‘Monocyte-Driven Atypical Cytokine Storm and Aberrant Neutrophil Activation as Key Mediators of COVID-19 Disease Severity’. *Nature Communications*, 12(1), p. 4117.

Vanderheiden, A. *et al.* (2020) ‘Type I and Type III Interferons Restrict SARS-CoV-2 Infection of Human Airway Epithelial Cultures’. *Journal of Virology*, 94(19), pp. 10–1128.

Varga, Z. *et al.* (2020) ‘Endothelial Cell Infection and Endotheliitis in COVID-19’. *The Lancet*, 395(10234), pp. 1417–1418.

Venet, M. *et al.* (2023) ‘Severe COVID-19 Patients Have Impaired Plasmacytoid Dendritic Cell-Mediated Control of SARS-CoV-2’. *Nature Communications*, 14(1), p. 694.

Veras, F.P. *et al.* (2020) ‘SARS-CoV-2–Triggered Neutrophil Extracellular Traps Mediate COVID-19 Pathology’. *Journal of Experimental Medicine*, 217(12), p. e20201129.

Vermillion, M.S. *et al.* (2018) ‘Estriol Reduces Pulmonary Immune Cell Recruitment and Inflammation to Protect Female Mice from Severe Influenza’. *Endocrinology*, 159(9), pp. 3306–3320.

Vogl, T. *et al.* (2007) ‘Mrp8 and Mrp14 Are Endogenous Activators of Toll-like Receptor 4, Promoting Lethal, Endotoxin-Induced Shock’. *Nature Medicine*, 13(9), pp. 1042–1049.

Voysey, M. *et al.* (2021) ‘Safety and Efficacy of the ChAdOx1 NCoV-19 Vaccine (AZD1222) against SARS-CoV-2: An Interim Analysis of Four Randomised Controlled Trials in Brazil, South Africa, and the UK’. *The Lancet*, 397(10269), pp. 99–111.

Walls, A.C. *et al.* (2020) ‘Structure, Function, and Antigenicity of the SARS-CoV-2 Spike Glycoprotein’. *Cell*, 181(2), pp. 281–292.

Wang, C. *et al.* (2003) ‘Alpha Interferon Induces Distinct Translational Control Programs to Suppress Hepatitis C Virus RNA Replication’. *Journal of Virology*, 77(7), pp. 3898–3912.

Wang, Jing. *et al.* (2023) ‘Individual Bat Virome Analysis Reveals Co-Infection and Spillover among Bats and Virus Zoonotic Potential’. *Nature Communications*, 14(1), p. 4079. DOI: 10.1038/s41467-023-39835-1.

Wang, K. *et al.* (2020) ‘CD147-Spike Protein Is a Novel Route for SARS-CoV-2 Infection to Host Cells’. *Signal Transduction and Targeted Therapy*, 5(1), p. 283. DOI: 10.1038/s41392-020-00426-x.

Wang, K.E. *et al.* (2020) ‘CD147-Spike Protein Is a Novel Route for SARS-CoV-2 Infection to Host Cells’. *Signal Transduction and Targeted Therapy*, 5(1), p. 283.

Wang, P. *et al.* (2021) ‘Antibody Resistance of SARS-CoV-2 Variants B. 1.351 and B. 1.1. 7’. *Nature*, 593(7857), pp. 130–135.

Wang, S. *et al.* (2021) ‘AXL Is a Candidate Receptor for SARS-CoV-2 That Promotes Infection of Pulmonary and Bronchial Epithelial Cells’. *Cell Research*, 31(2), pp. 126–140.

Wang, Siwen. *et al.* (2018) ‘S100A8/A9 in Inflammation’. *Frontiers in Immunology*, 9, p. 1298.

Wang, Xin. *et al.* (2024) ‘Nonconserved Epitopes Dominate Reverse Preexisting T Cell Immunity in COVID-19 Convalescents’. *Signal Transduction and Targeted Therapy*, 9(1), p. 160. DOI: 10.1038/s41392-024-01876-3.

Wang, Y. *et al.* (2020) ‘A Comprehensive Investigation of the MRNA and Protein Level of ACE2, the Putative Receptor of SARS-CoV-2, in Human Tissues and Blood Cells’. *International Journal of Medical Sciences*, 17(11), p. 1522.

Wauters, E. *et al.* (2021) ‘Discriminating Mild from Critical COVID-19 by Innate and Adaptive Immune Single-Cell Profiling of Bronchoalveolar Lavages’. *Cell Research*, 31(3), pp. 272–290.

Wei, J. *et al.* (2021) ‘Anti-Spike Antibody Response to Natural SARS-CoV-2 Infection in the General Population’. *Nature Communications*, 12(1), pp. 1–12.

Wendisch, D. *et al.* (2021) ‘SARS-CoV-2 Infection Triggers Profibrotic Macrophage Responses and Lung Fibrosis’. *Cell*, 184(26), pp. 6243–6261.

Whittaker, E. *et al.* (2020) ‘Clinical Characteristics of 58 Children with a Pediatric Inflammatory Multisystem Syndrome Temporally Associated with SARS-CoV-2’. *Jama*, 324(3), pp. 259–269.

Wickenhagen, A. *et al.* (2021) ‘A Prenylated DsRNA Sensor Protects against Severe COVID-19’. *Science*, 374(6567), p. eabj3624.

Wiersinga, W.J. *et al.* (2020) ‘Pathophysiology, Transmission, Diagnosis, and Treatment of Coronavirus Disease 2019 (COVID-19): A Review’. *Jama*, 324(8), pp. 782–793.

Winkler, C.W. *et al.* (2024) ‘CC Motif Chemokine Receptor 2 and 7 Synergistically Control Inflammatory Monocyte Recruitment but the Infecting Virus Dictates Monocyte Function in the Brain’. *Communications Biology*, 7(1), p. 494.

Winstone, H. *et al.* (2021) ‘The Polybasic Cleavage Site in SARS-CoV-2 Spike Modulates Viral Sensitivity to Type I Interferon and IFITM2’. *Journal of Virology*, 95(9), pp. 10–1128.

Wong, K.L. *et al.* (2011) ‘Gene Expression Profiling Reveals the Defining Features of the Classical, Intermediate, and Nonclassical Human Monocyte Subsets’. *Blood, The Journal of the American Society of Hematology*, 118(5), pp. e16–e31.

Woo, P.C.Y. *et al.* (2012) ‘Discovery of Seven Novel Mammalian and Avian Coronaviruses in the Genus Deltacoronavirus Supports Bat Coronaviruses as the Gene Source of Alphacoronavirus and Betacoronavirus and Avian Coronaviruses as the Gene Source of Gammacoronavirus and Deltacoronavirus’. *Journal of Virology*, 86(7), pp. 3995–4008.

World Health Organization. (2022) *Interim Recommendations for the Use of the Janssen Ad26.COV2.S (COVID-19) Vaccine*. Available at: https://iris.who.int/bitstream/handle/10665/355160/WHO-2019-nCoV-vaccines-SAGE-recommendation-Ad26.COV2.S-2022.1-eng.pdf?sequence=1 (Accessed: 24 April 2024).

World Health Organization. (2023) *Therapeutics and COVID-19: Living Guideline, Version 7*. World Health Organization Available at: https://iris.who.int/bitstream/handle/10665/365580/WHO-2019-nCoV-clinical-2023.1-eng.pdf (Accessed: 23 February 2024).

World Health Organization. (2024) *WHO Coronavirus (COVID-19) Dashboard > Deaths [Dashboard]*.

Wrapp, D. *et al.* (2020) 'Cryo-EM Structure of the 2019-NCoV Spike in the Prefusion Conformation'. *Science*, 367(6483), pp. 1260–1263.

Wrobel, A.G. *et al.* (2021) 'Structure and Binding Properties of Pangolin-CoV Spike Glycoprotein Inform the Evolution of SARS-CoV-2'. *Nature Communications*, 12(1), p. 837. DOI: 10.1038/s41467-021-21006-9.

Wu, L., Girgis, C.M. and Cheung, N.W. (2020) 'COVID-19 and Diabetes: Insulin Requirements Parallel Illness Severity in Critically Unwell Patients'. *Clinical Endocrinology*, 93(4), pp. 390–393.

Wu, Y. *et al.* (2020) 'Prolonged Presence of SARS-CoV-2 Viral RNA in Faecal Samples'. *The Lancet Gastroenterology & Hepatology*, 5(5), pp. 434–435.

Wylon, K., Dölle, S. and Worm, M. (2016) 'Polyethylene Glycol as a Cause of Anaphylaxis'. *Allergy, Asthma & Clinical Immunology*, 12(1), pp. 1–3.

Xiao, F. *et al.* (2020) 'Evidence for Gastrointestinal Infection of SARS-CoV-2'. *Gastroenterology*, 158(6), pp. 1831–1833.

Xie, J. *et al.* (2022) ‘Comparative Effectiveness of the BNT162b2 and ChAdOx1 Vaccines against Covid-19 in People over 50’. *Nature Communications*, 13(1), p. 1519. DOI: 10.1038/s41467-022-29159-x.

Xu, B. *et al.* (2017) ‘The Ratio of Circulating Follicular T Helper Cell to Follicular T Regulatory Cell Is Correlated with Disease Activity in Systemic Lupus Erythematosus’. *Clinical Immunology*, 183, pp. 46–53.

Yang, L. *et al.* (2021) ‘The Signal Pathways and Treatment of Cytokine Storm in COVID-19’. *Signal Transduction and Targeted Therapy*, 6(1), p. 255.

Yang, Q. *et al.* (2021) ‘Suppressive Monocytes Impair MAIT Cells Response via IL-10 in Patients with Severe COVID-19’. *The Journal of Immunology*, 207(7), pp. 1848–1856.

Yang, Shiyi. *et al.* (2020) ‘Decontamination of Ambient RNA in Single-Cell RNA-Seq with DecontX’. *Genome Biology*, 21, pp. 1–15.

Yang, Shu. *et al.* (2020) ‘Early Estimation of the Case Fatality Rate of COVID-19 in Mainland China: A Data-Driven Analysis’. *Annals of Translational Medicine*, 8(4).

Yaykasli, K.O. *et al.* (2021) ‘Neutrophil Extracellular Trap-Driven Occlusive Diseases’. *Cells*, 10(9), p. 2208.

Yin, X. *et al.* (2021) ‘MDA5 Governs the Innate Immune Response to SARS-CoV-2 in Lung Epithelial Cells’. *Cell Reports*, 34(2).

Yin, Y., Yajima, M. and Campbell, J.D. (2024) ‘Characterization and Decontamination of Background Noise in Droplet-Based Single-Cell Protein Expression Data with DecontPro’. *Nucleic Acids Research*, 52(1), pp. e4–e4.

Yoshida, M. *et al.* (2022) ‘Local and Systemic Responses to SARS-CoV-2 Infection in Children and Adults’. *Nature*, 602(7896), pp. 321–327.

You, J. *et al.* (2024) ‘Serum AXL Is a Potential Molecular Marker for Predicting COVID-19 Progression’. *Frontiers in Immunology*, 15, p. 1394429.

Young, M.D. and Behjati, S. (2020) ‘SoupX Removes Ambient RNA Contamination from Droplet-Based Single-Cell RNA Sequencing Data’. *GigaScience*, 9(12), p. giaa151. DOI: 10.1093/gigascience/giaa151.

Yu, G. *et al.* (2012) ‘ClusterProfiler: An R Package for Comparing Biological Themes among Gene Clusters’. *Omics: A Journal of Integrative Biology*, 16(5), pp. 284–287.

Yu, G. and He, Q.-Y. (2016) ‘ReactomePA: An R/Bioconductor Package for Reactome Pathway Analysis and Visualization’. *Molecular BioSystems*, 12(2), pp. 477–479.

Zaim, S. *et al.* (2020) ‘COVID-19 and Multiorgan Response’. *Current Problems in Cardiology*, 45(8), p. 100618.

Zerbinati, N. *et al.* (2020) ‘Chemical and Mechanical Characterization of Hyaluronic Acid Hydrogel Cross-linked with Polyethylen Glycol and Its Use in Dermatology’. *Dermatologic Therapy*, 33(4), p. e13747.

Zhai, Y. *et al.* (2015) ‘Host Transcriptional Response to Influenza and Other Acute Respiratory Viral Infections–a Prospective Cohort Study’. *PLoS Pathogens*, 11(6), p. e1004869.

Zhang, Q. *et al.* (2020) ‘Inborn Errors of Type I IFN Immunity in Patients with Life-Threatening COVID-19’. *Science*, 370(6515), p. eabd4570.

Zhang, Y.-Z. and Holmes, E.C. (2020) ‘A Genomic Perspective on the Origin and Emergence of SARS-CoV-2’. *Cell*, 181(2), pp. 223–227.

Zhao, M.-M. *et al.* (2021) ‘Cathepsin L Plays a Key Role in SARS-CoV-2 Infection in Humans and Humanized Mice and Is a Promising Target for New Drug Development’. *Signal Transduction and Targeted Therapy*, 6(1), p. 134.

Zhao, M.-M. *et al.* (2022) ‘Novel Cleavage Sites Identified in SARS-CoV-2 Spike Protein Reveal Mechanism for Cathepsin L-Facilitated Viral Infection and Treatment Strategies’. *Cell Discovery*, 8(1), p. 53.

Zhao, X. *et al.* (2022) ‘Interferon Control of Human Coronavirus Infection and Viral Evasion: Mechanistic Insights and Implications for Antiviral Drug and Vaccine Development’. *Journal of Molecular Biology*, 434(6), p. 167438.

Zheng, H.-Y. *et al.* (2020) ‘Elevated Exhaustion Levels and Reduced Functional Diversity of T Cells in Peripheral Blood May Predict Severe Progression in COVID-19 Patients’. *Cellular & Molecular Immunology*, 17(5), pp. 541–543.

Zheng, M. *et al.* (2021) ‘TLR2 Senses the SARS-CoV-2 Envelope Protein to Produce Inflammatory Cytokines’. *Nature Immunology*, 22(7), pp. 829–838.

Zhou, F. *et al.* (2020) ‘Clinical Course and Risk Factors for Mortality of Adult Inpatients with COVID-19 in Wuhan, China: A Retrospective Cohort Study’. *The Lancet*, 395(10229), pp. 1054–1062.

Zhou, R. *et al.* (2020) ‘Acute SARS-CoV-2 Infection Impairs Dendritic Cell and T Cell Responses’. *Immunity*, 53(4), pp. 864–877.

Zhu, L. *et al.* (2020) ‘Association of Blood Glucose Control and Outcomes in Patients with COVID-19 and Pre-Existing Type 2 Diabetes’. *Cell Metabolism*, 31(6), pp. 1068–1077.

Zou, X. *et al.* (2020) ‘Single-Cell RNA-Seq Data Analysis on the Receptor ACE2 Expression Reveals the Potential Risk of Different Human Organs Vulnerable to 2019-NCoV Infection’. *Frontiers of Medicine*, 14, pp. 185–192.

Zubchenko, S. *et al.* (2022) ‘Herpesvirus Infections and Post-COVID-19 Manifestations: A Pilot Observational Study’. *Rheumatology International*, 42(9), pp. 1523–1530.

Zuo, Y. *et al.* (2020) ‘Neutrophil Extracellular Traps in COVID-19’. *JCI Insight*, 5(11).

10. Appendix

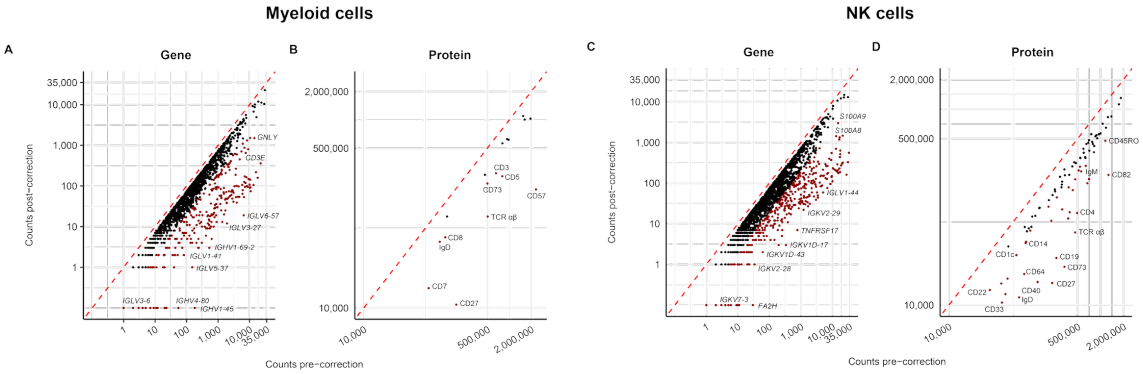

E

Gene	Raw	Corrected	Count Diff.	% Diff.
PTPRC	0.4M	0.3M	8760	2.5
LYZ	2.0M	2.0M	332	0.0
HLA-DRA	0.7M	0.7M	80	0.0
CD14	0.2M	0.2M	21	0.0
S100A8	4.5M	4.5M	924	0.0
S100A9	5.3M	5.3M	1218	0.0

F

Protein	Raw	Corrected	Count Diff.	% Diff.
CD45	6.4M	6.1M	329K	5.1
CD163	1.2M	1.1M	56K	4.7
HLA-DR	1.8M	1.7M	65K	3.6
CD14	1.7M	1.7M	15K	0.9
CD11c	8.5M	8.5M	45K	0.5
CD86	1.4M	1.4M	956	0.1

G

Gene	Raw	Corrected	Count Diff.	% Diff.
PTPRC	751.3K	750.1K	1143	0.2
NCAM1	78.6K	78.6K	5	0.0
KLRF1	200.1K	200.1K	11	0.0
FCGR3A	277.3K	277.3K	10	0.0

H

Protein	Raw	Corrected	Count Diff.	% Diff.
CD45	5.2M	4.8M	387K	7.4
CD56	6.5M	6.4M	176K	2.7
CD158	2.6M	2.6M	79K	3.0
CD16	12.5M	12.1M	402K	3.2

Supplementary Figure 1: Overview of most and least changed genes and proteins after ambient noise decontamination in myeloid and NK cells. Comparison of genes **(A, C)** and protein **(B, D)** expression before and after correction with a change of at least 25%. Red dots represent transcripts and proteins presenting reductions greater than 80% and 50% post-correction, respectively. Tables indicating initial and corrected counts of transcripts and proteins percentage decrease of marker genes for the myeloid **(E-F)** and NK **(G-H)** cell lineages.

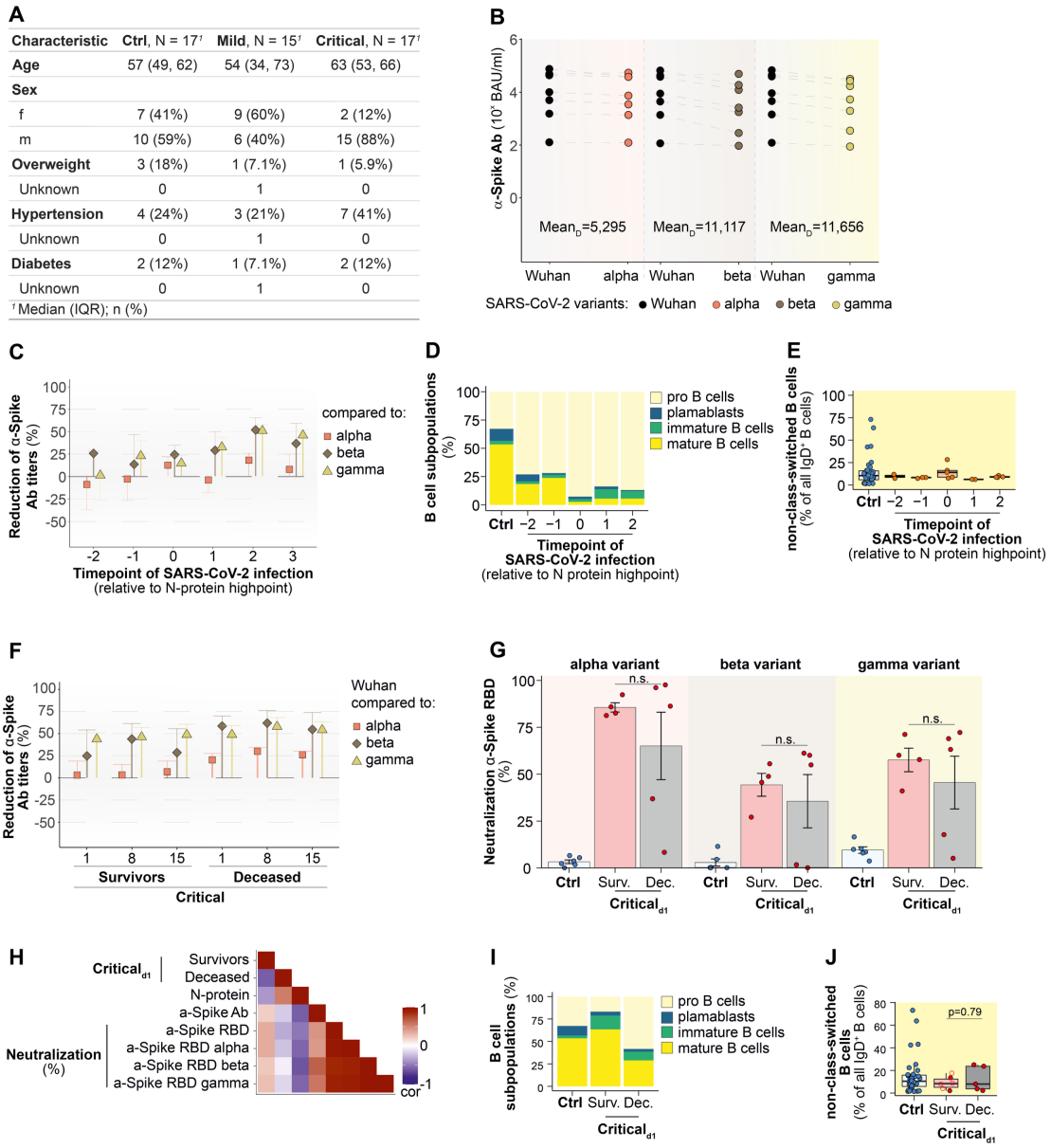

Supplementary Figure 2: Exploration of antibody titers against various SARS-CoV-2 strains across COVID-19 disease severities. (A) Table detailing patient demographics and comorbidities for cohorts infected with SARS-CoV-2 and control groups. **(B)** Dot plot exhibiting concentrations of specific α-Spike-Ab against different SARS-CoV-2 variants at the peak N-protein concentration moment (t2) in the serum of patients with mild SARS-CoV-2 infection. **(C, F)** Lollipop plots depicting the percentage reduction in α-Spike-Ab levels against SARS-CoV-2 variants relative to the Wuhan strain in both mild (C) and critical (F) COVID-19 cases, and for Long COVID patients (H). **(D, E, G, H)** Immune cell

frequencies in mild **(D, E)** and critical **(G, H)** COVID-19 cases, focusing on B cell populations **(D, G)** and non-class-switched B cells **(E, H)**. **(G)** Neutralizing potential of antibodies against the Spike-RBD for alpha, beta, and gamma SARS-CoV-2 variants in healthy, non-vaccinated controls versus critically ill patients. **(H)** Pearson correlation matrix for selected metrics including the neutralizing capacity of α-Spike-Ab for RBD among critically ill patients on the first hospitalization day. The mean concentration in healthy controls is represented by a blue line, with the 95% confidence interval indicated by a blue dashed line. Error bars in (C) and (F) denote the standard error of the mean; statistical significance is assessed via the Mann-Whitney U test with unadjusted p-values (H); significance levels are marked as * p value <0.05, ** p value <0.01, *** p value <0.001.

A

Characteristic	LC control, N = 8[1]	Long COVID, N = 20[1]
Age	40 (34, 46)	39 (30, 47)
Sex		
f	6 (75%)	12 (60%)
m	2 (25%)	8 (40%)
Overweight	0 (0%)	3 (23%)
Unknown	3	7
Hypertension	1 (12%)	2 (10%)
Unknown	0	0
Diabetes	0 (0%)	1 (5.0%)
Unknown	0	0

[1] Median (IQR); n (%)

B

Characteristic	LC control, N = 8[1]	Long-COVID, N = 20[1]	p-value[2]
Fatigue	7 (88%)	16 (80%)	>0.9
Cardiovascular System	5 (62%)	10 (50%)	0.7
Neurological	6 (75%)	16 (80%)	>0.9
Insomnia	2 (25%)	3 (15%)	0.6
Headaches	3 (38%)	6 (30%)	>0.9
Dyspnea	4 (50%)	11 (55%)	>0.9

[1] n (%)
[2] Fisher's exact test

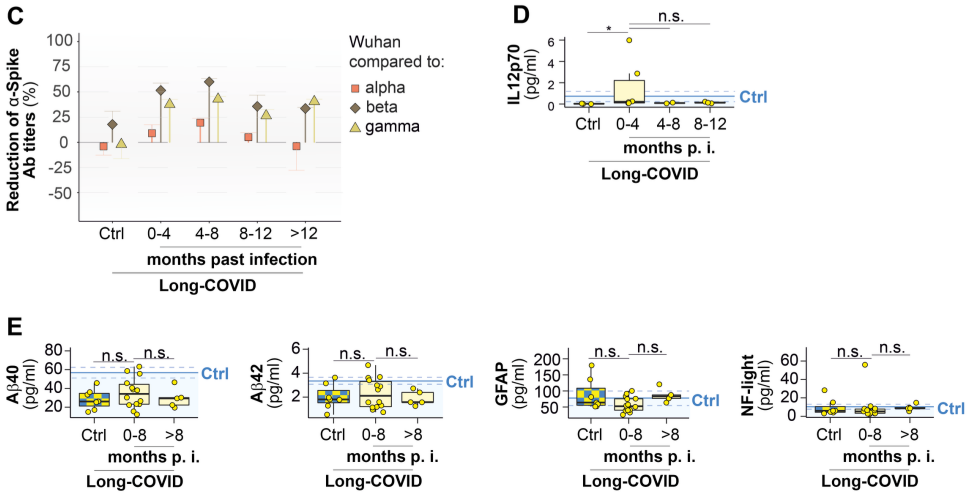

Supplementary Figure 3: Antibody Titers and Cytokine Levels in Long COVID. (A) Clinical data comparison table for Long COVID patients vs. control group. **(B)** Symptom frequency table for Long COVID vs. LC control cohorts. **(C)**

Charts of relative α-Spike-Ab titers to SARS-CoV-2 variants in Long COVID subjects. **(D)** Time series boxplots of IL12p70 cytokine levels in sera from Long COVID vs. control individuals. **(E)** Concentrations of neuroinflammation markers Aβ40, Aβ42, GFAP, NF-light in sera of Long COVID patients and LC controls. Mean concentration in healthy controls is represented by the blue line, 95% confidence interval shown with a blue dashed line. Error bars in (D) and (E) for standard error of the mean. Statistical analysis via Mann-Whitney U test; significance levels denoted as * p value <0.05, ** p value <0.01, *** p value <0.001 for (D, E).

A

Characteristic	Impf. Astra, N = 16[1]	Impf. Biontech, N = 45[1]	Impf. Moderna, N = 15[1]	p-value[2]
Age	50 (44, 54)	47 (37, 54)	27 (22, 36)	<0.001
Sex				0.013
f	15 (94%)	31 (69%)	7 (47%)	
m	1 (6.2%)	14 (31%)	8 (53%)	

[1] Median (IQR); n (%)
[2] Kruskal-Wallis rank sum test; Fisher's exact test

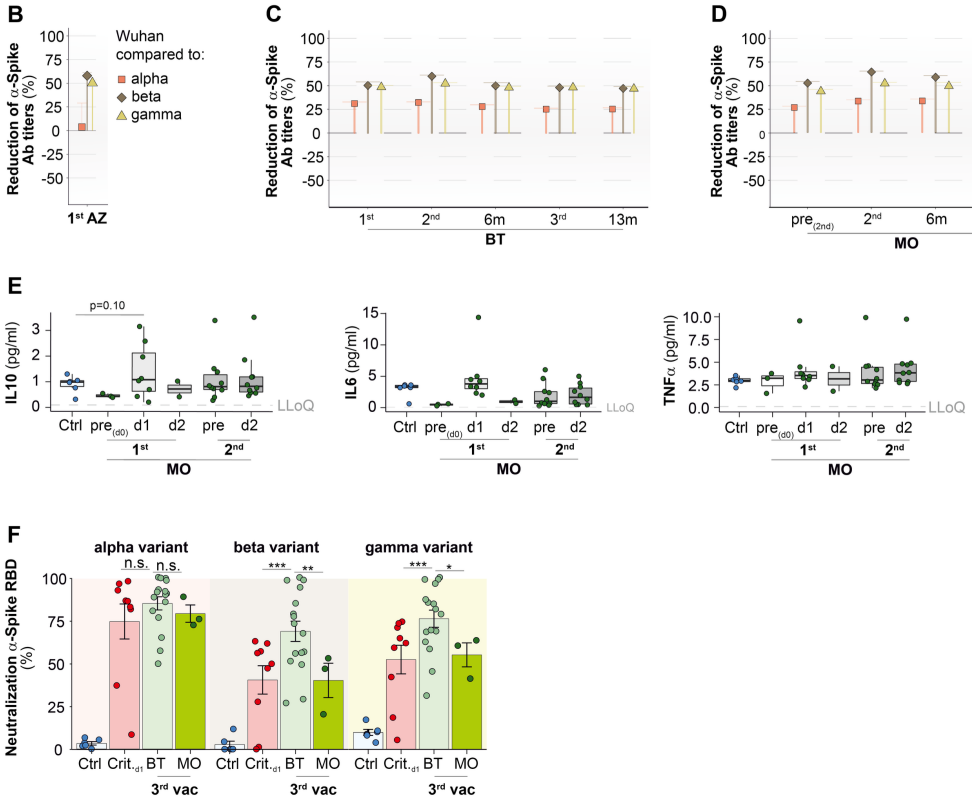

Supplementary Figure 4: Antibody titers and cytokine concentrations post-vaccination. (A) Demographic table detailing age and sex of participants receiving AZ, BT, and MO vaccines. Lollypop plots depicting percentage

reduction in α-Spike-Ab levels against SARS-CoV-2 variants relative to the Wuhan strain for AZ **(B)**, BT **(C)**, and MO **(D)** recipients at specified vaccination timepoints. **(E)** Cytokine levels of IL10, IL6, and TNFα measured in the peripheral blood of MO vaccine recipients pre- and post-inoculation. **(F)** Evaluation of the neutralizing ability of α-Spike-Ab against the RBD of SARS-CoV-2 alpha, beta, and gamma variants in non-vaccinated healthy controls, critically ill COVID-19 patients, and individuals vaccinated with BT and MO six months post-second booster (3rd vaccination). Standard error of the mean denoted by error bars in (C), (F), and (J). Statistical analysis conducted using the Mann-Whitney U test with unadjusted p-values for (E). Significance levels are * p value <0.05, ** p value <0.01, *** p value <0.001.

A

Characteristic	Astra/Astra/Biontech N = 3[1]	Astra/Biontech/Biontech N = 4[1]	J&J/Biontech N = 3[1]	Moderna/Moderna/Biontech N = 5[1]	Astra/Biontech N = 20[1]	p-value[2]
Age	60 (44, 61)	43 (30, 56)	35 (32, 42)	36 (22, 60)	32 (27, 46)	0.5
Sex						0.004
f	0 (0%)	4 (100%)	0 (0%)	2 (40%)	14 (70%)	
m	3 (100%)	0 (0%)	3 (100%)	3 (60%)	6 (30%)	

[1] Median (IQR); n (%)
[2] Kruskal-Wallis rank sum test; Fisher's exact test

B

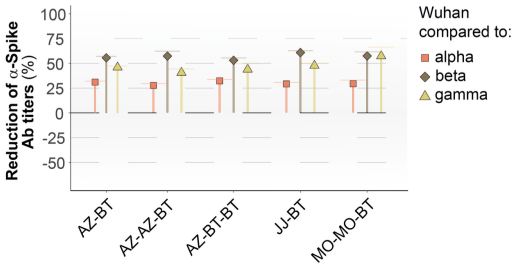

Supplementary Figure 5: Dynamics of Ab responses to SARS-CoV-2 variants following cross-vaccination with different vaccine bases. (A) Presents a table detailing the ages and genders of participants who received various vaccines, including Vaxzevria AstraZeneca (AZ), Jcovden Janssen-Cilag (JJ), Comirnaty Pfizer-BioNTech (BT), and Spikevax Moderna (MO), in multiple doses. **(B)** Comparative lollipop plot illustrating the reduction in α-Spike-Ab levels against different SARS-CoV-2 variants after being vaccinated with a combination of vaccines across various immunization strategies. Error bars represent the standard error of the mean.

A

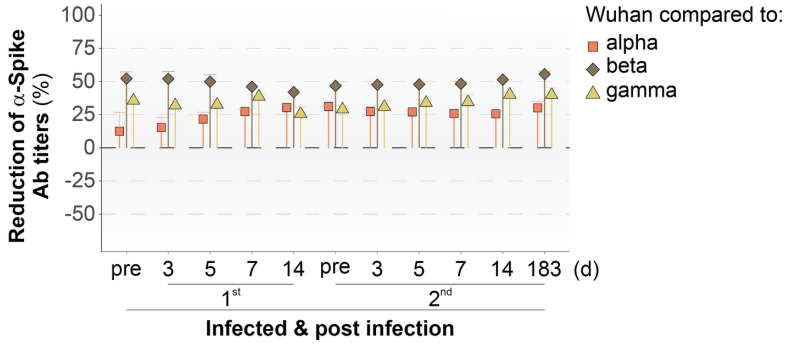

Supplementary Figure 6: Ab titer reduction in previously infected and subsequently vaccinated individuals. **(A)** A lollipop chart depicting the decrease in antibody titers against specified variants in comparison to the Wuhan strain. Error bars represent the standard error of the mean. Sample size: N = 3.

9. Acknowledgements

I would like to express my heartfelt gratitude to Susanne Schmidt, Eicke Latz, and Sammy Bedoui for creating the opportunity for me to pursue my PhD and participate in studies of such high importance. Their supervision, input, and unwavering support have been invaluable throughout my research journey.

Special thanks go to my family - my wife and son, my brother, my parents, and my grandparents - for their emotional support over the years. Their pride in me and my work has been a constant source of motivation. I also want to thank my best friend, Tim Treis, for his unwavering support during the hard times and for being a good friend.

My deepest appreciation goes to my best buddy in the lab, Jasper Spitzer, for his support, interactive discussions, and help in solving bioinformatics issues. His companionship made the time at work and outside truly enjoyable.

I am especially grateful to Stefano Mangiola and Jan Schroeder for their supervision in bioinformatics and their introduction to scRNAseq data analysis. My thanks also go to Tony Pappenfuss for providing access to the WEHI computational resources necessary for my analysis.

Thanks to Gunther Hartman for supporting my work during the final period of my PhD when we transitioned from the Institute of Innate Immunity to the Institute of Clinical Chemistry and Clinical Pharmacology.

A special mention goes to the Immunogenomics team, including Kai, Carolyn, Nushi, Ulrike, Marie and Maike, for their support in the lab and the pleasant time in the office. I am also grateful to the members of the Institute of Innate Immunity for their support.

Thanks to the Computational Science Initiative members - Dan, Ilariya, Justine, Tony, Lei, and Jenny - as well as the Bedoui Lab members, for welcoming me during my stay in Melbourne and making it a wonderful experience as a visiting PhD student. Their hospitality made me feel at home.

I extend my gratitude to the medical doctoral students Jakob, Simon, Tim and David for the fun in the lab and their support during the collection and processing of patient samples. Additional thanks go to all the probands who donated blood for the studies, making this work possible.

I also appreciate all the cooperation partners who facilitated numerous publications during my PhD.

Finally, thanks to the IRTG coordination office for their efficient handling of bureaucratic matters, ensuring smooth administrative processes throughout my studies.

10. Publications

- Wolf, C., Lim, E. L., Mokhtari, M., Kind, B., **Odainic, A.**, Lara-Villacanas, E., ... & Lee-Kirsch, M. A. (2024). UNC93B1 variants underlie TLR7-dependent autoimmunity. **Science immunology**
- Mangiola, S., Milton, M., Ranathunga, N., Li-Wai-Suen, C. S. N., **Odainic, A.**, Yang, E., ... & Papenfuss, A. T. (2024). A multi-organ map of the human immune system across age, sex and ethnicity. bioRxiv.
- de Boni, L., **Odainic, A.**,..., Petzold, G.C., 2023. No evidence for neuronal damage or astrocytic activation in cerebrospinal fluid of Neuro-COVID-19 patients with long-term persistent headache. **Neurological Research and Practice**, 5(1), p.49.
- Gressier, E., ..., **Odainic, A.**,..., Bedoui, S., 2023. CD4+ T cell calibration of antigen-presenting cells optimizes antiviral CD8+ T cell immunity. **Nature Immunology**, pp.1-12.
- Feng, W., ..., **Odainic, A.**, ..., Iyengar, S., 2023. NULISA: a novel proteomic liquid biopsy platform with attomolar sensitivity and high multiplexing. **Nature Communications**, 14(1), 7238.
- Hackstein, C.P., ..., **Odainic, A.**, ..., Abdullah, Z., 2023. Interferon-induced IL-10 drives systemic T-cell dysfunction during chronic liver injury. **Journal of Hepatology**, 79 (1), 150-166
- Niepmann, S.T., ..., **Odainic, A.**, ..., Latz, E., 2023. Toll-like receptor-3 contributes to the development of aortic valve stenosis. **Basic Research in Cardiology**, 118(1), p.6.
- **Odainic, A.** et al., 2022. Comparative analysis of antibody titers against the spike protein of SARS-CoV-2 variants in infected patient cohorts and diverse vaccination regimes. **International Journal of Molecular Sciences**, 23(20), p.12231.
- de Boni, L.,**Odainic, A.**, ..., Petzold, G. C. (2022). No serological evidence for neuronal damage or reactive gliosis in neuro-COVID-19 patients with

long-term persistent headache. **Neurological Research and Practice**, 4(1), 1-7.

- Rieke, G. J., ..., **Odainic, A.**, ..., Nattermann, J. (2022). Natural Killer Cell-Mediated Antibody-Dependent Cellular Cytotoxicity Against SARS-CoV-2 After Natural Infection Is More Potent Than After Vaccination. **The Journal of infectious diseases**, 225(10), 1688-1693.
- Jaskolski, M. R., **Odainic, A.**, ..., Flöck, A. (2022). Brain-Derived Neurotrophic Factor in Gestational Diabetes: Analysis of Maternal Serum and Cord Blood Pairs and Comparison of Dietary-and Insulin-Dependent GDM. **Metabolites**, 12(6), 482.
- Flöck, A., **Odainic, A.**, ..., Merz, W. M. (2022). High maternal BMI and low maternal blood BDNF may determine the limit of detection of amniotic fluid BDNF throughout gestation: Analysis of mother-fetus trios and literature review. **Plos one**, 17(3), e0265186.
- Scheiblich, H., ..., **Odainic, A.**, ..., Heneka, M. T. (2021). Microglia jointly degrade fibrillar alpha-synuclein cargo by distribution through tunneling nanotubes. **Cell**, 184(20), 5089-5106.
- Müller, P.L.,**Odainic, A.**, ..., Pfau, M. (2021). Inferred retinal sensitivity in recessive Stargardt disease using machine learning. **Scientific Reports**, 11(1), p.1466.
- Müller, P.L., Treis, T.,**Odainic, A**., ..., Holz, F.G. (2020). Prediction of function in ABCA4-related retinopathy using ensemble machine learning. **Journal of Clinical Medicine**, 9(8), p.2428.